2005

Hydrodynamics and gas holdup in a cocurrent air-water-fiber bubble column

Chengzhi Tang
Iowa State University

Hydrodynamics and gas holdup in a cocurrent air-water-fiber bubble column

by

Chengzhi Tang

A dissertation submitted to the graduate faculty

in partial fulfillment of the requirements for the degree of

DOCTOR OF PHILOSOPHY

Major: Mechanical Engineering

Program of Study Committee:
Theodore J. Heindel, Major Professor
Gerald M. Colver
Michael G. Olsen
Shankar Subramaniam
Dennis Vigil

Iowa State University

Ames, Iowa

2005

Graduate College
Iowa State University

This is to certify that the doctoral dissertation of

Chengzhi Tang

has met the dissertation requirements of Iowa State University

Signature was redacted for privacy.

Major Professor

Signature was redacted for privacy.

For the Major Program

To

My parents

TABLE OF CONTENTS

LIST OF FIGURES

LIST OF TABLES

NOMENCLATURE

Symbols

a	coefficient in Eq. (2.8) or Eq. (6.26)
a_1, a_2, a_3	model coefficients in Eq. (7.11)
A_1	intercept in Eq. (7.9), cm/s
A_c	bubble column cross-sectional area, m^2
b	exponential parameter in Eq. (2.8) or Eq. (6.26)
B_0	intercept in the Zuber-Findlay drift-flux model, m/s
$B_{0,1}$, $B_{0,2}$	intercepts in the two-segment gas holdup model (Eq. (7.3))
B_1	intercept in Eq. (7.7), m/s
C	fiber mass fraction in % ($0 \leq C \leq 100$)
c	empirically determined coefficient in Eq. (2.10)
C_1	slope of U_g/ε with superficial liquid velocity in Eqs. (7.9) and (7.11)
C_f	wall friction coefficient in Eq. (A.10)
C_g, C_l	radial distribution parameters for the modified drift-flux model (Eq. (5.7))
$C_{g,1}$	slope in the two-segment gas holdup model (Eqs (7.3), (7.7), (7.9), and (7.11))
$C_{g,2}$	slope in the two-segment gas holdup model (Eq. (7.3))
$C_{g,2\text{-}1}$	slope change when the flow regimes transitions from vortical-spiral to turbulent (Eqs. (7.7), (7.9), and (7.11))
C_v	volumetric fiber fraction ($0 \leq C_v \leq 1$)
C_0, C_1	slope in the drift-flux model
CV(L)	coefficient of variation of fiber length
D	bubble column diameter or floc diameter, m
D_c	bubble column diameter, m
d	fiber diameter, m

d_b	bubble diameter, m
d_{fi}	fiber inner diameter, m
d_{fo}	fiber outer diameter, m
d_o	gas distributor orifice diameter, m
E	fiber elastic modulus, Pa
$F(\varepsilon)$	function representing the influence of interactions between neighboring bubbles
f	fiber surface friction coefficient or friction factor calculated with Eq. (A.12)
f(L)	fiber length distribution
g	acceleration due to gravity, m/s^2
h	distance, m
I	moment of inertial of a fiber, m^4
I_0	model coefficient in Eq. (7.11)
I_c	characterization parameter for fiber suspension effects on gas holdup, defined in Eq. (6.29)
Fr^*	Froude number defined in Eq. (B.21)
j_{gl}, j_{gm}	drift-flux, m/s
K	power-law fluid consistency index, $Pa \cdot s^n$
L	average fiber length, m
L_A	arithmetic average fiber length, m
L_L	length-weighted average fiber length, m
L_W	weight-weighted average fiber length, m
l	length of a single fiber, m
l_f	average fiber length, m
M	total mass of a fiber sample, kg
N	total number of fibers in a fiber sample
N_c	crowding factor

$\overline{N}_c$	mean crowding factor
$N_{c,LA}$	crowding factor calculated with Eq. (6.4) using the arithmetic average fiber length
$N_{c,log}$	crowding factor assuming a log-normal fiber length distribution
N_{c1}	crowing factor defined by L_L and N_f (Eq. (6.24))
N_{c2}	crowing factor defined by L_A and N_f (Eq. (6.25))
N_f	fiber number density in fiber suspensions, $1/m^3$
n	exponential parameter in Eq. (2.17) or power-law index in Eq. (A.22)
n_c	contact number
n_f	number of fibers per unit mass of fiber sample, 1/kg
p	pressure, Pa
$p(N_c)$	probability density function of the crowding factor
$\dot{Q}_g$	volumetric gas flow rate, m^3/s
$\dot{Q}_l$	volumetric liquid flow rate, m^3/s
r	fiber aspect ratio
R_A	gas distributor open area ratio
Re	Reynolds number defined in Eq. (B.19)
Re_n	power law fluid flow Reynolds number defined in Eq. (A.24)
R_U	superficial velocity ratio defined in Eq. (7.16)
S_f, S_L	fiber length standard deviation, m
$U_{b\infty}$	terminal bubble rise velocity, m/s
U_g	superficial gas velocity, m/s
U_{gt}	superficial gas velocity where the gas flow regime transition from vortical-spiral to turbulent flow (Eqs. (7.3), (7.7), (7.9), and (7.11)), m/s
U_l	superficial liquid velocity, m/s
U_s	slip velocity, m/s
U_{sp}	superficial solid velocity, m/s

V_{sp} volume of a sphere swept by a fiber, m^3

We Weber number defined in Eq. (B.23)

z axial position along a bubble column, m

$\langle\rangle$ average over the cross section

Greek symbols

γ shear rate, s^{-1}

Δ roughness, m

$\Delta I_{c,t}$ width of the transitional region in Fig. 7.14

Δp pressure difference between two column axial locations, Pa

Δp_0 pressure difference between two column axial locations before aeration, Pa

Δp_τ pressure loss due to wall shear friction, Pa

Δz distance between two axial positions along a bubble column, m

$\Delta\varepsilon$ gas holdup uncertainty

$\Delta\bar{\varepsilon}_{II}$ gas holdup estimation error due to Method II

$\Delta\bar{\varepsilon}_{III}$ gas holdup estimation error due to Method III

δ a small number (Eqs. (7.28) and (7.29)) or fiber wall thickness, m

ε gas holdup

$\bar{\varepsilon}$ average gas holdup

$\varepsilon_{A\text{-}W}$ gas holdup in air-water bubble columns

ε_{expr} experimental gas holdup

ε_{pred} predicted or reproduced gas holdup

$\bar{\varepsilon}_{II}$ average gas holdup estimated with Method II

$\bar{\varepsilon}_{III}$ average gas holdup estimated with Method III

$\bar{\varepsilon}_\tau$ contribution of wall shear stress to the total gas holdup

θ_f liquid-fiber interfacial contact angle

μ_a apparent viscosity, Pa·s

μ_f fiber surface friction coefficient

μ_l	liquid dynamic viscosity, Pa·s
μ_s	suspending liquid viscosity, Pa·s
μ_{sp}	dimensionless specific viscosity defined in Eq. (2.14)
ν_g	gas phase kinematic viscosity, m^2/s
ν_l	liquid kinematic viscosity, m^2/s
$\Pi_l^{'}$	Fiber network confinement force to buoyancy force ratio defined by Eq. (B.28)
$\rho_{f,\,eff}$	effective fiber density, kg/m^3
ρ_f	fiber wall material density, kg/m^3
ρ_g	gas density, kg/m^3
ρ_l	liquid density, kg/m^3
ρ_m	fiber suspension density, kg/m^3
σ	surface tension, N/m
τ_w	wall shear stress, Pa
$\bar{\tau}_w$	average wall shear stress, Pa
$\bar{\tau}_{w0}$	average wall shear stress for single-phase liquid flow, Pa
τ_y	yield stress, N/m^2
ω	fiber coarseness, kg/m

Subscripts

0	without aeration
A	arithmetic average
A-W	in air-water bubble column
b	bubble
c	contact or cross-section
f	fiber
g	gas
gl	quantity of gas phase relative to liquid phase
gt	superficial gas velocity at which a flow regime transition occurs

H	at the higher end
i	identification number of a fiber in a sample or a column section
L	length-weighted average, lumen, or at the lower end
l	liquid
m	mixture
sp	solid particles
W	weight-weighted average
w	water or wall
τ	due to wall shear friction
∞	terminal

ACKNOWLEDGEMENTS

First I would like to thank my major professor, Dr. Theodore J. Heindel, for introducing me into this research and providing all the resources that makes this work possible. The countless recommendations and comments he continuously gave me through this project are essential to reach the research goals. The freedom to study and explore that I enjoyed in his group is greatly appreciated.

I would also like to thank my POS committee members, Dr. Gerald M. Colver, Dr. Michael G. Olsen, Dr. Shankar Subramaniam, and Dr. Dennis Vigil, for their generous contribution of time and valuable comments on this project.

Portions of this project were supported by the National Research Initiative of the USDA Cooperative State Research, Education and Extension Service, grant number 2001-35103-11259. The cellulose fiber supply and characterization was provided by Kimberly-Clark Corporation; their support is appreciated.

I would like to thank my father, Siqing Tang, and my mother, Manqing Li, for their love, support, and encouragement during all my life. They are great parents. I would like to dedicate this dissertation to them.

Last but not the least, I would like to thank my beloved wife, Xiaoping Wang. She was always with me during these years, supporting me both in my life and in my work. With her in my life, I was able to be strong and motivated through all the time. She also occasionally assisted me in the lab and was very helpful.

ABSTRACT

Gas-liquid-fiber flows are widely found in various unit operations in the pulp and paper industry and similar flow conditions may be found in other industrials, such as wastewater treatment, food processing, biological organism production, and pharmaceutical manufacturing.

Flocculated fiber suspensions are considered as mixtures of fiber and suspending liquid with network structures comprising flocs and inter-floc regions. The fundamental mechanisms of the fiber influences on bubble motions and gas holdup in gas-liquid-fiber bubble columns are connected to the unique structure and properties of fiber suspensions.

An experimental study is completed to investigate the hydrodynamics and gas holdup in a cocurrent air-water-fiber bubble column. Generally, gas holdup increases with increasing superficial gas velocity without a local maximum, decreases with increasing superficial liquid velocity, and changes nonlinearly with increasing fiber mass fraction. When flocculation is significant in the fiber suspension, gas holdup decreases with increasing fiber mass fraction. These trends are similar for all the studied fiber types. Gas distribution method significantly affects the gas holdup trends with increasing superficial liquid velocity or fiber mass fraction. Fiber type has a significant effect on gas holdup in the cocurrent air-water-fiber bubble column. Gas flow regimes in the air-liquid-fiber bubble column are identified based on the drift-flux model. Three gas flow regimes (i.e., dispersed bubble, vortical-spiral, and turbulent flow) are identified. When fiber mass fraction is higher than a certain value (which is a function of fiber type), the dispersed bubble flow regime disappears because bubble coalescence is enhanced at low superficial gas velocities by flocculating fibers. Superficial liquid velocity does not affect gas flow regime transition.

A parameter (I_c) is identified to characterize the fiber effects on gas holdup in the air-water-fiber bubble column that satisfies the following condition: when this parameter is constant, the gas holdup in different fiber suspensions is generally similar at most operating conditions.

A gas holdup model is developed for cocurrent air-water-fiber bubble flows based on the drift-flux model. The model coefficients are estimated with a nonlinear least square error curve fitting method using all data collected in the air-water-fiber system investigated in this study. The gas holdup model correlates gas holdup with superficial gas and liquid velocity and fiber type and mass fraction. The characterization parameter I_c is used to represent the effect of fiber type and mass fraction. The model reproduces most air-water-fiber system data within ±10% error. It also predicts the gas holdup data in air-water systems, which is not used in estimating the model coefficients, within ±10% error.

Chapter 1: INTRODUCTION

This chapter includes three sections. The first section gives the motivation of the current research project. The second section introduces the goals of the present study. The last section provides a brief description of the organization of this dissertation.

1.1 Motivation

Bubble columns are contactors in which a discontinuous gas phase, in the form of bubbles, moves relative to a continuous phase, which can be a liquid or a homogeneous suspension (Shah *et al.*, 1982). The main benefits of bubble columns compared to other multiphase contactors include (Shah *et al.*, 1982):

(i) Less maintenance is required because there are no moving parts;

(ii) Higher overall mass transfer coefficients can be obtained;

(iii) Higher heat transfer rates per unit volume can be achieved;

(iv) Solids can be handled without erosion or plugging;

(v) Less floor space is occupied;

(vi) Bubble column reactors cost less; and

(vii) Slow reactions can be carried out because of high liquid residence time.

Because of their large benefits, bubble columns are widely used to effect gas-liquid (GL) or gas-liquid-solid (GLS) transport processes, which are commonly found in many industries including pulp and paper processing, petroleum-based fuel production, commodity and specialty chemical production, mineral processing, wastewater treatment, food processing, biological organism production, and pharmaceutical manufacturing.

Recently, one area of GLS bubble columns involving suspensions with flexible fibers or fiber-like filamentous fungi constituting the solid phase has gained wide industrial applications. One application of gas-liquid-fiber (GLF) bubble columns is flotation deinking in the paper recycling industry. In flotation deinking, air is injected into a dilute suspension (typically has a fiber mass fraction on the order of $C \approx 1\%$) of recycled fiber and contaminants (mainly hydrophobic ink particles). The air bubbles are blended with the

suspension, and under appropriate conditions, contaminant-bubble aggregates are formed. The aggregates rise to the suspension surface where the contaminants are skimmed off as a dirt-laden layer of froth (Smook, 1992; Heindel, 2003). Traditionally, flotation deinking is achieved in flotation cells (Smook, 1992; Heindel, 1997; Chaiarrekij *et al.*, 2000), which are basically agitated tanks and usually equipped with electrical energy-consuming agitators. Recently, a flotation column in place of a typical flotation cell for deinking recycled paper was suggested (Gomez *et al.*, 1995). Benefits of column flotation deinking have been reported to include: (i) power savings while obtaining similar or better pulp brightness and ink particle removal efficiencies compared to conventional multistage flotation cell systems (Gomez *et al.*, 1995; Heindel, 1997; Dessureault *et al.*, 1998; Hardie *et al.*, 1999a; Chaiarrekij *et al.*, 2000), (ii) a potential in recovering usable fibers from the reject stream, and (iii) reducing the volume of deinking waste rejected into the environment (Chaiarrekij *et al.*, 2000).

In the pulp and paper industry, there are many other unit operations involving GLF flows such as direct-contact steam heating, gaseous fiber bleaching, and papermaking (Heindel, 2003).

GLF systems involving cellulose fibers are very complex because cellulose fibers are typically flexible with a large aspect ratio and have a density close to that of water. Cellulose fibers can also form coherent network structures (i.e., flocs) at fiber mass fractions (C) as low as ~0.3% and continuous fiber networks at fiber mass fractions larger than ~1% (Kerekes *et al.*, 1985). When gas is introduced into the fiber suspension, bubble movement can be retarded by the fiber network, and small bubbles can even be trapped and stop rising relative to the fiber suspension (Pelton and Piette, 1992; Ajersch and Pelton, 1999a). It is believed that fiber-fiber interaction can have a significant effect on the hydrodynamics and transport processes in GLF systems.

Knowledge of GLF bubble columns may also be useful for understanding the hydrodynamics and transport processes involved in submerged culture of filamentous fungi in bubble columns, where bubble columns have recently been used in their production (Malfait *et al.*, 1981; Zhi and Rorrer, 1996; Kawagoe *et al.*, 1997; Chisti, 1998; Kawagoe *et al.*, 1999; Gibbs *et al.*, 2000). Filamentous fungi are widely used in industry for a variety of

products of enormous social and economy importance, such as antibiotics, therapeutic metabolites, organic acids, insecticides and herbicides, food enzymes, cellulases, mycotoxins, and edible mushrooms (Finkelstein and Ball, 1992). One problem associated with submerged culture (aerobic fermentation) in bubble columns is to transfer sufficient oxygen to the active cells. The presence of the filamentous fungi produces a high viscosity slurry and thus, adds additional complications to the mass transfer (Gibbs *et al.*, 2000). Poor mixing resulting from the presence of filamentous fungi may also result in temperature control problems of the fermentation suspensions (Gibbs *et al.*, 2000).

Most filamentous fungi grow as branched filaments termed hyphae, which are collectively called mycelia (O'Donnell and Peterson, 1992). In submerged culture, the mycelia are either freely dispersed throughout the medium or form macroscopic aggregates. Bjorkman (2002; 2003a) showed that mycelia floc production and breakup were similar to that found in softwood fiber and Nylon fiber suspensions. Olsvik and Kristiansen (1994) stated that the rheological properties of mycelial suspensions are determined mainly by the concentration of fungi, its growth rate and morphology, which include factors such as hyphae geometry (length, diameter, branching frequency), hyphal flexibility and hyphal-hyphal interactions. Mycelial suspensions generally exhibit non-Newtonian behaviors and usually show pseudoplastic behaviors and a yield stress (Oolman and Blanch, 1986; Olsvik and Kristiansen, 1994). A Bingham plastic or yield-pseudoplastic model are commonly used to correlate the rheological data from mycelial suspensions (Deindoerfer and West, 1960; Zhong *et al.*, 1992; Olsvik and Kristiansen, 1994; Chen *et al.*, 1997). Cellulose fiber suspensions are also described with Bingham plastic models (Chase *et al.*, 1989) or yield-pseudoplastic models (Duffy *et al.*, 1976; Bennington *et al.*, 1990; Bennington *et al.*, 1995). All the aforementioned studies show that there is considerable similarity between GLF systems and gas-liquid-filamentous fungi suspensions. Hence, the study of the hydrodynamics in gas-liquid-cellulose fiber bubble columns can provide valuable information for the study and scale-up of filamentous fungi fermentation bubble columns.

Although bubble columns are easy to use, they are difficult to design because of their complex flow characteristics. Extensive efforts have been directed to the scale-up of bubble columns over the past several decades (e.g., Shah *et al.*, 1982; Joshi *et al.*, 1986; Joshi *et al.*,

1990; Joshi, 2001; Joshi *et al.*, 2002). However, few studies have been focused on hydrodynamics and transport processes of GLF bubble columns (Lindsay *et al.*, 1995; Reese *et al.*, 1996; Heindel and Monefeldt, 1997; Heindel and Garner, 1999; Heindel and Omberg, 2001; Xie *et al.*, 2003b). No model accounting for operating condition influences, fiber mass fraction, and fiber type based on extensive data collection is available for key nonadjustable process parameters of GLF bubble columns. One such parameter is gas holdup, which is one of the most important parameters used to characterize bubble column hydrodynamics (Shah *et al.*, 1982; Sarrafi *et al.*, 1999).

Gas holdup is defined as the volume fraction occupied by the gas phase in the total volume of the two or three-phase mixture in the bubble column. A higher gas holdup generally implies larger interfacial area between the gas and liquid and/or a larger gas residence time, both of which lead to a higher gas-liquid mass transfer rate. In flotation deinking processes, a higher gas holdup results in an increase in the ink removal efficiency (Lindsay *et al.*, 1995). Additional studies have also shown that hydrodynamics in flotation columns have a significant effect on ink removal efficiency (Dessureault *et al.*, 1998; Hardie *et al.*, 1999a; Janse *et al.*, 1999). Hence, the focus of this study is to develop a GLF gas holdup model to provide valuable information for optimizing and controlling the operating conditions of GLF bubble columns.

1.2 Goals of this Study

In the present experimental study on hydrodynamics and gas holdup in a cocurrent air-water-fiber bubble column, the following objectives will be reached.

First, the effects of cellulose and synthetic fiber addition on hydrodynamics and gas holdup will be examined. The effects of fiber mass fraction will be examined by comparing experimental results, i.e., gas holdup, in systems with fiber mass fractions ranging between 0 and 2%, which are typically the conditions met in paper recycling unit operations (e.g., flotation deinking). The effects of fiber type will also be determined. The fiber types to be studied include papermaking cellulose fibers like hardwood, softwood, and mechanical fibers, and synthetic (Rayon) fiber. The mechanisms by which fiber type and mass fraction

influence bubble motion and gas holdup in gas-liquid-fiber bubble columns will be summarized and applied to explain experimental data.

Second, the effects of superficial gas and liquid velocity on the hydrodynamics and gas holdup in the cocurrent air-water-fiber bubble column system will be studied. The superficial gas (U_g) and liquid (U_l) velocities investigated in this study will be $0 \leq U_g \leq 20$ cm/s and $0 \leq U_l \leq 10$ cm/s, which are typical conditions in various industries, so that the results from this study will have industrial relevance.

Third, based on the experimental results and analysis, a parameter will be identified to characterize the fiber influences on gas holdup in the air-water-fiber cocurrent bubble column. The parameter will account for effects of fiber mass fraction as well as fiber type. As far as the influences on gas holdup in gas-liquid-fiber suspensions are concerned, fiber types can be differentiated by a number of fiber physical properties, including fiber length, diameter, coarseness, surface friction coefficient, and flexibility. The identified parameter will simplify the quantification of fiber type effect by including important and available physical property parameters and neglecting less relevant ones.

Fourth, a gas holdup model will be developed for the cocurrent air-water-fiber bubble column, which correlates gas holdup with the superficial gas and liquid velocity and the identified parameter, which characterizes influences of fiber type and mass fraction. The model can be used by various industries to predict the system performance when fibers are added to the process. The model will also be useful to control air-water-fiber systems by adjusting superficial gas velocity, superficial liquid velocity, and/or amount of fibers into the systems, so that optimal or required performance can be reached.

To obtain the gas holdup model, a curve fitting method based on the drift-flux model will be used. A nonlinear least-square estimation method will be used for the model coefficient estimation. The first task is to check the applicability of the drift-flux model on the cocurrent air-water-fiber bubble column in identifying gas flow regimes and to correlate gas holdup and superficial gas velocity to specific superficial liquid velocities, fiber mass fractions, and fiber types. The coefficients obtained for the drift-flux gas holdup model will be correlated as functions of superficial liquid velocity, fiber mass fraction, and fiber type.

1.3 Organization of this Dissertation

This dissertation includes eight chapters and two appendixes.

Chapter 1 introduces the motivation and objectives of this research and the organization of this dissertation.

Chapter 2 is a review of literature related to the present research. Results from previous studies on cellulose fiber properties, liquid-fiber suspension properties and flow behaviors, gas-liquid-solid flow in bubble columns, gas-liquid-fibers flows in bubble columns, and gas holdup modeling in bubble columns are surveyed and summarized.

Chapter 3 outlines the experimental program used in this study on gas holdup in a cocurrent air-water-fiber bubble column. Details on experimental facility, experimental conditions, experimental procedures, data reduction, and experimental uncertainty are included.

Chapter 4 discusses the influences of fiber suspensions on bubble motion and gas holdup based on the unique structure and properties of flocculated fiber suspensions.

Chapter 5 presents the experimental results of this study in detail. Discussions regarding the mechanisms of these results are included. Comparison between the results obtained in this study and those reported in literature are also provided.

Chapter 6 describes an effort to quantify the fiber suspension effect on gas holdup in gas-liquid-fiber bubble columns with a single parameter, which can quantitatively accounts for the effects of both fiber mass fraction and fiber type.

Chapter 7 provides a detailed procedure to develop a gas model for air-water-fiber bubble columns based on the drift-flux model and experimental data. A model correlating gas holdup with superficial gas and liquid velocity and fiber mass fraction and type is resulted and evaluated. Discussions on the model coefficients are also included.

Chapter 8 lists the conclusions obtained in this study. Recommendations on future work to further this study are also provided.

Appendix A provides details of the gas holdup estimation method used in this study via pressure difference measurements. Appendix B presents a dimensional analysis on gas holdup in cocurrent gas-liquid-fiber bubble columns.

Chapter 2: LITERATURE REVIEW

In this chapter, previous results on topics related to this research project are surveyed and summarized. Five sections are included in this chapter. The first section gives a brief review on cellulose fiber properties. The second section provides a summary on liquid-fiber suspension properties and flow behaviors. The third section reviews gas-liquid-solid flow in bubble columns. The fourth section focuses on gas-liquid-fiber flows in bubble columns. The last section reviews previous research on gas holdup modeling in bubble columns.

2.1 Cellulose Fiber Properties

In this study, cellulose fibers made from wood will be used. There are two major wood classes: (1) angiosperms or broad-leaf trees (e.g., eucalyptus, birch, elm, and oak, etc.), usually called hardwoods; and (2) gymnosperm or conifers (e.g., pine, fir, and hemlock, etc.), usually called softwoods. One difference between hardwoods and softwoods is their vertical structures. Softwood vertical structure is composed almost entirely of long, tapering cells called tracheids, while hardwood is composed of both relatively long, narrow cells, named libriform fibers, and much shorter, wider cells, named vessels. Papermaking cellulose fibers made from these two wood classes are called hardwood fibers and softwood fibers, respectively. Cellulose fibers from different sources have different morphological and mechanical properties (McIntosh, 1970; Ilvessalo-Pfaffli, 1995). A major difference between hardwood and softwood fiber is their length. Typically, the average length of softwood fibers is up to two times longer than that of hardwood fibers (Smook, 1992).

Cellulose fibers are reduced from wood (or other fibrous raw materials) via different pulping methods, systematically rupturing the bonds within the wood structure. Existing pulping processes are classified as mechanical, chemical, or semichemical. In mechanical pulping processes, wood is pulped by mechanical energy with a small amount of chemicals and heat. In chemical pulping processes, wood is pulped with chemicals and heat with little or no mechanical energy. In semichemical pulping processes, wood is pulped with a

combination of chemical and mechanical treatments. Details about different pulping methods can be found in Smook (1992).

The chemithermomechanical pulping process is a chemically modified mechanical pulping process. Wood chips are presteamed with a chemical treatment at a high temperature (> 100°C) before a two-stage mechanical process, in which at first the chips are refined at higher temperature (> 100°C), and then refined under atmospheric conditions (Smook, 1992). Kraft pulping is a widely used chemical pulping process where wood chips are cooked in a solution of sodium hydroxide (NaOH) and sodium sulfide (Na_2S) at elevated pressure and temperature. The lignin, an amorphous, highly-polymerized substance cementing the fibers together, is degraded and dissolved away in the chemical solutions, leaving behind most of the cellulose and hemicellulose (both compositions of wood) in the form of intact fibers (Smook, 1992).

The difference between chemically pulped fibers and mechanically pulped fibers includes: (1) mechanical pulp retains a majority of the lignin; while chemical pulp is primarily lignin-free; (2) mechanical pulp fibers have a larger stiffness than chemical pulp fibers; and (3) chemical pulp fibers are longer than mechanical pulp fibers. Forgacs *et al.* (1958) showed that removal of lignin from wood pulp increased fiber flexibility. Hence, most wood fibers with lignin are fairly rigid, while fibers with most of the lignin removed are very flexible.

Cellulose fiber is a hygroscopic material. For hardwood fibers like Aspen, its moisture content can be up to about 100% of its ovendry mass; for softwood, the moisture content can be even larger. For example, the moisture content of redwood sapwood (i.e., newly formed outer wood) can be 210% of its ovendry mass; however, the moisture content of softwood heartwood (i.e., older, inactive central wood) is about the same as that of hardwood (Forest Products Laboratory, 1999).

The relative density of cellulose, i.e., the cell wall material, is about 1.5 times that of water, but because there are voids called lumens inside the fibers, the densities for common commercial cellulose fiber species range from 0.3 to 0.7 times that of water density, based on the swollen volume (Forest Products Laboratory, 1999). Thus, for cellulose fiber in a pulp

suspension, the density of the fiber with the water inside its body is very close to the density of water.

Due to the existence of lumens (i.e., the hollow centers in cellulose fibers), cellulose fibers collapse when the moisture content decreases. When the moisture content increases, fibers swell, resulting in larger cross-sections. Fiber shrinking or swelling occurs mainly in the tangential directions of the fiber; there is little shrinkage or swelling in the fiber axial direction (Forest Products Laboratory, 1999). Dry fibers tend to be brittle, however, when they are soaked in water, the fibers swell and become very flexible, soft, and pliable, and have higher elasticity and plasticity and lower stiffness (Casey, 1960).

Rayon fibers are synthetically produced from regenerated cellulose and have much more uniform physical properties (e.g., fiber length and diameter). Other differences between Rayon and cellulose fibers include: (i) cellulose fibers have hollow centers called a "lumen", while Rayon fibers are flexible solid cylinders; (ii) cellulose fibers have locations along the fiber attributed to biological characteristics or mechanical damages resulting from processing operations (i.e., beating), producing "hinges" or "knees", while Rayon fibers usually lack such nonuniformity (Stenuf and Unbehend, 1986); and (iii) cellulose fibers are usually subject to external fibrillation and micro-compressions in mechanical treatment and thus have surfaces morphologically different from those of smooth Rayon fiber surfaces (Seth *et al.*, 1993). These differences make cellulose fibers much more flexible than Rayon fibers, and the fiber-fiber contact mechanisms for cellulose fibers differ from those of Rayon.

Fiber length is a very important fiber property and affects flocculation. Natural fibers are not uniform in length due to the biological structure of pulpwood and the pulping processes. Usually average fiber length is used. There are three types of average fiber lengths:

(i) Arithmetic average fiber length L_A:

$$L_A = \frac{1}{N}\sum_{i=1}^{N} l_i \tag{2.1}$$

(ii) Length-weighted average fiber length L_L:

$$L_L = \frac{\sum_{i=1}^{N} l_i^2}{\sum_{i=1}^{N} l_i} \tag{2.2}$$

(iii) Weight-weighted average fiber length L_W:

$$L_W = \frac{\sum_{i=1}^{N} l_i^3}{\sum_{i=1}^{N} l_i^2} \tag{2.3}$$

where N is the number of fibers in the sample, and l_i is the length of fiber i.

The arithmetic average fiber length (L_A) is seldom used to represent fiber length. Cellulose pulp suspensions include shorter elements, typically referred to as "fines", down to submicroscopic lengths and there tends to be a larger quantity of fines as fiber length decreases. These short elements artificially skew L_A to small values. On the other hand, L_L or L_W are commonly used as a fundamental pulp fiber property because the very short fiber elements do not significantly affect their values. L_L and L_W can be measured with the projection method (TAPPI, 2002d) or the classification method (TAPPI, 2002c), with the latter giving the most accurate estimation. L_L and L_W can also be automatically measured by an optical analyzer using polarized light (TAPPI, 2002b).

Another important fiber property is coarseness, which is defined as the weight of fiber wall material in a specified fiber length. Its unit is given by milligram per 100 meters, called a decigrex with abbreviation "dg". Fiber coarseness can be measured with a standard TAPPI method (TAPPI, 2002a).

2.2 Liquid-Fiber Suspension Flows

2.2.1 Motion of isolated fibers in liquids

In extremely dilute fiber suspensions without fiber-fiber interactions, fibers can move in translation and rotation, with rotation being much more important (Mason, 1954). A fiber can sweep out a much larger volume, exceeding its own volume by a factor of r^2, where r is the fiber aspect ratio, thus rotational motion results in more collisions than translational motion.

Mason (1954) observed four classes of typical fiber rotational orbits in a shear field, namely, rigid (class I), springy (class II), "snake turn" or "loop turn" (class III), and complex

(class IV), as shown in Fig. 2.2, and related fiber rotational orbits to fiber flexibility. (Note, figures in this document can be found at the end of the respective chapter.) A rigid fiber will rotate in a shear field following the class I orbit. The fiber does not bend or change shape. Flexible fibers will rotate following Class II-IV orbits and are deformed by the shear field during the rotation. How a fiber shape is changed is a function of fiber flexibility and uniformity.

2.2.2 Fiber-fiber interactions in fiber suspensions

2.2.2.1 Crowding factor

Mason (1948) suggested that fiber-fiber interaction becomes important when the number of fibers in the sphere swept by a fiber is larger than 1. Kerekes *et al.* (1985) extended this idea and proposed a "crowding factor" to characterize fiber-fiber contact regimes. The crowding factor (N_c) is defined as the number of fibers inside a spherical volume with a diameter equal to the fiber length (Kerekes *et al.*, 1985; Kerekes and Schell, 1992). It reflects the level of inter-fiber contact and restraint of rotational motion, and hence, the tendency to form flocs in a fiber suspension (Kerekes and Schell, 1992). The crowding factor is calculated by (Kerekes and Schell, 1992):

$$N_c = \frac{2}{3} C_v \left(\frac{L}{d}\right)^2 \tag{2.4}$$

where L is the fiber length, d is the fiber diameter, and C_v is the volumetric fiber concentration ($0 \leq C_v \leq 1$).

For cellulose fiber suspensions, it is more convenient to estimate N from the mass concentration (Kerekes and Schell, 1992, 1995; Kerekes, 1996):

$$N_c \approx \frac{5}{\omega} C L^2 \tag{2.5}$$

where ω, in kg/m, is the fiber coarseness; C, in percent, is the fiber mass fraction ($0 \leq C \leq 100$); and L, in m, is the fiber length. Note Eq. (2.5) requires specific dimensions for the various parameters for the crowding factor to remain dimensionless.

The fiber length (L) is not clearly defined in Eqs. (2.4) and (2.5). Kerekes and Schell (1995) calculated crowding factors using length-weighted average fiber length (L_w). The used of L_w to estimate N_c for a polydisperse fiber suspension was later theoretically justified (Huber and Martinez, 2003) based on mass conservation.

The crowding factor is viewed as a dimensionless concentration which accounts for fiber morphology (Huber *et al.*, 2003) and has been proven to be useful to describe fiber flocculation (Kerekes and Schell, 1992; Kerekes, 1995; Huber *et al.*, 2003).

2.2.2.2 Fiber-fiber contacts

There are three broad fiber-fiber contact types in a fiber suspension, i.e., occasional collisions, forced collisions, and continuous contacts (Kerekes and Schell, 1992). These regimes can be characterized by the crowding factor (N_c). When $N_c < 1$, fibers are free to move, they occasionally collide through translation, temporarily remain together, and then completely disperse; as N_c increases, more collisions take place through translation and eventually through rotation; when N_c increases to ~60, which corresponds an average number of contacts per fiber of 3, fibers become restrained in rotation relative to one another through 3-point contacts and start to form a continuous network; when $N_c > 60$, the continuous network remains and is enhanced as N_c increases (Kerekes and Schell, 1992). Corresponding to the fiber-fiber contact types, fiber suspensions are classified into 3 regimes: dilute, semi-concentrated, and concentrated. The characteristics of the 3 regimes are summarized in Table 2.1 (Kerekes and Schell, 1992).

Table 2.1: Fiber suspension regimes and interfiber contact types (adopted from (Kerekes and Schell, 1992)).

Regimes	**Type of Fiber Contact**	**N_c**
Dilute	Chance Collision	$N_c < 1$
Semi-Concentrated	Forced Collision	$1 < N_c < 60$
Concentrated	Continuous Contact	$N_c > 60$

2.2.2.3 Inter-fiber forces

When fiber-fiber contact occurs, inter-fiber forces exist. Generally, there are 4 types of inter-fiber forces inside a fiber suspension (Kerekes *et al.*, 1985):

(i) Type A - Colloidal: These are electrostatic and electro-kinetic forces. They cause retention of small particles on the fiber surface.

(ii) Type B - Mechanical Surface Linkage: This is a hooking force. It is generated by mechanical entanglement of fibers having kinked or curled configurations and/or fibrillated surfaces.

(iii) Type C - Elastic Fiber Bending: This force results from friction resistance induced by normal forces at fiber-fiber contact points.

(iv) Type D - Surface Tension: This interfacial force is caused by bubbles of undissolved gas at fiber interstices.

The four force types are not always present in a fiber suspension, and some forces often have a dominating effect at a given condition. Mason (1954) reported that mechanical entanglement, which was later attributed to Type C force (Soszynski and Kerekes, 1988a), was the main factor and far more important than colloidal forces in fiber flocculation. Kerekes *et al.* (1985) summarized that types A, B, C forces all exist with type C force dominating when $0.3\% < C < 5\%$ and the domination of the type C force decreases with decreasing fiber mass fraction until $C = 0.3\%$, when the type C force ceases to exist.

2.2.2.4 Flocculation in fiber suspensions

When there are a sufficient number of fibers in a fiber suspension volume so that fiber-fiber contact is inevitable, the fiber suspension has a tendency to form regions where the fibers aggregate (i.e., flocculate). The state of flocculation relates to the degree of nonuniformity in a fiber suspension at a given moment of time (Soszynski and Kerekes, 1988a). Kerekes *et al.* (1985) reported that this could occur at fiber mass fractions as low as $C = 0.3\%$. Mason (1950) showed that collisions and subsequent entanglement of fibers resulted from shear motion of the suspending liquid were the primary factors influencing cellulose fiber flocculation. He named this type of fiber aggregation "mechanical"

flocculation and clearly separated it from "chemical" (i.e., colloidal) flocculation while recognizing the existence of both types of flocculation in fiber suspensions. Later Mason (1954) concluded that mechanical entanglement was the main factor and far more important than colloidal forces in fiber flocculation, even at a fiber mass fraction when flocculation just starts.

At the beginning of flocculation as fiber mass fraction increases, flocs continually form and disperse. The flocs are temporary and possess no network strength (Kerekes, 1983). As the fiber suspension becomes more concentrated, flocs appear to have sufficient strength to withstand rupture in the flow where they form. These type of fiber flocs are called "coherent flocs" (Soszynski and Kerekes, 1988a).

Meyer and Wahren (1964) proposed a concept of coherent floc formation. They wrote: "... when a fiber suspension is agitated, the fibers are exposed to viscous and dynamic forces, which bend and twist the fibers. When agitation ceases, the fibers tend to regain their original unstrained shape. However, if there are many fibers per unit volume, the fibers cannot straighten out freely but will come in contact with other fibers. A fraction of the fibers will come in contact with so many other fibers that they will come to rest in strained positions, and forces will be transmitted from fiber to fiber." Soszynski and Kerekes (1988b) reported coherent flocs formed due to local fiber crowding caused by flow deceleration when suspension concentration exceeds the "threshold concentration". Jacquelin (1972) developed a method to make mechanically entangled fiber aggregates of regular shape (e.g., spheroid) by applying continuous agitation of moderate intensity to concentrated suspensions. Soszynski and Kerekes (1988a) showed that the mechanical entanglement was due to interlocking by the elastic bending of fibers. They also reported that flocs having elastically interlocked fibers usually formed and persisted above a "threshold concentration", which was found to be a function of fiber aspect ratio (i.e., length to diameter ratio) and coarseness. The data were later generalized with the concept of the "crowding factor (N_c)" and were plotted into curves showing the condition at which coherent flocs form in a suspension, as shown in Fig. 2.1 (Kerekes and Schell, 1992). According to Fig. 2.1, coherent flocs first appear in the suspension when $60 < N_c < 130$.

Robertson and Mason (1954) showed that floc size could be affected by the turbulence intensity and the decay rate of turbulence in fully developed flows. It has also been shown that floc size depends on turbulent eddy size, and small eddies are required to create small fiber flocs (Kerekes, 1983). A difficulty in characterizing flocculation is that fiber floc sizes are not uniform. Research has shown that they have a lognormal size distribution (Hourani, 1988a, 1988b). Floc size also appears to be a characteristic of a given suspension, the minimum dominant size being one to two times of the longest fiber length (Kerekes *et al.*, 1985).

Dodson (1996) tried to estimate mean floc diameter(D) in a fiber suspension. He gave the following relationship:

$$D = (L/2)[1 + (n_c/3)] \tag{2.6}$$

where L is the fiber length and n_c is the contact number, which can be calculated from the volumetric concentration C_v and fiber aspect ratio r, with the following equation (Pan, 1993).

$$n_c = (4rC_v)/(2 + \pi C_v) \tag{2.7}$$

where $r = L/d$.

According to Eq. (2.6), fiber length has a very significant effect on floc size, not only influencing the contact number, but also affecting the floc diameter directly. When the fiber length increases, the floc diameter will increase, which is consistent with the experimental study of Kerekes and Schell (1995). It is also interesting to note, according to Eq. (2.6), that increasing fiber diameter will reduce floc size.

2.2.2.5 Floc rupture in fiber suspensions

It is important to point out that floc formation and rupture always exist at the same time. Mason (1954) observed that fiber flocs continually form and disperse and the two processes reached a "dynamic equilibrium," when the average floc size was determined by the shear level.

Steen (1989a) developed a fiber flocculation concept, where the flocculation process was described as a combination of floc aggregation and rupture processes. Flocculation in

turbulent flows results from the interaction between fibers and the "turbulent energy cascade" (i.e., the turbulent energy transfer from larger to smaller scales by vortex stretching). In turbulent fiber suspensions, the large-scale eddies contain local fiber networks or flocs, while the smallest vortices contain only single fibers or no fibers. Floc aggregation results from small-scale flocs being transported by large scale eddies, inside which small flocs collide and create larger ones. Floc rupture is a process whereby the larger flocs are broken up by the stretching of high energy turbulent eddies of the same scale as the floc. Floc break-up is possible if the deformation forces are larger than the flocs internal network strength. On a much smaller scale, dissipative eddies residing between the large eddies erode the outer surfaces of the flocs, making rupture of the flocs by large scale eddy stretching more probable. Because the two opposite processes occur simultaneously in a fiber suspension, an equilibrium floc scale exists for a given turbulence level. Based on the fiber flocculation concept, Steen (1991) modeled the flocculation process in a turbulent fiber suspension using a transport equation which includes source terms for both the rate of floc aggregation and rupture.

There are three fiber network rupture regimes: macro (inter-network) scale, micro (intra-network) scale, and fluidized state (Wikstrom *et al.*, 2002). At a low shear rate, the macro scale rupture dominates, and fiber networks breakup between flocs where the local fiber mass fraction is the lowest and the fiber network strength the weakest. As the shear rate increases, relative movement occurs within individual fiber flocs. This is the micro scale fiber network rupture. When the shear rate is increased to a certain level, the fiber network is completely dispersed. This state is denoted as "fluidized". A fluidized fiber suspension usually behaves as a Newtonian fluid (Gullichsen and Harkonen, 1981).

For a single cellulose fiber floc formed in a liquid, Lee and Brodkey (1987) proposed two floc dispersion mechanisms: (i) stochastic global-scale disruptions, including deformation, stretching, breaking, shedding, and fragmentation of the flocs; and (ii) local small-scale surface erosion, a rate process occurring over the entire floc surface, in which the surface fibers are washed away. The global-scale disruption is caused by turbulence with scales on the order of the floc size and a mean velocity gradient, with the latter being the major factor when the turbulent stress levels are small. The small-scale erosion process is

caused by turbulence of scales smaller than the floc size. The rate of floc size reduction is a function of the turbulence level and the floc size, which not only determines the total exposed surface area available for erosion, but also affects the relative fluid velocity. According to Lee and Brodkey (1987), to disperse a floc to the fiber level, local small-scale surface erosion must be present.

It has been shown that different flow conditions have different effects on fiber floc dispersion (Kerekes *et al.*, 1985). Kao and Mason (1975) found that irrotational shear flow was more effective in dispersing fiber aggregates than was rotational shear flow. Kerekes *et al.* (1985) recommended that turbulence having a high intensity and small scale could be used to rupture flocs in a suspension. The energy dissipation associated with this turbulence is related to the power dissipation. Various correlations are given in the literature to estimate the power dissipation required to fluidize fiber suspensions (Kerekes *et al.*, 1985; Bennington and Kerekes, 1996; Kerekes, 1996).

2.2.3 Liquid-fiber suspension flow

Forgacs *et al.* (1958) reviewed fiber suspension flow regimes. When the fiber mass fraction is very small (i.e., $C < 0.01\%$), fibers are isolated from one another, except for occasional collisions. Isolated fibers rotate in well-defined orbits (Fig. 2.2) and follow a preferential orientation in the direction of flow. As the fiber mass fraction gradually increases, fiber flocs start to form and a dynamic equilibrium exists between floc formation and rupture due to flow shear. When fiber mass fraction is increased to those commonly found in papermaking, e.g., 0.58%, three flow regimes, namely, laminar plug flow, mixed flow, and turbulent flow, are identified for fiber suspension flows in pipes. Figure 2.3 schematically represents these three flow regimes. Laminar plug flow occurs at very low velocities. This regime is characterized by the existence of a plug flow region in which no relative movement exists between the fibers, and the formation of a fiber-free water layer near the wall, whose thickness grows as the velocity is increased. In the fiber-free layer, water flows in a laminar manner. As the velocity increases, the flow in the fiber-free layer becomes unstable and a turbulent annulus forms outside the plug, causing disintegration of

the plug. Until the velocity is increased to a critical point when the plug is completely broken up, the flow is called mixed flow. After the breakdown of the plug, the flow is turbulent. In both the mixed and turbulent flow regimes, there is no fiber-free layer.

Xu and Aidun (2005) observed 5 types of cross-sectional velocity profiles (Fig. 2.4a) for fiber suspension flows in a rectangular channel and identified their corresponding regions in a fiber concentration (nl^3) versus Reynolds number (Re) plane (Fig. 2.4b). Type 1 velocity profile (Region 1 in Fig. 2.4b) is the same as that of single-phase Newtonian liquid turbulent flow. Type 2 velocity profile (Region 2 in Fig. 2.4b) is sharper than the first one and the velocity gradient becomes larger with increasing nl^3 and/or decreasing Re. As nl^3 increases and/or Re decreases, the velocity profile becomes blunter again in the Type 3 profile (Region 3 in Fig. 2.4b). Type 4 velocity profile (Region 4 in Fig. 2.4b) is similar to the mixed flow observed by Forgacs *et al.* (1958). Type 5 velocity profile (Region 5 in Fig. 2.4b) is typical for plug flow (Forgacs *et al.*, 1958): there is a central plug region of uniform velocity and a turbulent flow region between the plug boundary and the channel wall.

The friction pressure drop in a fiber suspension flow in a pipe is different from that of water pipe flow (TAPPI, 1985). Figure 2.5 shows the typical friction pressure loss versus bulk velocity curve for a fiber suspension pipe flow. Generally, the pressure loss increases with increasing velocity in the low velocity range and passes through a local maximum and minimum before entering a zone where the pressure loss continually increases with increasing velocity again. There is a drag reduction regime where the pressure loss is lower for a fiber suspension flow than for a water flow, providing other conditions are the same. From Fig. 2.5, it is also clear that the pressure loss increases with increasing fiber mass fraction at low velocities. In the drag reduction regime, the pressure loss at a higher fiber mass fraction can be lower than that at a lower fiber mass fraction.

2.2.4 Fiber suspension yield stress and viscosity

2.2.4.1 Yield stress

When coherent fiber networks form, they possess a certain level of tensile and shear strength (Meyer and Wahren, 1964; Kerekes *et al.*, 1985). Meyer and Wahren (1964)

attributed the fiber network strength to the fiber bending and entangling and the resulted friction forces. Because of the mechanical entanglement between fibers, for a given fiber suspension, a certain level of stress is required to cause relative motion in the suspension. The level of stress required to create relative motion among fibers in a fiber suspension is defined as the yield stress. It is an important parameter to characterize fiber network strength. With a yield stress, cellulose fiber suspensions have been described by Bingham plastic models (Chase *et al.*, 1989) or yield-pseudoplastic models (Duffy *et al.*, 1976; Myreen, 1989; Bennington *et al.*, 1990; Bennington *et al.*, 1995; Kerekes, 1996).

The yield stress of a fiber suspension was found to depend on fiber mass fraction, average fiber length, freeness (i.e., a property showing how fast water drains out from a fiber suspension), lignin content, fiber type, and amount of entrained gas (Chase *et al.*, 1989; Bennington *et al.*, 1990; Bennington *et al.*, 1995; Wikstrom and Rasmuson, 1998; Youn and Lee, 2002). Wikstrom and Rasmuson (1998) further concluded that the fiber length distribution had a greater effect on fiber network strength than the average fiber length.

Kerekes (1985) found that for cellulose fiber suspensions, the yield stress can be typically correlated with fiber mass fraction using equations of the form:

$$\tau_y = aC^b \tag{2.8}$$

with a and b being empirically derived coefficients. Kerekes (1996) gave some empirical correlations for common fiber suspension types. For example, yield stress of semi-bleached kraft (SBK) suspensions with $0.5 \leq C \leq 10\%$ was given as

$$\tau_y = 10.3C^{2.3} \tag{2.9}$$

where C is in percent and τ_y is in Pa.

Bennington *et al.* (1990) argued that the volumetric concentration C_v is more descriptive for fiber suspension composition when yield stress is concerned and derived a relationship showing that the yield stress is proportional to C_v^3, which agreed well with experimental results.

Assuming the gas phase is negligible and fibers are hollow cylinders, Wikstrom and Rasmuson (1998) derived a theoretical model for the yield stress of fiber suspensions which

accounts for a variety of fiber properties including fiber length (L), diameter (d), wall thickness (δ), coarseness (ω), elastic modulus (E), and water absorption

$$\tau_y = cE\left(\frac{L}{d}\right)^2\left[1-\left(\frac{d-2\delta}{d}\right)^4\right]C_v^3 \tag{2.10}$$

where c is an empirically determined coefficient and the volumetric concentration is calculated by

$$C_v = \frac{\pi d^2 \rho_w C}{4\omega\left[1+C\left(\frac{\rho_w}{\rho_f}-1\right)\right]} \tag{2.11}$$

where ρ_f is the fiber material density and ρ_w is the water density.

2.2.4.2 Apparent viscosity

When fibers are added to a liquid, the fiber suspension has a certain level of viscosity when the suspension is treated as a pseudofluid. The apparent viscosity of the fiber suspension is unusually different from that of the suspending liquid. Chase *et al.* (1989) showed that the viscosities of both hardwood and softwood fiber suspensions increase linearly with fiber mass fraction and generally decrease with fiber suspension freeness. Bennington and Kerekes (1996) proposed a correlation for the apparent viscosity μ_a of a fluidized SBK (softwood bleached kraft) fiber suspension:

$$\mu_a = 1.5\times10^{-3}C^{3.1} \quad (1\% < C < 12.6\%) \tag{2.12}$$

where μ_a is in Pa·s and C is in percent.

Based on extensive data using falling ball rheometry, Powell *et al.* (2001) obtained the following correlation for apparent viscosity of suspensions of randomly oriented non-flexible fibers covering a wide range of aspect ratios and concentrations.

$$\mu_{sp} = \begin{cases} 0.050(N_f L^3)^{1.00}, N_f L^3 < 50 \\ 4.5\times10^{-5}(N_f L^3)^{2.7}, N_f L^3 > 50 \end{cases} \tag{2.13}$$

where

$$\mu_{sp} = \frac{\mu_a}{\mu_s} - 1 \tag{2.14}$$

and μ_s is the suspending liquid viscosity; N_f is the fiber number density and L is the average fiber length.

2.2.5 Effects of fibers on liquid turbulence in fiber suspensions

Numerous fiber suspension flow studies have shown that the presence of fibers significantly suppress small-scale velocity fluctuations (Forgacs *et al.*, 1958; Norman *et al.*, 1978; Steen, 1989b; Andersson and Rasmuson, 2000; Xu and Aidun, 2005). Norman *et al.* (1978) suggested fibers damp turbulence intensity by supplying a force-bearing link between nearby fluid elements moving at different velocities, and thus suppressing the velocity difference. Increasing the fiber mass fraction, length, and flexibility resulted in a higher reduction in the turbulence intensity. Steen (1989b) showed that the turbulence structure in fiber suspension pipe flow was changed due to the presence of fibers, and the change was related to the crowding factor. For most situations, the turbulence intensity was reduced, primarily at small length scales. The turbulence intensity increased in the small length scales only when the crowding factor was small (e.g., $N_c \approx 3.6$), or when the crowding factor was in the medium range and the flow was in the wall region. The suppression of the small-scale components of the turbulence spectrum by fiber addition was also reported by Andersson and Rasmuson (2000) and Forgacs *et al.* (1958), who further concluded that the suppression was stronger at higher fiber mass fractions.

2.3 Gas-Liquid-Solid Flow in Bubble Columns

2.3.1 Flow regimes

Flow regimes are usually used to define the morphological arrangement of a gas phase moving through a liquid phase (Wallis, 1969). In a bubble column, properties such as the gas holdup (i.e., volumetric gas fraction), pressure drop, gas-liquid interfacial area, and heat and mass transfer are strongly dependent on the flow regime (Shah *et al.*, 1982).

Gas flow regimes have been identified based on visual observation or flow visualization (Chen *et al.*, 1994; Heindel, 2000; Xie *et al.*, 2003b), pressure fluctuation analysis (Drahos *et al.*, 1991; Letzel *et al.*, 1997; Lin *et al.*, 1999; Lin *et al.*, 2001; Xie *et al.*, 2003a), conductivity probe signal analysis (Barnea *et al.*, 1980; Zhang *et al.*, 1997), and application of the drift-flux model (Zahradnik *et al.*, 1997; Sarrafi *et al.*, 1999; Su and Heindel, 2003).

In gas-liquid or gas-liquid-solid bubble columns, three different flow regimes, including dispersed bubble, coalesced bubble, and slugging regimes are commonly observed (Fan, 1989). The slugging flow can only be observed in small diameter large aspect ratio bubble columns at high superficial gas velocities. The dispersed bubble regime is also called bubbly or homogeneous flow, while the coalesced bubble regime is also called churn-turbulent or heterogeneous flow. In the homogeneous regime, bubbles uniform in size are generated at the gas distributor and are dispersed homogeneously throughout the liquid phase. In the heterogeneous regime, bubbles generated at the gas distributor coalesce within a certain distance above the distributor and form large bubbles with large rise velocities, which follow vortical and spiral trajectories; some of them undergo coalescence and breakup, resulting in a wide bubble size distribution. Generally, the transition from homogeneous to heterogeneous flow occurs at a superficial gas velocity between 2 to 6 cm/s (Sarrafi, 1999). Ruzicka *et al.* (2001b) considered the homogeneous and heterogeneous flows as two basic flow regimes occurring in bubble columns and gave an excellent review of typical features in both regimes, as well as the conditions that produce such regimes.

Because gas flow regimes are a complex function of operational conditions, column geometry, gas distribution method, particle concentration and geometry, and liquid and gas phase properties, various results have been reported by different investigators. Chen *et al.* (1994) identified three flow regimes, namely, dispersed bubble, vortical-spiral, and turbulent flow regimes, in a three-phase bubble column. They emphasized that the commonly identified coalesced bubble or churn-turbulent flow regime should be subdivided into vortical-spiral flow and turbulent flow based on inherently different flow mechanisms and flow structures observed in their study. Using the bubble passing frequency, Sauter mean bubble chord length, and the time taken by a bubble to pass a given point, Zhang *et al.* (1997)

identified 7 regimes: namely, dispersed bubble flow, discrete bubble flow, coalesced bubble flow, slug flow, churn flow, bridge flow, and annular flow, in a 2 m high 82.6 mm diameter three-phase cocurrent bubble column with $0.0018 \leq U_g \leq 7.7$ m/s and $0 \leq U_l \leq 0.4$ m/s. Using visual observation, gamma-ray densitometry, and flash x-ray radiography, Xie *et al.* (2003b) recorded five distinct flow regimes in an air-water-cellulose fiber suspension, including dispersed bubbly, layered bubbly, (incipient plug and) plug, churn-turbulent, and slug flows, in a 2.80 m tall 5.1 cm diameter cocurrent bubble column. Using the Zuber-Findlay drift-flux model (Zuber and Findlay, 1965), the homogeneous and heterogeneous flow regimes were successfully identified based on a relationship between gas holdup and superficial gas velocity (Zahradnik *et al.*, 1997; Sarrafi *et al.*, 1999; Su and Heindel, 2003).

It is extremely difficult to predict gas flow regimes in a bubble column because the gas flow behavior is a complex function of column diameter, settled bed height, distributor type, particle geometry (size and shape), particle density and wettability, liquid phase surface tension, and operational pressure (Bejar *et al.*, 1992; Dudukovic *et al.*, 1999; Fan *et al.*, 1999). Bejar *et al.* (1992) developed a flow chart to distinguish the dispersed bubble flow from the coalesced bubble flow regimes in a three-phase fluidized fermenter with immobilizing particles. Zhang *et al.* (1997) summarized criteria represented by gas flow regime maps and empirical correlations for determining flow regime transitions in two-phase and three-phase bubble columns. Sarrafi *et al.* (1999) and Ruzicka *et al.* (2001b) proposed various models to predict conditions at which the flow transitions from the homogeneous to heterogeneous regime based on the Zuber-Findlay drift-flux model. Xie *et al.* (2003b) developed a flow regime map for a gas-liquid-fiber cocurrent bubble column based on flow visualization. Xie *et al.* (2003a) further proposed a method based on artificial neural networks (ANNs) to identify gas flow regimes in air-water-cellulose fiber systems using the statistical characteristics of pressure fluctuations measured by a single pressure sensor. Chaos analysis of the pressure fluctuation signals has also been shown to be very promising for characterizing gas flow regimes and predicting regime transitions (Drahos *et al.*, 1991; Letzel *et al.*, 1997; Lin *et al.*, 2001).

2.3.2 Flow structure in bubble columns

Three regions or zones can be identified in a bubble column: the entrance region, the bulk region, and the free surface region (Joshi *et al.*, 1986; Reese and Fan, 1994). The entrance region is the zone immediately above the distributor in which the gas-liquid flow develops, including the liquid velocity and gas holdup profiles. The bulk region consists of a significant portion of the bubble column, and thus, most of the research on bubble columns has focused on this region (Chen *et al.*, 1994; Lindsay *et al.*, 1995; Groen *et al.*, 1996; van den Akker, 1998). The free surface region exists in the upper part of the column and is characterized by a large radial component of the liquid velocity (Joshi *et al.*, 1986).

2.3.2.1 Entrance region

Reese and Fan (1994) studied the entrance region in a semi-batch bubble column and found that the length of the entrance region decreases with increasing superficial gas velocity. In the coalesced bubble regime, bubble coalescence occurs in the entrance region and the flow develops much faster. At high superficial gas velocities, the flow develops so fast that only a small area immediately above the gas distributor is required for the flow and coherent flow structures to develop. The length of the region does not change significantly with further increases in superficial gas velocity.

2.3.2.2 Bulk region

Fan and his group (Tzeng *et al.*, 1993; Chen *et al.*, 1994) described coherent flow structures in the bulk region of bubble columns. Dispersed bubble flow in the bulk region is characterized as homogeneous in the sense that bubbles of relatively uniform size rise rectilinearly along the column axis with insignificant coalescence and the liquid flows straight downward between the rising bubbles. In the vortical-spiral flow regime, the gross structure for gas-liquid and gas-liquid-solid bubble columns is divided into 4 distinct flow regions based on the local liquid flow characteristics and bubble dynamics, i.e., descending flow, vortical-spiral flow, fast bubble flow, and central plume regions (Fig. 2.6). The

descending flow region is adjacent to the wall and characterized by downward liquid and/or solid streams with few bubbles. Adjacent to the descending flow region is the vortical-spiral flow region, characterized by the existence of spiral-downward liquid and/or solid vortices, whose descending velocity is a function of superficial liquid and gas velocity. Good mixing is found in this region. The fast bubble flow region is located between the vortical-spiral flow region and the central plume region. It is characterized by clusters of bubbles or coalesced bubbles moving upward in a spiral manner with high velocity. Significant bubble coalescence and breakup occur in this region. This region prevents mass transfer for both liquid and solid phases between the central plume region and the vortical-spiral flow region. It is the dominant macroscopic flow structure when the vortical-spiral flow regime is established. The central plume region is located in the column center and is surrounded by the fast bubble flow regime; it is characterized by a relatively uniform bubble size distribution and less bubble-bubble interaction. This region is indistinguishable when the column diameter is small because it merges with the fast bubble region. In the turbulent flow regime, intense bubble coalescence causes large discrete bubbles to form with diameters of the order of the column diameter. These large bubbles are separated by a certain distance along the bubble column and suppress the spiral flow pattern in the central bubble stream. Liquid flow is induced and transported by the so called bubble wake mechanism (Tang and Fan, 1989; Tsuchiya *et al.*, 1992), with a pattern much more chaotic and dynamic than that in the vortical-spiral flow regime. The mixing between the bottom and top of the bubble column is not as rapid as that in the vortical-spiral flow regime.

2.3.2.3 Free surface region

In the free surface region, bubbles rise to the surface and burst, ejecting liquid jets and droplets (Boultonstone and Blake, 1993; Duchemin *et al.*, 2002). The disengagement of gas bubbles results in voids to be filled by liquid. When the superficial liquid velocity is small, but the superficial gas velocity is large, the voids are mainly filled by liquid backflow. The liquid backflow entrains small air bubbles and carries them downward along the bubble column. Bubble entrainment is especially significant when the liquid phase is a fiber

suspension, which can trap small bubbles when the fiber mass fraction is sufficiently large to form fiber networks (Pelton and Piette, 1992; Lindsay *et al.*, 1995; Ajersch and Pelton, 1999a).

2.3.3 Gas holdup in gas-liquid-solid bubble columns

Gas holdup is defined as the volume fraction occupied by the gas phase in the total volume of the two- or three-phase mixture in the bubble column. It is one of the most important parameters used to characterize bubble column hydrodynamics (Shah *et al.*, 1982). Gas holdup in two-phase systems provides information about the volumetric fractions of both phases present and thus their residence time. In addition, gas holdup together with knowledge of average bubble diameter allows calculation of gas-liquid interfacial area, which is important when identifying the gas-liquid mass transfer rate (Shah *et al.*, 1982).

Gas holdup in bubble columns depends on operational conditions (i.e., superficial liquid and gas velocity, pressure, and temperature), column geometry (column diameter and aspect ratio), gas distribution method (distributor type, hole number, open area ratio, etc.), liquid and gas phase properties, and, for gas-liquid-solid systems, particle density, concentration, and geometry (shape and size).

The relationship between gas holdup and superficial gas velocity is a function of flow regime (Zahradnik *et al.*, 1997). In homogeneous flow, gas holdup increases linearly with increasing superficial gas velocity. In heterogeneous flow, gas holdup also increases with superficial gas velocity, but with a smaller slope. In the transition from homogeneous to heterogeneous flow, gas holdup first increases before reaching a local maximum, then decreases until it reaches a local minimum, where the transition is considered completed (curve a in Fig. 2.7). Under some operating conditions, a local maximum and minimum may not be observed, but a transition is still observed by a change in slope (curve b in Fig. 2.7). Homogeneous flow may not appear even at very low superficial gas velocities under certain conditions, e.g., high solid concentration, large gas distributor holes, high liquid viscosity, etc. In this situation, pure heterogeneous flow appears (curve c in Fig. 2.7) and gas holdup increases monotonically with increasing superficial gas velocity (Zahradnik *et al.*, 1997).

Superficial liquid velocity can reduce the size of newly generated bubbles and inhibit bubble coalescence near the gas distributor, however, increasing superficial liquid velocity significantly decreases bubble residence time. Therefore, gas holdup usually decreases with increasing superficial liquid velocity, e.g., Xie *et al.* (2003b) reported gas holdup in a cocurrent air-water-fiber bubble column decreased with superficial liquid velocity in a range of 21 cm/s < U_l < 51 cm/s.

Luo *et al.* (1999) reported that gas holdup decreased with increasing solids concentration, especially at ambient pressure. However, the effect of solids concentration was smaller at elevated pressures and at superficial gas velocities above 25 cm/s. They also reported that gas holdup increased with increasing pressure and the pressure effects were more pronounced in higher concentration slurries. The increase in gas holdup with increasing pressure was also reported by Kemoun *et al.* (2001). Yang *et al.* (2000) reported that changing system temperature resulted in liquid viscosity changes, and thus, affected gas holdup.

Krishna and coworkers (Krishna and Ellenberger, 1996; Krishna *et al.*, 1997) divided the churn-turbulent flow in a bubble column into a "dense" phase and a "dilute" phase. The "dilute" phase was identified with the fast-rising "large" bubbles, while the "dense" phase was identified with the liquid phase and the entrained "small" bubbles. Accordingly, they split the total gas holdup into a dilute-phase portion and a dense-phase portion. It was found that the dense-phase portion was independent of the bubble column diameter, while the dilute-phase portion was significantly affected by the column diameter when $D \leq 0.38$ m (Krishna *et al.*, 1997). It was further shown that the bubble column diameter had a significant effect on the centerline liquid velocity and the axial liquid dispersion coefficient, when the diameter was up to 0.38 m (Krishna *et al.*, 1999b). However, Shah *et al.* (1982) noticed that gas holdup values obtained in a bubble column with a diameter larger than 0.15 m were sufficiently close to those obtained in larger diameter columns.

Camarasa *et al.* (1999) showed that gas distributor design can affect bubble size distribution and bubble frequency, and the influence of the distributor was enhanced in non-coalescing media. As a result, gas distribution methods can affect bubble column flow regimes, including whether homogeneous flow appears or not (Zahradnik *et al.*, 1997;

Camarasa *et al.*, 1999), as well as the flow regime transition. It was also shown that a different orientation of the gas sparger in a bubble column can cause a significant change in gas holdup in an air-water cocurrent bubble column (Tang and Heindel, 2004b). Additional studies on the effect of gas distributor on gas holdup and bubble column hydrodynamics appear in the literature (Park *et al.*, 1977; Miyahara *et al.*, 1983; Tsuchiya and Nakanishi, 1992; Krishna and Ellenberger, 1996; Ruzicka *et al.*, 1999; Terasaka *et al.*, 1999; Lee *et al.*, 2001).

Gas and solid densities were also reported to have effects on gas holdup and bubble column hydrodynamics. Bly and Worden (1992) reported that bubble rise velocities decrease with increasing solids fraction and density. Larachi *et al.* (1994) presented that an increase in gas density resulted in an increase in the two-phase pressure drop and gas holdup at a given superficial fluid velocity.

Surfactants in the liquid phase can significantly change the surface tension, and thus, gas holdup and bubble column hydrodynamics (Kelkar *et al.*, 1983; Gorowara and Fan, 1990; Zahradnik *et al.*, 1997; Janse *et al.*, 1999; Kluytmans *et al.*, 2001). Unknown trace surfactants have also been found to be a source of experimental error (Tang and Heindel, 2004b).

2.4 Gas-Liquid-Fiber Flows in Bubble Columns

2.4.1 Flow regimes

Using a 10.2 diameter cylindrical semi-batch bubble column filled with a fiber suspension, Reese *et al.* (1996) found that the discrete bubble regime and the vortical-spiral flow regime could still be identified when the fiber mass fraction was low ($C \leq 0.5\%$), while only turbulent flow was recorded at high fiber mass fractions ($C > 0.5\%$). Some fiber buildup at the bottom of the column was also observed when $C > 0.5\%$.

In a 1 m tall 2-D semi-batch bubble column with a rectangular cross-section of 20 cm × 2 cm, Heindel (2000) observed vortical, churn-turbulent, surge churn-turbulent, and discrete channel flow as the fiber mass fraction increased from 0% to 5% with a fixed superficial gas velocity of 0.83 cm/s.

In a 1% fiber slurry semi-batch bubble column, Lindsay *et al.* (1995) observed that the regime transition between bubbly flow and churn-turbulent flow was similar to the features observed in water. However, the presence of fiber promoted the transition to churn-turbulent flow, which occurred at a much lower superficial gas velocity when compared to a similar air-water system. At higher fiber mass fractions, channeling was observed. They also showed that flow regimes in a cocurrent bubble column filled with a fiber suspension resembled those of the semi-batch bubble column.

Walmsley (1992) reported that as fiber mass fraction increased, the transition from bubbly flow to turbulent flow became less apparent. Superficial gas velocity and fiber mass fraction clearly affected the observed flow regimes in a bubble column filled with a fiber suspension. It was also shown that the column aspect ratio (the liquid height to diameter ratio) affected the transition point from bubbly flow to churn-turbulent flow for an air-water system, with the transition occurring at lower superficial gas velocity when the aspect ratio increased. However, the aspect ratio had no effect on the transition when fiber was added to the column.

In a 1.80 m tall 5.1 cm diameter cocurrent bubble column, Xie *et al.* (2003b) recorded five distinct flow regimes in an air-water-cellulose fiber suspension, including dispersed bubbly, layered bubbly, (incipient plug and) plug, churn-turbulent, and slug flows. The superficial gas velocity at which flow regime transitioned decreased with fiber addition. Similar results for a 2-D semi-batch bubble column were observed by Heindel and Monefeldt (1998). Based on visual observation, Xie *et al.* (2003b) produced a flow regime map which identified the range of superficial gas and liquid velocities for each regime. Later, Xie *et al.* (2003a) proposed an objective method based on artificial neural networks to identify gas flow regimes in gas-liquid-fiber bubble columns using fluctuations of the pressure signal.

2.4.2 Bubble motion in fiber suspensions

Pelton and Piette (1992) pointed out that the main mechanism for bubble holdup in a fiber suspension was the mechanical entrapment of bubbles in fiber networks. Two criteria for bubble holdup were determined: (i) sufficient fiber-fiber contact points to prevent a

bubble from rolling off or around the fiber network, and (ii) the network must be strong enough to sustain the buoyant force exerted by the bubble.

Reese *et al.* (1996) observed that bubble behavior in a fiber suspension was established at the lower part of a bubble column and the bubble behavior remained constant throughout the column. Bubbles in the fiber suspension were flatter than in pure water and the bubbles at the bottom of the column were also flatter than those near the top. They also observed that the bubble rise velocity decreased with increasing fiber mass fraction. It was proposed that bubble coalescence increased in the fiber suspension because the flatter bubbles rose slower in the lower part of the column and lead to an increase in bubble-bubble interactions.

Walmsley (1992) reported that adding only 0.1% cellulose fiber to water could significantly change bubble behavior. Fibers act as barriers to bubble rise with some bubbles rising and getting trapped beneath fiber networks and others rising upward between fiber flocs (in regions of locally low fiber mass fraction). The trapped bubbles remain at the locations where they get trapped, while other rising bubbles may catch the trapped bubbles and coalesce with them. Once the size of the trapped bubble increases to a critical diameter where the buoyancy force is sufficient to cleave the fiber network, the trapped bubble breaks the network and rises upward. Network rupture by the large bubble may open a path for many small bubbles to follow, creating bubble rise channels (termed channeling). Walmsley (1992) observed that when the fiber mass fraction was greater than 1.4%, continuous channels of fast rising bubbles appear.

Ajersch and Pelton (1999a) summarized 4 mechanisms by which bubbles escape from a fiber network (Fig. 2.8):

(i) Bubbles may escape a fiber floc by slipping through the void space between individual fibers. The bubble diameter must be less than the smallest void space between the fibers for this to occur.

(ii) Bubbles may escape by disrupting the fiber network and provide aid in the release of other trapped bubbles. The probability of floc disruption depends on both the bubble buoyant force (and thus bubble size) and the network strength

of the floc, which depends on the fiber physical properties and mass fraction of the suspension.

(iii) Under turbulent flow conditions, flocs can disperse by deformation, stretching, breaking, and fragmentation due to local shear forces (Lee and Brodkey, 1987). Hence, bubbles may escape during these actions.

(iv) Translational motion of the flocs resulting from large scale turbulence can cause velocity gradients between flocs and the surrounding fluid (Lee and Brodkey, 1987), resulting in local shear forces that act at the bubble-floc interface and therefore, may cause bubble detachment from under a floc.

2.4.3 Bubble size distribution in gas-liquid-fiber flows

Bubble size and its distribution are very influential to gas holdup in a cellulose slurry bubble column. Small bubbles have a small buoyant force and low rise velocity, and can be more easily trapped inside a fiber suspension. Large bubbles have a high velocity and a large buoyant force, so they easily break through the fiber network. Furthermore, large bubbles have large wakes that can trap many small bubbles, making them rise faster, and enhance coalescence between bubbles. Lee *et al.* (1999) showed 70% of the small bubbles were entrained in large bubble wakes and had a velocity close to that of the large bubbles in churn-turbulent flow.

Bubble size can be modified in one of three ways: (i) by bubble coalescence, i.e., small bubbles coalesce into large bubbles; (ii) by bubble breakup, i.e., large bubbles are broken into small bubbles; and (iii) bubble size increase due to hydrostatic pressure decrease as the bubbles rise from the bottom of the bubble column to the top. It is believed that bubble coalescence and breakup are the main reasons for the change in bubble size (Clift *et al.*, 1978; Walter and Blanch, 1986; Hesketh *et al.*, 1991; Risso, 2000; Tse *et al.*, 2003). The third mechanism is usually insignificant because the pressure difference between the column bottom and top is typically very small compared with the ambient pressure.

Various investigations have been completed on bubble size in gas-liquid-fiber systems. Reese *et al.* (1996) reported that larger bubbles were observed at higher fiber mass

fractions. With flash X-ray radiography, Heindel measured bubble size in a semi-batch bubble column (Heindel, 1999; Heindel and Garner, 1999) and a cocurrent bubble column (Heindel, 2002) in which both bubble columns were filled with fiber suspensions at various mass fractions. In both the semi-batch and cocurrent bubble columns, it was found that the bubble size varied with fiber mass fraction. The number of small bubbles decreased and number of large bubbles increased as the fiber mass fraction increased. It was also observed that when $C \leq 1.5\%$, the bubble size could be described by a lognormal distribution. In the cocurrent bubble column, when $C = 1.5\%$, there was a significant change in the hydrodynamic behavior of the slurry; however, the small bubbles were still characterized by a lognormal distribution. In the semi-batch bubble column, it was also found that gas injection methods could significantly affect bubble size. Janse *et al.* (1999) pointed out that surface-active agents typically found in industrial-scale fiber suspensions had a significant effect on bubble size, affecting bubble rise velocity and gas holdup in a bubble column.

Fiber type has a small effect on bubble size. Garner and Heindel (2000) observed the number of large bubbles increased with increasing fiber length while the number of small bubbles decreased when flow regime was churn-turbulent. The small bubble size distribution could be characterized by a lognormal distribution and was independent of fiber type. Heindel (2002) found that bubbles generated in an old newsprint (ONP) fiber slurry were slightly smaller than those in a copy paper (CP) fiber slurry with all else being equal. However, the mechanism was not revealed by which the fiber types influenced the bubble size. Heindel and Omberg (2001) found that synthetic (Rayon) fiber length had a negligible effect on bubble size. As inferred by Janse *et al.* (1999), it appears that chemical agents found in different types of natural fibers, i.e., ONP or CP, affect the bubble size.

2.4.4 Gas holdup in gas-liquid-fiber bubble columns

In the past decade, gas holdup in gas-liquid-fiber systems has been studied in both semi-batch (Walmsley, 1992; Went *et al.*, 1993; Lindsay *et al.*, 1995; Reese *et al.*, 1996; Janse *et al.*, 1999; Su and Heindel, 2003; Su and Heindel, 2004b, 2004a) and cocurrent (Lindsay *et al.*, 1995; Schulz and Heindel, 2000; Xie *et al.*, 2003b; Tang and Heindel, 2004a,

2005c) bubble columns. Effects of superficial gas and liquid velocity, fiber mass fraction, and gas distribution method on gas holdup were extensively studied in these investigations. Effect of fiber type on gas holdup in semi-batch gas-liquid-fiber bubble columns was also investigated (Walmsley, 1992; Su and Heindel, 2003, 2004a). Local (axial and radial) gas holdup variation was also reported (Lindsay *et al.*, 1995; Schulz and Heindel, 2000; Hol and Heindel, 2005).

2.4.4.1 Effect of superficial gas velocity

It was shown that gas holdup increased with increasing superficial gas velocity both in semi-batch (Lindsay *et al.*, 1995; Janse *et al.*, 1999) and in cocurrent (Lindsay *et al.*, 1995; Schulz and Heindel, 2000; Xie *et al.*, 2003b) bubble columns filled with cellulose fiber suspensions. However, the influence of superficial gas velocity is more complex, as observed by Su and Heindel (2003), where increasing superficial gas velocity resulted in a local maximum gas holdup in a semi-batch air-water-synthetic fiber bubble column.

Schulz and Heindel (2000) also investigated the effects of superficial gas velocity on the cross-sectional average gas holdup as a function of column height. The study showed that the higher the superficial gas velocity, the larger was the increase in cross-sectional average gas holdup with position. Their study also showed that the superficial gas velocity affected the radial gas holdup distribution, with a parabolic chord-average gas holdup distribution flattening out at lower superficial gas velocities.

2.4.4.2 Effect of superficial liquid velocity

Lindsay *et al.* (1995) found that for pure water, superficial liquid velocity had a very small effect on gas holdup; but for a fiber suspension with a certain fiber mass fraction, the gas holdup was higher than that of water at the same flow conditions. Two explanations for this observation were proposed: (i) there was a small amount of trapped gas in the fiber network, i.e., extrapolating the linear change in gas holdup to a zero superficial gas velocity resulted in a non-zero gas holdup; and (ii) the up-flowing liquid prevented bubbles from coalescing with neighboring bubbles. The first reason is reasonable but cannot account for all

the change. The second reason is better justified by Lindsay *et al.* (1995) and has also been cited in other gas-liquid-solid cocurrent flows (Mitra-Majumdar *et al.*, 1998). Janse *et al.* (1999) also reported that when the superficial liquid velocity increased, gas holdup increased, but this column was a counter-current flow column, where the liquid flowed downward in the column.

Schulz and Heindel (2000) showed that in the lower part of the column the cross-sectional average gas holdup increased with increasing superficial liquid velocity. This was attributed to the fast flowing fluid removing bubbles from the injector port at a faster rate, keeping the bubbles small and well dispersed while increasing the amount of backmixing. However, this trend was not apparent in the upper column region, with the cross-sectional average gas holdup changing in a complicated way with increasing superficial liquid velocity and fiber mass fraction.

Recently, using a 5.08 cm ID cocurrent bubble column, Xie *et al.* (2003b) showed that gas holdup significantly decreased with increasing superficial liquid velocity in a range of 21 cm/s < U_l < 51 cm/s.

2.4.4.3 Effect of fiber mass fraction

Most studies on semi-batch bubble columns filled with fiber suspensions (Went *et al.*, 1993; Lindsay *et al.*, 1995; Reese *et al.*, 1996) showed that adding a very small amount of fiber in a bubble column reduced the overall gas holdup due to enhanced bubble coalescence by the added fiber. The studies also showed that the decrease in gas holdup with increasing fiber mass fraction diminished when the fiber mass fraction reached a certain value. Went *et al.* (1993) reported that the gas holdup remained constant when the fiber mass fraction was varied from 1% to 1.5%. This was attributed to the formation of a large, low porosity fiber agglomeration at the bottom of the column. However, Walmsley (1992) reported that the addition of a small mass fraction of chemical pulp into an air-water system could cause up to a 40% rise in gas holdup and additional fiber addition reduced the gas holdup to less than that of an air-water system under the same flow conditions. Walmsley (1992) also reported that the addition of a mechanical pulp continuously reduced gas holdup. Using a counter-current

flow bubble column, Janse *et al.* (1999) also showed the overall gas holdup decreased with increasing fiber mass fraction.

Studies using cocurrent bubble columns filled with a fiber suspension (Lindsay *et al.*, 1995; Schulz and Heindel, 2000) showed quite different and more complex effects of fiber mass fraction on gas holdup. Lindsay *et al.* (1995) reported that when the column was filled with a fiber suspension with a certain fiber mass fraction, the gas holdup was higher than that of an air-water system under the same flow conditions. Schulz and Heindel (2000) showed that the column-average gas holdup was highest at C = 0.8% and lowest at C = 1.2% when all other conditions were constant. They proposed that there was an optimal fiber mass fraction where the gas holdup reached a maximum for a given combination of superficial gas and liquid velocity. However, they only used mass fractions of 0, 0.8 and 1.2% in their study. Similar complex effects of fiber mass fraction on gas holdup was also observed by Xie *et al.* (2003b), who reported that the effect of fiber mass fraction on gas holdup was opposite at two different superficial liquid velocities (U_l = 32 cm/s or 51 cm/s).

There are very few reports about the increase in gas holdup with fiber mass fraction in a bubble column and the phenomenon is far from understood. Further work must to be completed in order to identify the interactions between fiber mass fraction and superficial gas and liquid velocities.

2.4.4.4 Effect of fiber type

For different fiber types, the geometric characteristics and mechanical properties, as well as chemical contaminants existing on or in the fibers, can be quite different. Fiber geometric characteristics and mechanical properties affect formation, strength, and dispersion of fiber flocs. This directly influences bubble-fiber network interaction, which is critical to the gas holdup in a bubble column filled with the fiber suspension. The resident chemicals on/in the fibers affect liquid-phase physical properties and influence bubble formation, growth, coalescence, breakup, and movement, and hence gas holdup.

Walmsley (1992) reported significant differences between gas holdup in suspensions of chemically and mechanically pulped fibers under similar operation conditions. In his

research, the addition of a very small mass fraction of chemically pulped fiber into an air-water bubble column increased the overall gas holdup level by up to 40%, while the addition of a mechanically pulped fiber only reduced the gas holdup. Walmsley (1992) attributed the difference to the fiber length.

Su and Heindel (2003; 2004a) reported that gas holdup in a 15.24 cm ID semi-batch air-water-Rayon fiber bubble column decreased with increasing fiber length (3, 6, and 12 mm) when fiber mass fraction was less than 1.4%, and the fiber length effect was negligible when fiber mass fraction was higher than 1.4%.

However, there are many other possibilities like different chemical agents in the fibers, different aspect ratios, or different mechanical properties, etc. This is an area that requires further study.

2.4.4.5 Local gas holdup distribution

In homogeneous flow, gas holdup is considered homogeneous in a bubble column. However, in most situations, gas holdup in a bubble column is not uniform in the axial or radial direction.

In both semi-batch (Lindsay *et al.*, 1995) and cocurrent (Lindsay *et al.*, 1995; Schulz and Heindel, 2000) bubble columns, the cross-sectional average gas holdup was reported to increase with vertical distance from the column bottom. The increase was attributed to fiber suspension recirculation downward to the column bottom (Lindsay *et al.*, 1995). Schulz and Heindel (2000) also observed that the increase in the cross-sectional average gas holdup with position was strengthened when the superficial gas velocity was above 2.0 cm/s.

The radial gas holdup distribution was also studied. Lindsay *et al.* (1995) and Schulz and Heindel (2000) reported that the radial distribution of the chord-average gas holdup was parabolic, with the maximum chord average gas holdup near the column center and gas holdup decreased with increasing offset distance from the column center. This was attributed to wall effects and back mixing near the column wall.

2.5 Gas Holdup Models in Bubble Columns

2.5.1 Slip velocity model

Slip velocity has been shown to be a fundamental parameter in bubble column flows (Lapidus and Elgin, 1957) and is widely used in modeling bubbly flow conditions in gas-liquid systems (Shah *et al.*, 1982; Joshi *et al.*, 1990; Krishna *et al.*, 1993; Zahradnik *et al.*, 1997; Sarrafi *et al.*, 1999). For cocurrent flow, the slip velocity U_s is defined as the vertical component of the relative velocity between the bubbles and the liquid (Lapidus and Elgin, 1957),

$$U_s = \frac{U_g}{\varepsilon} - \frac{U_l}{1-\varepsilon} \tag{2.15}$$

where U_g and U_l are the superficial gas and liquid velocities, respectively, while ε is the gas holdup. U_s is a characterizing parameter of bubble columns and is only a function of the terminal bubble rise velocity $U_{b\infty}$ and the gas holdup (Lapidus and Elgin, 1957; Zahradnik *et al.*, 1997),

$$U_s = U_{b\infty} F(\varepsilon) \tag{2.16}$$

where $F(\varepsilon)$ is a function that represents the influence of the interactions between neighboring bubbles. It generally has a form of

$$F(\varepsilon) = (1-\varepsilon)^{n-1} \tag{2.17}$$

with n varying in different investigations from –1 to +3. Excellent summaries on $F(\varepsilon)$ can be found in the literature (Shah *et al.*, 1982; Zahradnik *et al.*, 1997; Sarrafi *et al.*, 1999).

The terminal bubble rise velocity $U_{b\infty}$ is defined as the velocity at which a bubble rises in a boundless volume of liquid. It is only a function of bubble size and gas and liquid phase properties, and it can be evaluated with the generalized equation proposed by Jamialahmadi *et al.* (1994). With the information of terminal bubble rise velocity and Eqs. (2.15) - (2.17), the gas holdup can be predicted given the superficial gas and liquid velocities.

2.5.2 Drift-flux model

The gas drift-flux (j_{gl}) was defined by Wallis (1969) as the volumetric flux of gas relative to a surface moving at a velocity equal to the total of the superficial gas and liquid velocity. It is analogous to the diffusion flux in the molecular diffusion of gases and provides a convenient way of modifying homogeneous theory to account for the relative motion (Wallis, 1969). The concept of drift-flux is very important since all the properties of a gas-liquid flow, such as gas holdup, average density, and momentum flux, can be expressed as the homogeneous flow values together with a correction factor or an additional term that is a function of the ratios of the drift flux to the component flux (Wallis, 1969). For a cocurrent gas-liquid flow, it was derived that (Wallis, 1969)

$$j_{gl} = U_s \varepsilon (1-\varepsilon) \tag{2.18}$$

or

$$j_{gl} = U_g (1-\varepsilon) - U_l \varepsilon \tag{2.19}$$

The drift-flux model is essentially a separated-flow model in which attention is focused on the relative motion rather than on the motion of the individual phases (Wallis, 1969). It is based on the assumption that the mean void fraction occurring in two-phase gas-liquid flows can be attributed to two different phenomena: (i) the radial gas holdup and velocity distribution caused by transverse forces, and (ii) the relative velocity between the phases, due to density differences. The effects of those two contributions are then taken into account by two parameters: the distribution parameter and the gas holdup weighted mean drift velocity (Clark *et al.*, 1990; Guet *et al.*, 2004). In derivation of the drift-flux model, the compressibility of each phase is neglected and the density of each phase within any cross-sectional area is considered to be uniform since for most practical two-phase flows, the transverse pressure gradient within a channel is relatively small (Ishii, 1977). The drift-flux model is an approximate formulation in comparison with the more rigorous two-fluid formulation; however, because of its simplicity and applicability to a wide range of two-phase-flow problems of practical interests, the drift-flux model is of considerable importance (Hibiki and Ishii, 2002).

For heterogeneous flow, the Zuber and Findlay (1965) drift-flux theory is widely recommended for modeling gas holdup in bubble columns (Shah *et al.*, 1982; Zahradnik *et*

al., 1997; Ruzicka *et al.*, 2001b; Xie *et al.*, 2003b). It accounts for the radial flow non-uniformity and gas holdup distribution typically found in the heterogeneous flow. For cocurrent flow, Eq. (2.19) can be written as

$$\frac{U_g}{\varepsilon} = (U_g + U_l) + \frac{j_{gl}}{\varepsilon} \tag{2.20a}$$

or

$$U_g = (U_g + U_l)\varepsilon + j_{gl} \tag{2.20b}$$

By averaging Eq. (2.20b) over the bubble column cross-section and dividing by the average gas holdup $<\varepsilon>$, the following can be obtained:

$$\frac{<U_g>}{<\varepsilon>} = C_l <U_g + U_l> + \frac{<j_{gl}>}{<\varepsilon>} \tag{2.21}$$

where $<>$ indicates averaging over the cross section and

$$C_l = \frac{<\varepsilon(U_g + U_l)>}{<\varepsilon><U_g + U_l>} \tag{2.22}$$

is a coefficient that gauges the radial non-uniformity of the flow. Since all values in the present study are averaged, the $<>$ nomenclature will be omitted in the following descriptions.

According to Eq. (2.18),

$$\frac{j_{gl}}{\varepsilon} = U_s(1-\varepsilon) \tag{2.23}$$

It was shown that the slip velocity U_s was approximately constant within the same flow regime (Nicklin, 1962; Ueyama and Miyauchi, 1979). It is reasonable to assume the weighted average drift velocity (j_{gl}/ε) is constant without resulting in significant error because the change of gas holdup in bubble columns is typically small compared to (1- ε) (since $\varepsilon < 0.25$ in most situations) when the superficial gas and liquid velocities are changed within a given flow regime (Clark *et al.*, 1990). In practice, j_{gl}/ε is usually assumed to be the terminal bubble rise velocity ($U_{b\infty}$) in an infinite medium (Clark *et al.*, 1990). Hence, Eq. (2.21) becomes

$$\frac{U_g}{\varepsilon} = C_0(U_g + U_l) + B_0 \tag{2.24}$$

where the slope C_0 and intercept B_0 can be obtained by plotting U_g/ε versus (U_g+U_l). C_0 and B_0 are generally functions of liquid phase properties (Chhabra *et al.*, 1984). For a given bubble column flow regime, the slope C_0 is constant. A change in C_0 corresponds to a flow regime transition. Kara *et al.* (1982) modified the Zuber-Findlay theory slightly to use it to model gas holdup in gas-liquid-solid three phase slurries. Once the parameters C_0 and B_0 are determined, the gas holdup can be estimated with Eq. (2.24) giving knowledge of U_g and U_l. Note that the drift-flux model is better suited for less viscous, water-like fluids and fails in highly viscous fluids (Kelkar *et al.*, 1984).

2.5.3 Other gas holdup models

There are various gas holdup correlations proposed in literature and they are well reviewed by Shah *et al.* (1982), Fan (1989), and Deckwer (1992). These correlations are typically for specific bubble column geometries, operating conditions, and liquid and solid media. They show large scatter and a single general correlation is not available in the open literature.

2.5.4 Gas holdup model for gas-liquid-fiber bubble columns

Although gas holdup correlations are numerous for gas-liquid-solid (GLS) bubble columns, correlations for gas holdup in gas-liquid-fiber (GLF) system are scarce. Only a few correlations based on limited data can be found in literature (Walmsley, 1992; Xie *et al.*, 2003b). Walmsley (1992) reported that the gas holdup in a semi-batch bubble column filled with eucalyptus fiber was independent of fiber mass fraction C and was related to superficial gas velocity with the following equation:

$$\varepsilon = 0.016U_g^{0.8} \tag{2.25}$$

when fiber mass fraction was in the range of $1.0 \leq C \leq 4.0\%$.

Recently, Xie *et al.* (2003b) showed that the drift-flux model, i.e., Eq. (2.24), could be successfully used to model gas holdup in a GLF bubble column, assuming that the liquid-fiber suspension was a psuedofluid. The coefficients B_0 and C_0 were shown to be a function

of flow regime and fiber mass fraction. C_0 approached unity as the fiber mass fraction increased, indicating a higher fiber mass fraction results in a flatter radial gas holdup profile. B_0 was a complex function of fiber mass fraction due to the two opposing effects: (i) a higher fiber mass fraction means a stronger fiber network to trap bubbles and thus a smaller B_0, and (ii), a higher C results in larger bubbles due to enhanced bubble coalescence and thus tends to increase B_0.

In this study, initial work to be done will determine how well the gas flow in a fiber suspension follows the drift-flux model; then a gas holdup model based on the drift-flux model, if it is applicable, will be developed which accounts for not only the operational conditions, but the fiber suspension and fiber properties.

2.6 Summary

A literature review has been conducted on cellulose fiber properties, liquid-fiber suspension properties and flow behaviors, gas-liquid-solid and gas-liquid-fiber flows in bubble columns, and previous research on gas holdup modeling in bubble columns. The review shows that gas-liquid-fiber flows have different characteristics from conventional gas-liquid-solid flows because of the unique fiber suspension behaviors mainly resulting from fiber flocculation. There are many investigations on the hydrodynamics and gas holdup in gas-liquid, gas-liquid-solid, and gas-liquid-fiber bubble columns, especially those operated in a semi-batch mode. These study showed that the hydrodynamics and gas holdup in bubble columns are affected by many factors including operating conditions, bubble column geometry, gas distributor design, and gas, liquid, and solid physical properties. Although the influences of such factors on gas holdup in gas-liquid and gas-iquid-solid bubble columns were systematically studied and gas holdup models were developed to correlate the gas holdup with important influencing factors, no systematic investigation has been done on the influeces of operating consitions (superficial gas and liquid velocity and fiber mass fraction) and fiber physical properties (e.g., fiber length, diameter, coarseness, and flexibility) on hydrydynamics and gas holdup in gas-liquid-fiber bubble columns. No gas holdup model

based on systematic data acquisition, which is very important for relating industrial process design and control, has been developed.

In this study, an experimetnal study will be completed to quatitatively examine the influeces of operating consitions and fiber physical properties on hydrydynamics and gas holdup in a cocurrent gas-liquid-fiber bubble column. Based on large amount of data systematically aquired in this study, a gas holdup model will be developed to correlate the gas holdup with the operating consitions and fiber physical properties for the cocurrent gas-liquid-fiber bubble column.

Figure 2.1: The condition at which nylon fibers formed coherent flocs in a suspension in a rotating, inclined cylinder (adopted from Soszynski and Kerekes (1988a)).

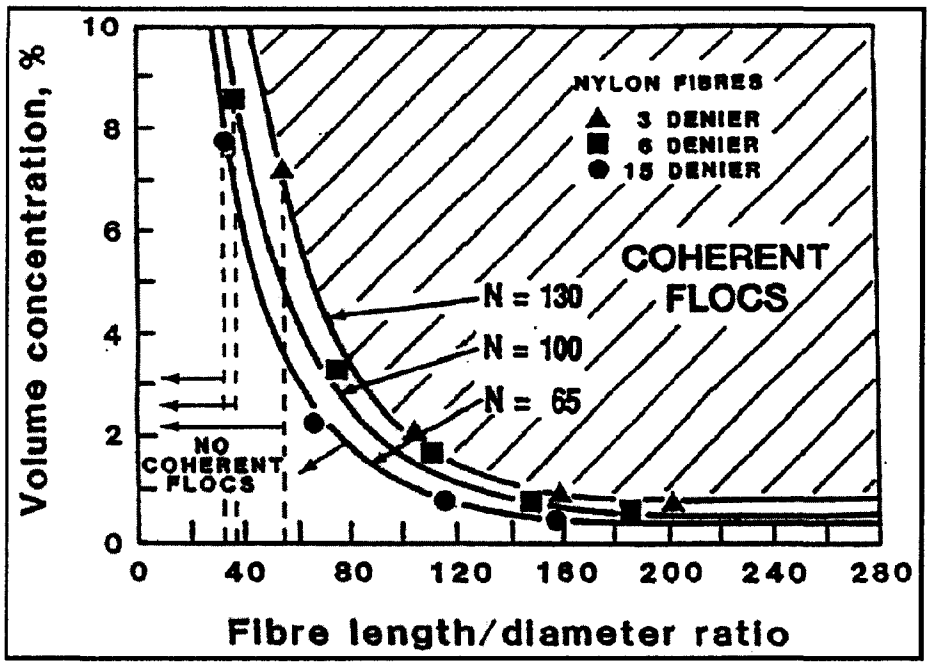

Figure 2.2: Typical rotational orbits of fibers in the X-Y plane (adopted from Forgacs *et al.* (1958)).

(Note: the relation between the coordinate system and the shear field is shown in the top left of the figure; Classes I-IV are in increasing order of flexibility.)

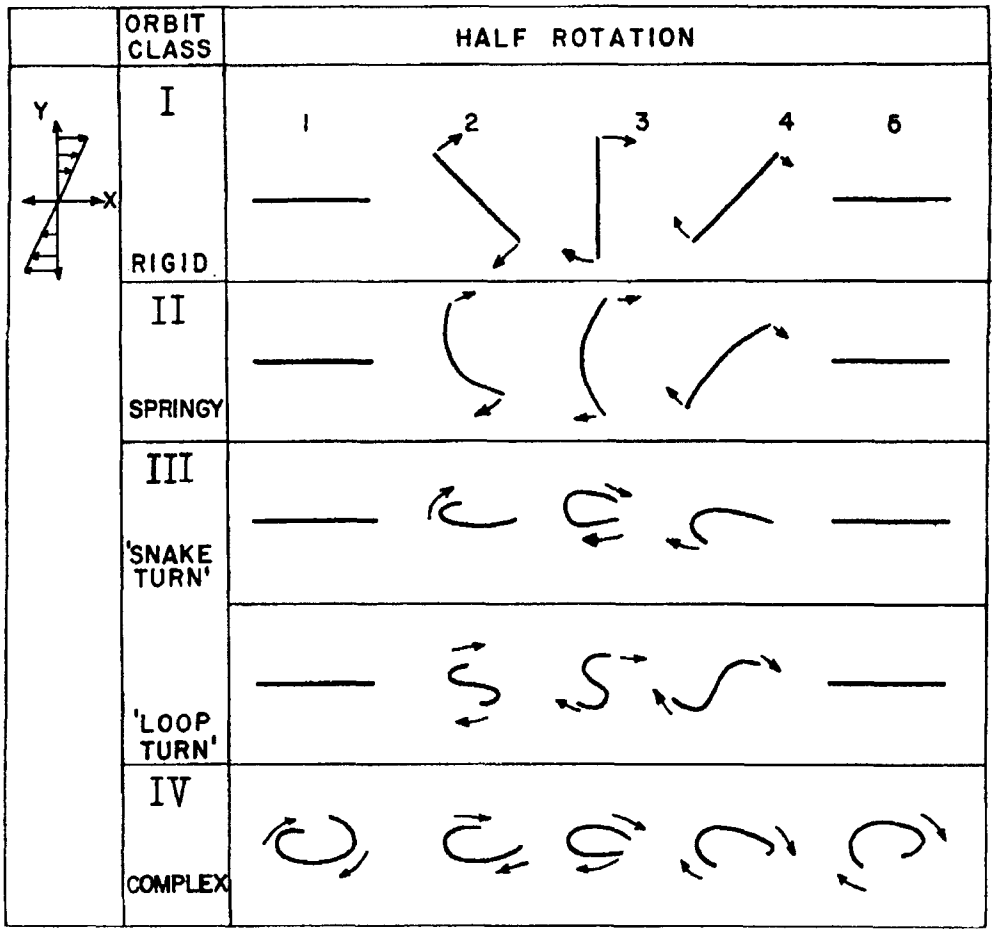

Figure 2.3: Schematic drawings of the three fiber suspension flow regimes (adopted from Forgacs *et al.* (1958)).
(Note the orientation of fibers near the wall in plug flow and the persistence of the plug in the mixed flow region.)

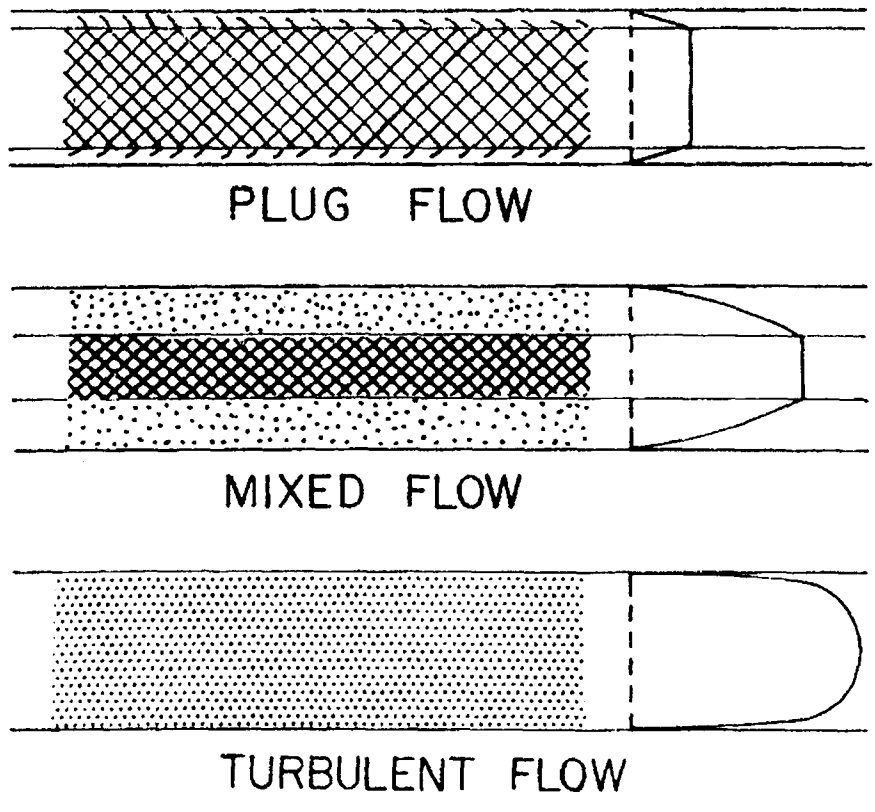

Figure 2.4: Different velocity profiles and their corresponding flow regions observed in fiber suspension flows in a rectangular channel (adopted from Xu and Aidun (2005)): (a) different velocity profiles and (b) corresponding flow regions.

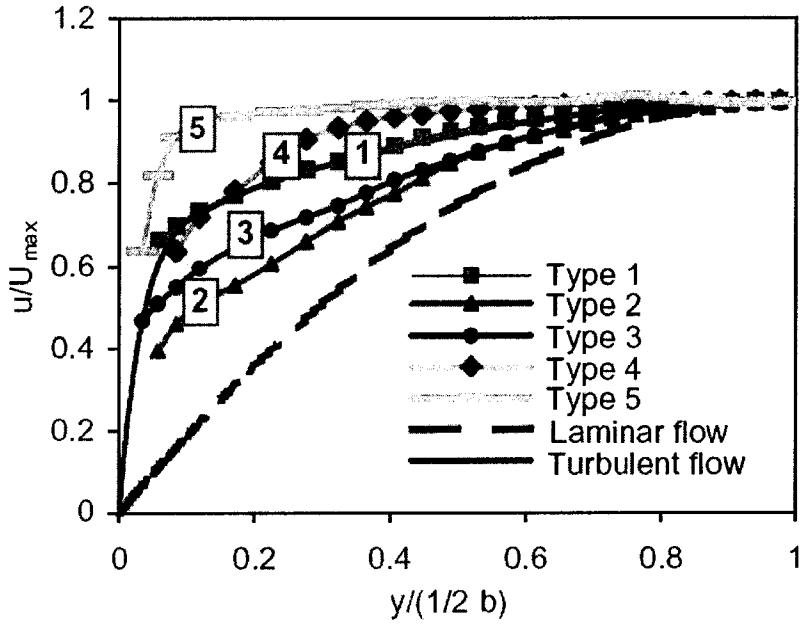

(a)

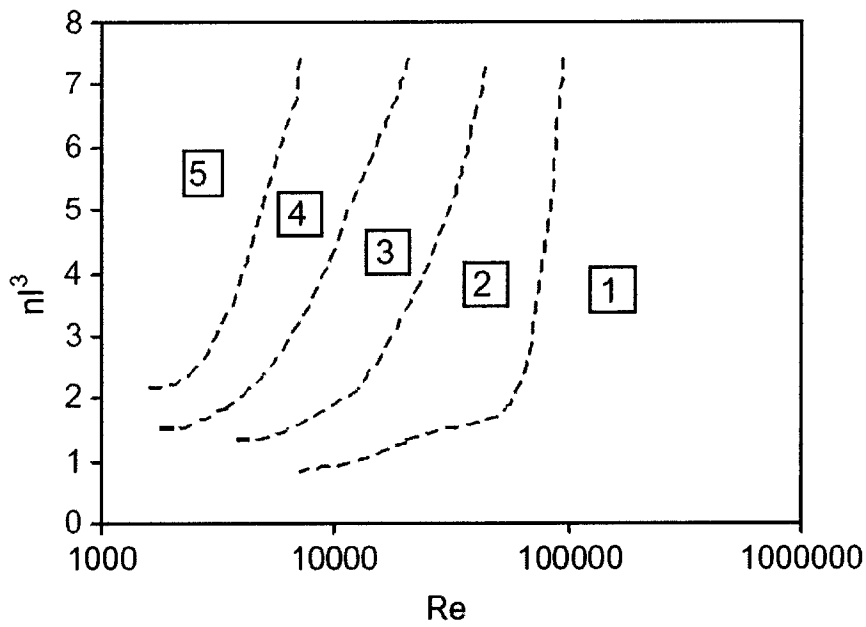

(b)

Figure 2.5: Typical curves of friction loss vs. bulk velocity for cellulose fiber suspension pipe flows (adopted from TAPPI (1985)).

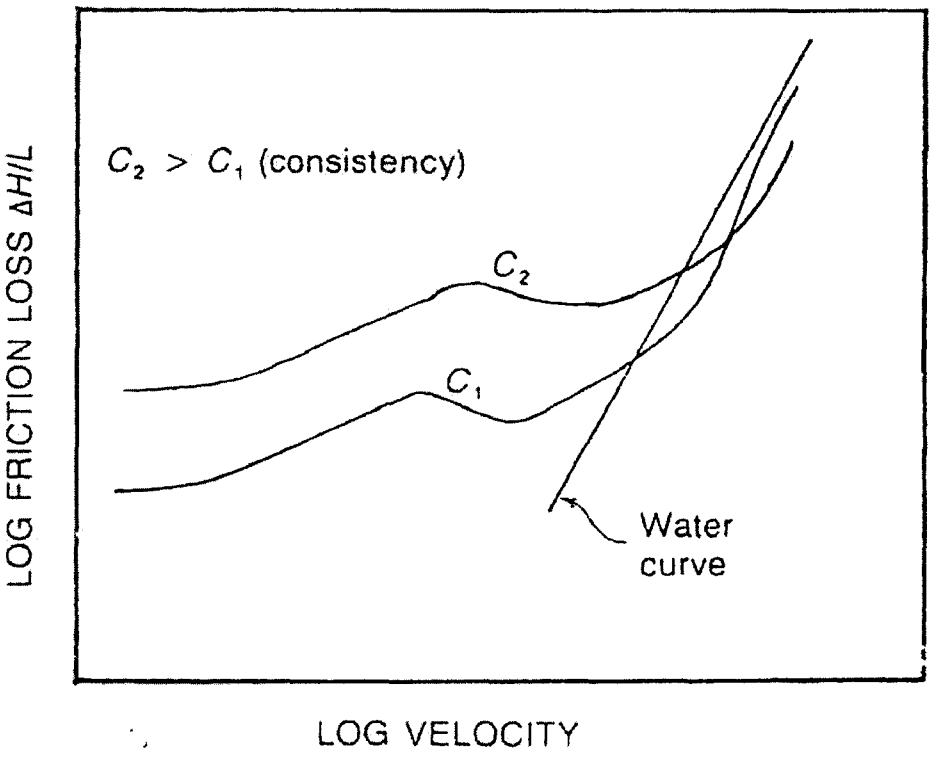

Figure 2.6: Flow structure in the vortical-spiral flow regime in a 3-D gas-liquid or gas-liquid-solid bubble column (adopted from Chen *et al.* (1994)).

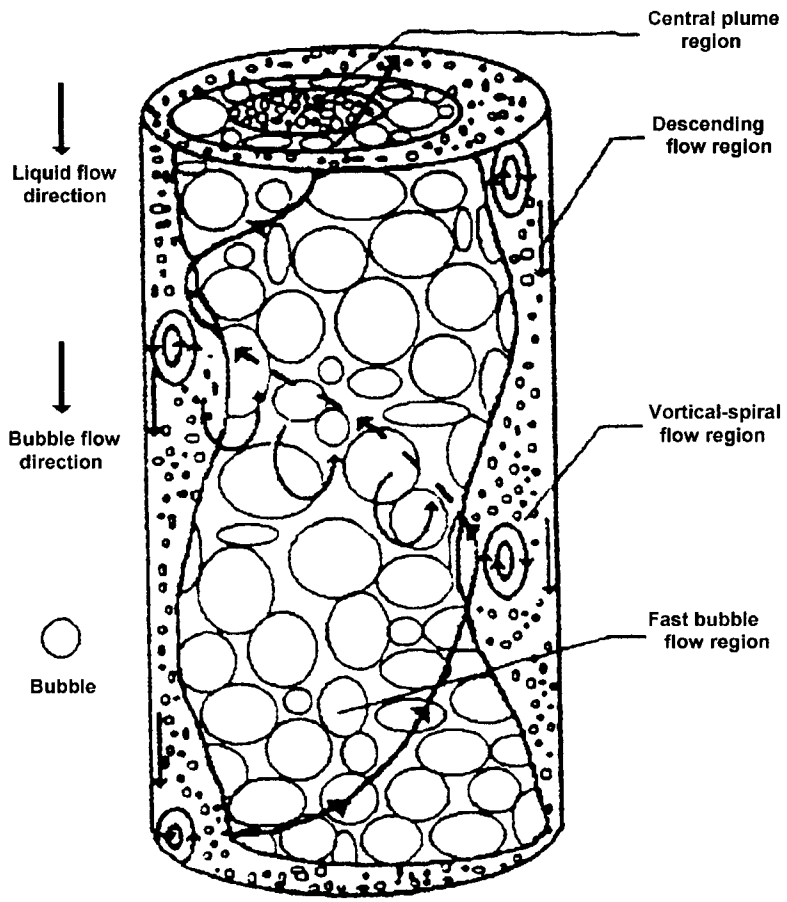

Figure 2.7: Schematic representation of typical gas holdup versus superficial gas velocity relationship.

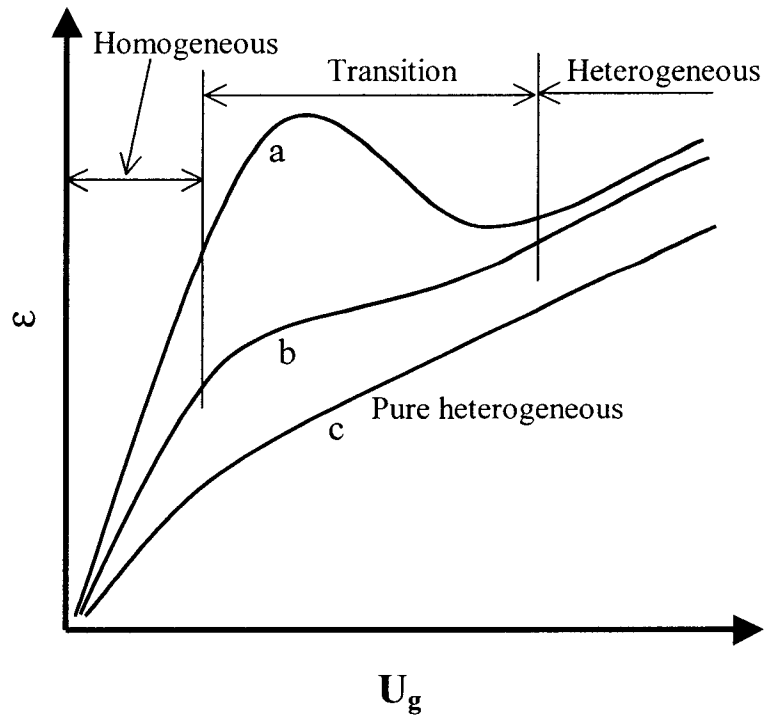

Figure 2.8: Mechanisms by which bubbles escape from fiber networks (adopted from Ajersch and Pelton (1999)).

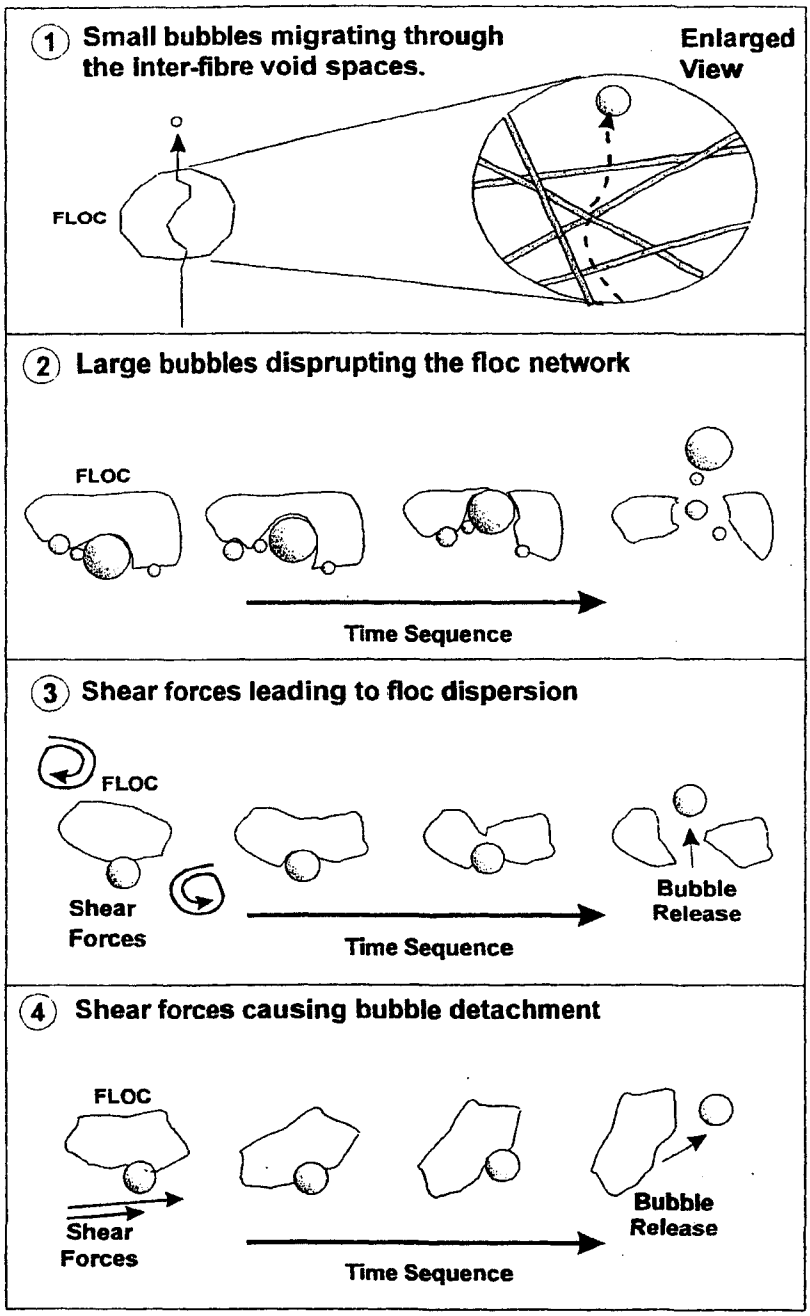

Chapter 3: EXPERIMENTAL METHOD

This chapter provides a description of the experimental method used in this study on gas holdup in a cocurrent air-water-fiber bubble column. Details concerning the experimental facility, experimental conditions, experimental procedures, data reduction, and experimental uncertainty are included.

3.1 Experimental Cocurrent Bubble Column System

The experiments for this study are conducted in a cylindrical cocurrent bubble column, which consists of four 0.914 m tall acrylic tubes with 15.24 cm internal diameter. Five delrin collars, each 5.1 cm tall, and 11 buna-n gaskets are used to connect the acrylic tubes for a total column height of 4 m. Figure 3.1 shows a schematic of the entire system. Figure 3.2 is a picture of the actual experimental set-up. Filtered air is supplied by a compressor and enters the bubble column from the bottom via a spider sparger, which is installed at the same height of the bottom collar. The air flowrate is adjusted with a regulator and measured with one of three gas flowmeters (Aalborg, Model: GFM 371s, 471, and 671s, respectively), each covering a different flowrate range. The fiber suspension from a 379 L reservoir is pumped into the column. The pump is connected to the reservoir with a 2.44 m long 7.62 cm diameter PVC pipe. A 2.85 m long 2.54 cm diameter PVC pipe connects the pump to the column. The fiber suspension flowrate is measured with a magnetic flowmeter (COPA-XE^{TM} Series 4000, Model: 10DX4311) and varied via a pump power frequency controller. The fiber suspension enters the column through a flow expander located immediately below the spider sparger. A gas-liquid separator is located on top of the column where air is separated from the fiber slurry while the slurry returns to the reservoir through a PVC pipe. Along the column, 5 pressure transducers (Cole-Parmer, Model: 68075, labeled as P_1, P_2, P_3, P_4, and P_5 in Fig. 3.1) are installed, one in each of the five delrin collars. Each acrylic tube section is numbered 1 to 4 from the bottom of the column. Two type-T thermocouples are also located at the bottom and top of the column, respectively.

A schematic and picture of the spider sparger are shown in Fig. 3.3. The sparger has eight arms made of 12.7 mm diameter stainless steel tubes. Thirty-three 1.6 mm diameter holes are located on one side of each arm and distributed as shown in Fig. 3.3. The arms are soldered to the center cylinder of the sparger such that all the holes face the same direction. Air enters the spider sparger from the central cylinder and exits from the arm holes. The sparger is installed with the holes facing upward.

3.2 Experimental Conditions

3.2.1 Fiber types and their properties

Three types of cellulose fibers and Rayon fiber of three lengths are used in this study. The cellulose fibers have been provided by Kimberly-Clark and are hardwood (Acacruz ECF (Elemental Chlorine-Free) Eucalyptus wood fiber), softwood (northern softwood kraft – LL–19), and bleached chemithermomechanical pulp (BCTMP). Their key physical properties were also provided by Kimberly-Clark and are listed in Table 3.1.

Table 3.1: Cellulose fiber properties.

Fiber type / Properties	**Hardwood**	**Softwood**	**BCTMP**
Wood species	Eucalyptus	65-75% Northern Black Spruce, 20-25% Jackpine, 5-10% Balsam Fir	Softwood
Arithmetic average length (L_A) (mm)	0.69	1.2	0.8
Length weighted average length (L_L) (mm)	0.78	2.31	1.91
Coarseness (ω) (mg/100m)	6.9	13.08	29.5
Number of fibers per unit mass (n_f) (millions/g)	21.4	6.37	4.25

The Rayon fibers used in this study have a nominal length of 1 mm, 3 mm, or 6 mm and were provided by Clarmont Flock Corp., Leominster, MA (1 mm) or Mini Fibers, Inc., Johnson City, TN (3 mm and 6mm). All Rayon fibers have a coarseness of 50 mg/100m, which corresponds to a fiber diameter of 20.6 μm.

3.2.2 Other experimental conditions

All experiments in this study are carried out under atmospheric pressure and ambient temperature. The superficial gas velocity range is 0 cm/s $\leq U_g \leq$ 20 cm/s, the superficial liquid velocity range is 0 cm/s $\leq U_l \leq$ 10 cm/s.

Fiber mass fraction C is defined as the ratio of oven-dry fiber mass to the suspension mass. In this study, the fiber mass fraction range is $0 \leq C \leq 1.5\%$ for all fiber types except hardwood and 6 mm Rayon fibers. For hardwood fiber, a range of $0 \leq C \leq 2.0\%$ is used. Due to clogging in the 2.54 cm PVC pipe at fiber mass fractions higher than 0.4%, 6 mm Rayon fiber is only studied in a range of $0 \leq C \leq 0.4\%$.

3.3 Experimental Procedures

3.3.1 Fiber suspension preparation

All the cellulose fibers are disintegrated from dry lap fiber sheets. The fiber sheets are originally torn into small pieces and then a specified mass of oven-dry fiber is weighed. It is then soaked in tap water for 24 hours before the pieces of fiber sheet are disintegrated in a Black-Clawson laboratory hydropulper. The concentrated fiber suspension is then transferred to the reservoir and additional tap water is added to raise the fiber mass fraction to a predetermined level.

Rayon fibers are prepared slightly differently from the cellulose fibers because of additives attached to the fiber surface, which are gradually released into the fiber suspension and significantly affect the surface tension of Rayon fiber suspensions. First, a specified mass of oven-dry fiber is weighed. Then the fiber is soaked in tap water for 24 hours before it is repeatedly washed and soaked using tap water until the surface tension of the filtered water

reaches a steady value of about 70 mN/m. This process removes a majority of the additives and thus their possible influences on bubble column hydrodynamics. The washed Rayon fiber is then added to the reservoir and additional tap water is added to adjust the fiber mass fraction to a predetermined level.

3.3.2 Data measurement

For each data point, volumetric gas ($\dot{Q}_g$) and liquid ($\dot{Q}_l$) flow rates and pressure from each of the 5 gage pressure transducers are recorded. All pressure and flowmeter signals are collected via a computer controlled data acquisition system. A LABVIEW data acquisition program is used to select signals to be collected, visualize signal temporal variations, and collect and save data.

Superficial gas and liquid velocities are controlled by a gas regulator and pump power frequency controller (Fig. 3.1), respectively.

To acquire gas holdup data at a given superficial gas and liquid velocity, 4800 readings are collected from each instrument every 10 ms and averaged after quasi-steady conditions are reached. For a given fiber type and fiber mass fraction, data are acquired while the superficial liquid velocity is fixed and the superficial gas velocity is gradually increased in a stepwise fashion from 0 to 20 cm/s. The pump frequency controller is slightly adjusted to maintain a nominal superficial liquid velocity whenever the gas flowrate is changed. When data acquisition is completed at a given superficial liquid velocity, the superficial liquid velocity is adjusted to another nominal value and the superficial gas velocity is again varied from 0 to 20 cm/s. A gas holdup versus superficial gas velocity curve is obtained for each superficial liquid velocity.

When data collection is completed at a given cellulose fiber mass fraction, the used fiber suspension is discarded. A specified amount of new fiber and tap water is prepared and added to the reservoir to reach a new fiber mass fraction. For Rayon fibers, the used fiber suspension is retained while an additional amount of Rayon fiber is added to increase the fiber mass fraction to a given value. Additionally, water in the reservoir is added and/or filtered out to reach the target fiber mass fraction.

Once a new suspension of a given fiber mass fraction is ready, it is then agitated with the mixer and the bubble column is operated at U_l = 10 cm/s and U_g = 18 cm/s for at least 15 minutes. Data are then collected at the same superficial gas and liquid velocity every minute for at least one hour to condition the system. The collected data is used to identify any temporal gas holdup variation. It has been shown (Su and Heindel, 2004b; Tang and Heindel, 2004b) that data collected at the beginning of the experiment may show a temporal variation and may not be reproducible. Data acquisition is finally initiated when no temporal gas holdup trend is observed.

During data acquisition, surface tension and pH of the water filtrate from the fiber suspension are measured with a Sigma 703 digital tensiometer and a Milwaukee SM 802 pH/EC/TDS meter, respectively.

3.4 Data Reduction

3.4.1 Calculation of superficial velocities

The superficial liquid velocity is determined from

$$U_l = \frac{\dot{Q}_l}{A_c} \tag{3.1}$$

where $\dot{Q}_l$ is the volumetric liquid flow rate and A_c is the column cross-sectional area. This assumes the water-fiber suspension is a pseudofluid and the fibers follow the water flow. This is a good assumption because cellulose fiber or Rayon fiber densities are typically close to that of water and the overall fiber mass fraction is less than 2%.

The superficial gas velocity is determined from

$$U_g = \frac{\dot{Q}_g}{A_c} \tag{3.2}$$

where $\dot{Q}_g$ is the volumetric gas flow rate.

3.4.2 Calculation of gas holdup

For a cocurrent bubble column, gas holdup is generally determined from (Hills, 1976; Merchuk and Stein, 1981; Kumar *et al.*, 1997)

$$\varepsilon = \left(1 - \frac{\Delta p}{\rho_l g h}\right) + \frac{U_l^2}{g}\frac{d}{dh}\left(\frac{1}{1-\varepsilon}\right) + \frac{4\tau_w}{\rho_l D g} \tag{3.3}$$

where ε is the gas holdup in a column section between two locations separated by a distance h; Δp is the pressure drop between the same locations; ρ_l is the liquid density; g is the acceleration due to gravity; D is the column inner diameter; and τ_w is the wall shear stress. The first term in Eq. (3.3) accounts for the hydrostatic head; the second term represents fluid acceleration due to void changes; and the third term is a contribution from wall shear effects. It is known that the fluid acceleration term is negligible when the superficial liquid velocity U_l is small (Hills, 1976; Merchuk and Stein, 1981). The gas holdup evaluated by the summation of the first and third terms, i.e.,

$$\varepsilon = \left(1 - \frac{\Delta p}{\rho_l g h}\right) + \frac{4\tau_w}{\rho_l D g} \tag{3.4}$$

is found to be very close to the gas holdup evaluated by

$$\varepsilon = 1 - \frac{\Delta p}{\Delta p_0} \tag{3.5}$$

where Δp_0 is the pressure drop between the same locations corresponding to Δp at the same conditions (fiber suspension and superficial liquid velocity) except with $U_g = 0$. More details are given in Appendix A.

With five measured pressure signals, the time-averaged gas holdup in each section is calculated from

$$\varepsilon_i = 1 - \frac{\Delta p_i}{\Delta p_{0,i}} \tag{3.6}$$

where $\Delta p_i = p_{L,i} - p_{H,i}$ is the pressure difference between the lower ($p_{L,i}$) and higher ($p_{H,i}$) ends of column section i (i =1, 2, 3, 4); $\Delta p_{0,i}$ is the corresponding pressure difference when the column is filled only with the specified water-fiber suspension flowing at the same U_l.

The overall column gas holdup is defined as

$$\varepsilon = \frac{1}{3}(\varepsilon_1 + \varepsilon_2 + \varepsilon_3) \tag{3.7}$$

which corresponds to the average gas holdup in the three lower sections. The gas holdup in the top section is not included in the overall gas holdup because the measurement error due to the void caused by large bubbles escaping the column top is significant during some experimental conditions.

Gas holdup values can also be estimated with the bed expansion method (i.e., from liquid level changes between the ungassed and gassed condition) (Kumar *et al.*, 1997). Figure 3.4 compares the average gas holdup values in sections 1-3 estimated with the bed expansion method and those obtained using the pressure difference method represented by Eq. (3.5) for air-water systems at $U_l = 0$ cm/s. The gas holdup values from these two methods at a given operating condition are very close.

3.5 Experimental Uncertainty

The gas holdup uncertainty is a result of pressure measurement error. The superficial gas velocity uncertainties are mainly due to gas flow rate measurement error. The contribution of column diameter uncertainty to the superficial gas velocity uncertainty is neglected. The pressure and gas flow rate errors include two parts: signal fluctuation and calibration error. All these quantities are calculated following procedures presented in Figliola and Beasley (2000).

The pressure transducer error is less than 0.25% of full scale (34.475 kPa) for a single measurement. When pressure signal fluctuation is significant, the variation between two measurements is larger. However, with multiple (e.g., 4800) measurements, the resultant average pressure is much more precise. The standard deviation of the average pressure value is much smaller. For example, for an average pressure of 4800 measurements, the standard deviation of the average pressure is only ~1/70 of that of a single measurement.

Figure 3.5 shows two examples of pressure fluctuation signals obtained with pressure transducer P_2 in air-water systems at $U_g = 20$ cm/s and $U_l = 0$ cm/s and 10 cm/s, respectively. It shows that the pressure fluctuations are different at different superficial liquid velocities.

The level of pressure fluctuation also depends on superficial gas velocity, fiber mass fraction, and transducer location. The variation in a single pressure measurement can be from less than 100 Pa to ~1000 Pa. However, the standard deviation of the average pressure of 4800 measurements is typically up to ±15 Pa. Considering the influence of operating condition, absolute gas holdup uncertainty is estimated to be $\Delta\varepsilon \approx \pm 0.005\sim0.01$.

When gas channeling occurs, the measurement accuracy of gas holdup will decrease because (i) the fiber-water suspension is not homogeneous; and (ii) gas flows through the channels with large velocity, resulting in significant pressure drop due to shear friction. However, in the present experimental study, fiber mass fraction is only up to 1.5% and channeling takes place only near the spider sparger and only at the high fiber mass fractions.

Using a similar procedure to that for gas holdup uncertainty, the typical uncertainty for superficial gas velocity is estimated to be ±2~4% for $U_g \geq 1.0$ cm/s.

The uncertainty of superficial liquid velocity is different from that of superficial gas velocity because during data acquisition, superficial liquid velocity is fixed at a constant value. Thus, the superficial liquid velocity uncertainty is resulted from not only liquid flow rate fluctuation uncertainties, but also a human adjustment uncertainty. The liquid flow rate fluctuation and magnetic flowmeter calibration uncertainties are found much smaller than their counterparts for gas flow rate uncertainty. The main source of uncertainty is the human adjustment uncertainty. By studying actually obtained superficial liquid velocities and their corresponding adjustment goals (i.e., the superficial liquid velocities that are to be reached by adjusting pump frequency), the typical uncertainties associated with superficial liquid velocity is estimated as ±1.5~5% for $U_g \geq 2.0$ cm/s, with a larger uncertainty found at a higher fiber mass fraction because pump performance is less steady when it is pumping at more concentrated fiber suspension.

When gas bubbles are entrained in the fiber suspensions, the accuracy of the magnetic flow meter can possibly be affected. In this study, although it was found a small amount of gas is entrained at the highest mass fractions, the amount is very small; it is assumed to have a negligible effect on the overall slurry flowrate.

Figure 3.1: Schematic of the cocurrent bubble column experimental facility.

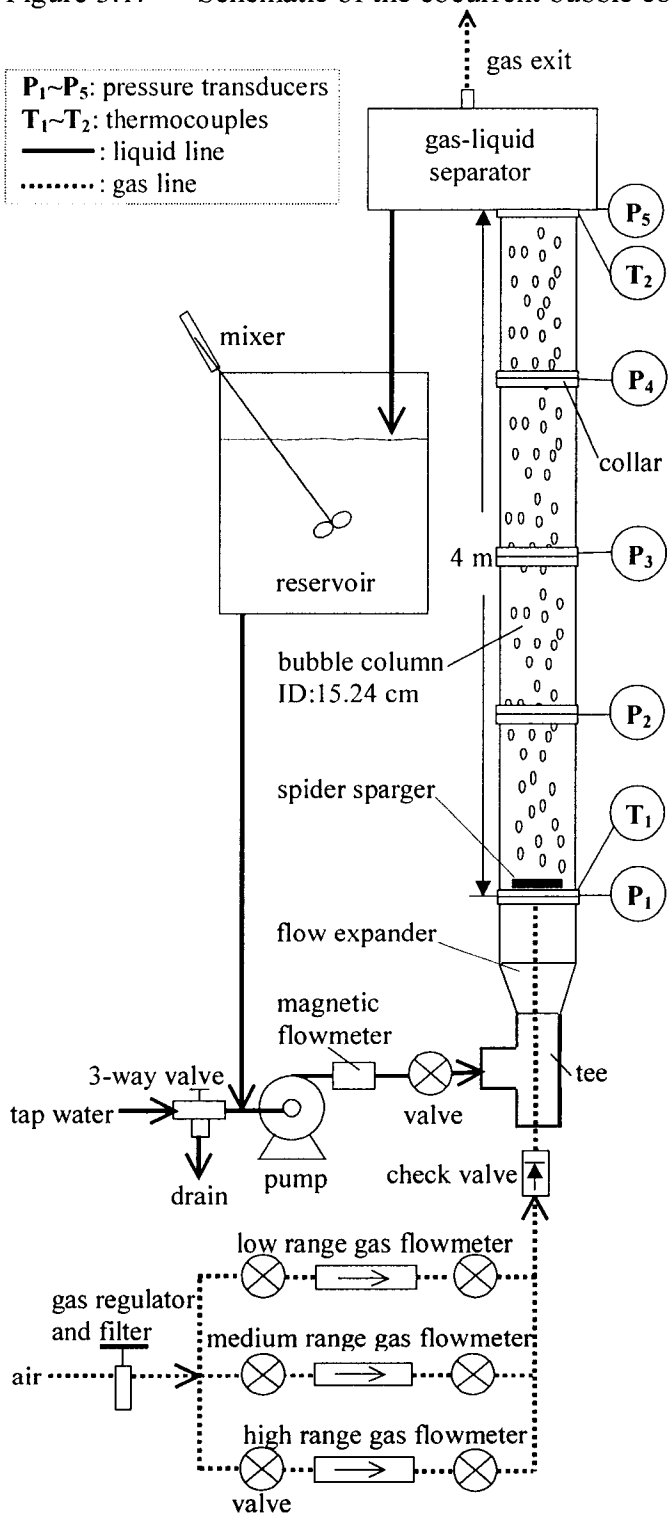

Figure 3.2: Picture of the cocurrent bubble column experimental facility.

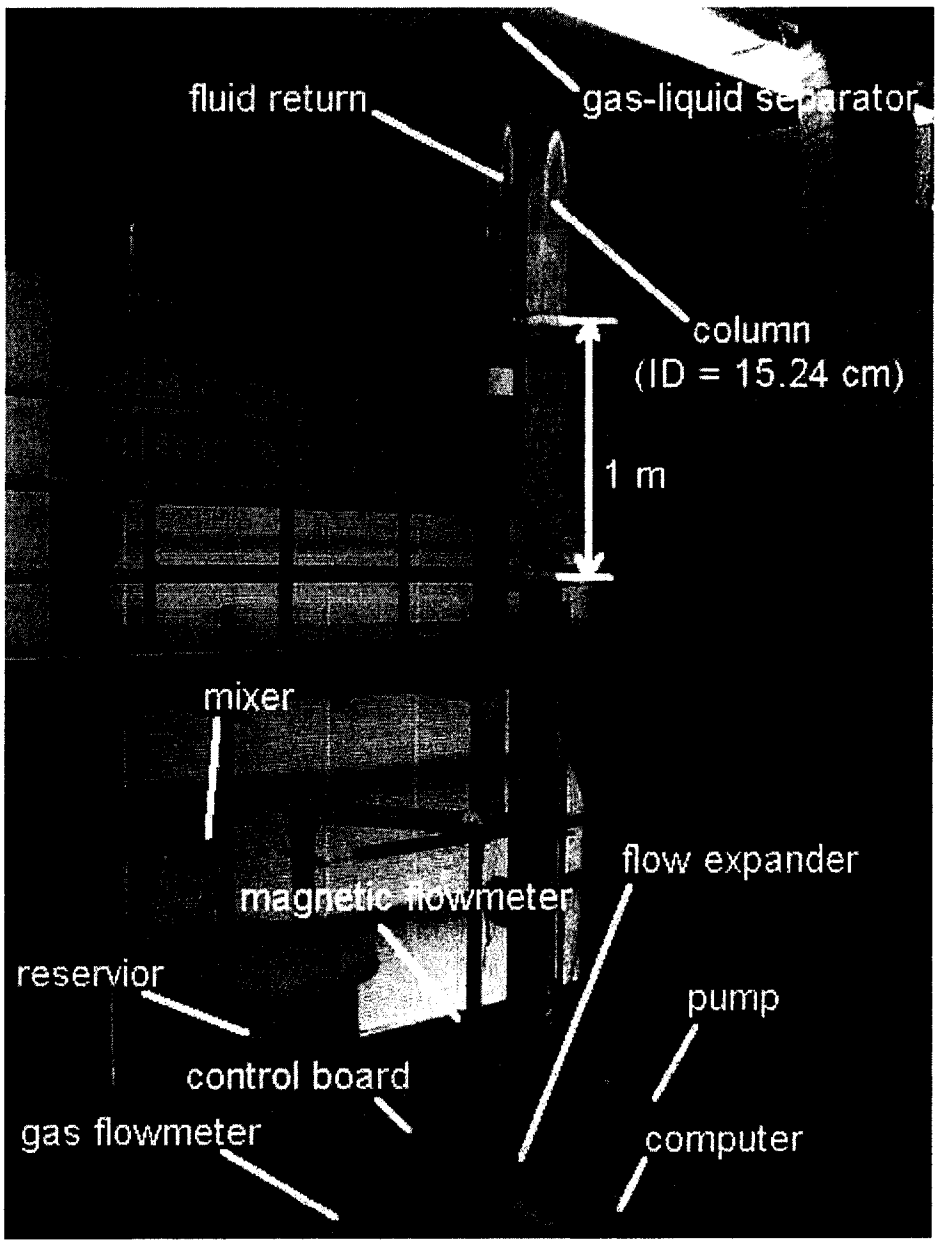

Figure 3.3: Schematic and picture of the spider sparger.

(a)

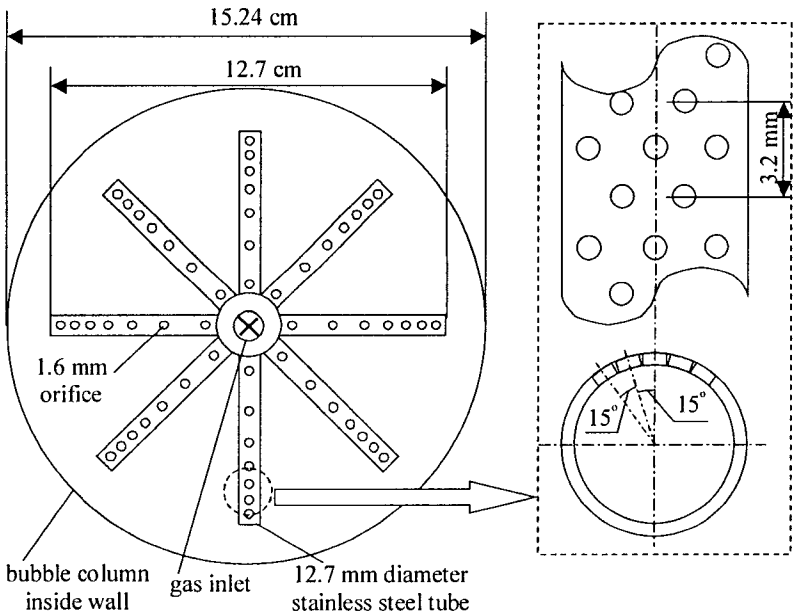

(b)

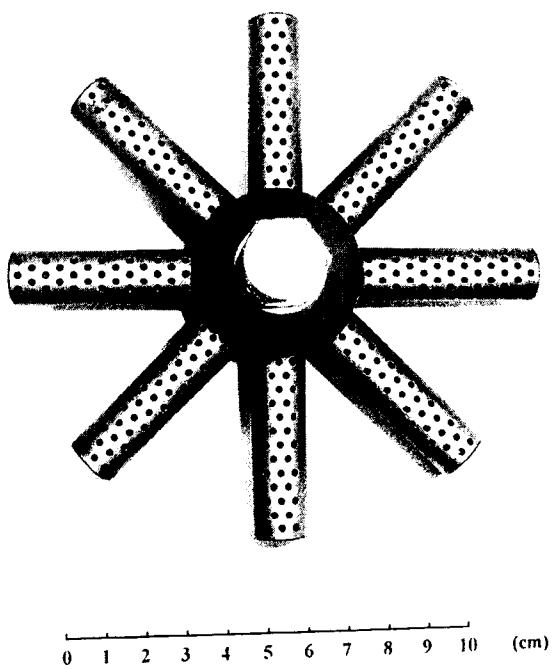

Figure 3.4: Comparison between gas holdup values in air-water semi-batch bubble columns obtained with the bed expansion and pressure difference methods.

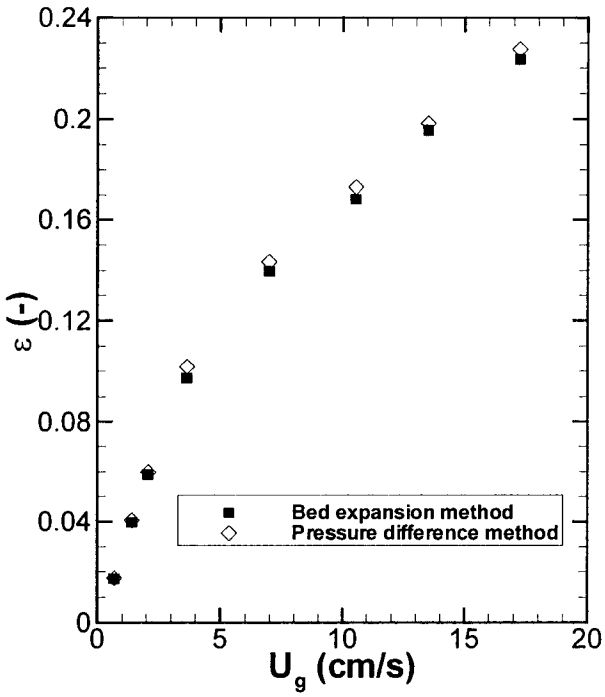

Figure 3.5: Examples of pressure fluctuation signals obtained with pressure transducer P_2 in air-water systems at U_g = 20 cm/s: (a) U_l = 0 cm/s and (b) U_l = 10 cm/s.

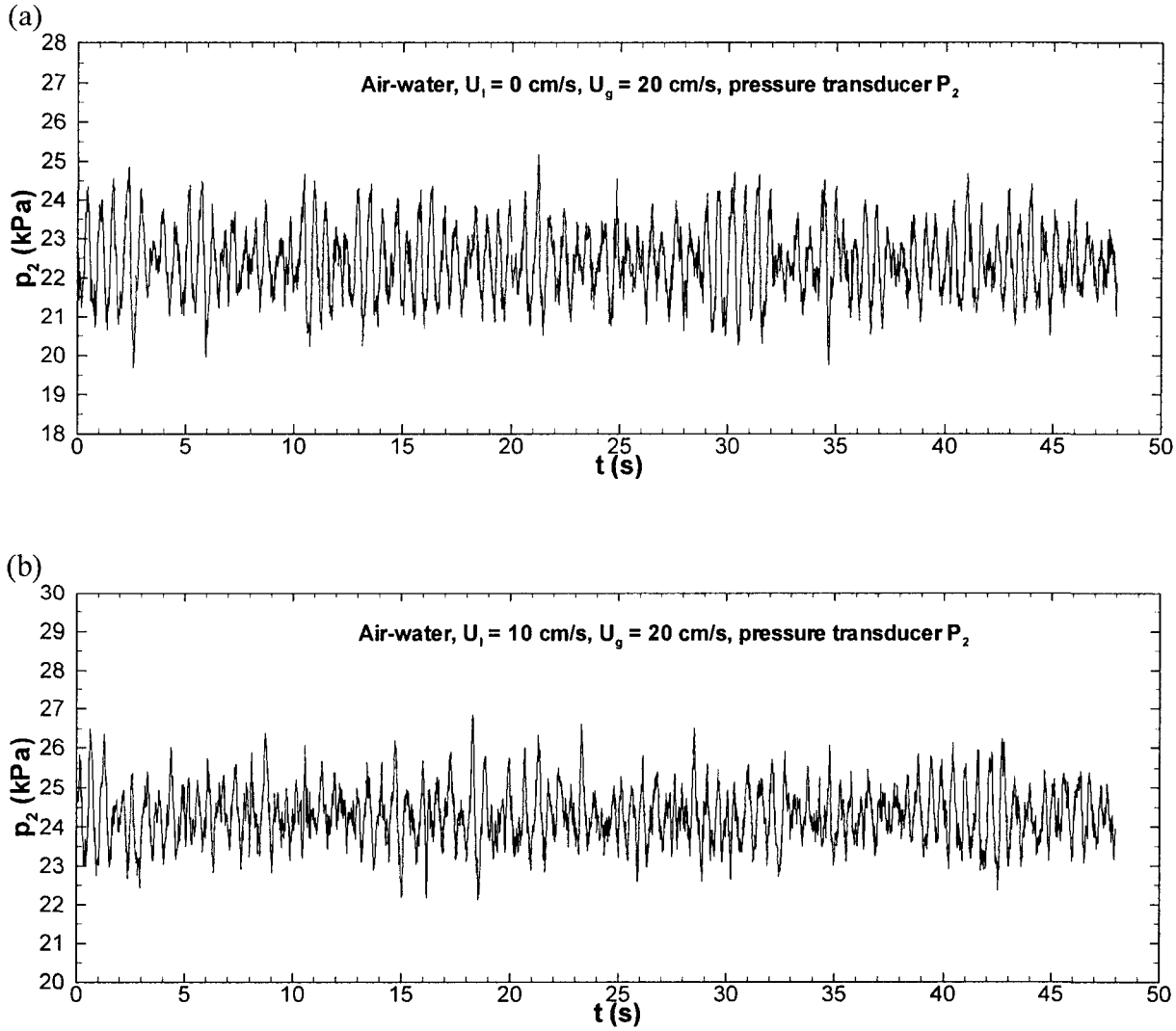

Chapter 4: THE INFLUENCE OF FIBER SUSPENSIONS ON BUBBLE MOTION AND GAS HOLDUP

When flexible fibers (cellulose or synthetic) are mixed in a liquid, flocculation occurs if the fiber mass fraction is higher than a critical value, which depends on fiber type, flow conditions, and liquid viscosity. Flocculation results in a nonuniform fiber distribution and fiber network structures, which possess a certain level of strength and significantly influence bubble motion in fiber suspensions and hence, gas holdup in bubble columns. In this chapter, the first section discusses fiber suspension structures, considering a fiber suspension comprises flocs and inter-floc regions, which surrounds and connects adjacent flocs. The second section examines the influence of fiber suspensions on bubble motion based on the understanding of fiber suspension structures. The third section identifies the major mechanisms by which fibers affect gas holdup in gas-liquid-fiber bubble columns.

4.1 Fiber Suspension Structures

In an extremely dilute fiber suspension with negligible fiber-fiber interactions, a well mixed fiber suspension is uniform, i.e., the fibers are uniformly distributed throughout the suspension volume. As the fiber mass fraction (C) of the suspension increases, fiber-fiber interaction becomes more significant and eventually, when C is higher than a certain critical value, fiber flocculation occurs and fiber networks form (Kerekes *et al.*, 1985). A fiber network is an interconnected system in which each fiber is in contact with other fibers (Kerekes *et al.*, 1985). The fiber distribution in a fiber suspension is usually not uniform. The local fiber mass fraction variation has been extensively studied (Norman *et al.*, 1978; Yokogawa *et al.*, 1985; Steen, 1989a; Ringner and Rasmuson, 2000). The coefficient of variation of the local fiber mass fraction was defined as the flocculation intensity (Wahren, 1967). In a flocculated fiber suspension, there are usually regions where fibers aggregate and result in a local fiber mass fraction higher than the average fiber mass fraction of the suspension. These high fiber mass fraction regions (including fibers and the suspending

liquid) are called flocs (Kerekes *et al.*, 1985). Flocs are different from the low fiber mass fraction regions in that the flocs have higher strength and in flowing conditions may act as independent entities (Kerekes *et al.*, 1985). More information on floc characterization and behavior can be found in Jagannadh *et al.* (1991) and Bjorkman (2002).

A flocculated fiber suspension can be considered as a fiber-liquid mixture comprising two parts: (i) flocs and (ii) inter-floc regions. Figure 4.1 is a sketch showing the structure of a flocculated fiber suspension. There are no distinct boundaries between flocs and inter-floc regions, which are considered transitional regions between flocs. The local fiber mass fraction in the inter-floc region is lower than that in the adjacent flocs. The flocs are surrounded and connected by the inter-floc regions.

A floc is compressible in that when it is squeezed, the liquid held inside the floc flows out, leaving the squeezed floc (i.e., the fiber material of the floc plus residual liquid) having a larger compactness and occupying a smaller volume. However, the total volume of the squeezed floc and the liquid squeezed out of the floc is still the same as the original floc because the fiber material (considering a fiber as a solid cylinder) and the suspending liquid are incompressible. The compactness of a fiber floc can be gauged by its mass fractal dimension, which is a measure of the space-filling capacity of a object (Glover *et al.*, 1999). In a three-dimensional Euclidean space, the compactness is between 1 and 3, with a solid object (without interior voids) having a compactness of 3.

A floc usually has an irregular shape and a given strength. Flocs are usually not uniform in size and follow a certain distribution (Hourani, 1988b; Syrjala *et al.*, 2003). The number of fiber flocs and the size distribution in a suspension is a function of fiber mass fraction, fiber physical properties, suspending liquid properties, chemical additives, and flow conditions (Mason, 1948; Mason, 1954; Kerekes, 1983; Kerekes *et al.*, 1985; Hourani, 1988b; Steen, 1989a, 1991; Kerekes and Schell, 1992; Zhao and Kerekes, 1993; Beghello, 1998; Syrjala *et al.*, 2003). In a turbulent flow field, usually an equilibrium floc size distribution is determined by the interaction between flocculation and flow turbulence (Steen, 1989a, 1991); this floc size is smaller at a higher turbulence level.

In an inter-floc region, some fibers have one or both ends entangled inside neighboring flocs; other fibers are not part of any neighboring flocs, but are in contact with

other fibers. In turbulent flow fields, there are frequent interactions between the flocs and the inter-floc regions: (i) fibers can leave from a floc via erosion (Lee and Brodkey, 1987) and enter a floc via entanglement with fibers at the floc surface; (ii) when a floc moves, it may exert tension on and even break up its neighboring inter-floc region. At very high fiber mass fractions, the inter-floc regions become very thin because many flocs form and they are crowded. In this situation, the inter-floc regions are negligible and direct contacts between flocs prevail.

There are several examples where modeling fiber suspensions with a structure similar to that shown in Fig. 4.1 resulted in the successful prediction and explanation of experimental observations on processes involving liquid-fiber suspensions. Ajersch and Pelton (1999b) modeled flocculated fiber suspensions as a mixture comprising uniform fiber flocs and low fiber mass fraction inter-floc regions where uniformly distributed individual fibers are present, and successfully explained and predicted fiber losses due to entrainment during flotation deinking. Ringner and Rasmuson (2000) considered that a flocculating fiber suspension consisted of flocs and low fiber mass fraction inter-floc regions and estimated inter- and intra- floc fiber mass fractions using X-ray computed tomography and image analysis. With different fibers, and in devices with different flow geometries, Bjorkman (2003a) demonstrated that suspended fiber networks (at C = 1-4%) break up through creating voids with negligible fibers parallel to the largest local compression. Viewing the suspended fiber networks as particulate systems comprising closed packed non-adherent compressible flocs suspending in an incompressible penetrating matrix, Bjorkman (2003b) successfully explained the formation mechanism of the voids and concluded that the voids opened up between flocs due to the compressibility difference between the suspending liquid (incompressible) and the floc phase (i.e., the fiber aggregate of a floc without including the suspending liquid, which is compressible).

When a shear force is exerted on a fiber network, it likely breaks up once the force is larger than a critical value. When a fiber network breaks up into two parts, it is due to fracture at interfaces via fiber slipping and not fiber breakage (Jagannadh *et al.*, 1991). The resistances that these fibers receive during the slipping include friction and hook forces. The total resistance force of all these fibers consists of a large portion of the force required to

break the fiber network, i.e., the network strength, which also includes the force required to make enough space so that fiber slipping is possible (by means of, for example, squeezing and/or pushing aside related flocs in shear flow). In the inter-floc regions, the network is weak because there are fewer fibers and inter-fiber contact points, and the resistance will be smaller if the fiber network ruptures at these regions. Hence, when a fiber suspension is subject to a shear stress, fiber network breakup at first occurs at the inter-floc regions. The fiber network strength depends on the number of fibers in the inter-floc region, the total fiber length that is entangled in the neighboring flocs, and the compactness of local flocs. It also depends on the fiber physical properties, such as the fiber surface friction coefficient and elastic modulus. When the inter-floc region is negligible, the force required to breakup a fiber network mainly results from floc packing (Bjorkman, 2003b).

The network breakup from inter-floc regions when the flocs remain unbroken was called macro scale breakup by Wikstrom *et al.* (2002). Similar observations were also made by Ringner and Rasmuson (2000) and Bjorkman (2003a). The stress required to breakup fiber networks in a suspension and cause relative movement between flocs is the yield stress of the fiber suspension, which has been extensively studied (Bennington *et al.*, 1990; Bennington *et al.*, 1995; Wikstrom and Rasmuson, 1998). Wikstrom *et al.* (2002) also identified two other network states: micro scale breakup and a fluidized state. The micro scale breakup involves the rupture of flocs, which occurs at higher shear rates than that required by the macro scale breakup. When the shear stress increases to a critical value, all the flocs completely breakup and the fiber suspension becomes very uniform. This was called a fluidized state by Wikstrom *et al.*(2002). To achieve a complete breakup of fiber networks in a suspension (i.e., fluidization), much more energy is required (Kerekes *et al.*, 1985; Bennington and Kerekes, 1996; Wikstrom *et al.*, 2002).

In a flowing flocculated fiber suspension, generally there may be three types of movements according to their corresponding length scales. The first type is global scale movement. At this scale, the suspension behaves as a pseudofluid and it moves in an orderly manner with a certain flow pattern and average velocity. The second type is floc scale movement. In this scale, each floc moves as an entity. Although the flocs collectively follow a certain global flow pattern, there are relative movements between the flocs. The flocs may

collide and coalesce with each other; two contacted flocs may also deviate from each other; flocs may rotate and when they contact, sliding may occur between them. During floc movement, single flocs may be subjected to deformation, stretching, breaking, and fragmentation (Lee and Brodkey, 1987), which result in changes in the floc shape, size distribution, and number. The third type of movement is fiber scale movement. This includes fiber movements in the inter-floc region, relative motion between fibers in a floc, and fibers leaving and joining flocs via surface erosion and entanglement, respectively.

4.2 Bubble Motion in Fiber Suspensions

In this section, at first a brief review of previous studies on bubble motion in fiber suspensions is given. Then the effects of a fiber suspension on the motion of single and multiple in both quiescent (or semi-batch) and flowing suspensions are discussed.

4.2.1 Review of previous bubble motion studies

Many researchers have investigated bubble motion in fiber suspensions; these include studies on bubble entrainment (Isler and Widmer, 1979; Pelton and Piette, 1992; Ajersch and Pelton, 1993; Schulz and Scott, 1993b, 1993a; Helle, 2000) and movement (Walmsley, 1992; Reese *et al.*, 1996; Heindel and Monefeldt, 1998; Ajersch and Pelton, 1999a) in fiber suspensions.

4.2.1.1 Bubble entrainment

Isler and Widmer (1979) observed the tendency of air bubbles to rise through fiber suspensions flowing in a horizontal pipe and reported that bubbles smaller than 60 μm were bounded to the fiber network and did not rise, while larger bubbles rose toward the top of the pipe.

Pelton and Piette (1992) showed that in a quiescent fiber suspension, at a given fiber mass fraction, a single bubble was trapped by fibers when it was smaller than a critical size, which increased with increasing fiber mass fraction and varied with fiber type. The entrained

bubble was usually released when the fiber suspension was stirred. They pointed out that the main mechanism for bubble holdup in a fiber suspension was the mechanical entrapment of bubbles in fiber networks. Two criteria for bubble holdup were determined: (i) sufficient fiber-fiber contact points to prevent a bubble from rolling off or around the fiber network, and (ii) the network must be strong enough to sustain the buoyant force exerted by the bubble.

Schulz and Scott (1993a) reported that air was entrained in fiber suspensions at various locations throughout a paper recycling system and the entrained air corresponded to a gas holdup ranging from 0.006 to 0.055. Schulz and Scott (1993b) reported that air entrainment varied between different fiber suspensions. They considered that the dissolved and colloidal hydrophobic substances, which served to stabilize entrained air bubbles and varied between different fiber suspensions, as a major reason.

Ajersch and Pelton (1993) found that new bubbles could not grow on fully wetted fibers and carbon black surfaces under conditions likely to arise in pulp and paper mills; however, repulped paper had trapped pockets of air which are active sites for bubble growth from supersaturated solutions. They reported that adhesion of air bubbles to fibers was rarely observed and concluded that bubble-fiber adhesion was not an important mechanism for bubble holdup in fiber fiber suspensions.

Helle (2000) reported that entrained bubbles rarely adhered to fibers and bubbles bounded by fibers could be removed by applying a centrifugal force.

4.2.1.2 Bubble movement

Ajersch and Pelton (1999a) reported that in a C = 0.27% quiescent fiber suspension, large bubbles (but not sufficiently large to disrupt the fiber network) were trapped in the fiber network; small bubbles (~80 μm) migrated following a tortuous path as it collided with individual fibers and passed around them before resting at a localized region of high fiber density. In a flowing fiber suspension at the same fiber mass fraction, air bubbles moved in a series of random discrete steps because these bubbles were repeatedly trapped and released from fiber flocs; the overall floc shape changed during this bubble-floc interaction process, indicating a shear force that deformed the floc.

Walmsley (1992) reported that adding only 0.1% cellulose fiber to water could significantly change bubble behavior. Fibers act as barriers to bubble rise with some bubbles rising and getting trapped beneath fiber networks and others rising upward between fiber flocs (in regions of locally low fiber mass fraction). The trapped bubbles remain at the locations where they get trapped, while other rising bubbles may catch the trapped bubbles and coalesce with them. Once the size of the trapped bubble increases to a critical diameter where the buoyancy force is sufficient to cleave the fiber network, the trapped bubble breaks the network and rises upward. Network rupture by the large bubble may open a path for many small bubbles to follow, creating bubble rise channels (termed channeling). Walmsley (1992) observed that when the fiber mass fraction was greater than 1.4%, continuous channels of fast rising bubbles appear.

Reese *et al.* (1996) observed that bubble behavior in a fiber suspension was established at the lower part of a bubble column and the bubble behavior remained constant throughout the column. Bubbles in the fiber suspension were flatter than in pure water and the bubbles at the bottom of the column were also flatter than those near the top. They also observed that the bubble rise velocity decreased with increasing fiber mass fraction. It was proposed that bubble coalescence increased in the fiber suspension because the flatter bubbles rose slower in the lower part of the column and lead to an increase in bubble-bubble interactions.

Heindel and Monefeldt (1998) used flash X-ray radiography to observe that in an air-water-cellulose fiber suspension: (i) the gas flow regime changed from homogeneous to heterogeneous flow when the superficial gas velocity was increased or when more fibers were added to the suspension while other conditions remained constant; (ii) increasing the fiber mass fraction resulted in large bubbles and gas channeling; and (iii) the overall flow patterns were significantly affected by increasing fiber mass fraction.

4.2.2 Single bubble motion in quiescent fiber suspensions

When a single bubble is released into a quiescent fiber suspension, like that described in Ajersch and Pelton (1999a), the bubble can be trapped in the fiber suspension or move upward in the suspension, as shown in the sketches in Fig. 4.2.

The bubble may be trapped in the fiber suspension in two situations: (i) when the bubble size is smaller than the voids between fibers in a floc, it can enter the floc through the voids and then get trapped when the fiber spacing becomes smaller than the bubble size (Fig. 4.2a); and (ii) when the bubble size is larger than the fiber spacing but its buoyant force is not sufficiently large to push aside neighboring flocs (Fig. 4.2b).

The bubble may move upward through the suspension in three cases: (i) when the bubble is smaller than the minimum fiber spacing in the fiber suspension, the bubble can flow upward through the voids between fibers (Fig. 4.2c); (ii) when the bubble is larger than the fiber spacing in the flocs, it can move upward through the inter-floc region if it is smaller than the inter-floc region width and able to breakup the network in the inter-floc region (Fig. 4.2d); and (iii) a bubble larger than the inter-floc region width can move upward when its buoyant force is sufficient to push aside neighboring flocs, breakup the fiber network, and create a path (Fig. 4.2e). The difference between cases (ii) and (iii) is that in case (ii) the bubble movement does not cause significant deformation and displacement of flocs while in case (iii) it does. In case (iii), after the bubble passes by the location where the fiber network has been broken (i.e., flocs are deformed and/or displaced), the suspension will recover to a state similar to that before it was broken if sufficient time is provided, which increases with increasing fiber concentrations. This recovery will close the bubble path created by the bubble.

When a bubble moves in the fiber suspension, it interacts with the adjacent fiber network. The fiber network may slow down bubble movement or change its direction, resulting in more tortuous paths and a smaller rise velocity compared to its movement without the presence of flocculated fibers. When the bubble is large, the fiber network may also cause its shape to change and even breakup, resulting in smaller bubbles, which may disperse into a wider area. The rising large bubble may also induce stresses and turbulence, which have significant effects on deformation and breakup of both flocs and bubbles.

4.2.3 Multiple-bubble motion in semi-batch fiber suspensions

When multiple bubbles are in a fiber suspension, the suspension will affect the motion of each bubble in similar ways as described in the previous section. In addition, when the distance between two or more bubbles is smaller than a critical length, which decreases with increasing fiber mass fraction and length, interactions between bubbles become significant. The bubble-bubble interactions are important and can dominate bubble motion in many bubble column operations.

In a gas-liquid system, four typical inter-bubble interaction modes are identified:

(i) Interaction between a trailing bubble and the wake of its leading bubble results in coalescence and generates a larger bubble. Fan and Tsuchiya (1990) summarized that coalescence of a pair of bubbles occurs in four steps: (1) both bubbles align along the same axis in the vertical direction; (2) the trailing bubble accelerates and elongates due to wake suction; (3) the trailing bubble closely contacts the leading bubble; and (4) the thin liquid layer between the two bubbles drains and ruptures. They pointed out that the leading bubble wakes are the most important factor responsible for the bubble contact. Otake *et al.* (1977) observed that when the leading bubble is larger than the trailing one, the latter has a tendency to coalesce with the leading bubble.

(ii) Interaction between a trailing bubble and the wake of a leading bubble may also cause bubble breakup. Otake *et al.* (1977) observed that the bubble breakup process also includes three stages: (1) approaching of the trailing bubble to the leading bubble, (2) the elongation of the trailing bubble, and (3) trailing bubble breaking up. They also observed that when the leading bubble is smaller than the trailing bubble, the latter tends to break up.

(iii) Bubble-wake interaction may merely cause the acceleration and deformation of the trailing bubble. Because bubble coalescence and breakup require a sufficient bubble contact time or elongation (degree and time period), respectively, there is a possibility that the final stages of bubble coalescence and breakup cannot be satisfied.

(iv) Bubble wakes drag the liquid along with the rising bubble and cause local liquid upflow. To balance this, a liquid down flow region is found surrounding the bubble

rise region. When wall effects are significant, significant global liquid circulation occurs, which in turn causes small bubble lateral migration and backmixing.

It is important to note that bubble-wake interaction plays a very important role in these four inter-bubble interaction modes. Bubble wakes are significantly affected by liquid viscosity. Crabtree and Bridgwater (1967) reported that in a highly viscous liquid (ν_l = 8.34 cm^2/s), a negligible vortex was observed behind a single bubble but a systematic vortex eventually appeared as ν_l was reduced, which became stronger and larger as ν_l was further decreased. They also founded that vortex decay was slower at a lower ν_l. Bessler and Littman (1987) also reported that the primary wake behind a circularly capped bubble was smaller when the liquid viscosity was higher. The apparent viscosity of a fiber suspension increases exponentially with its fiber mass fraction (Bennington and Kerekes, 1996; Powell *et al.*, 2001). Thus, the bubble wakes in a fiber suspension will be significantly damped as its fiber mass fraction increases. Therefore, although these 4 inter-bubble interaction modes are also present in gas-liquid-fiber flows, their influence on gas bubble behavior will be less significant than in gas-liquid flow.

In a gas-liquid-fiber suspension, the global circulation is also affected by the ability of the fiber flocs to flow laterally toward the voids left behind a rising bubble. This ability decreases significantly with increasing fiber mass fraction. Thus, in a fiber suspension of higher fiber mass fraction, the global circulation is weaker and the suspension region covered by the global circulation is smaller. This agrees with Heindel (1999), who observed that in an air-water bubble column, air bubbles rose in a serpentine pattern and the bubbles were dispersed well in the upper part of the column, while in an air-water-fiber bubble column with C = 1.0% and the other conditions remained the same, the serpentine bubble rise pattern disappeared and bubbles only moved in a narrow region in the suspension, even at the column top. Heindel (2000) also observed that turbulent backmixing was less significant at a higher fiber mass fraction and it completely disappeared at C = 2.5%.

It should be pointed out that although the descriptions of the above modes are about two bubbles, similar interactions have been observed between more than two bubbles (Stewart, 1995).

The four inter-bubble interaction modes described above for gas-liquid systems are also present in gas-liquid-fiber systems. Additionally, there are three other inter-bubble interaction modes uniquely present in gas-liquid-fiber flows:

(v) A fiber network may slow down or even stop a leading bubble and a fast moving trailing bubble hits it, causing bubble coalescence. This mode of bubble coalescence does not require bubble-wake interaction and becomes more significant when the fiber mass fraction is high.

(vi) A leading bubble breaks the fiber network and trailing bubbles follow, rising with a smaller rising resistance. This effect is usually called gas channeling, which means that gas bubbles flow through the fiber suspension via preferential paths. The preferential paths usually exist for a short period of time as the passing bubbles gradually cause damages (e.g., erosion on floc surfaces) to the surrounding fiber network. When the total damage reaches a certain degree, the surrounding fiber networks collapses. The preferential paths last longer if the fiber mass fraction is high.

(vii) The bubble motion generates disturbances, reducing the fiber network strength, or even causing fiber network breakup and thus, fewer bubbles are entrained and bubbles rise faster. A severe case of this phenomenon is when multiple bubble motions may actually fluidize the fiber suspension.

4.2.4 Bubble motion in flowing fiber suspensions

In this section, a "flowing" fiber suspension means that there is a net suspension flowrate in a certain direction. Thus, in a cocurrent bubble column, the fiber suspension is a "flowing" one, while the suspension is a semi-batch bubble column is not.

4.2.4.1 Effects of flowing fiber suspensions on single bubble motion

When a single bubble is released into a flowing fiber suspension, it will assume the same velocity in the suspension flow direction in a short period of time because the bubble inertia is negligible compared to that of fiber suspension. The bubble may also move upward

relative to the fiber suspension if its size is sufficient to produce a large buoyant force. This relative upward movement is similar to the bubble motion in a quiescent fiber suspension, i.e., terminal bubble velocity. However, the fiber suspension flow induces turbulence, which reduces the fiber network strength, especially when the fiber suspension has a high velocity. Thus, for a given bubble, it has a lower tendency to become trapped in a flowing fiber suspension than in a quiescent fiber suspension. Under turbulent flow conditions, Ajersch and Pelton (1999a) observed that in addition to passing through voids between fibers and moving while disrupting the fiber network, a bubble can escape from a floc (i) when flocs are deformed, stretched, and broken due to local shear forces; and (ii) when the bubble is detached from under a floc due to velocity gradients between the floc and the surrounding fluid.

4.2.4.2 Effects of flowing fiber suspensions on bubble residence time and coalescence

There are three simple bubble translation modes in a flowing fiber suspension according to the local suspension flow direction: (i) cocurrent flow (local suspension flow upward), (ii) countercurrent flow (local suspension flow downward), and (iii) cross flow (local suspension flow in a horizontal direction), as shown in Fig 4.3.

In a cocurrent flow (Fig. 4.3a), the absolute bubble rise velocity (i.e., the bubble rise velocity relative to the suspension boundary, e.g., the column wall in a bubble column) is increased by the suspension. Thus, in a bubble column, cocurrent suspension flow reduces bubble residence time in the column. If a series of bubbles are released from the same locations successively with a certain frequency, the cocurrent suspension flow reduces the number of bubble-bubble contacts and thus, the probability of bubble coalescence.

In a countercurrent flow (Fig. 4.3b), the absolute bubble rise velocity is reduced by the fiber suspension and can be negative (i.e., the bubble actually flows downward) when the local suspension velocity is larger than the bubble terminal velocity. Some researchers also called it downward cocurrent flow when the absolute bubble rise velocity is negative, (e.g., Yamagiwa *et al.* (1990)). In a bubble column, bubble residence time is usually increased and

bubble coalescence is enhanced by the countercurrent liquid flow because the suspension tends to retain the bubbles for a longer time period in the region near the gas distributor.

In a cross flow (Fig. 4.3c), the bubble rise velocity is not affected and hence, the bubble residence in a fiber suspension remain the same, as far as the residence time is defined as the time required for a bubble to rise to the suspension surface. However, bubble coalescence is greatly reduced if a series bubbles is released from a given location because the fiber suspension will carry a bubble away from the distributor immediately after it is released and separate it from subsequent bubbles that are released.

4.2.4.3 Effects of flowing fiber suspensions on bubble formation

Bubble formation at a gas distributor has been reported to be significantly affected by local liquid flow conditions. Sada *et al.* (1978) observed that the bubble size formed in a cross-flowing liquid decreased with increasing superficial liquid velocity. Three bubble formation modes, i.e. single bubbles, coalescent bubbles and gas jets, were observed at different superficial gas and liquid velocities. Johnson *et al.* (1982) proposed a model indicating that the equivalent diameter of the bubbles decreased significantly with increasing liquid cross-flow velocity. Waldie *et al.* (1999) found that the Sauter mean diameter of bubbles formed in a liquid cross-flow was proportional to $V_c^{-1.64}$, where V_c is the liquid cross-flow velocity. Forrester and Rielly (1998) reported that increasing the liquid cross-flow velocity resulted in a significant decrease in the bubble size between a liquid velocity of 1 and 3 m/s for a constant gas injection flow rate, and further increases in the liquid velocity had a much smaller effect on bubble size.

The bubble sizes formed in a cocurrent gas-liquid flow also decrease with increasing liquid velocity when the gas distributor orifices face upward. Fawkner *et al.* (1990) found bubble size formed in a column increased with increasing superficial liquid velocity when the liquid was cocurrently pulsed into the column. Terasaka *et al.* (1999) reported that the bubble volume formed at a nozzle submerged in a cocurrent upward flow decreased with increasing liquid velocity. In a reduced gravity environment, Tsuge *et al.* (1997) also found bubble

volume formed in a cocurrent liquid flow decreased with increasing liquid velocity. Using a theoretical analysis, Chen and Tan (2002) also predicted a similar trend.

In a countercurrent gas-liquid flow with gas distributor orifices facing upward, the bubble generated at an aeration orifice is larger than that formed in a quiescent liquid. This is because the bubble detaches from the distributor aeration orifice in the opposite direction as that of the liquid flow. To detach from the aeration orifice, the bubble must overcome the resistance to the liquid flow. This makes the bubble subjected to a higher pressure from the aeration orifice and increases the bubble size. Tsuge *et al.* (1997) compared the effect of liquid flow direction on bubble size for a constant superficial liquid velocity and found that the bubble formed in the cross-flow conditions is the smallest while that in the countercurrent flow is the largest.

Liquid flows have also been reported to significantly influence bubble frequency and growth rate, which are two additional parameters in the bubble formation process (Tsuge *et al.*, 1997; Terasaka *et al.*, 1999; Chen and Tan, 2002).

In gas-liquid-fiber flow, the fiber suspension flow is expected to have a similar effect on gas bubble formation, especially when the fiber suspension is in a fluidized state. However, no direct observation of gas bubble formation in flowing fiber suspensions has been found in the literature. Further study is needed to characterize the effect of fiber suspensions on bubble formation.

4.3 Fiber Suspension Influences on Gas Holdup

When fibers are added to an air-water bubble column, bubble behavior will change due to the presence of fibers. Based on detailed observations from this study and available literature citations, six major mechanisms are proposed by which fibers influence gas holdup in a bubble column; they are summarized in Table 4.1 and details are provided below. Additional details can be found in Tang and Heindel (2005a).

Table 4.1: Major mechanisms influencing gas holdup in a gas-liquid-fiber bubble column.

Mechanism	Influence	Effect on gas holdup
I	Suppression of bubble coalescence	Increase
II	Increased bubble residence time	Increase
III	Enhanced bubble coalescence	Decrease
IV	Gas channeling	Decrease
V	Suppression of bubble breakup	Decrease
VI	Fluid property change	Increase

4.3.1 Mechanism I – Suppression of bubble coalescence

Fibers can work as separation "walls" between bubbles, reduce their contact opportunity, and thus suppress bubble coalescence. This effect is particularly significant when bubbles are uniformly distributed in a fiber suspension at a high fiber mass fraction where continuous fiber networks form (Tang and Heindel, 2005c). The ability of the fiber network to separate bubbles increases with increasing fiber mass fraction, but decreases with increasing bubble size and flow disturbance. Hence, in heterogeneous flows, characterized by large bubbles and turbulent mixing, Mechanism I has little influence on the large bubbles. However, small bubble coalescence can still be reduced by Mechanism I. This agrees with Heindel (2002), who observed more small bubbles in a fiber suspension than an air-water system operating under the same condition. Bubble coalescence can still be reduced even when the fiber mass fraction is not high enough to form continuous fiber networks. Temporary fiber flocs usually form under this condition (Kerekes *et al.*, 1985). The fiber flocs remain between bubbles and reduce their collision probability. In a bubble column, Mechanism I usually results in an increase in gas holdup.

4.3.2 Mechanism II – Increased bubble residence time

Fiber addition in a bubble column can increase bubble residence time. Fibers can form flocs or continuous fiber networks at high fiber mass fractions. The fiber networks can

hinder bubble motion, especially when bubbles are small and the fiber suspension velocity is lower than the bubble rise velocity. Walmsley (1992) observed that fiber-bubble collisions in a semi-batch bubble column slowed bubble rise velocity. Ajersch and Pelton (1999a) reported that a common phenomenon in flocculated fiber suspensions, was that "air bubbles migrated upwards in a series of random discrete steps as these bubbles became repeatedly trapped and released from the pulp flocs." Reese *et al.* (1996) recorded that the bubble rise velocity decreased with fiber mass fraction in a semi-batch air-water-fiber bubble column. They also reported that bubble rise velocity was higher near the column bottom, and the velocity difference between two fixed axial locations was larger at higher fiber mass fractions. These observations were attributed to the resistance and tortuosity of bubble rise paths, both of which increased with increasing fiber mass fraction. The fiber network can also entrain small bubbles and make them move with the network (Ajersch and Pelton, 1999a). This further enhances the bubble residence time because the residence time of a fiber suspension in a bubble column is typically longer than the gas phase residence time. One extreme example is that small bubbles stay in the fiber network even after the fiber suspension leaves the bubble column and is pumped back to the bubble column, causing a positive gas holdup even when no gas is released to the bubble column (Lindsay *et al.*, 1995). In semi-batch bubble columns or at low superficial liquid velocities in cocurrent bubble columns, Mechanism II causes a gas holdup increase in a bubble column, especially when small bubbles dominate the flow.

4.3.3 Mechanism III – Enhanced bubble coalescence

When fibers form continuous networks, the fiber network can slow down and trap smaller bubbles, allowing coalescence with trailing bubbles (Walmsley, 1992; Ajersch and Pelton, 1999a). This mechanism dominates the bubble behavior when three conditions are satisfied: (i) the diameter of the leading bubble is larger than the fiber spacing in the network; (ii) the leading bubble is not too large such that the buoyant force is not sufficient to break through the fiber network; and (iii) the bubble approaches the fiber network with a velocity higher than the local fiber suspension velocity. These three conditions hinder bubble rise and

allow coalescence with trailing bubbles. One situation where these conditions are easily satisfied is in a bubble column aeration zone where gas is directly distributed into the column by a sparger (Tang and Heindel, 2005c) or perforated plate (Reese *et al.*, 1996; Su and Heindel, 2003). Condition (i) is satisfied when C is high enough to form a fiber network. For a suspension having a fiber mass fraction between 0.5% - 1.0%, most fiber spacing is on the order of ten microns and it decreases with increasing fiber mass fraction (Ajersch and Pelton, 1999a). Bubbles generated in the aeration zone are generally much larger, on the order of several millimeters (Heindel, 1999, 2002). Condition (ii) is satisfied when C is high enough such that the fiber network is sufficiently strong to hold a newly generated bubble. Condition (iii) is always satisfied in a semi-batch bubble column, and easily satisfied in the entrance region of a cocurrent bubble column, where bubbles are released at relatively high speed from the gas distributor. Mechanism III causes a significant decrease in gas holdup, which is more evident at higher fiber mass fractions.

4.3.4 Mechanism IV – Gas channeling

When the fiber mass fraction is high, gas channeling occurs, significantly reducing the gas phase residence time. Channeling can occur at high fiber mass fractions (e.g., $C \approx 1.5\%$) when small bubbles are still found; in this case, a large bubble having a sufficient buoyancy force breaks through the fiber network and a non-static channel of low bubble rise resistance forms behind the bubble (Heindel, 2000). As the large bubble cleaves the fiber network, many small bubbles confined in the network near the path are released into the low fiber mass fraction channel, following behind the fast rising large bubble (Walmsley, 1992; Ajersch and Pelton, 1999a). When the fiber suspension is very dense (e.g., $C \gtrsim 3.5\%$), a different type of channel forms. It becomes difficult for discrete bubbles to rise through the suspension and discrete semi-static gas channels are formed to allow the gas to pass. These channels remain active for periods of time ranging from a few seconds to a few minutes (Heindel, 2000). Both types of channels severely shorten the gas phase residence time. Mechanism IV results in a gas holdup decrease in a bubble column.

4.3.5 Mechanism V – Suppression of bubble breakup

The presence of fibers in a bubble column can also suppress bubble breakup. It is very common that bubble breakup and coalescence occur simultaneously in a bubble column (Otake *et al.*, 1977; DeSwart *et al.*, 1996). The bubble size distribution in the bubble column is determined by the dynamics of these two processes. It is widely accepted that only velocity fluctuations over a distance approximately equal to the bubble diameter are capable of causing bubble deformation and breakup while larger eddies merely transport the bubble (Clift *et al.*, 1978; Walter and Blanch, 1986). Several studies have shown that the presence of fibers significantly changes velocity fluctuations in a turbulent flow field (Forgacs *et al.*, 1958; Norman *et al.*, 1978; Steen, 1989b; Andersson and Rasmuson, 2000). For most situations, turbulence intensity is reduced and turbulence damping occurs mainly at small length scales (Steen, 1989b). Thus, the addition of fibers can affect bubble shape and reduce bubble breakup. Mechanism V decreases gas holdup.

4.3.6 Mechanism VI – Fluid property changes

Fiber addition can modify fluid properties, such as surface tension, when surface-active agents leach from the fiber into the liquid. Surfactants may also be added to the slurry for desired process characteristics (e.g., foam formation) (McCool, 1993; Dessureault *et al.*, 1995; Hardie *et al.*, 1999b). Changes in the fluid properties can affect bubble size and bubble behavior. This can occur with certain types of cellulose (Janse *et al.*, 1999) or synthetic (Su and Heindel, 2004b) fibers. The surface-active agents usually cause a decrease in liquid surface tension, and produce a smaller, more stable bubble (i.e., one less prone to coalescence). Mechanism VI will increase gas holdup.

4.3.7 Summary of the fiber suspension influence on gas holdup

Mechanisms I-V are all functions of fiber suspension properties, which are in turn affected by fiber mass fraction and fiber physical properties. In a bubble column filled with a suspension made of longer, more flexible, and less coarse fibers, Mechanisms I-V tend to be

stronger, providing other conditions (including fiber mass fraction, flow conditions, and lignin content, etc.) are similar. Since fiber physical properties vary with fiber type, gas holdup can change significantly in different fiber suspensions.

It is important to note that Mechanisms I–VI are not equal in their influence on gas holdup. Only a few of the mechanisms influence gas holdup for a given condition, and their importance changes with operating conditions. In most cases with semi-batch or cocurrent gas-liquid-fiber bubble columns, Mechanism III will dominate the flow; Mechanisms I, II, and V may also affect bubble behavior, but are less significant. However, if the fiber suspension has a vertical velocity larger than the bubble rise velocity of newly released bubbles, Mechanism III is negligible. Also, if the bubbles are distributed within a fiber suspension before they enter a bubble column, Mechanism I will dominate the bubble behavior in the lower region of the bubble column (Lindsay *et al.*, 1995; Schulz and Heindel, 2000; Xie *et al.*, 2003b; Tang and Heindel, 2005c). Finally, if surfactants are present, Mechanism VI may dominate the entire system (Janse *et al.*, 1999).

4.4 Summary

Flocculated fiber suspensions are considered as a mixture of fiber and suspending medium comprising flocs and inter-floc regions. Fiber suspension properties are discussed based on this fiber suspension structure. Single bubble motions in fiber suspensions are explained using the proposed fiber suspension structure theory. Seven inter-bubble interaction modes are identified and the effects of the fiber suspension on them are examined. Following the discussion of fiber suspension structure and bubble motion, six mechanisms are outlined for fiber influences on gas holdup in gas-liquid-bubble columns; these mechanisms are used in the following chapters to explain the observed results

Figure 4.1: Sketch of a flocculated fiber suspension structure.

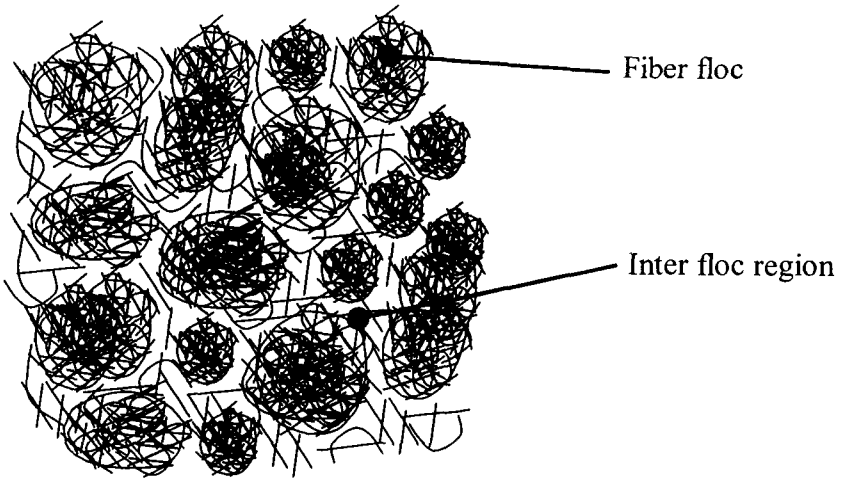

Figure 4.2: Sketches of single bubble entrainment and movement in a fiber suspension.

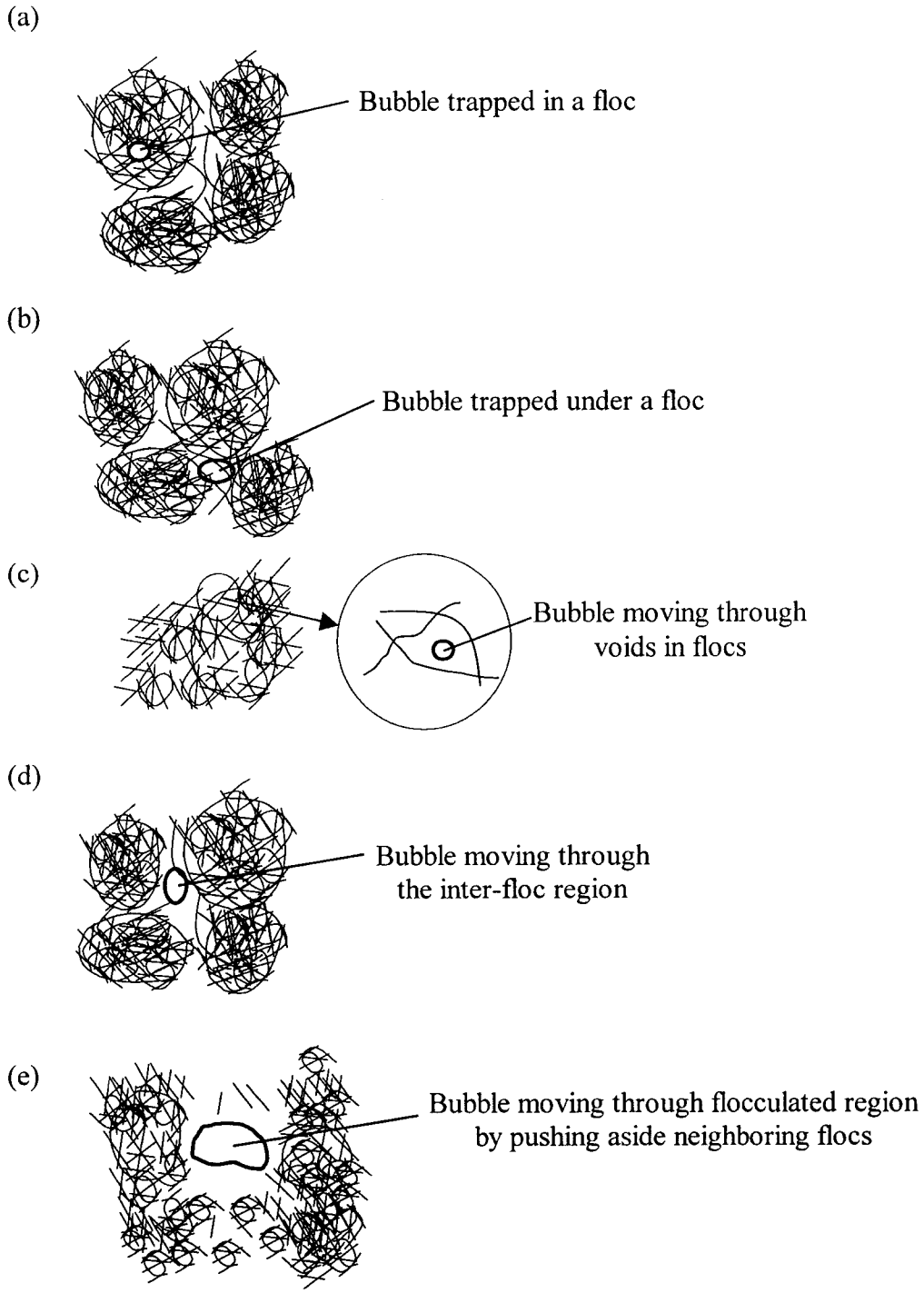

Figure 4.3: Three simple bubble translation modes in flowing fiber suspensions: (a) cocurrent flow; (b) countercurrent flow; and (c) cross flow.

(a)

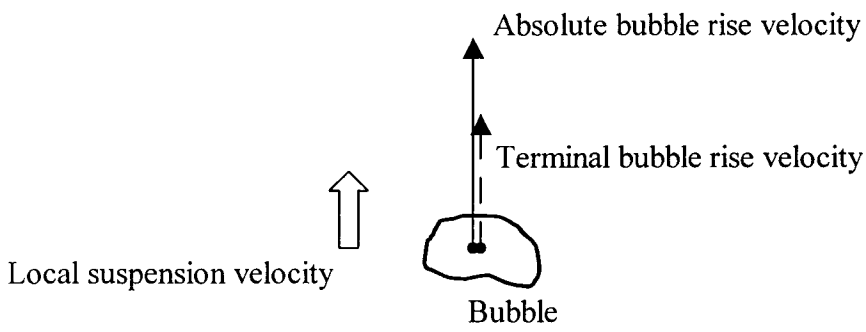

(b)

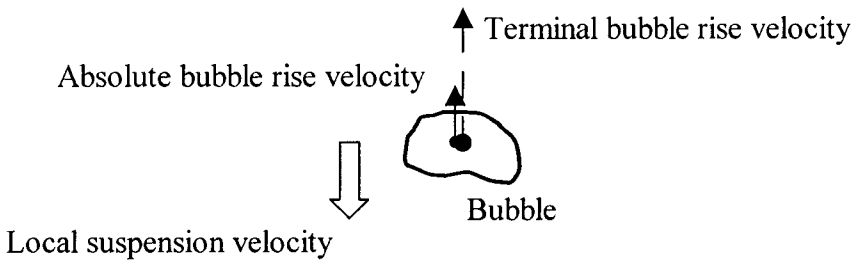

(c)

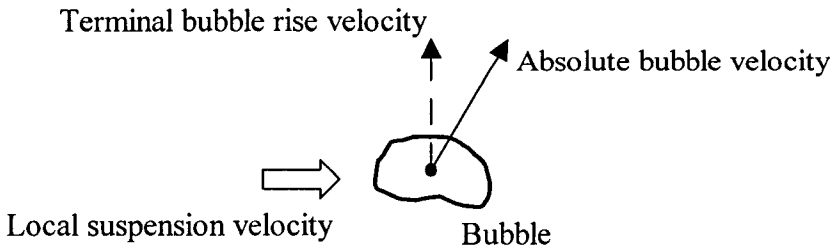

Chapter 5: EXPERIMENTAL RESULTS

In this chapter, the experimental results of the present study are presented in detail. The first section discusses the general trends of gas holdup in the cocurrent air-water-fiber bubble column in which variations in the superficial gas and liquid velocity and fiber mass fraction are analyzed, with a primary focus on hardwood fiber suspensions. The second section presents influences of fiber type. The third section uses the drift-flux model to identify distinct gas flow regimes. Finally, this chapter concludes with a brief summary.

5.1 Gas Holdup in Hardwood Fiber Suspensions

The data collected in hardwood fiber suspensions are first presented. The effect of operating conditions, including superficial gas and liquid velocity and fiber mass fraction, on gas holdup in hardwood fiber suspensions are analyzed in detail. Axial gas holdup variations are also discussed. A significant portion of the results in this section have been presented in Tang and Heindel (2005c).

5.1.1 Effect of superficial gas velocity

Figure 5.1 shows the variation of ε with U_g at different U_l and C in a cocurrent bubble column. Gas holdup increases with increasing U_g for all conditions addressed in this study. There is no local gas holdup maximum, which is observed at low fiber mass fractions in a 15.24 cm air-water-Rayon fiber semi-batch bubble column with a perforated plate gas distributor (Su and Heindel, 2003). At low fiber mass fractions (C = 0.1%, Fig. 5.1b), the gas holdup is similar to that of an air-water system (C = 0%, Fig. 5.1a). When $U_g \lesssim 4$ cm/s, gas holdup increases proportionally with U_g. At $U_g \approx 0$ cm/s, gas holdup is very close to zero, suggesting no air entrainment in the fiber suspension. When $U_g \gtrsim 13$ cm/s, gas holdup increases linearly with U_g, but the slope is less than that when $U_g \lesssim 4$ cm/s. At high fiber mass fractions (C = 1.0%), gas holdup also increases with U_g. At $U_g \approx 0$ cm/s, gas holdup is

nonzero, due to a small amount of air entrained in the fiber suspension ($\varepsilon \approx 0.005$). The small amount of entrained air can actually be observed in the pump suction line. Similar results were reported by Lindsay *et al.* (1995) and were attributed to the same reason.

5.1.2 Effect of superficial liquid velocity

5.1.2.1 Results from the present study

Generally, gas holdup decreases with increasing U_l providing U_g and C are constant. Figure 5.1 shows the results for C = 0%, 0.1% and 1.0%. The effect of U_l on ε is similar when C = 0.1% and 0%. When C = 1.0% (Fig. 5.1b), gas holdup still decreases with increasing U_l, albeit over a smaller ε range. The decrease is attributed to the bubble residence time decrease due to increasing superficial liquid velocity.

Figure 5.2 compares the trend of ε with increasing U_l at different C when U_g = 4, 13, and 20 cm/s. The effect of U_l on ε is more significant at lower fiber mass fractions (e.g., C $\lesssim$ 0.6%). This is more evident at a low superficial gas velocity (e.g., U_g = 4 cm/s, Fig. 5.2a), where gas holdup nearly remains constant at higher fiber mass fractions (e.g., C =1.5%), than at a high superficial gas velocity (e.g., U_g = 20 cm/s, Fig. 5.2c), where the gas holdup clearly decreases with increasing superficial liquid velocity at 1.5%. The difference between the superficial liquid velocity effect at low and high fiber mass fractions can be explained by the fact that the number of large bubbles increases with increasing fiber mass fraction (Heindel, 2002). Large bubbles dominate the flow in the bubble column at the higher fiber mass fractions and have a much smaller residence time. Hence, increasing the superficial liquid velocity does not significantly decrease their residence time.

5.1.2.2 Literature comparisons

The effect of U_l on ε in this study agrees with the results reported by (Xie *et al.*, 2003b) for the cross-sectional average gas holdup in a 5.08 cm cocurrent bubble column filled with a kraft softwood fiber suspension and 21 cm/s $\leq U_l \leq$ 51 cm/s. However, Schulz

and Heindel (2000) reported that the cross-sectional average gas holdup increased with increasing U_l (2.5 cm/s $\leq U_l \leq$ 7.5 cm/s) when C = 0%, 0.8% or 1.2% at a lower position (H = 50.8 cm), this trend was significant only when C = 0.8% at a higher column position (H = 132.1 cm) in a 12.7 cm diameter cocurrent bubble column using old news paper (ONP) fiber. The difference in results is attributed to the method of gas distribution.

Schulz and Heindel (2000) used forced air injection, where air was dispersed by shear forces into the fiber suspension in a 2.5 cm pipe prior to a conical diffuser at the bottom of their bubble column. With this method, bubbles that are formed in the 2.5 cm pipe are carried away by the fiber suspension right after they are released. The velocity of the fiber suspension in the 2.5 cm pipe is about 0.625 m/s to 1.875 m/s when 2.5 cm/s $\leq U_l \leq$ 7.5 cm/s. As a result, bubbles are uniformly distributed in the fiber suspension and bubble coalescence after gas injection is minimized. Bubble coalescence is further inhibited by the presence of fiber networks, which work as separating "walls" between bubbles. The effective thickness of the "walls" is larger at higher fiber suspension flowrates (i.e., the relative bubble rise velocity is minimized).

Furthermore, it is well documented that when bubbles form in a liquid cross-flow, bubble size decreases significantly with increasing liquid velocity (Maier, 1927; Johnson *et al.*, 1982; Forrester and Rielly, 1998; Waldie *et al.*, 1999). Maier (1927) reported that bubble size decreased with increasing cross-flow velocity, typically by a factor of about 3, over the liquid velocity range 0 – 3.74 m/s. Johnson *et al.* (1982) proposed a model indicating that the equivalent diameter of the bubbles decreased significantly with increasing liquid cross-flow velocity. Waldie *et al.* (1999) found that the Sauter mean diameter of bubbles formed in a liquid cross-flow was proportional to $V_c^{-1.64}$, where V_c is the liquid cross-flow velocity. Forrester and Rielly (1998) reported that increasing the liquid cross-flow velocity resulted in a significant decrease in the bubble size between a liquid velocity of 1 and 3 m/s for a constant gas injection flow rate, and further increases in the liquid velocity had a much smaller effect on bubble size.

As a result, the smaller bubbles formed in the entrance region of Schulz and Heindel (2000), coupled with the large effective separating "wall" thickness found in fiber suspensions, increased gas holdup with increasing U_l.

As the bubbles and fiber suspension flow upward along the bubble column, more and more bubble-bubble interaction is observed, resulting in bubble coalescence. At higher column positions, bubble coalescence dominates the flow. The resulting large bubbles have a very large velocity. Hence, the relative bubble rise velocity is sufficient to be unaffected by the superficial liquid velocity. As a result, the effect of superficial liquid velocity on gas holdup at high positions is less significant than at low positions.

This explanation also agrees with the result of Schulz and Heindel (2000) that the effect of superficial liquid velocity on gas holdup was more evident at lower column positions, where the entering bubble size had a significant influence on gas holdup.

Xie *et al.* (2003b) used a hydrosonic mixer to create gas-liquid mixing. Gas was first introduced to the liquid line and relatively large bubbles were formed. The gas-liquid mixture then passed through a hydrosonic mixer, where the large bubbles were reduced in size by a specially designed rotating disk, creating millions of uniformly distributed micro-bubbles due to cavitation and a cavitation induced shock wave (Hudson and Kazem, 2003). When the well-mixed gas-liquid mixture exited the mixer, the micro-bubbles began to agglomerate into larger bubbles. The agglomeration of micro-bubbles is homogeneous inside the suspension, and when the bubble size is larger than the fiber spacing, bubble movement is confined by the fiber network and bubble agglomeration stops. The agglomeration process of micro-bubbles is not significantly affected by the liquid velocity because the process occurs in a smaller length scale than fiber flocs, most of which flow in their entireties. As a result, the gas holdup decreases with increasing U_l due to a decrease in bubble residence time.

In the current study, however, air was released from a spider sparger with uniformly distributed 1.6 mm holes at the bottom of the bubble column after the water-fiber suspension enters the column. Gas exits the sparger holes in the same direction as the liquid. Under most operating conditions, the bubble rise velocity at release from the sparger holes is higher than the suspension velocity. This and the liquid circulation in the bubble column cause the bubbles to migrate toward the column center (Tzeng *et al.*, 1993; Chen *et al.*, 1994), resulting in bubble coalescence. The presence of fiber networks significantly enhances bubble coalescence. At higher fiber mass fractions, bubble coalescence occurs right above the sparger. Increasing U_l in the range of 0 cm/s $\leq U_l \leq$ 10 cm/s does not provide a uniform

bubble distribution in the fiber suspension. Hence, the decrease in gas holdup due to a decreasing bubble residence time with increasing U_l is not offset by the potential gas holdup increase due to the inhibition of bubble coalescence by increasing U_l.

5.1.3 Effect of fiber mass fraction

5.1.3.1 Results from the present study

Figure 5.3 shows the effect of fiber mass fraction on gas holdup when U_l = 8 cm/s and 0 cm/s ≤ U_g ≤ 20 cm/s. When C ≤ 0.2%, the ε-U_g curves overlap, indicating an insignificant influence of fiber mass fraction on gas holdup. This is because at C = 0.1% and 0.2%, fiber flocculation does not occur and bubble movement in the fiber suspension is similar to that of water. When U_g ≥ 2 cm/s, starting with C = 0.4%, ε decreases significantly with C when C ≤ 1.5% and U_g and U_l are constant, and this is attributed to fiber flocculation. As fibers flocculate, bubble movement near the sparger is suppressed by the fiber network, resulting in enhanced coalescence between leading and trailing bubbles. This is supported by observations of Ajersch and Pelton (1999a) and Walmsley (1992). As a result, much larger bubbles appear in the lower column positions (Heindel, 1999; 2002), and they rise faster, reducing gas holdup. The resistance to bubble movement due to fiber network formation increases with fiber mass fraction. Thus, bubble coalescence also increases with increasing fiber mass fraction, which results in a significant decrease in gas holdup with increasing fiber mass fraction.

The presence of fibers also reduces gas holdup by inhibiting bubble breakup. It is widely accepted that in turbulent flow fields, only eddies of scales close to the bubble diameter are capable of causing large bubble deformation and breakup; larger eddies merely transport the bubbles (Clift *et al.*, 1978; Walter and Blanch, 1986; Hesketh *et al.*, 1991; Risso, 2000). As fibers are added, small-scale eddies are suppressed and the suppression is stronger at higher fiber mass fraction (Forgacs *et al.*, 1958; Norman *et al.*, 1978; Steen, 1989b; Andersson and Rasmuson, 2000). Hence, bubble shape is affected and bubble breakup is reduced in fiber suspensions. This is supported by observation of Heindel and Monefeldt

(1998) that the bubbles in a C = 0.5% fiber suspension were more spherical than those in pure water in the same semi-batch bubble column.

When $U_g \approx 0$, ε at higher C is a little higher than those at lower C because of gas entrainment ($\varepsilon \approx 0.005$) in the fiber suspension. When C is increased to 2.0%, the gas holdup is higher than that at C = 1.0%, 1.2% and 1.5% over the entire range of superficial gas velocities. This is attributed to a significant increase in the amount of gas entrained in the fiber suspension, which is not released in the gas-liquid separator or the reservoir when C = 2.0%. This is supported by visual observations of small gas bubbles in the pump suction line when C = 2.0%. The increase in the amount of retained gas in the fiber network is larger than the decrease in gas holdup associated with an increase in fiber mass fraction. This agrees with Lindsay *et al.* (1995), who found the amount of gas retained in the fiber suspension increased with U_g much faster when C = 2.0% than when C = 1.0%.

Figures 5.4 and 5.5 reveal specific gas holdup changes as a function of fiber mass fraction. According to both figures, gas holdup is not significantly affected by fiber mass fraction when $C \leq 0.2\%$. In some conditions (e.g., U_g = 5 cm/s and U_l = 6 cm/s), gas holdup at C = 0.1% may be slightly higher than that of C = 0% or C = 0.4%. When $0.4\% \leq C \leq 1.0\%$, gas holdup declines sharply with increasing C. When $1.2\% \leq C \leq 1.5\%$, the gas holdup decline is less severe with increasing C, and in some cases, negligible. This is attributed to 2 factors: (i) the amount of entrained gas in the fiber suspension increases with increasing fiber mass fraction and compensates for the decrease in gas holdup due to increasing fiber mass fraction; and (ii) when $C \geq 1.2\%$, most newly generated bubbles coalesce in the aeration zone so increasing fiber mass fraction does not enhance bubble coalescence as effectively as the same increase in fiber mass fraction in the range of $0.4\% \leq C \leq 1.0\%$.

At U_g = 20 cm/s (Fig. 5.4), ε decreases with C in the same manner for all U_l, indicating a negligible influence of U_l on the effects of fiber mass fraction at high superficial gas velocities. However, when U_g = 5 cm/s and $C \geq 1.0\%$, all gas holdup values converge. The difference is attributed to the effect of the suspension flow. When U_g = 20 cm/s, a large number of bubbles are released from the sparger holes with velocities higher than the suspension velocity. Significant bubble coalescence and backmixing occurs at all superficial

liquid velocities. Thus, increasing fiber mass fraction at each U_l results in a similar gas holdup variation. When U_g = 5 cm/s, only a small number of bubbles are released from the sparger holes and their velocity is small. At zero and low superficial liquid velocities, bubble velocity is higher than the suspension velocity. Bubble coalescence and backmixing are significant. Thus, increasing fiber mass fraction results in a similar gas holdup variation as the trend observed at U_g = 20 cm/s. At high superficial liquid velocities, the bubble velocity is lower than the suspension velocity. Bubbles are carried away from the sparger and bubble coalescence and backmixing are inhibited. The gain in gas holdup due to inhibition of bubble coalescence is offset by loss in gas holdup due to a decrease in the bubble residence time. As a result, increasing C does not significantly affect gas holdup. This explanation can also be used to explain the results presented in Fig. 5.5, which shows that at both high (e.g., U_l = 8 cm/s, Fig. 5.5a) and low (e.g., U_l = 0 cm/s, Fig. 5.5b) superficial liquid velocities, the shape of the ε-C curve is similar for all superficial gas velocities except at very low values (U_g = 2 cm/s), where gas holdup is nearly constant for the range of fiber mass fractions in this study.

5.1.3.2 Literature comparisons

It is noticed that the trend of gas holdup variation with fiber mass fraction in this study is different from the observations of Lindsay *et al.* (1995), Schulz and Heindel (2000), and Xie *et al.* (2003b). They all reported that gas holdup increased with increasing fiber mass fraction in cocurrent bubble columns in certain ranges of fiber mass fractions. Lindsay *et al.* (1995) observed gas holdup at C = 1% was higher than that at C = 0% when U_l = 2.5 cm/s or 5 cm/s. Using the same bubble column, Schulz and Heindel (2000) observed cross-sectional average gas holdup reached its maximum when C = 0.8%. Xie *et al.* (2003b) reported that cross-sectional gas holdup in a 5.08 cm cocurrent bubble column was much higher when C = 1.0% or 1.5% than C = 0.5%. The difference is mainly caused by the different gas distribution methods used in these studies. Lindsay *et al.* (1995) and Schulz and Heindel (2000) used a forced air injection method, while Xie *et al.* (2003b) used a hydrosonic pump to mix air into the fiber suspension. Both methods are described in the

previous section. One important characteristic of both gas distribution methods is that gas can be uniformly distributed in the fiber suspension and bubble coalescence at the bubble column entrance region is inhibited. At higher fiber mass fractions, the fiber network strength and thus the inhibition of bubble coalescence is stronger, when well-dispersed bubbles are initially present in the suspension.

The decrease in gas holdup observed by Schulz and Heindel (2000) when C was increased from 0.8% to 1.2% is not fully understood. One possible explanation is that when C = 1.2%, the fiber network was strong such that the high velocity air-suspension mixture from the 2.5 cm pipe was not uniformly distributed via the conical expansion, which was assumed to occurred at C = 0.8%. This may have caused channeling in the entrance region (bubbles traveling in a preferential path), resulting in enhanced bubble coalescence and a corresponding reduction in gas holdup.

5.1.4 Axial gas holdup variation

Figure 5.6 presents the sectional average gas holdup distribution at different superficial liquid velocities when U_g = 18.5 cm/s and C = 0.1% or 1.0%. Generally, the difference between the sectional average gas holdups in sections 2 and 3 is much less significant than that between sections 1 and 2 or sections 3 and 4. The average gas holdup in section 1 is significantly lower because in section 1, especially in the region right above the sparger, bubbles flow upward rather fast with paths less tortuous than those in sections 2-4, where gas backmixing is significant, which enhances bubble residence time. It is also noticed that the difference between ε_1 and ε_2 increases with increasing U_l, particularly at low fiber mass fractions (e.g., C = 0.1%). This is due to a shorter bubble residence time in section 1 at higher U_l.

The higher average gas holdup in section 4 than that in section 3 can be attributed to two reasons: (i) large voids that are formed when large bubbles are violently released at the top of the column; and (ii) small bubbles are entrained from the column exit and carried downward with backmixed liquid (Lindsay *et al.*, 1995; Schulz and Heindel, 2000). At low fiber mass fractions (e.g., C = 0.1%), flocculation is insignificant and no fiber networks form,

thus, bubble entrainment at the column exit is insignificant, but the void formation at the column exit is very significant at high superficial gas velocities (e.g., U_g = 18.5 cm/s). When the large voids form, they temporarily reduce the liquid surface in the bubble column to a height below pressure transducer P_5 for a time period that decreases with increasing U_l. If the superficial liquid velocity is smaller than a critical value, the time period is long enough to produce a significant error in ε_4 due to the liquid height being below P_5. The error makes the ε_4 larger than its real value, and it increases with decreasing superficial liquid velocity, as shown in Fig. 5.6. When the superficial liquid velocity is sufficiently large (e.g., U_l = 10 cm/s, Fig. 5.6), the voids are quickly filled by liquid upflow, making the error less significant. The gas holdup error due to void formation at the column exit is the reason why ε_4 is not included in the average column gas holdup. At high fiber mass fractions (e.g., C = 1.0%), fiber network formation and bubble entrainment at the column exit are significant. This influences ε_4 most because the entrained small bubbles coalesce with other bubbles and rise, and only a small fraction of the small bubbles migrate to lower column sections. Additionally, visual observations for C = 1% reveal pressure transducer P_5 is seldom exposed to air (i.e., the large bubble release is less violent at the higher fiber mass fractions). Hence, $\varepsilon_3 - \varepsilon_4$ does not change with superficial liquid velocity at C = 1% (Fig. 5.6).

Figure 5.7 compares the average gas holdups in sections 1, 2, and 3 as a function of fiber mass fraction at U_l = 8 cm/s. The difference between gas holdup in sections 2 and 3 is negligible when U_g = 5 cm/s, but is apparent and increases slightly with fiber mass fraction when U_g = 18 cm/s and $C \geq 0.6\%$. This is due to bubble entrainment, which is insignificant when U_g = 5 cm/s for all $C \leq 1.5$, but is significant and increases with increasing fiber mass fraction when U_g = 18 cm/s and $C \geq 0.6\%$. As indicated in Fig. 5.7, the gas holdup in section 1 is significantly lower than that in sections 2 and 3 for all studied conditions due to a shorter bubble residence time in section 1. In addition, there are two points to notice in Fig. 5.7 regarding the difference between ε_1 and ε_2 (or ε_3) as a function of fiber mass fraction. First, when $0 \leq C \leq 0.4$, the difference between ε_1 and ε_2 (or ε_3) at U_g = 5 is very similar to that at 18 cm/s. However, when $C \geq 0.6\%$, the difference is smaller at U_g = 5 cm/s. This is because at $C \geq 0.6\%$, bubble entrainment at the column exit and backmixing is significant and it is more evident at higher superficial gas velocities. Second, the difference between ε_1 and ε_2 (or

ε_3) increases when C increases from 1.2% to 1.5% at both high and low superficial gas velocities. This is because at a fiber mass fraction as high as 1.5%, the gas-fiber slurry in section 1 is not fully mixed, resulting in temporary channeling or preferential paths of bubble movement, which makes the gas holdup decrease sharply in section 1, as indicated in Fig. 5.7. However, the gas-fiber mixture in sections 2 and 3 are still well mixed; thus the difference ε_2 - ε_1 increases.

5.1.5 Air-water-fiber to air-water gas holdup ratio

The effect of fiber on gas holdup in air-water-fiber bubble columns is also revealed by comparing the gas holdup obtained with and without fiber addition in the same bubble column at the same operating conditions. The air-water-fiber to air-water gas holdup ratio ($\varepsilon/\varepsilon_{A\text{-}W}$), simplified as "gas holdup ratio" in the following description, is defined as the ratio of gas holdup in an air-water-fiber bubble column (ε) to the gas holdup in the same bubble column with only air and water flowing ($\varepsilon_{A\text{-}W}$) at the same superficial liquid and gas velocity. It reflects the change in gas holdup resulting from fiber addition in an air-water bubble column. It also represents the degree to which an air-water-fiber bubble column behaves like an air-water bubble column.

Figure 5.8 shows the variation of gas holdup ratio ($\varepsilon/\varepsilon_{A\text{-}W}$) with increasing superficial gas velocity at different fiber mass fractions in hardwood fiber suspensions with U_l = 8 cm/s. When $0.05\% \leq C \leq 0.2\%$, the gas holdup ratio is initially slightly larger than 1, indicating a slight increase in gas holdup is obtained in the air-water-fiber bubble column than in the air-water bubble column; when the superficial gas velocity is larger than a value between 5 and 10 cm/s, the gas holdup ratio approaches 1.0 and remains constant. This is because at very low fiber mass fractions, fibers can slightly slow down and separate bubbles. Thus, the bubble residence time slightly increases and a slight gas holdup increase is obtained at low superficial gas velocities. At high superficial gas velocity, turbulent mixing is very strong in the bubble column and the bubble size is much larger, the very dilute fiber suspensions behave very similar to water. It is also noticed that as superficial gas velocity increases, the

gas holdup approaches 1.0 asymptotically without a significant local minimum, which is different from the results at $0.4\% \leq C \leq 1.5\%$.

When $0.4\% \leq C \leq 1.5\%$, the gas holdup ratio becomes less than 1 for most conditions, indicating a significant fiber effect on gas holdup at all studied superficial gas velocities. The gas holdup ratio decreases with increasing fiber mass fraction because gas holdup decreases with increasing fiber mass fraction in this C range. A general trend in this fiber mass fraction range is the gas holdup ratio at first decreases with increasing superficial gas velocity and reaches a minimum value at $U_g \approx 4\sim5$ cm/s, then increases with increasing superficial gas velocity. The initial decrease of the gas holdup ratio can be explained by the bubble coalescence enhancement. At very low superficial gas velocities, the fiber suspension is not well fluidized and consists of fiber networks, which can slow down or trap gas bubbles and make them coalesce with trailing bubbles. This bubble coalescence enhancement mechanism is especially significant at the sparger zone, where bubbles are released at a much larger velocity than the local fiber suspension velocity. As the superficial gas velocity increases, more gas bubbles are released and thus, more bubbles coalescence occurs in the fiber suspension. Consequently, the gas holdup ratio decreases. However, as the superficial gas velocity increases and more large bubble forms, the mixing in the fiber suspension becomes stronger, and thus, the fiber suspension behaves more like water. This is a mechanism that causes the gas holdup ratio to increase with increasing U_g. It is negligible at very low superficial liquid velocities, but dominates the flow at high superficial velocities. When this mechanism dominates, the gas holdup ratio reaches a minimum and then increases with increasing superficial gas velocity. The increase in the gas holdup ratio after the local minimum is also explained by the following fact: at high superficial gas velocities, bubble coalescence becomes strong in air-water bubble columns; addition of fibers into the bubble column can further enhance the bubble coalescence; however, this enhancement will not cause a gas holdup decrease as significant as that resulting from an addition of the same amount of fiber at a low superficial gas velocity (but higher than 4~5 cm/s), at which bubble coalescence is much less significant.

The difference between the $\varepsilon/\varepsilon_{A\text{-}W}$ versus U_g curve before and after $C = 0.4\%$ (i.e., without or with a local minimum) can be explained by the fact that there is negligible fiber

flocculation when $0.05\% \leq C \leq 0.2\%$ (even when U_g is small), which is not the case at when $C \geq 0.4\%$.

Figure 5.9 shows the effect of superficial liquid velocity on $\varepsilon/\varepsilon_{A\text{-}W}$. At C = 0.1% (Fig. 5.9a), the gas holdup ratio is not affected by superficial liquid velocities when $U_l > 0$. This is explained by the fact that the fiber suspension at C =0.1% behaves similar to water and changing superficial liquid velocity does not change the suspension rheological properties. At C = 1.0% (Fig. 5.9b), the gas holdup ratio generally increases with increasing superficial liquid velocity. The effect is more significant at low superficial gas velocities. This is because increasing superficial liquid velocity enhances fluidization of the fiber suspension, which is rheologically different from tap water and enhances gas bubble coalescence before fluidization. The superficial liquid velocity effect is less significant at high superficial gas velocities because the fiber suspension is usually well mixed even at low superficial liquid velocities due to the strong turbulent mixing caused by large fast-rising bubbles. It is also noticed that the gas holdup ratio at $U_l = 0$ cm/s is quite different from that at $U_l > 0$ cm/s. This is not fully understood and may be attributed to the difference between semi-batch and cocurrent bubble columns. The data at C = 0.05 and 0.2% show results similar to that presented in Fig. 5.9a, while the data when $C \geq 0.4\%$ show results similar to Fig. 5.9b.

Figure 5.10 compares the gas holdup ratio for sections 1, 2, and 3 at two fiber mass fractions (C = 0.1% and 1.5%) when $U_l = 8$ cm/s. Generally, the gas holdup ratio is larger in a higher section. This is attributed to the stronger mixing in the higher section. It is also noticed that the difference between the gas holdup ratio in different sections is less significant at the lower fiber mass fraction (i.e., C = 0.1%), because mixing is more uniform at C = 0.1%.

5.2 Effect of Fiber Type on Gas Holdup

In section 5.1, the influence of various factors (including superficial gas and liquid velocity, fiber mass fraction, and axial position) on gas holdup in hardwood fiber suspensions was discussed in detail. Gas holdups in suspensions of five other fiber types have also been investigated. In this section, the gas holdup values in the six types of fiber suspensions are

compared and the effect of fiber type on gas holdup is discussed. In Chapter 4, six mechanisms, of fiber influences on gas holdup were identified. They are used in this section to explain the experimental results, which have also been summarized in Tang and Heindel (2005a).

5.2.1 Fiber suspension surface tension and pH

There is no significant change in pH for the various operational conditions and fiber mass fractions addressed in this study. The pH for the different fiber types range 7.0~8.5, which is close to that of tap water.

The surface tension (σ) of the filtrate from softwood and BCTMP fiber suspensions as a function of fiber mass fraction is compared in Fig. 5.11, where the error bars show the standard deviation of multiple measurements. The surface tension of the softwood fiber suspension filtrate does not significantly vary with fiber mass fraction, staying in the 63~69 mN/m range. This is close to that of tap water (~70 mN/m). Measurements in hardwood fiber suspensions at both low and high fiber mass fractions show similar surface tension values to that of softwood fiber. The surface tension of the BCTMP fiber suspension filtrate, however, decreases significantly with increasing fiber mass fraction in the range $0.05\% \leq C \leq 0.8\%$ and remains relative constant at about 50 mN/m when $1.0\% \leq C \leq 1.5\%$. This is reflected by a significant amount of foam observed in the reservoir and pump suction line. The BCTMP fiber used in this study was produced using sodium sulfite. Although the resulting pulp was washed and neutralized after beaching, it may still contain a small amount of lignosulfonates. Since lignosulfonate is water-soluble and a soap, it is believed that it was responsible for the foam that was produced with BCTMP fiber. The surface tension of the Rayon fiber suspensions filtrate is similar to that of water because it is the goal of the Rayon fiber processing procedure (see Sec. 3.3.1).

Since only BCTMP fiber suspension surface tension is significantly different from the other fibers, Mechanism VI (see Chapter 4 and Table 4.1) will be considered in the following discussion only when BCTMP results are mentioned.

5.2.2 Gas holdup variation with fiber mass fraction

Typical gas holdup variation with fiber mass fraction in different fiber suspensions are presented in Fig. 5.12 for 6 combinations of superficial gas and liquid velocities (U_l = 8, 4 cm/s and U_g = 20, 10, 4 cm/s). Similar trends are observed for all 6 cases. They are also seen for data taken at other superficial gas and liquid velocities. The general trends are described in the following paragraphs mainly based on the results obtained at U_l = 8 cm/s and U_g = 20 cm/s (Fig. 5.12a).

An overview of Fig. 5.12 indicates that the gas holdup for softwood and 6 mm Rayon fiber suspensions are very similar for all studied conditions. Gas holdup similarity between hardwood and 3 mm Rayon fiber suspensions is also observed. It is not fully understood why the gas holdup for the two pairs of fiber types are similar. However, it is possible that the effects of longer, stiffer Rayon fibers are offset by shorter, more flexible cellulose fibers. Additionally, cellulose fibers are hollow and have surface nonuniformities including "hinges" or "knees", as well as smaller diameters. Based on Fig. 5.12, fiber type effects will be analyzed mainly between hardwood, softwood, BCTMP, and 1 mm Rayon fibers, assuming the effects of 3 (6) mm Rayon fiber are similar to that of hardwood (softwood) fiber.

When a very small amount of fiber is added (C = 0.05%) to the bubble column, gas holdup increases slightly when compared to an air-water system (C = 0%) operating under the same superficial gas and liquid velocities. This result was also observed by Walmsley (1992). The slight increase is attributed primarily to Mechanism I (see Chapter 4 and Table 4.1). The gas holdup increase in the BCTMP fiber suspension is larger, because Mechanism VI (see Chapter 4 and Table 4.1) also contributes to the gas holdup increase, whereas it is not significant for the other fiber types.

As fiber mass fraction increases, gas holdup eventually decreases in a nonlinear fashion. For softwood fiber suspensions, gas holdup starts to decrease with increasing fiber mass fraction at C = 0.1%. This is because in softwood fiber suspensions, fiber networks begin to form and Mechanisms III and V (see Chapter 4 and Table 4.1) begin to contribute to the influence on gas holdup. For hardwood, 1 mm Rayon, and BCTMP fiber suspensions, the maximum gas holdup reached at C = 0.05% is relatively unchanged with increasing fiber

mass fraction until C = 0.4% (for hardwood and 1 mm Rayon fibers) or C = 0.6% (for BCTMP fibers), where gas holdup begins to decrease sharply with increasing fiber mass fraction. The gas holdup at first remains constant because negligible fiber flocculation is observed in this fiber mass fraction range for these fiber types and the effect of Mechanism III is negligible. Once the fiber mass fraction reaches a critical value where significant fiber networks form, Mechanism III dominates the flow and gas holdup decreases with increasing C.

The fiber mass fraction at which gas holdup starts to decrease with increasing C varies for different fiber types because fiber flocculation is affected by fiber physical properties, including fiber length, coarseness, and flexibility. A suspension with longer or more flexible fibers begins to form flocs and fiber networks at lower fiber mass fractions and Mechanism III begins to dominate the flow. However, gas holdup in a BCTMP fiber suspension does not follow this trend because Mechanism VI dominates the flow until C = 0.6%, when Mechanism III becomes significant.

When the gas holdup begins to decrease for all fiber types except 1 mm Rayon fiber, the decline is very steep until C $\approx$ 0.8~1.0%. The sharp decrease in gas holdup is attributed mainly to Mechanism III when C $\lesssim$ 0.8%. As fiber mass fraction increases, fiber network strength increases and the gas holdup decrease resulting from Mechanism III increases. The decline in gas holdup with increasing fiber mass fraction is steeper for softwood fibers than for hardwood or BCTMP fibers, while the slope for the latter two fiber types are similar (Fig. 5.12a). This is attributed to fiber physical properties. Softwood fiber will cause more flocculation and increase fiber network strength more effectively than hardwood fiber at the same mass fraction because softwood fiber is much longer than hardwood fiber. Although BCTMP fiber is longer than hardwood fiber, it is less flexible because of the lignin content, which offsets the fiber length effect.

When C $\gtrsim$ 1.0%, the gas holdup decrease is less severe than when C $\lesssim$ 0.8% (Fig. 5.12a). For softwood fiber, gas holdup does not significantly change with increasing fiber mass fraction. The asymptotic reduction in gas holdup at the higher mass fractions is attributed to the following two reasons: (i) the amount of entrained gas in the fiber suspension increases with increasing fiber mass fraction and compensates for the decrease in

gas holdup due to increasing fiber mass fraction; and (ii) enhanced bubble coalescence (Mechanism III) is not as significant because the fiber network strength is strong enough to make most newly generated bubbles coalesce in the aeration zone, especially for softwood fiber suspensions.

For 1 mm Rayon fibers, gas holdup decreases with increasing fiber mass fraction more gradually when $0.4 \leq C \leq 1.5\%$ (Fig. 5.12a). No significant slope change is found because this Rayon fiber is short compared to the others, and Rayon is less flexible than cellulose fibers. Additionally, Rayon fiber surface morphology is smoother than cellulose, allowing the relatively short 1 mm Rayon to slide over each other as opposed to forming flocs in cellulose and longer Rayon fiber suspensions. Hence, the addition of 1 mm Rayon fibers into the suspension produces a much smaller enhancement of the fiber network strength when compared to the other fiber types.

It is also noticed from Fig. 5.12 that the gas holdup difference between hardwood (3 mm Rayon) and BCTMP fiber suspensions changes with superficial gas and liquid velocity. At $U_g = 20$ cm/s (Fig. 5.12a), the difference is significant for $0.05\% \leq C \leq 1.2\%$ when $U_l = 8$ cm/s, while it is only significant for $0.05\% \leq C \leq 0.6\%$ (Fig. 5.12b) when $U_l = 4$ cm/s. This is still seen when the superficial gas velocity decreases to $U_g = 10$ cm/s (Figs. 5.12c and d). However, the magnitude of the difference is smaller. When $U_g = 4$ cm/s, the gas holdup in the three types of fiber suspensions shows negligible difference for $0.05\% \leq C \leq 1.5\%$ (Figs. 5.12e and f). This is attributed to the foam generated in the BCTMP fiber suspensions and will be discussed in more detail in the following two sections.

5.2.3 Gas holdup variation with superficial gas velocity

Typical results on gas holdup variation with superficial gas velocity in different fiber suspensions at low ($C = 0.1\%$) and high ($C = 1.0\%$) fiber mass fractions and a fixed superficial liquid velocity ($U_l = 8$ cm/s) are shown in Fig. 5.13. Air-water data under similar operating conditions are also presented for reference. Similar plots have also been made for other fiber mass fractions and operating conditions. They are not included because they all show a similar ε vs. U_g trend as shown in Fig. 5.13. The general trend for all fiber types is

that gas holdup increases with increasing superficial gas velocity without a local maximum. This is consistent with previous studies (Walmsley, 1992; Reese *et al.*, 1996; Xie *et al.*, 2003b; Tang and Heindel, 2005c). Hence, fiber type does not have an effect on the pattern of gas holdup trends with superficial gas velocity in this study. Other studies using semi-batch bubble columns (Su and Heindel, 2004b, 2004a) have concluded that fiber type and fiber length can influence gas holdup trends. The difference is primarily due to the gas distributors used in these studies.

Gas holdup in all fiber suspensions is compared in the range $0 \leq U_g \leq 20$ cm/s (Fig. 5.13). Superficial gas velocity does not affect gas holdup trends among the different fiber suspensions. However, in Fig. 5.13a, the difference between the gas holdup in the BCTMP fiber suspension and that of the hardwood and 1 mm Rayon fiber suspensions is more significant at $U_g > 15$ cm/s than at $U_g < 15$ cm/s. Similarly, in Fig. 5.13b, the difference between the gas holdup in the BCTMP fiber suspension and that of the hardwood fiber suspension is more significant at $U_g > 8$ cm/s than at $U_g < 8$ cm/s. This is explained by the fact that at high superficial gas velocities (i.e., $U_g > 15$ cm/s at C = 0.1%, or $U_g > 8$ cm/s at C = 1.0%), a significant amount of foam is generated at the top of the bubble column in the BCTMP suspension and it is entrained into the bubble column due to backmixing, resulting in an additional increase in gas holdup. Backmixing is not significant at lower superficial gas velocities, so the gas holdup in the BCTMP fiber suspension is similar to other fiber suspensions. Foam in BCTMP suspensions begins to appear at a lower superficial gas velocity at C = 1.0% than C = 0.1%, because there is more foam producing material (i.e., lignosulfonate) in the suspension when C = 1.0%.

Extrapolating the gas holdup versus superficial gas velocity curves to $U_g = 0$ cm/s can be used to estimate if there is significant gas entrainment in the fiber suspension (Lindsay *et al.*, 1995). Hence, Fig. 5.13a indicates no air entrainment at C = 0.1% for all fiber types. However, a nonzero gas holdup ($\varepsilon \approx 0.005$) at $U_g = 0$ cm/s in Fig. 5.13b indicates a noticeable amount of gas entrained in for BCTMP, hardwood, softwood, and 3 mm Rayon fibers when C = 1.0%. Extrapolating the 1 mm Rayon fiber data to $U_g = 0$ yields $\varepsilon \approx 0$, implying no gas entrainment in this fiber suspension, even at C = 1.0%.

5.2.4 Gas holdup variation with superficial liquid velocity

In Sec. 5.1.2, it is shown that gas holdup decreases with increasing superficial liquid velocity due to a reduced bubble residence time, and the decrease is more significant at a lower fiber mass fraction. This trend is generally true for all fiber types investigated in this study except BCTMP fiber at some fiber mass fractions (Figs. 5.14a-c). As shown in Fig. 5.14b for C = 0.6% and U_g = 20 or 5 cm/s, gas holdup in the BCTMP fiber suspension increases when U_l is increased from 0 to 2 cm/s, reaching a maximum at U_l = 2 cm/s, and then decreases with increasing U_l. This general BCTMP trend is also found at other fiber mass fractions. However, as shown in Fig. 5.15, the superficial liquid velocity at which the gas holdup reaches a local maximum varies with fiber mass fraction. This behavior is the result of the foam formation in BCTMP fiber suspensions. Visual observations reveal foam forms inside the reservoir and at the top of the bubble column. The bubble column gas holdup increase from foam can be attributed to: (i) part of the foam formed in the reservoir is entrained in the fiber suspension and transferred into the bubble column by the pump when $U_l > 0$ cm/s; and (ii) the foam formed in the bubble column accumulates at the column top, where part of the foam is entrained in the fiber suspension and transferred back to the bubble column due to backmixing. The complex interaction between these two effects, the superficial liquid velocity, and fiber mass fraction is not yet fully understood. More work is needed to fully understand why the gas holdup variation with superficial liquid velocity for BCTMP fiber suspensions deviates from the trends for other fiber suspensions.

5.2.5 Air-water-fiber to air-water gas holdup ratio

In Sec. 5.1.5, a detailed analysis is presented on the influences of superficial gas and liquid velocity, fiber mass fraction, and axial column position on gas holdup ratio for hardwood fiber suspensions. Similar trends regarding the influences of these factors have also been observed for other fiber types. In this section, the effect of fiber type on the gas holdup ratio is discussed.

Figure 5.16 compares the variation of gas holdup ratio with superficial gas velocity for different fiber suspensions at four different fiber mass fractions (C = 0.1%, 0.2%, 1.0%,

and 1.5%) with U_l = 8 cm/s. At C = 0.1% (Fig. 5.16a), the gas holdup ratio for all 6 fiber types are very close to 1.0 at most superficial gas velocities. The difference between fiber types is insignificant. No significant local minimum is observed for any fiber type. This is because at C = 0.1%, no fiber flocculation occurs and all fiber suspensions have very similar rheological properties to water. At C = 0.2% (Fig. 5.16b), the gas holdup ratio for softwood and 6 mm Rayon fibers is less than 1 for most conditions and a local minimum starts to appear (although not as obvious as that at higher fiber mass fractions) at $U_g \approx 5$ cm/s on the $\varepsilon/\varepsilon_{A-W} \sim U_g$ curves. This is because flocculation begins in the softwood and 6 mm Rayon fiber suspensions and affects the gas bubble behavior. The $\varepsilon/\varepsilon_{A-W} \sim U_g$ curves for the other 4 fiber types remain similar to those at C = 0.1%, indicating negligible flocculation in these fiber suspensions. When C increases to 1.0% (Fig. 5.16c), a local minimum appears on the $\varepsilon/\varepsilon_{A-W} \sim U_g$ curve for each fiber type. The superficial gas velocity at which the local minimum is located does not change significantly with fiber type. For most conditions, the gas holdup ratio for 1 mm Rayon (softwood) fiber is largest (smallest) while the gas holdup ratios for hardwood and 3 mm Rayon fibers are very close for all U_g. The gas holdup ratio for BCTMP fiber is similar to that for hardwood and 3 mm Rayon fibers when $U_g \lesssim 10$ and becomes larger when $U_g > 10$ cm/s. Such a relationship between the gas holdup ratios for all the fiber types agrees with the comparison of the gas holdup in the fiber suspensions in Sec. 5.2.2. At C = 1.5% (Fig. 5.16d), the $\varepsilon/\varepsilon_{A-W} \sim U_g$ curve for 1 mm Rayon fiber does not change much from that at C = 1.0%. This is because an addition of only 0.5% of short, stiff, and smooth 1 mm Rayon fiber can not enhance the fiber flocculation very significantly in the bubble column. The change in the $\varepsilon/\varepsilon_{A-W} \sim U_g$ curve for softwood fiber is also insignificant. However, this is because adding more softwood fiber does not cause further change in the bubble column hydrodynamics. The $\varepsilon/\varepsilon_{A-W} \sim U_g$ curves for the other three fiber types are similar to the softwood curve, indicating that at C = 1.5%, the hydrodynamics for the four fiber types are similar.

5.3 Gas Flow Regime Transition

Flow regimes are usually used to define the morphological arrangement of a gas phase moving through a liquid phase (Wallis, 1969). In a bubble column, properties such as gas holdup (i.e., volumetric gas fraction), pressure drop, gas-liquid interfacial area, and heat and mass transfer are strongly dependent upon flow regime (Shah *et al.*, 1982). With an identified gas flow regime, the modeling and simulation of the transport processes in a bubble column flow become simpler and more accurate.

In this section, the drift-flux model, which is widely recommended for modeling gas holdup in bubble columns (Shah *et al.*, 1982; Clark and Flemmer, 1986; Miller and Cain, 1986; Zahradnik *et al.*, 1997; Ruzicka *et al.*, 2001b; Xie *et al.*, 2003b), is used to identify the gas flow regime transitions.

5.3.1 Drift-flux model

The drift-flux model accounts for the radial nonuniformity of flow and holdup profiles typically encountered in the heterogeneous flow regime. The drift-flux (j_{gm}) is defined by Wallis (1969) as the volumetric flux of gas relative to a surface moving at a velocity equal to the total of the superficial gas and liquid velocities (i.e., the volumetric flux of the gas-liquid mixture). For a cocurrent bubble column, it can be shown that (Shah *et al.*, 1982)

$$\frac{\langle U_g \rangle}{\langle \varepsilon \rangle} = C_0 \langle U_l + U_g \rangle + \frac{\langle j_{gm} \rangle}{\langle \varepsilon \rangle} \tag{5.1}$$

where $\langle\rangle$ indicates averaging over the cross section and

$$C_0 = \frac{\langle \varepsilon (U_g + U_l) \rangle}{\langle \varepsilon \rangle \langle U_g + U_l \rangle} \tag{5.2}$$

is a distribution parameter gauging the uniformity in the radial velocity and holdup profiles and $\langle j_{gm} \rangle / \langle \varepsilon \rangle$ is a weighted average drift velocity accounting for local slip. Since all values in the present study are averaged, the $\langle\rangle$ nomenclature will be omitted when describing the data in the present study. The weighted average drift velocity is usually assumed as the

terminal bubble rise velocity ($U_{b\infty}$) in an infinite medium because the local slip velocity U_s (= $\frac{U_g}{\varepsilon} - \frac{U_l}{1-\varepsilon}$) changes little over the pipe diameter and $j_{gm} = U_s(1-\varepsilon)$, with $\varepsilon < 0.25$ in most situations for bubble column flows (Clark *et al.*, 1990). C_0 can be found by plotting $\langle U_g \rangle / \langle \varepsilon \rangle$ as a function of $\langle U_g + U_l \rangle$. For a given gas flow regime, C_0 and $U_{b\infty}$ are constant because the radial velocity, gas holdup distribution, and average bubble size do not change significantly. Zahradnik *et al.* (1997) observed that changes in the slope of the drift-flux plot indicate changes in flow regime. Xie *et al.* (2003b)showed that the Zuber-Findlay model could successfully model the gas holdup data in a cocurrent air-water-fiber bubble column when the flow regime is other than dispersed bubbly flow or layered bubbly flow. Using this method, Su and Heindel (2003) demarcated the superficial gas velocities at which flow regime transitions occurred in a 15.24 cm semi-batch air-water-Rayon fiber bubble column.

However, data acquired in the present study shows that Eq. (5.1) fails to correlate the gas holdup. Figure 5.17 plots U_g/ε versus $(U_g + U_l)$ at different fiber mass fractions for hardwood fiber suspensions. Data at a constant superficial liquid velocity fall along on a curve comprising two (C = 1.0% and 1.5%, Figs. 5.17c and d) or three (C = 0.1% and 0.4%, Figs. 5.17a and b) straight-line segments. However, data for different U_l values scatter on each plot and are not correlated with a single straight line. The position of a curve on the U_g/ε versus $(U_g + U_l)$ plot depends on its corresponding superficial liquid velocity. This dependence on superficial liquid velocity can not be accounted for with only one radial distribution parameter C_0 in Eq. (5.1).

Miller and Cain (1986) also reported that the Zuber-Findlay drift-flux model (Eq. (5.1)) failed to correlate gas holdup data in a gas-liquid-solid three phase cocurrent bubble column when the superficial slurry (liquid + solid) velocity varied over a wide range. However, they derived a modified drift-flux model by adding a second radial distribution parameter into the Zuber-Findlay drift-flux model:

$$\frac{\langle U_g \rangle}{\langle \varepsilon \rangle} = C_l \langle U_l + U_{sp} \rangle + C_g \langle U_g \rangle + \frac{\langle j_{gm} \rangle}{\langle \varepsilon \rangle} \tag{5.3}$$

where

$$C_l = \frac{\langle \varepsilon(U_{sp} + U_l) \rangle}{\langle \varepsilon \rangle \langle U_{sp} + U_l \rangle} \tag{5.4}$$

and

$$C_g = \frac{\langle \varepsilon U_g \rangle}{\langle \varepsilon \rangle \langle U_g \rangle} \tag{5.5}$$

are two radial distribution parameters and

$$j_{gm} = U_g - \varepsilon(U_g + U_l + U_{sp}) \tag{5.6}$$

is the volumetric flux of gas relative to a surface moving at a velocity equal to the total of the superficial gas, liquid, and solid velocities (i.e., drift-flux) and $\langle j_{gm} \rangle / \langle \varepsilon \rangle$ is a weighted average drift velocity. In Eq. (5.3), ($U_l + U_{sp}$) is the slurry superficial velocity (i.e., the sum of the superficial liquid and solid velocity). Miller and Cain (1986) showed that this modified drift-flux model (Eq. (5.3)) was able to correlate their data in a wide range of slurry superficial velocities. They also reported that the radial distribution parameters (C_l and C_g) and weighted drift-velocity were constant for a specific gas flow regime and varied when flow regime changes. Hence, the modified drift-flux model can be used to discriminate between different gas flow regimes.

Clark and Flemmer (1986) also observed that their data acquired in a gas-liquid 100 mm diameter cocurrent bubble column were not correlated with the Zuber-Findlay drift-flux model (Eq. (5.1)), but were well-correlated with the modified two-radial-distribution-parameter drift-flux model (Eq. (5.3)) when the slurry superficial velocity ($U_l + U_{sp}$) is replaced with superficial liquid velocity:

$$\frac{\langle U_g \rangle}{\langle \varepsilon \rangle} = C_l \langle U_l \rangle + C_g \langle U_g \rangle + \frac{\langle j_{gm} \rangle}{\langle \varepsilon \rangle} \tag{5.7}$$

Equation (5.7) can be rewritten as

$$\frac{\langle U_g \rangle}{\langle \varepsilon \rangle} = C_g \langle U_g \rangle + B_0 \tag{5.8}$$

where $B_0 = C_1\langle U_1\rangle + \frac{\langle j_{gm}\rangle}{\langle \varepsilon\rangle}$ is a constant for a given flow regime and U_l. Hence, the U_g/ε versus U_g plot can be used to identify the superficial gas velocity at which flow regime transition occurs for a given U_l.

5.3.2 Gas flow regimes in hardwood fiber suspensions

Figure 5.18 shows the effect of U_l on U_g/ε as a function of U_g at low (C = 0.1%) and high (C = 1.0%) fiber mass fractions in hardwood fiber suspensions. When C = 0.1%, as shown in Fig. 5.18a, each U_g/ε versus U_g curve for different U_l can be divided into 3 regions according to their slope. According to visual observations and the flow regimes described by Chen *et al.* (1994) and Reese *et al.* (1996), the three regions correspond to dispersed bubble flow (region a), vortical-spiral flow (region b), and turbulent flow (region c). Each of the three regions on one of the U_g/ε versus U_g curves has the same slope as the counterparts on the other curves. The superficial gas velocity corresponding to each transition is nearly independent of U_l. At each superficial liquid velocity, the transition from dispersed bubble flow to vortical-spiral flow occurs at $U_g \approx 4$ cm/s, while the transition from vortical-spiral flow to turbulent flow occurs at $U_g \approx 13\sim14$ cm/s. The boundaries between neighboring flow regimes are different from results in Reese *et al.* (1996), which is attributed to the difference in bubble column size and gas distribution method. The slope of the vortical-spiral flow regime is slightly different from that of the turbulent flow regime while both of them are distinctly different from that of the dispersed bubble flow regime. The superficial liquid velocity only influences the intercept at $U_g = 0$, which is consistent with Eq. (5.8).

When C = 1.0%, as shown in Fig. 5.18b, the dispersed bubble flow regime does not appear. There is only one regime transition on the curves, which occurs at $U_g \approx 13\sim14$ cm/s, and is independent of U_l. When $U_g \gtrsim 5$ cm/s, the slopes of regions a and b are independent of U_l and very close to those of regions b and c in Fig. 5.18a, respectively, suggesting that the corresponding flow regimes at C = 1.0% are vortical-spiral flow and turbulent flow. However,

when $U_g \lesssim 5$ cm/s, the slopes increase with U_l and are greater than the slope at higher U_g. This is attributed to gas entrainment, which composes a significant fraction of the measured gas holdup at $U_g \lesssim 5$ cm/s and C = 1.0%. For example, at C = 1.0%, the entrained gas fraction is estimated to be ~25% of the total gas holdup when U_g = 0.52 cm/s and U_l = 10 cm/s, and ~8% when U_g = 5.1 cm/s and U_l = 10 cm/s.

Figure 5.19 shows the effect of fiber mass fraction on gas flow regime transitions in hardwood fiber suspensions when U_l = 8 cm/s; similar results are found at other superficial liquid velocities. When C = 0.1% or 0.2%, the U_g/ε versus U_g curves overlap with the curves at C = 0%. Both slopes and intercepts of the curves are independent of C. When C is increased to 0.4%, the U_g/ε versus U_g curve is still parallel to the curves of lower fiber mass fractions at every U_g; only the intercept of the curve is changed. It is clear that there are three gas flow regimes when $C \leq 0.4\%$, i.e., dispersed bubble flow, vortical-spiral flow, and turbulent flow. In fiber suspensions with $C \leq 0.4\%$, the superficial gas velocity at which the gas flow regime transitions from dispersed bubble flow (vortical-spiral flow) to vortical-spiral flow (turbulent flow) is ~4 cm/s (~13.5 cm/s). When $0.6\% \leq C \leq 1.5\%$, only the vortical-spiral flow and turbulent flow regimes appear, and the superficial gas velocity at which transition occurs is 13–14 cm/s, with the slightly lower U_g corresponding to the higher C. The disappearance of the dispersed bubble flow regime when $C \geq 0.6\%$ is attributed to the enhancement of bubble coalescence by the fiber network. This is consistent with the observations of Reese *et al.* (1996) and Heindel (2000) in semi-batch bubble columns. When $U_g \gtrsim 5$ cm/s, the slopes of the U_g/ε versus U_g curves are not significantly different from those at $C \leq 0.4\%$. The separation distance between neighboring U_g/ε versus U_g curves varies nonuniformly with C, suggesting that the intercept B_0 in Eq. (5.8) is a nonlinear function of C. When $U_g \lesssim 5$ cm/s and $C \geq 0.6\%$, the slope increases with increasing C due to gas entrainment, which composes a significant fraction of the measured gas holdup at $U_g \lesssim 5$ cm/s and $C \geq 0.6\%$.

5.3.3 Effect of fiber type on gas flow regimes

The flow regimes in softwood, BCTMP, and Rayon (1, 3, 6 mm) fiber suspensions are also analyzed using the Zuber-Findlay drift-flux model. Three regimes similar to those found in hardwood fiber suspensions are identified for each fiber type. The effect of superficial liquid velocity on the flow regime transition is insignificant, i.e., the slope of the U_g/ε versus U_g curves does not significantly change with U_l, nor does the superficial gas velocity at which the flow regime transitions. However, the fiber mass fraction at which the U_g/ε versus U_g curve changes from 3-segment to 2-segment (i.e., the dispersed bubble flow regime disappears) varies with fiber types. This is summarized in Table 5.1, where it is seen that in 1 mm Rayon fiber suspensions, the three flow regimes is always found when $C \leq 1.5\%$. The variation of the fiber mass fraction at which the U_g/ε versus U_g curve changes from 3 to 2 segments with fiber type is attributed to the influence of fiber physical properties on flocculation in fiber suspensions.

Table 5.1: The fiber mass fraction at which the U_g/ε versus U_g curve changes from 3 to 2 segments.

Fiber type	Approximate fiber mass fraction where the dispersed bubble flow disappears
Hardwood	0.6%
Softwood	0.4%
BCTMP	0.8%
1 mm Rayon	> 1.5%
3 mm Rayon	1.0%
6 mm Rayon	0.4%

Figure 5.20 compares the U_g/ε versus U_g curves for different fiber types at fixed U_l and C. The same curve for air-water at the same U_l is also included for reference. When C = 0.1% (Fig. 5.20a), there are three gas flow regimes identified for all fiber types. Fiber type has a negligible effect on the curve slope, gas flow regime transition points, and even curve intercept. This is because all fiber suspensions behave very similar to that of water. When C = 0.4% (Fig. 5.20b), the dispersed bubble flow regime disappears from the softwood and 6

mm Rayon fiber suspensions, but still appears in other fiber suspensions. The distance between the U_g/ε versus U_g curves for softwood (6 mm Rayon) fiber and other fiber types is significant, while the difference between the curves for hardwood, BCTMP, and Rayon (1 and 3 mm) fibers is still negligible. This indicates significant flocculation occurs in the softwood and 6 mm Rayon fiber suspensions. As C increases to 1.0% (Fig. 5.20c), flocculation also becomes significant in hardwood, BCTMP, and 3 mm Rayon fiber suspensions. Thus, the U_g/ε versus U_g curves for these three fiber types become 2-segment and deviate from the air-water curve. When C increases to 1.5% (Fig. 5.20d), the curves for hardwood, softwood, BCTMP, and 3 mm Rayon overlap again, indicating the effect of these fiber suspensions on gas holdup approaches a "saturation point", where further fiber addition does not significantly influence gas holdup in the bubble column. In all four cases in Fig. 5.20, the superficial gas velocities at which the flow regime transitions are not significantly affected by fiber type.

5.4 Summary of the Experimental Results

In this chapter, the experimental data of this study are presented in detail.

The influence of superficial gas and liquid velocity and fiber mass fraction on gas holdup in the cocurrent air-water-fiber bubble column are analyzed, mainly based on the data acquired in hardwood fiber suspensions. Generally, gas holdup increases with increasing superficial gas velocity without a local maximum, decreases with increasing superficial liquid velocity, and changes nonlinearly with increasing fiber mass fraction. When flocculation is significant in the fiber suspension, gas holdup decreases with increasing fiber mass fraction. Similar trends are also found in other 5 fiber suspensions (softwood, BCTMP, and Rayon (1, 3, and 6 mm) fibers).

Fiber type also has a significant effect on gas holdup in the cocurrent air-water-fiber bubble column because fiber physical properties affect flocculation significantly in fiber suspensions, and consequently influence bubble column hydrodynamics.

The air-water-fiber to air-water gas holdup ratio ($\varepsilon/\varepsilon_{A-W}$) represents the effect of fiber addition on gas holdup and the degree to which an air-water-fiber bubble column flow

deviates from an air-water flow. The gas holdup ratio is a nonlinear function of superficial gas velocity. It reaches a local minimum at $U_g \approx 4\sim5$ cm/s when fiber mass fraction is sufficiently high to form fiber flocs.

Gas flow regimes are identified using the modified drift-flux model (Eq. (5.8)). Three gas flow regimes (i.e., dispersed bubble, vortical-spiral, and turbulent flow) are identified. When fiber mass fraction is higher than a certain value (which is a function of fiber type), the dispersed bubble flow regime disappears because bubble coalescence is enhanced at low U_g by flocculating fibers. Superficial liquid velocity does not affect gas flow regime transition.

Figure 5.1: Variation of gas holdup with superficial gas velocity at different superficial liquid velocities: (a) C = 0% and (b) C = 0.1% and 1.0% (hardwood fiber suspensions).

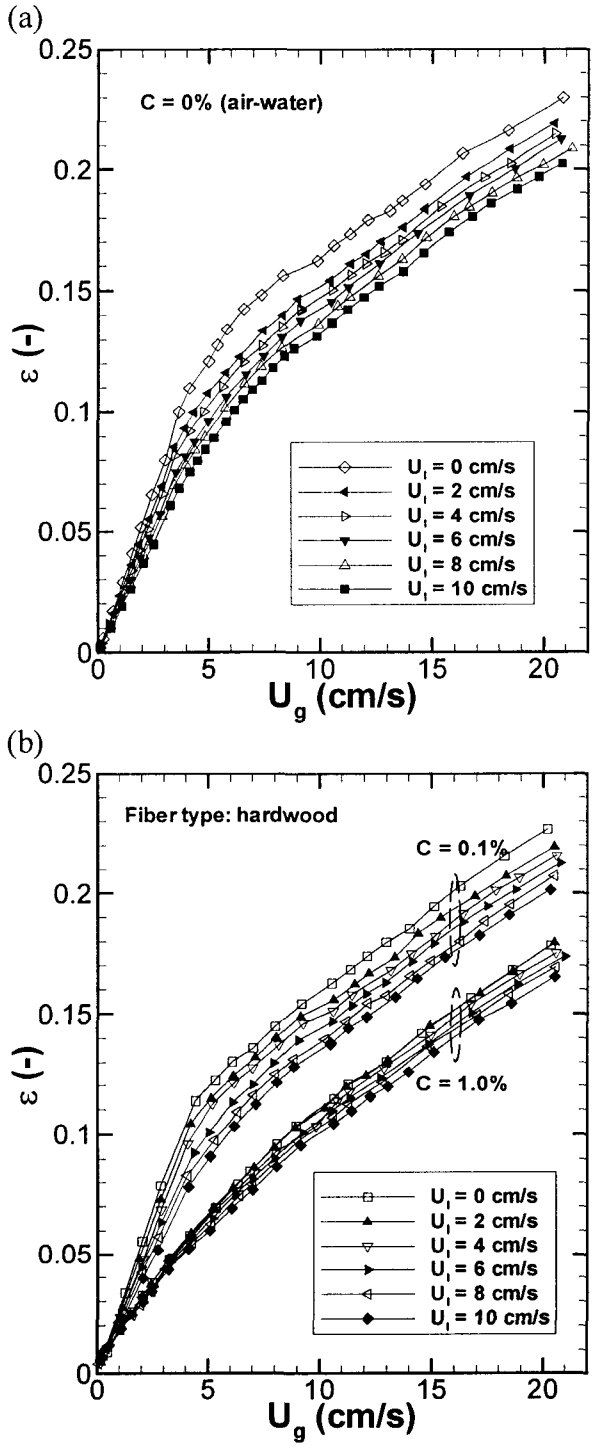

Figure 5.2: Variation of gas holdup with superficial liquid velocity at different fiber mass fractions in hardwood fiber suspensions: (a) U_g = 4 cm/s; (b) U_g = 13 cm/s; and (c) U_g = 20 cm/s.

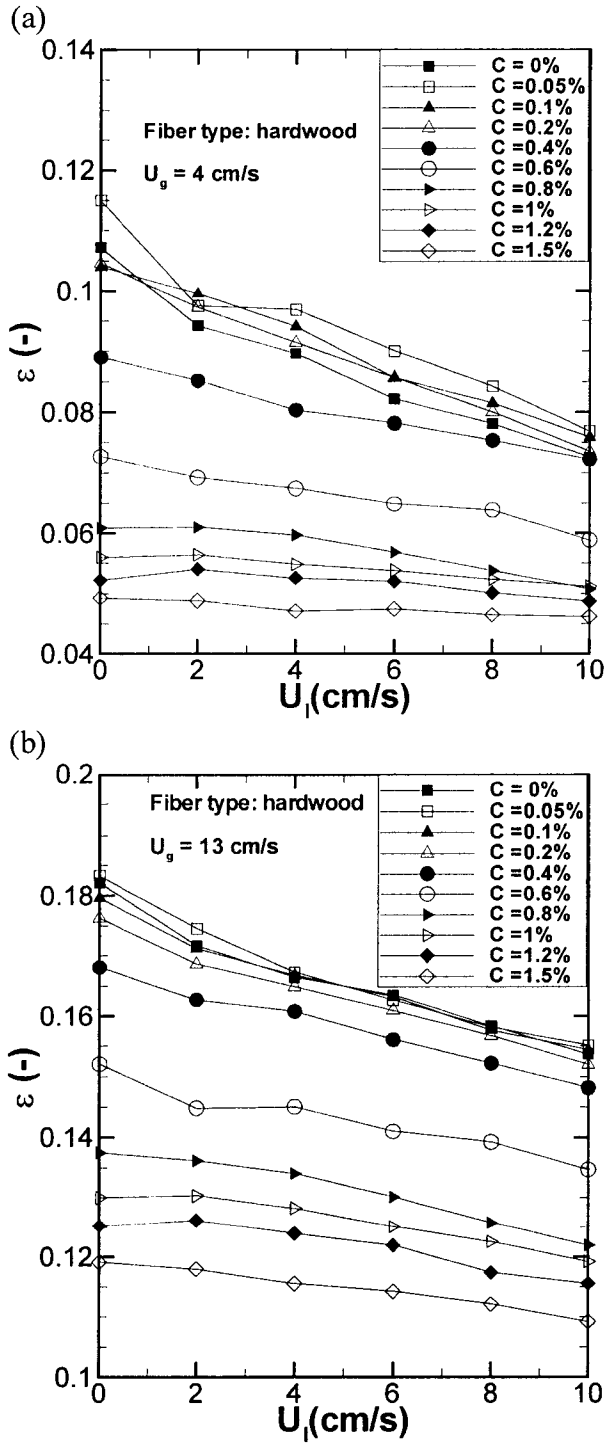

Figure 5.2: Continued.

(c)

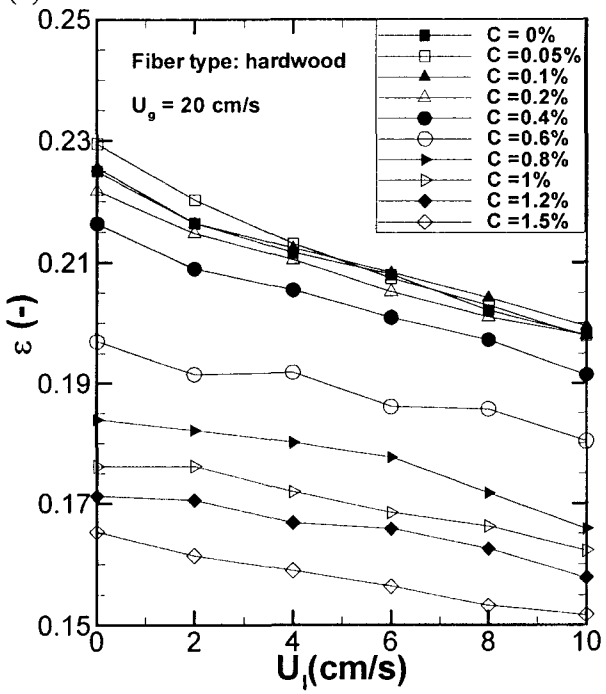

Figure 5.3: Variation of gas holdup with superficial gas velocity in suspensions of different fiber mass fractions in hardwood fiber suspensions (U_l = 8 cm/s).

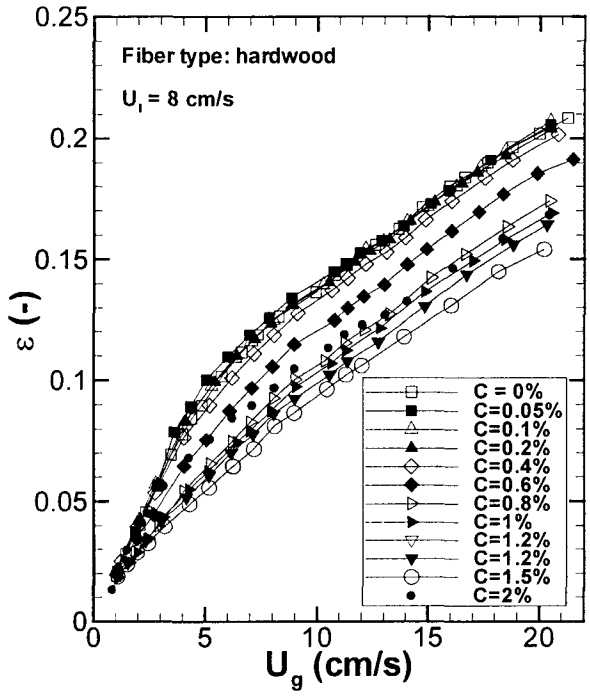

Figure 5.4: Variation of gas holdup with fiber mass fraction at different superficial liquid velocities in hardwood fiber suspensions.

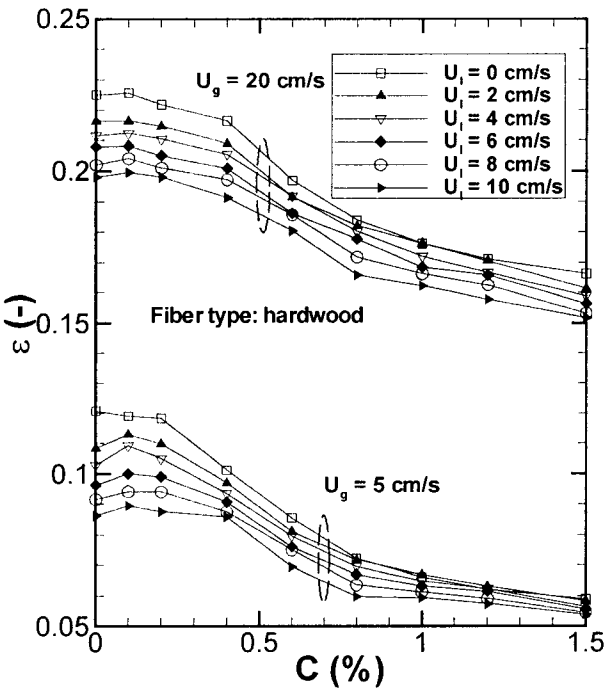

Figure 5.5: Variation of gas holdup with fiber mass fraction at different superficial gas velocities in hardwood fiber suspensions: (a) U_l = 8 cm/s and (b) U_l = 0 cm/s.

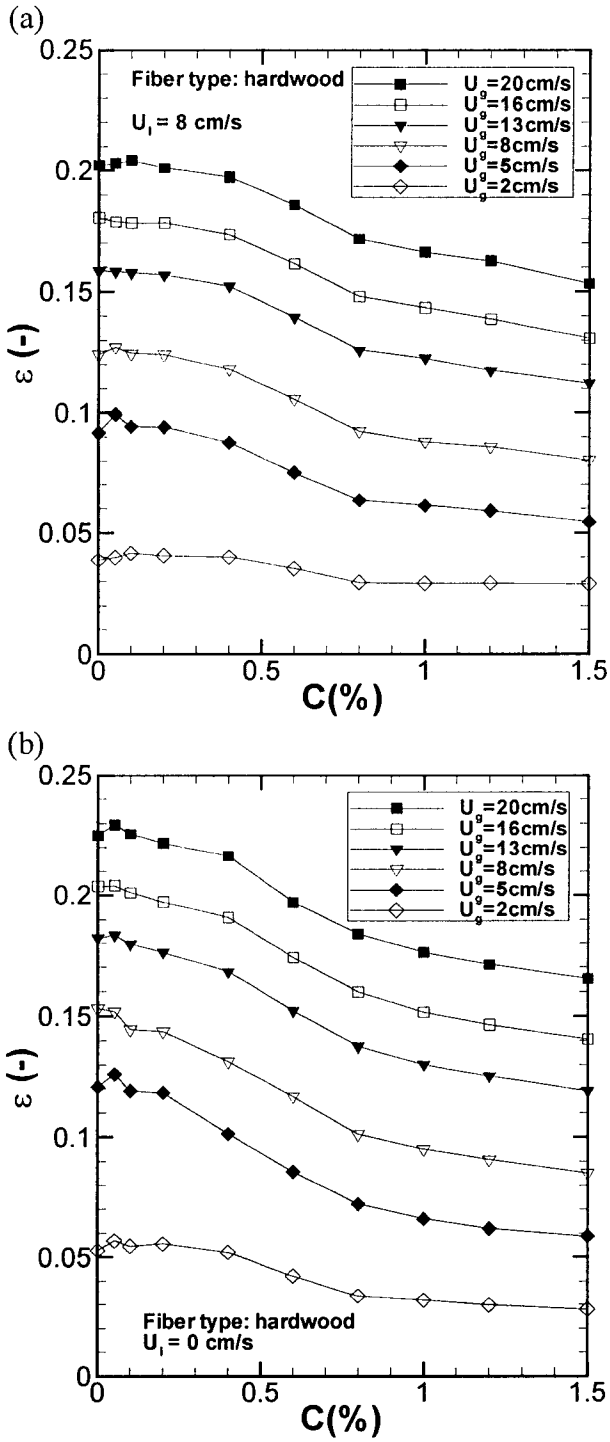

Figure 5.6: Axial gas holdup variation at different superficial liquid velocities in hardwood fiber suspensions (U_g = 18.5 cm/s).

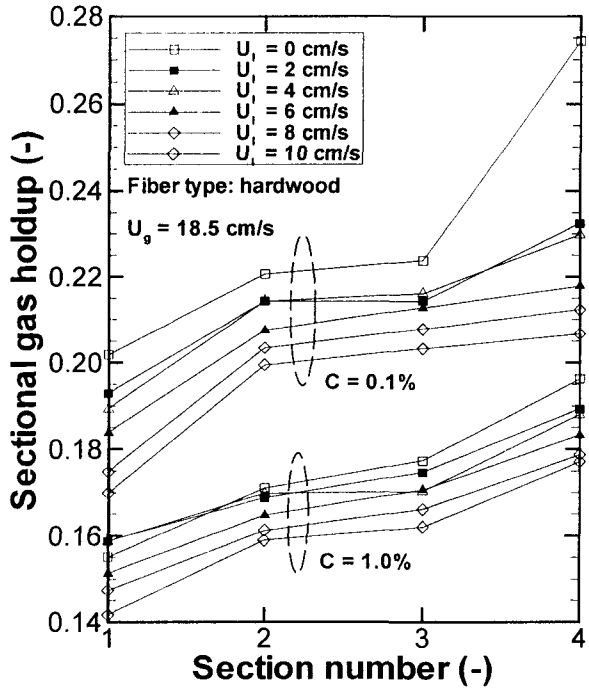

Figure 5.7: Influence of fiber mass fraction on gas holdup in hardwood fiber suspensions in different column sections.

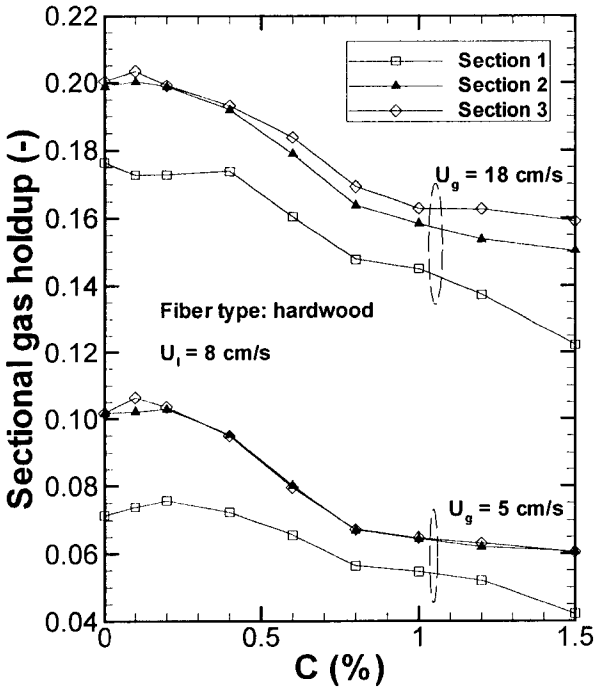

Figure 5.8: Variation of gas holdup ratio with superficial gas velocity for at different fiber mass fractions in hardwood fiber suspensions when U_l = 8 cm/s.

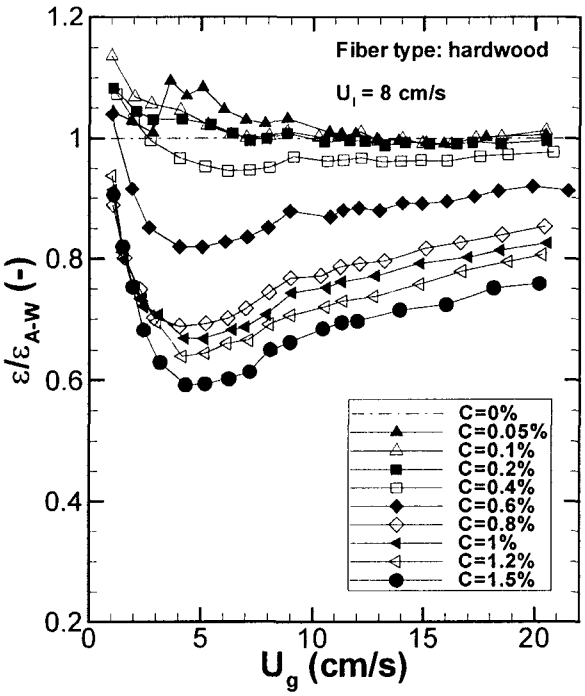

Figure 5.9: Variation of gas holdup ratio with superficial gas velocity for at different superficial liquid velocities in hardwood fiber suspensions: (a) C = 0.1% and (b) C =1.0%.

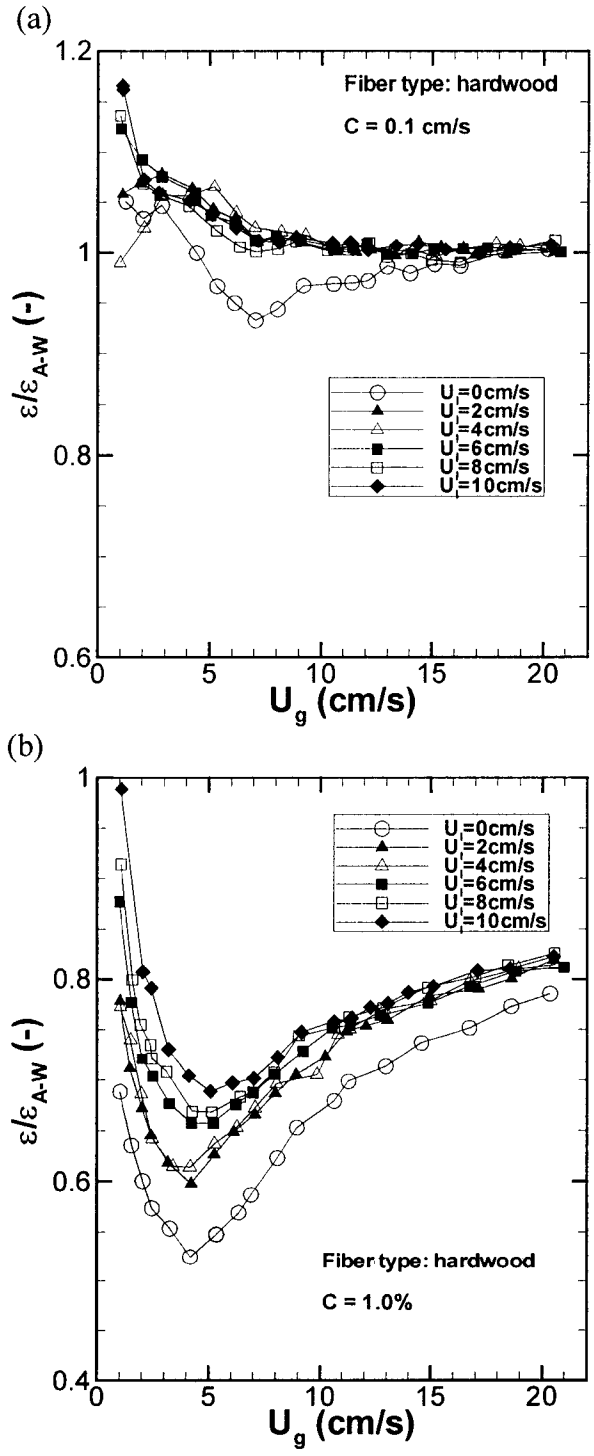

Figure 5.10: Comparison between gas holdup ratio for sections 1, 2, and 3 in hardwood fiber suspensions when U_l = 8 cm/s: (a) C = 0.1% and (b) C =1.5%.

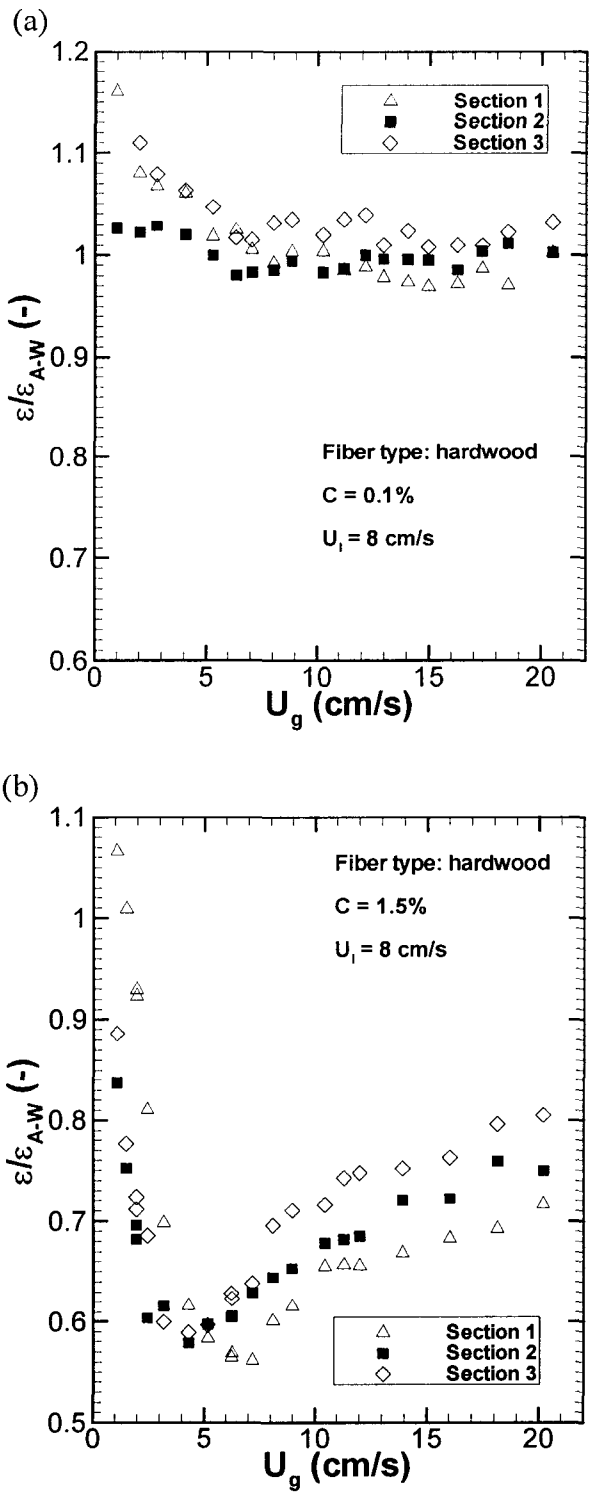

Figure 5.11: Variation of fiber suspension surface tension with fiber mass fraction.

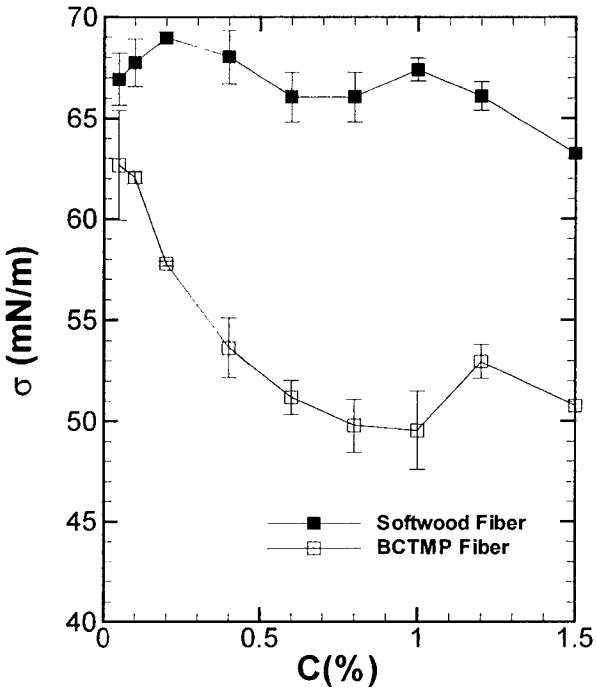

Figure 5.12: Variation of overall average gas holdup with fiber mass fraction in different fiber suspensions: (a) U_g = 20 cm/s, U_l = 8 cm/s; (b) U_g = 20 cm/s, U_l = 4 cm/s; (c) U_g = 10 cm/s, U_l = 8 cm/s; (d) U_g = 10 cm/s, U_l = 4 cm/s; and (e) U_g = 4 cm/s, U_l = 4 cm/s.

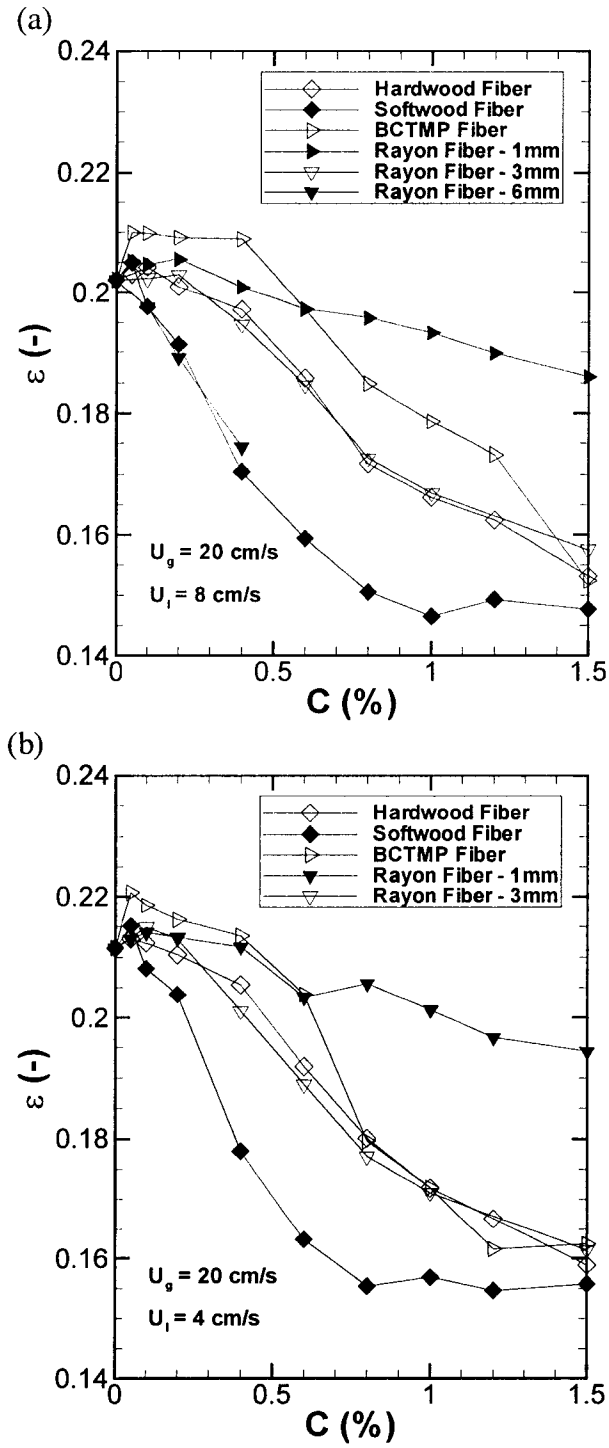

Figure 5.12: Continued.

(c)

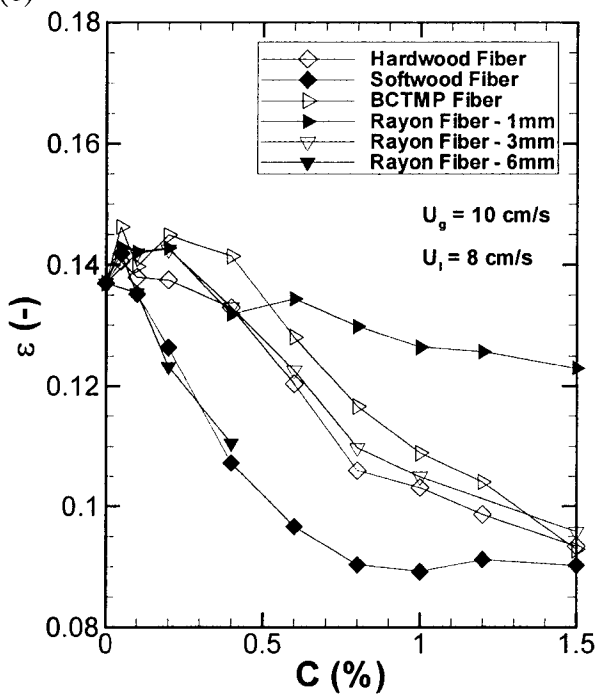

(d)

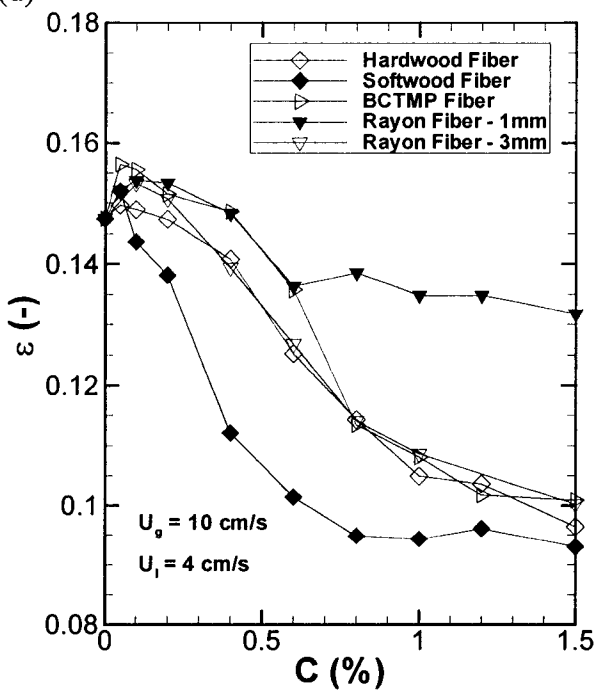

Figure 5.12: Continued.

(e)

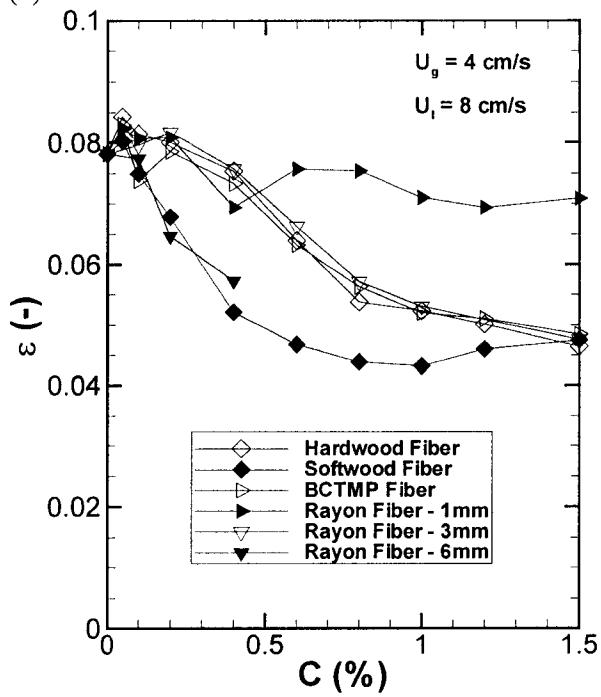

(f)

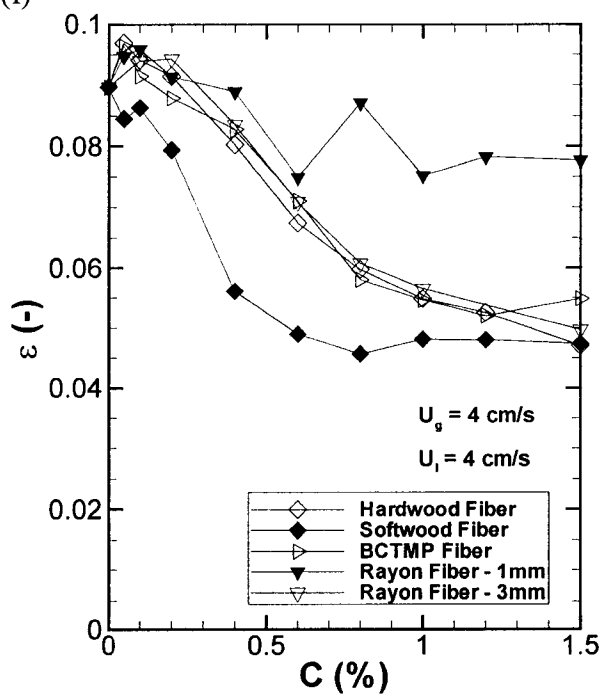

Figure 5.13: Variation of overall average gas holdup with superficial gas velocity in different fiber suspensions when U_l = 8 cm/s: (a) C = 0.1% and (b) C = 1.0%.

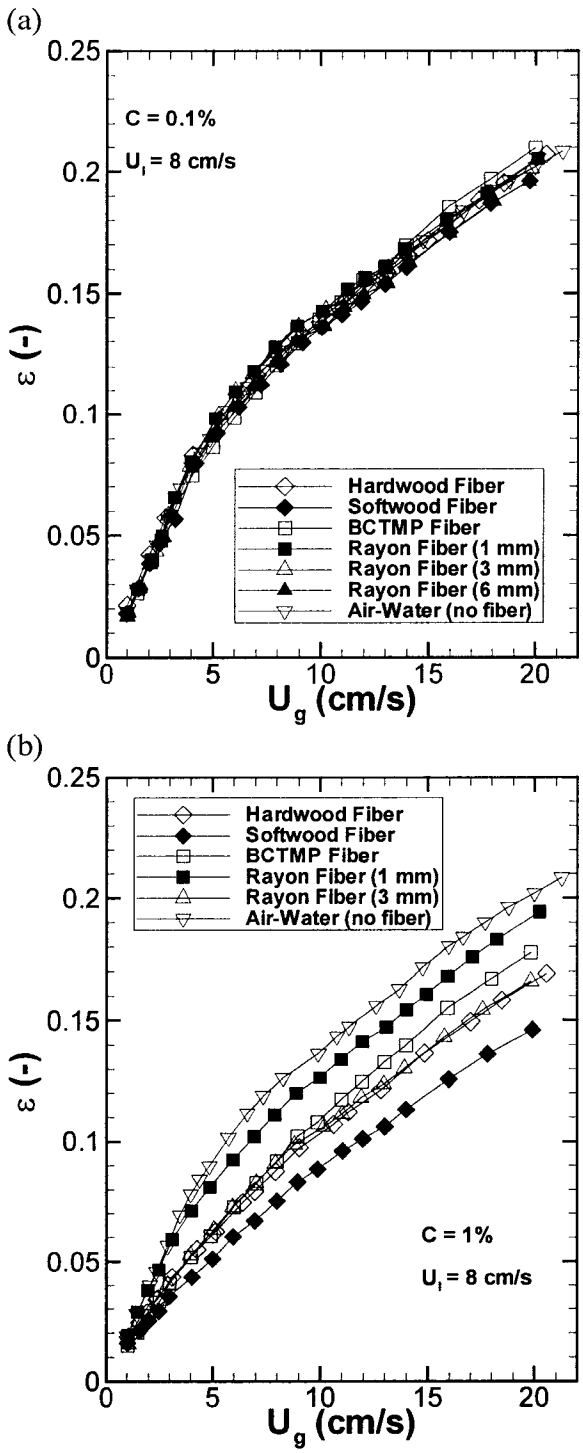

Figure 5.14: Variation of gas holdup with superficial liquid velocity in different fiber suspensions when U_g = 20 or 5 cm/s at different fiber mass fractions: (a) C = 0.1%; (b) C = 0.6%; and (c) C = 1.5%.

(a)

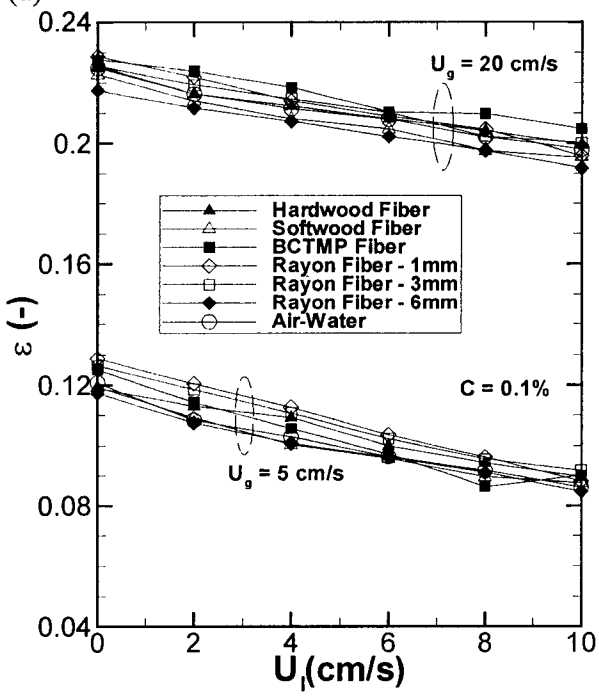

(b)

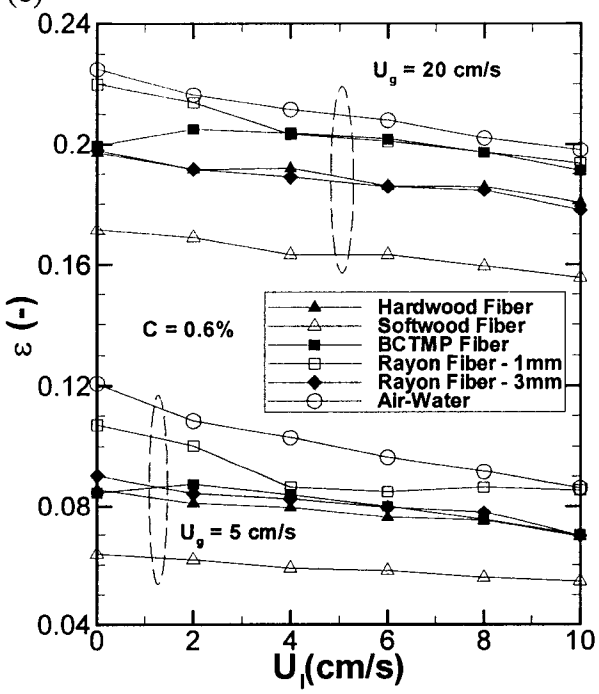

Figure 5.14: Continued.

(c)

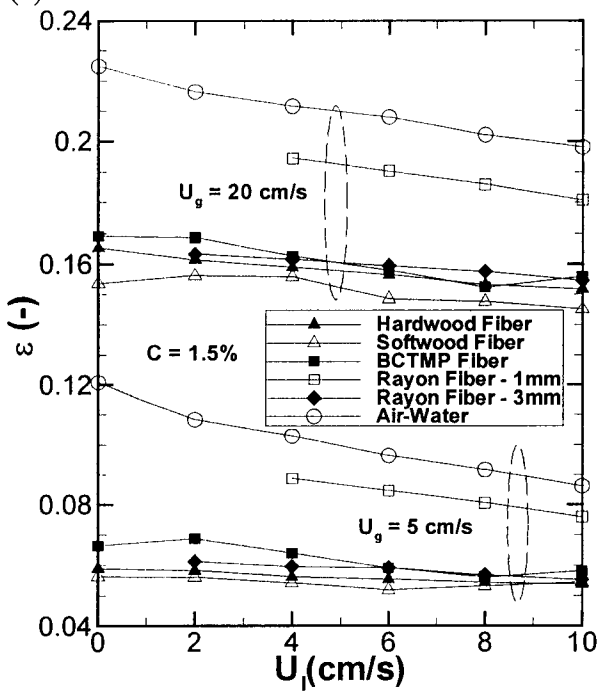

Figure 5.15: Variation of gas holdup with superficial liquid velocity in BCTMP fiber suspension at different fiber mass fraction when U_g = 20 cm/s.

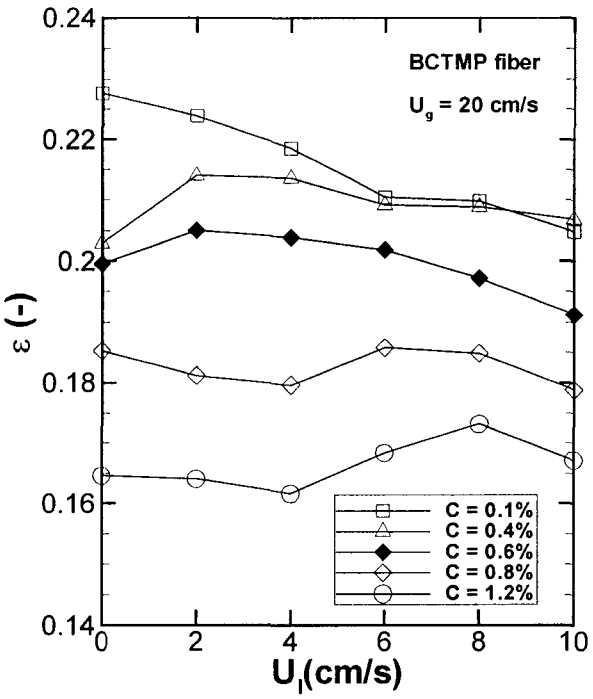

Figure 5.16: Variation of gas holdup ratio with superficial gas velocity for different fiber suspensions when U_l = 8 cm/s: (a) C = 0.1%; (b) C = 0.2%; (b) C =1.0%; and (c) C = 1.5%.

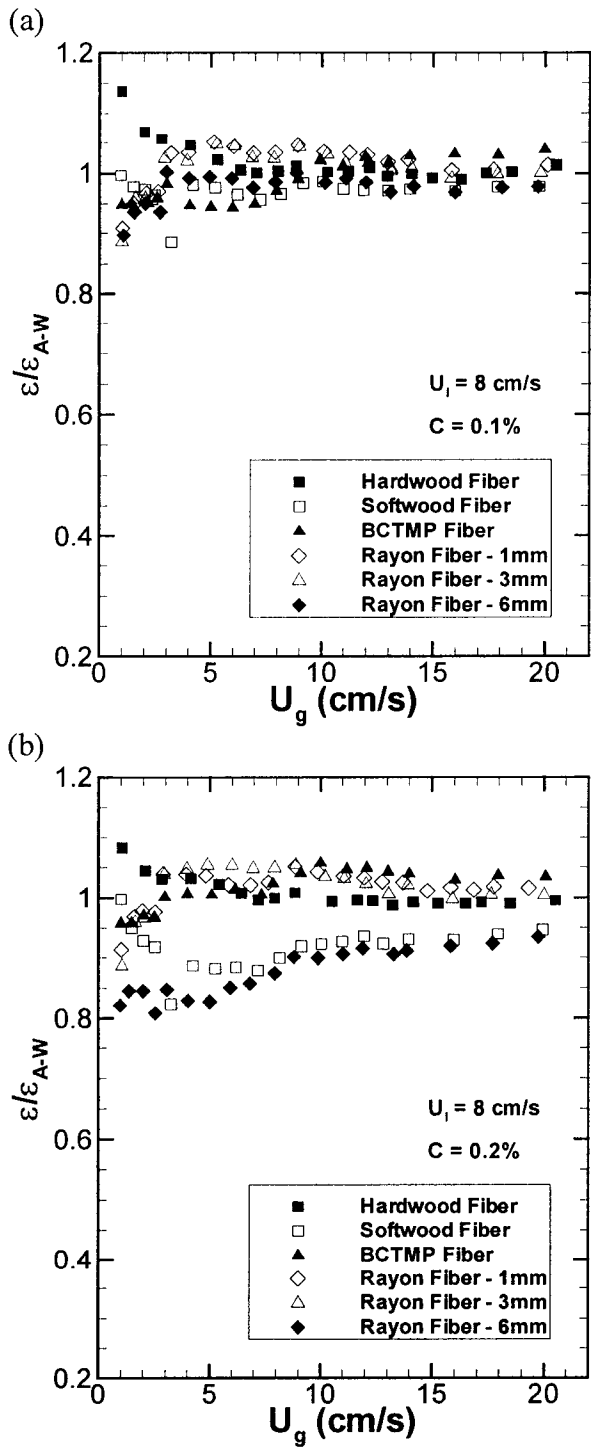

Figure 5.16: Continued.

(c)

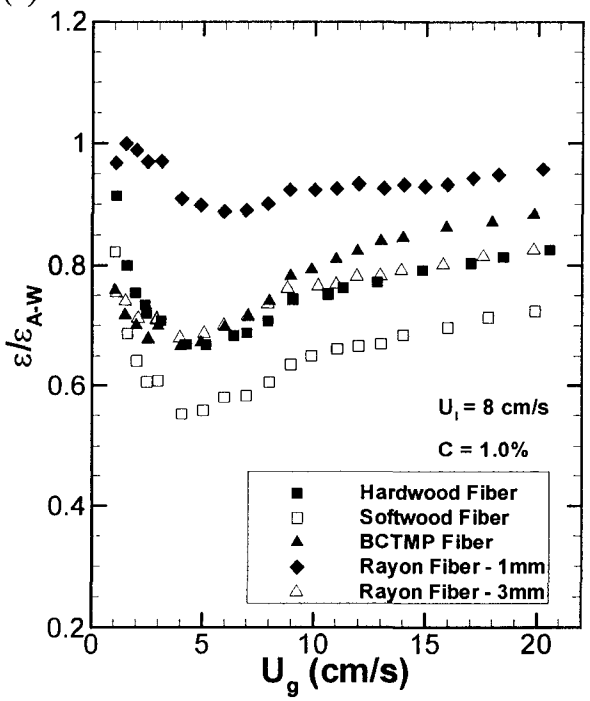

(d)

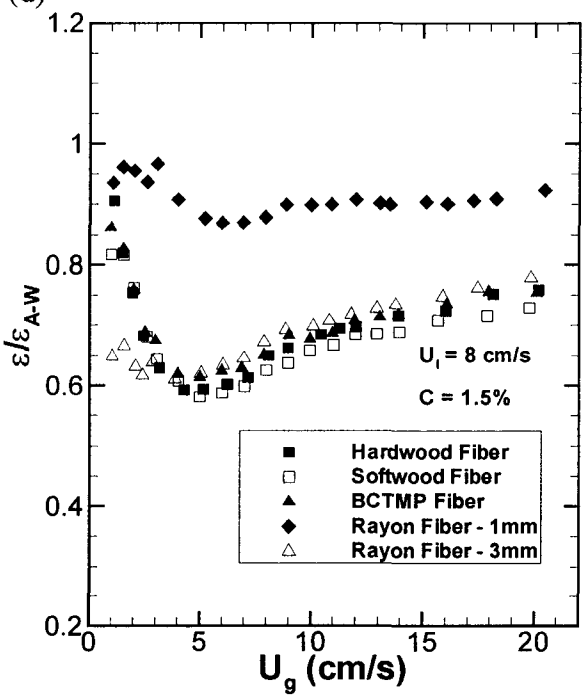

Figure 5.17: Variation of U_g/ε with total superficial velocity in hardwood fiber suspensions at different fiber mass fraction: (a) C = 0.1%; (b) C = 0.4%; (c) C = 1%; and (d) C = 1.5%.

(a)

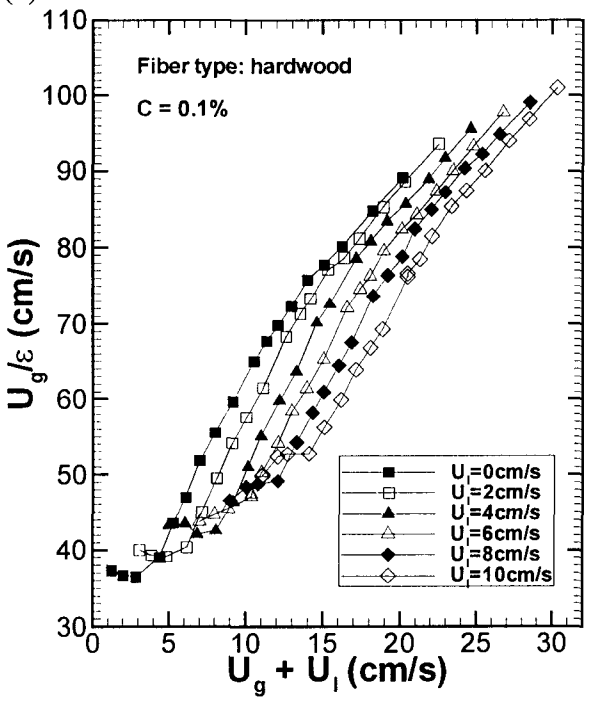

(b)

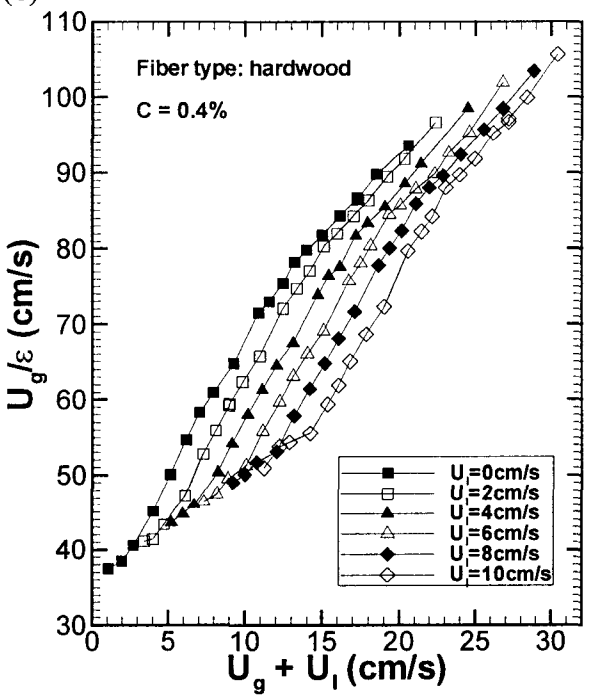

Figure 5.17: Continued.

(c)

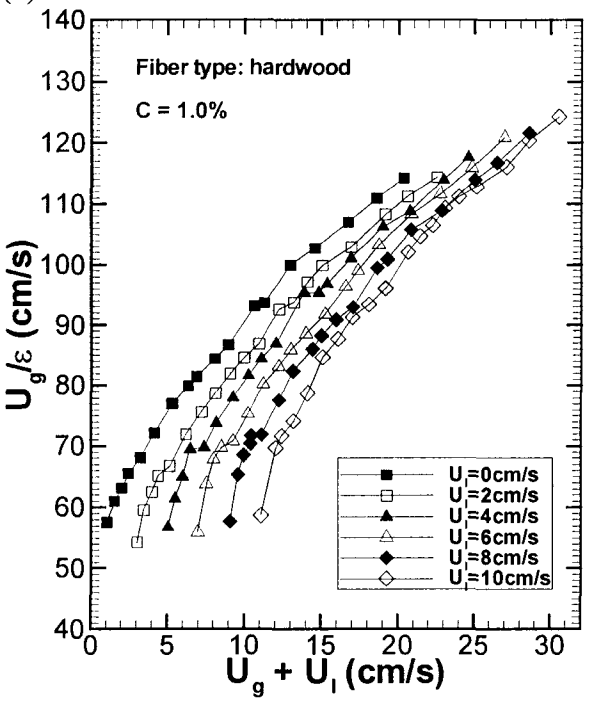

(d)

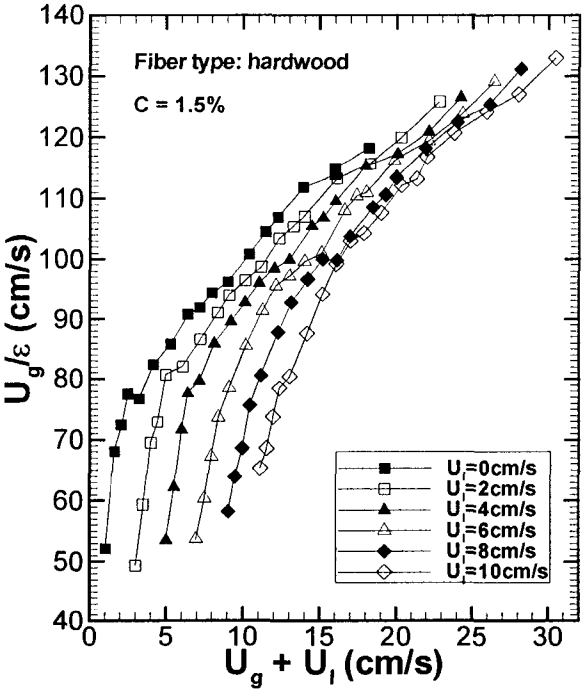

Figure 5.18: Variation of U_g/ε with superficial gas velocity at different superficial liquid velocities in hardwood fiber suspensions; (a) C = 0.1% and (b) C = 1.0%.

(a)

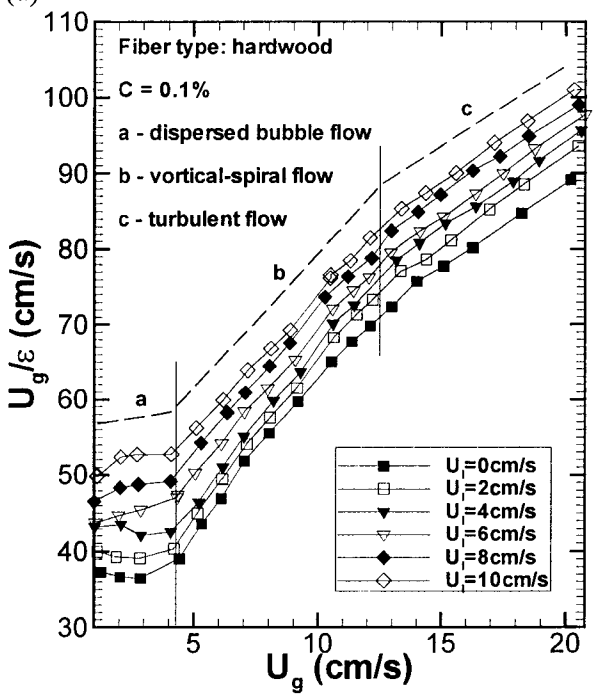

(b)

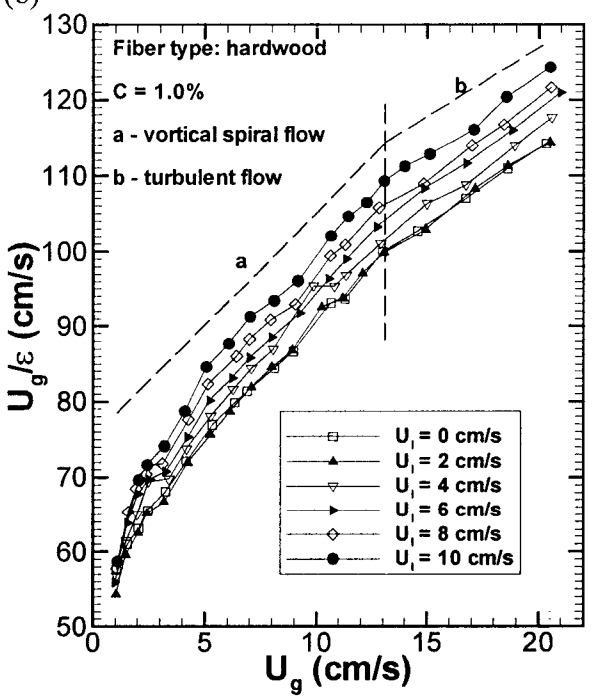

Figure 5.19: Variation of U_g/ε with superficial gas velocities at different fiber mass fractions in hardwood fiber suspensions (U_l = 8 cm/s).

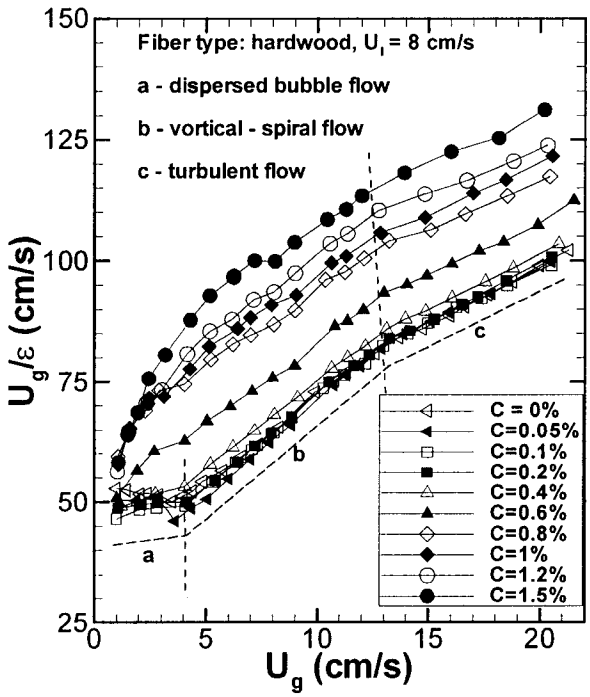

Figure 5.20: Variation of U_g/ε with superficial gas velocities in different fiber suspensions when U_l = 8 cm/s: (a) C = 0.1%; (b) C = 0.4%; (c) C = 1.0%; and (d) C = 1.5%.

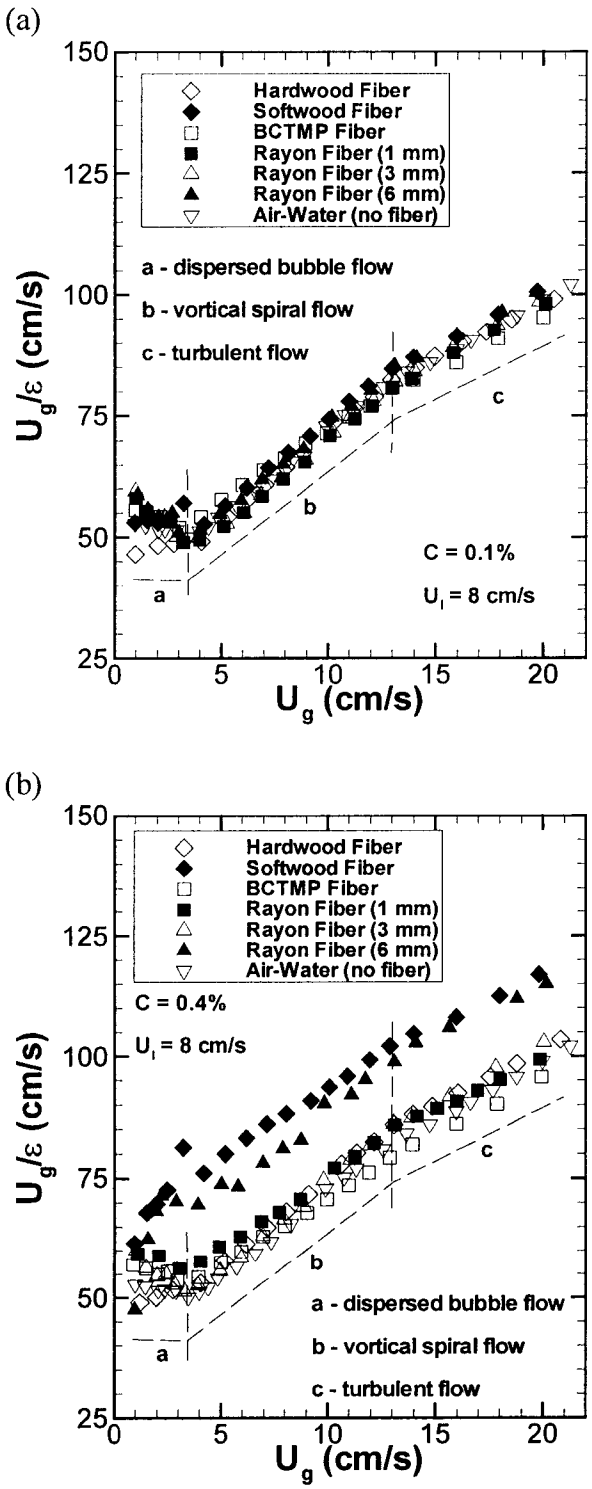

Figure 5.20: Continued.

(c)

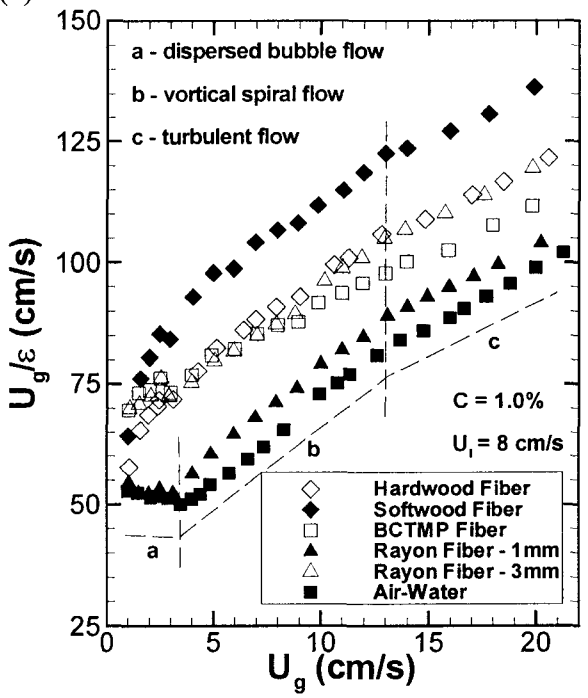

(d)

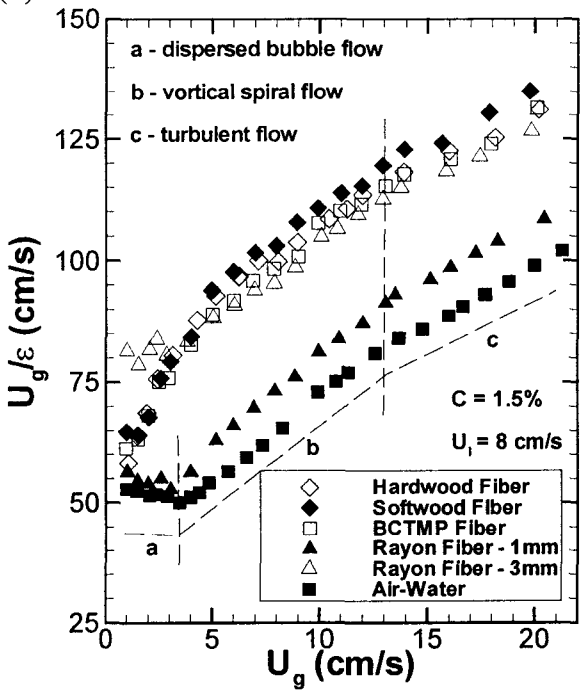

Chapter 6: QUANTIFYING THE FIBER EFFECT ON GAS HOLDUP

In Chapter 5, fiber mass fraction and type are found to have significant effects on gas holdup. At a constant fiber mass fraction and the same operating condition, the gas holdup is different in different fiber suspensions. The goal of this chapter is to identify a parameter that satisfies the following criterion: *when this parameter is constant, the gas holdup in different fiber suspensions is the same at a given operating condition.* This is important because with such a parameter: (i) the influences of adding different fibers on gas holdup in bubble columns can be quantitatively compared; and (ii) the gas holdup data acquired with different fiber types can be correlated by a single model.

To identify such a characterization parameter is not easy. No similar work has been found in the literature. The parameter should account for the effects of both fiber mass fraction and fiber type. Fiber type is only a qualitative factor. It includes chemical composition and physical and chemical properties. In the present study, the chemical composition of all six fiber types is cellulose and no chemical reactions are involved. Thus, only fiber physical properties will be considered when identifying the characterization parameter.

It is assumed that the influences of fiber mass fraction and fiber type can be characterized with a single parameter. This assumption is checked with the experimental data acquired in the present study.

This chapter is organized into several sections. The first section identifies and discusses the major influential factors related to fiber effects on gas holdup. Then the applicability of crowding factor (N_c) and fiber number density (N_f) for characterizing fiber effects are evaluated; they are two widely used parameters in describing fiber suspension rheological properties. A method is then described to identify a new parameter for characterizing the fiber effects on gas holdup, and its applicability is evaluated with experimental data. This chapter concludes with a summary.

6.1 Influential Factors Related to Fiber Effects on Gas Holdup

In Chapter 4, six mechanisms were identified that influence gas holdup in bubble columns filled with fiber suspensions; five of which (i.e., Mechanisms I, II, III, IV, and V in Table 4.1) are related to fiber flocculation and network strength, and these are functions of fiber mass fraction and physical properties. Thus, the factors influencing gas holdup in a fiber suspension are those affecting fiber flocculation.

Various studies (Forgacs *et al.*, 1958; Kerekes, 1983; Kerekes *et al.*, 1985; Kerekes and Schell, 1995; Wikstrom and Rasmuson, 1998) have showed that fiber flocculation is a complex function of fiber mass fraction (C), length (L), coarseness (ω), aspect ratio (r), stiffness (EI), surface friction coefficient (f), and flow conditions. For cellulose fiber suspensions, Kerekes and Schell (1995) concluded that fiber length affects the number of contacts per fiber and floc size and is the most important fiber property affecting floc formation. They also reported that fiber coarseness significantly affects the number of contacts per fiber, floc size, and suspension mobility (which is determined by the number of contacts per fiber and the force per contact). Wikstrom and Rasmuson (1998) reported that the fiber length distribution had a greater effect on fiber network strength than the average fiber length.

In summary, the factors influencing gas holdup in a fiber suspension include:

(i) Fiber mass fraction (C);

(ii) Average fiber length (L) and distribution;

(iii) Fiber coarseness (ω);

(iv) Fiber flexibility (1/EI), where E is fiber elastic modulus and I is the moment of inertia of a fiber; and

(v) Fiber surface friction coefficient (f).

The fiber coarseness (ω) is proportional to the cross-sectional area of the fiber; hence, it is related to fiber diameter. Fiber diameter is related to the moment of inertia of the fiber (I). Thus, including fiber coarseness can actually reflect information on fiber flexibility. The fiber elastic modulus (E) and surface friction coefficient (f) are difficult to obtain. Furthermore, in this study, fiber mass fraction is relatively small (only up to C = 1.5%); interfiber friction is assumed to be insignificant because for most conditions, the fiber

suspension is dilute or semi-dilute. Thus, a new characterization parameter will be formed including the information of fiber mass fraction, length and length distribution, and coarseness.

Two parameters currently widely used in characterizing fiber suspension behaviors are crowding factor (N_c) and fiber number density (N_f). In the following sections, these two parameters are discussed in detail.

6.2 Crowding Factor

6.2.1 Concept of the crowding factor

Mason (1948) suggested that fiber-fiber interaction becomes important when the number of fibers in the sphere swept by a fiber is larger than 1. Kerekes *et al.* (1985) extended this idea and proposed a "crowding factor" to characterize fiber-fiber contact regimes. The crowding factor (N_c) is defined as the number of fibers inside a spherical volume with a diameter equal to the fiber length (Kerekes *et al.*, 1985; Kerekes and Schell, 1992).

For suspensions of cylindrical fibers with uniform length (L) and diameter (d), the crowding factor is calculated by dividing the total fiber volume in a fictitious sphere of diameter L by the volume of a single fiber, i.e.,

$$N_c = \frac{V_{tot,f}}{V_f} = \frac{\frac{1}{6}\pi L^3 C_v}{\frac{1}{4}\pi d^2 L} \tag{6.1}$$

or

$$N_c = \frac{2}{3} C_v \left(\frac{L}{d}\right)^2 \tag{6.2}$$

where C_v is the volumetric fiber fraction ($0 \leq C_v \leq 1$).

For cellulose fibers, it is not convenient to calculate the crowding factor using Eq. (6.2) because a direct measure of C_v and d are difficult. Assuming all fibers have identical

length (L) and coarseness (ω), the crowding factor can also be calculated by dividing the total fiber mass in the fictitious spherical volume by the mass of a single fiber, i.e.,

$$N_c = \frac{M_{tot,f}}{M_f} = \frac{\frac{1}{6}\pi L^3 \rho_m C/100}{\omega L} = \frac{\pi L^2 \rho_m C}{600\omega} \tag{6.3}$$

where C is the suspension fiber mass fraction in percent (i.e., $0 \le C \le 100$) and ρ_m is the fiber suspension density. When fiber mass fraction is small (e.g., $0 \le C \le 1.5\%$), the fiber suspension density is close to water, i.e., $\rho_m \approx 1000$ kg/m^3. If the units of L and ω are m and kg/m, respectively, we have

$$N_c \approx \frac{5\pi C L^2}{3\omega} \tag{6.4}$$

This agrees with Kerekes and Schell (1992), who further approximated π with 3 and obtained

$$N_c \approx \frac{5CL^2}{\omega} \tag{6.5}$$

The fiber length (L) is not clearly defined in Eqs. (6.4) and (6.5). Notice that cellulose fiber lengths are usually not uniform; in this case, Kerekes and Schell (1995) used the length weighted average fiber length (L_L) in calculating the crowding factor. The use of L_L to estimate N_c for a polydisperse fiber suspension was later theoretically justified by Huber and Martinez (2003) based on mass conservation.

Kropholler and Sampson (2001) argued that cellulose fibers typically have a length distribution and the number of fibers within the spherical volume swept by a given fiber follows a distribution dependent upon the fiber length distribution. Assuming a lognormal fiber length distribution, Kropholler and Sampson (2001) derived the probability density function, mean, and variance of the crowing factor for fiber suspensions. The results showed that the distribution of crowding factors resembles a lognormal distribution and the mean crowding factor ($N_{c,log}$) significantly increases with the coefficient of variation of fiber length (CV(L)):

$$N_{c,log} = N_{c,LA} \cdot \{1 + [CV(L)]^2\}^4 \tag{6.6}$$

where $N_{c,LA}$ is the crowding factor calculated with Eq. (6.4) using the arithmetic average fiber length (L_A).

Huber *et al.* (2003) argued that the cellulose fiber length does not necessarily follow a lognormal distribution. As an extension of the Kropholler and Sampson (2001) theory, Huber *et al.* (2003) derived an expression for the probability density function of the crowding factor for a general fiber length distribution f(L); it was calculated by integrating the product of the probability of having fibers generating a spherical volume V_{sp} and the probability of having N_c fibers present in that volume, over the whole possible volume range (i.e., from 0 to infinity):

$$p(N_c) = \frac{10}{3}\left(\frac{6}{\pi}\right)^{1/3} \frac{C}{\omega N_c^{\,2}} \int_0^{\infty} V_{sp}^{1/3} \cdot f\left(\left(\frac{6V_{sp}}{\pi}\right)^{1/3}\right) \cdot f\left(\frac{10 \cdot C \cdot V_{sp}}{\omega N_c}\right) dV_{sp} \qquad (6.7)$$

where V_{sp} is the volume of the sphere swept by a fiber and is related with fiber length (L) by:

$$V_{sp} = \frac{\pi}{6} L^3 \qquad (6.8)$$

With Eq. (6.7), the mean crowding factor ($\overline{N}_c$) is calculated by

$$\overline{N}_c = \int_0^{\infty} N_c \cdot p(N_c) \cdot dN_c \qquad (6.9)$$

6.2.2 Application of the crowding factor

The crowding factor is viewed as a dimensionless concentration which accounts for fiber morphology (Huber *et al.*, 2003) and has been proven to be useful to describe fiber flocculation (Kerekes and Schell, 1992; Kerekes, 1995; Huber *et al.*, 2003). It reflects the level of inter-fiber contact and restraint of rotational motion, and hence, the tendency to form flocs in a fiber suspension (Kerekes and Schell, 1992, 1995). Kerekes (1995) claimed that the crowding factor is a useful tool for describing fiber suspensions over the whole range of fiber mass fractions used in papermaking and is superior to fiber mass fraction alone. Huber *et al.* (2003) reported that the crowding factor calculated with Eq. (6.9) or that obtained with Eq. (6.4) using L_L can provide a satisfactory description of the fiber flocculation behaviors in their study.

Dodson (1996) derived a relationship between the crowing factor and the contact number (n_c) for a random three-dimensional suspension formed by fibers of uniform length (L) and diameter (d):

$$n_c = \frac{3}{r} N_c \tag{6.10}$$

where r is the fiber aspect ratio, i.e., r = L/d. The contact number (n_c) is widely used in the analysis of fiber suspension prosperities, such as flocculation, network strength, and local density distribution (Meyer and Wahren, 1964; Wahren, 1979; Farnood *et al.*, 1994; Dodson, 1996; Dodson and Sampson, 1999).

Using the crowding factor, Kerekes and Schell (1992) identified three broad fiber-fiber contact types in fiber suspensions, i.e., occasional collisions, forced collisions, and continuous contacts. When $N_c < 1$, fibers are free to move, they occasionally collide through translation, temporarily remain together, and then completely disperse; as N_c increases, more collisions take place through translation and eventually through rotation; when N_c increases to ~60, which corresponds an average number of contacts per fiber of 3, fibers become restrained in rotation relative to one another through 3-point contact and start to form a continuous network; when $N_c > 60$, the continuous network remains and is enhanced as N_c increases.

While it is useful to characterize fiber suspensions, there are cases where the crowding factor alone is found insufficient for the characterization. Kerekes and Schell (1995) found that at the same crowding factor, changing fiber length yielded a different change in fiber suspension uniformity than changing fiber mass fraction. Su and Heindel (2003) reported that the crowding factor alone is not sufficient to characterize the fiber influence on gas holdup in an air-water-Rayon fiber semi-batch bubble column.

The reason that crowding factor is insufficient for characterization of fiber suspensions includes: (i) fiber length usually is not uniform and the effect of fiber length distribution is not considered when Eqs. (6.2), (6.4), or (6.5) are used to calculate the crowding factor; and (ii) the crowding factor only considers fiber mass fraction and two major influential fiber physical properties - length and coarseness, while there are other

factors, including flexibility and surface friction coefficient, etc., that can significantly influence fiber suspension properties.

6.2.3 Effect of crowding factor on gas holdup

In this section, the applicability of the crowding factor in characterizing fiber effect on gas holdup in the present cocurrent air-water-fiber bubble column is assessed. The following two crowding factor estimation methods are used:

(i) $N_{c,LA}$ - the crowding factor estimated with Eq. (6.4) using the arithmetic average fiber length (L_A); and

(ii) N_c - the crowding factor estimated with Eq. (6.4) using the length weighted average fiber length (L_L).

Figure 6.1 shows the variation of gas holdup with crowding factor based on the length-weighted average fiber length (N_c) for different fiber types at two superficial liquid velocities (U_l = 10 or 2 cm/s). For both high (U_l = 10 cm/s, Fig. 6.1a) and low (U_l = 2 cm/s, Fig. 6.1b) superficial liquid velocities, the gas holdup trend with increasing crowding factor is similar. The similarity is also seen for each fiber type between the trends at low (U_g = 10 cm/s) and high (U_g = 20 cm/s) superficial gas velocities. Gas holdup is at first approximately constant when N_c is small (i.e., $N_c \lesssim 10$), then decreases significantly with increasing crowding factor when $10 \lesssim N_c \lesssim 100$, and eventually remains approximately constant when $N_c \gtrsim 100$ (although this is only seen for the fiber types having a crowding factor higher than 100 at $0 < C < 1.5\%$, it is believed that a similar trend can be seen for other fiber types if, at higher fiber mass fractions, the crowding factors can reach a value higher than ~100). However, it is clear that there is a significant difference between the gas holdup values for different fiber types when N_c is fixed. This shows the insufficiency of the crowding factor (N_c) in characterizing the fiber influence on gas holdup. Figure 6.2 shows the effect of $N_{c,LA}$ on gas holdup. The gas holdup trend with $N_{c,LA}$ is similar to the trend presented in Fig. 6.1. However, the order of gas holdup values for different fiber types at the same $N_{c,LA}$ is different from that at the same N_c and the difference between the gas holdup for different fiber types at the same $N_{c,LA}$ is even larger. Thus, the crowding factor $N_{c,LA}$, as calculated

with the arithmetic average fiber length, can not sufficiently characterize the fiber influence on gas holdup either.

The major reasons that the crowding factor alone does not describe the gas holdup trends for different fiber types are identified in Sec 6.2.2. In order to characterize the fiber type effect on gas holdup, new information should be included in the characterization parameter in addition to fiber mass fraction, length, and coarseness.

6.3 Fiber Number Density

6.3.1 Concept of the fiber number density

Fiber number density (N_f) is defined as the number of fibers in a unit volume of fiber suspension. Note that the unit volume should have a characteristic length much larger than the average fiber length.

It is difficult to count the fibers in a fiber suspension. However, the number of fibers per unit mass (n_f) can be obtained using a Fibre Quality Analyzer (Huber and Martinez, 2003) or standard methods (TAPPI, 2002d, 2002b). Assuming fibers are uniformly distributed in the suspension, the fiber number density can be calculated from the number of fibers per unit mass (n_f) by

$$N_f = n_f \cdot C \cdot \rho_m / 100 \tag{6.11}$$

where C is the fiber mass fraction; and ρ_m is the fiber suspension density.

In the present study, for cellulose fibers, n_f is given in Table 3.1. For Rayon fibers, because they have uniform length and coarseness, the number of fiber per unit mass is calculated by

$$n_f = \frac{1}{\omega L} \tag{6.12}$$

where ω is Rayon fiber coarseness and L is fiber length.

In the present study, the fiber mass fraction is $C \leq 1.5\%$. Hence, the difference between the fiber suspension and the suspending liquid (i.e., water) densities is negligible. Thus, $\rho_m \approx \rho_l$.

6.3.2 Relationship between fiber number density and fiber length distribution

For a fiber sample with a total mass M and non-uniform fiber length, by definition, the arithmetic average fiber length (L_A) of a sample is calculated by

$$L_A = \frac{1}{M \cdot n_f} \sum_{i=1}^{M \cdot n_f} l_i \tag{6.13}$$

where n_f is the number of fibers per unit mass; l_i is the length of a single fiber; M is the mass of the fiber sample.

The length weighted average fiber length L_L is calculated by

$$L_L = \frac{\sum_{i=1}^{M \cdot n} l_i^2}{\sum_{i=1}^{M \cdot n} l_i} = \frac{1}{n_f L_A} \sum_{i=1}^{M \cdot n} l_i^2 \tag{6.14}$$

If the total fiber number ($M \cdot n_f$) is large, the fiber length standard deviation (S_L) is

$$\begin{aligned} S_L^2 &= \frac{1}{M \cdot n_f} \sum_{i=1}^{M \cdot n_f} (l_i - L_A)^2 \\ &= \frac{1}{M \cdot n_f} \left(\sum_{i=1}^{M \cdot n_f} l_i^2 - 2L_A \sum_{i=1}^{M \cdot n_f} l_i + M \cdot n_f L_A^2 \right) \\ &= \frac{1}{M \cdot n_f} \left(\sum_{i=1}^{M \cdot n_f} l_i^2 - M \cdot n_f L_A^2 \right) \\ &= \frac{1}{M \cdot n_f} \left(M \cdot n_f L_L L_A - M \cdot n_f L_A^2 \right) \\ &= L_A (L_L - L_A) \end{aligned} \tag{6.15}$$

The number of fibers per unit mass (n_f) is calculated with Eq. (6.12) using the arithmetic average fiber length (L_A):

$$n_f = \frac{1}{\omega L_A} \tag{6.16}$$

Thus, for a fiber sample, n_f is related to the fiber coarseness (ω), length weighted average length (L_L), and fiber length standard deviation (S_L) by

$$n_f = \frac{2}{\omega \left(L_L + \sqrt{L_L^2 - 4S_L^2} \right)} \tag{6.17}$$

Using Eq. (6.11), the fiber number density (N_f) is related to the fiber length standard deviation (S_L) and mass fraction (C) by

$$N_f = \frac{\rho_m C}{50 \cdot \omega\left(L_L + \sqrt{L_L^2 - 4S_L^2}\right)} \tag{6.18}$$

When the fiber mass fraction is small, $\rho_m \approx \rho_l$. Hence,

$$N_f \approx \frac{\rho_l C}{50 \cdot \omega\left(L_L + \sqrt{L_L^2 - 4S_L^2}\right)} \tag{6.19}$$

This means that the fiber number density is related to the length-weighted average fiber length and its standard deviation.

If a fiber sample has a uniform length, $L_A = L_L$ and $S_L = 0$. Equations (6.17) and (6.18) become Eqs. (6.12) and (6.11), respectively.

6.3.3 Application of the fiber number density

The fiber number density (N_f) is an important parameter to characterize a fiber suspension. Two dimensionless parameters, $N_f L^3$ and $N_f L^2 d$, are usually used in describing fiber suspension rheological properties (Doi and Edwards, 1978b, 1978a, 1987; Sundararajakumar and Koch, 1997; Schmid *et al.*, 2000; Xu and Aidun, 2005).

According to the theory of Doi and Edwards (1987), fiber suspensions can be classified into dilute, semi-dilute, and concentrated suspensions. In a dilute suspension, the fiber volume fraction C_v is usually so small that hydrodynamic interaction between fibers or between a fiber and a flow boundary are negligible (Petrie, 1999). Fibers in such a suspension can rotate freely without interference with other fibers. The fiber number density (N_f) and fiber length satisfy the following relationship (Doi and Edwards, 1987):

$$N_f L^3 << 1 \tag{6.20}$$

In a semi-dilute fiber suspension, the fiber number density N_f is much larger. The rotation of each fiber is restricted by other fibers. Fiber dynamic properties are affected by inter-fiber interactions. However, the fiber static properties (fiber properties at an equilibrium state) are not influenced. Fiber orientation is still random and the fiber suspension can be

treated as isotropic. The fiber number density satisfies the following relationship (Doi and Edwards, 1987):

$$N_f d \cdot L^2 << 1 << N_f L^3 \tag{6.21}$$

In a concentrated fiber suspension, the fiber-fiber interaction affects fiber static properties. Fibers tend to orient in the same direction as their neighbors. For this condition, the fiber number density satisfies (Doi and Edwards, 1987)

$$N_f d_f L^2 > 1 \tag{6.22}$$

In this regime, there is a critical fiber number density (N_f^*), which is on the order of $1/(d \cdot L^2)$. When $N_f < N_f^*$, the fiber suspension is still isotropic; when $N_f > N_f^*$, the suspension becomes anisotropic. In the latter case, the fiber suspension is called a liquid crystalline suspension (Doi and Edwards, 1987).

The dimensionless parameter $N_f L^3$ is actually the number of fibers in a cube with an edge equal to the fiber length (L). It is closely related to the crowding factor (N_c). For a suspension of fibers with uniform length and diameter,

$$N_f L^3 = \frac{6N_c}{\pi} \tag{6.23}$$

If the fiber length is not uniform, $N_f L^3$ can be different from $6N_c/\pi$ because the fiber number density (N_f) can change with fiber length distribution even when the average fiber length (L) is the same.

6.3.4 Effect of fiber number density on gas holdup

In this section, the gas holdup trend with fiber number density (N_f) is presented (Fig. 6.3). Notice that the unit of N_f is one per cubic centimeter ($1/cm^3$). The applicability of two new crowding factors (N_{c1} and N_{c2}) to characterize the fiber effect on gas holdup is also studied by plotting gas holdup versus the crowding factors for various fiber types (Figs. 6.4 and 6.5).

The crowing factor N_{c1} is defined as

$$N_{c1} = \frac{\pi}{6} L_L^3 N_f \tag{6.24}$$

where L_L is the length weighted average fiber length. N_{c1} represents the number of actual fibers in a sphere with a diameter equal to L_L.

The crowing factor N_{c2} is defined as

$$N_{c2} = \frac{\pi}{6} L_A^3 N_f \tag{6.25}$$

where L_A is the length weighted average fiber length. N_{c2} represents the number of actual fibers in a sphere with a diameter equal to L_A.

From Fig. 6.3, it can be seen that gas holdup is not significantly affected by fiber number density when N_f is small. When N_f is larger than some critical value (e.g., ~1000 cm^{-3} for 3 mm Rayon fiber at U_g = 20 cm/s, and U_l = 10 cm/s, Fig. 6.3a), it decreases with increasing fiber number density. The critical value is a function of fiber type. Further comparison shows that the critical N_f value decreases with increasing arithmetic average fiber length (L_A) at all the addressed conditions. Since the difference between the ε vs. N_f curves of different fiber types is significant, N_f alone is not sufficient to characterize the fiber effect.

As shown in Figs. 6.4 and 6.5, including the fiber number density (N_f) in the evaluation of the crowding factor does not improve the ability of the crowding factor to fully account for the fiber effect on gas holdup in the air-water-fiber bubble column. The trends of gas holdup with increasing N_{c1} (Fig. 6.4) and N_{c2} (Fig. 6.5) are similar to those shown in Figs. 6.1 and 6.2 except the order of gas holdup from different fiber types at a constant crowding factor changes with the crowding factor evaluation method.

6.4 A New Fiber Characterization Parameter

In the preceeding sections, the crowding factor (N_c) and fiber number density (N_f) are found insufficient in characterizing the fiber effect on gas holdup in air-water-fiber bubble columns. This is because the crowding factor does not account for the fiber length distribution, flexibility, and surface friction coefficient while the fiber number density does not even provide information on average fiber length. Crowding factors estimated using fiber number density (Eqs. (6.24) and (6.25)) also failed to fully account for the fiber effect. Hence,

it is necessary to find a new parameter that will account for more factors that characterize the effect fibers have on gas holdup in a gas-liquid-fiber suspension.

In this section, efforts are made to find a new parameter to fully characterize the fiber effect by considering combinations of the crowding factor (N_c) and fiber number density (N_f). This approach is chosen because including N_f can provide fiber length distribution information (Sec. 6.3.2), which is absent in N_c. To simplify the problem, other factors including fiber surface friction coefficient and elastic modulus are not considered because they are difficult to measure and, in most cases in the present study, fiber-fiber friction is not significant because the fiber suspensions are considered dilute ($C \leq 1.5\%$).

According to Figs. 6.1-6.5, gas holdup can be represented as a function of $\ln(N_c)$ and $\ln(N_f)$. Hence, it is expected that gas holdup is also a function of the natural logarithm of the combination of these two parameters. Hence, define:

$$I_c = \ln(N_c^a N_f^b) \tag{6.26}$$

where a and b are two exponents to be determined using the experimental data collected in the present study. Note that I_c can be written as

$$I_c = a \ln(N_c N_f^{b/a}) = a \ln(N_c N_f^x) \tag{6.27}$$

Thus, the exponent a is trivial and can be an arbitrary value. Hence, only one exponent is necessary to determine the form of I_c. Without losing generality, we set

$$a + b = 1 \tag{6.28}$$

According to Sections 6.2 and 6.3, gas holdup decreases with increasing N_c and N_f. Thus, we expect that the exponents a and b have the same sign and $0 < a < 1$ and $0 < b < 1$. Hence, the following is the form of the new parameter we are trying to identify:

$$I_c = \ln(N_c^{1-b} N_f^b) \tag{6.29}$$

where $0 < b < 1$.

The exponent b is determined by plotting gas holdup values versus I_c (at a guessed b value) for all fiber types at a fixed operating condition. If the selected b value collapses all the ε versus I_c curves for all fiber types to a single curve, then the b value is selected.

Notice that in the definition of I_c, N_c is dimensionless while N_f is dimensional. However, the selection of N_f unit does not influence the value of b. Assume that N_f has two

different units and the conversion factor between them is a constant X. When the first unit is used, I_c is calculated by

$$I_{c1} = \ln(N_c^{1-b} N_f^b) \tag{6.30}$$

When the second unit is used, I_c is calculated by

$$I_{c2} = \ln(N_c^{1-b}(XN_f)^b) = \ln(N_c^{1-b} N_f^b) + b \ln X = I_{c1} + b \ln X \tag{6.31}$$

which means that changing the units on N_f will only move every data point on the ε versus I_c plot by a constant distance (blnX) in the positive I_c direction; this will not change the relative position of each point on the plot.

In the present study, *the fiber number density is used with units of* $1/cm^3$.

After comparing various b values in the range of $0 < b < 1$, it is found that when b = 1/5, the data points from different fiber suspensions gather on a single curve at fixed superficial gas and liquid gas velocities. Figure 6.6 shows some examples of the variation of gas holdup with I_c for different fiber types at high and low superficial gas and liquid velocities. In Fig. 6.6, the gas holdup difference between different fiber types is very small at a constant I_c value. This is especially true for hardwood, softwood, and 3 and 6 mm Rayon fibers. Although it is seen that some of the BCTMP and 1 mm Rayon fiber data points deviate slightly from the curve, the new parameter

$$I_c = \ln(N_c^{4/5} N_f^{1/5}) \tag{6.32}$$

is a significant improvement over the fiber number density or crowding factor alone. The slight deviation of the BCTMP and 1 mm Rayon fiber data is attributed to the fact that I_c still does not account for the influential factors such as the foam promoting lignosulfonates particularly contained in the BCTMP fiber, fiber elastic modulus, and surface friction coefficient. Nevertheless, the parameter I_c defined in Eq. (6.32) is a suitable indictor of the fiber influence on gas holdup.

From Fig. 6.6, it is clear that the gas holdup trend with increasing I_c is similar at all operating conditions. Gas holdup approximately remains constant when $I_c \lesssim 6.5$; then decreases significantly with increasing I_c when $6.5 \lesssim I_c \lesssim 9$; when $I_c \gtrsim 9$, the gas holdup is again nearly constant with I_c.

Figure 6.7 compares the variation of I_c with fiber mass fraction (C) for the 6 fiber types used in this study. I_c increases linearly with the natural logarithm of C, which agrees with its definition:

$$I_c = \ln(N_c^{4/5} N_f^{1/5}) \approx \ln(C) + \frac{1}{5}\ln\left[\left(\frac{\rho_l n_f}{100}\right)\left(\frac{\pi L_L^{\,2}\rho_l}{600\omega}\right)^4\right] \qquad (6.33)$$

It is interesting to see that at a given fiber mass fraction, the I_c values of softwood and 6 mm Rayon fibers are very close (Fig. 6.7). This is also seen for hardwood, BCTMP, and 3 mm Rayon fibers. Recall that in Sec. 5.2.2 (Fig. 5.12), the gas holdup in softwood and 6 mm Rayon fiber suspensions are very similar at a given C for all studied conditions; the gas holdup similarity between hardwood and 3 mm Rayon fiber suspensions is also observed. The gas holdup trend with increasing C for BCTMP fiber is similar to that for hardwood and 3 mm Rayon fibers, although the gas holdup in BCTMP fiber suspensions is higher due to the existence of foam promoting lignosulfonates. These results further support that I_c is a suitable parameter to characterize the fiber effect on gas holdup.

6.5 Summary

In this chapter, a parameter that characterizes the fiber effect on gas holdup in gas-liquid-fiber bubble columns is identified and satisfies the following condition: when this parameter is constant, the gas holdup in different fiber suspensions is generally similar at most operating conditions. The crowding factor estimated with various methods and fiber number density did not satisfy this criterion. A method is proposed to identify a characterization parameter by combining the crowding factor and fiber number density. With this method, a parameter $I_c = \ln(N_c^{4/5} N_f^{1/5})$ is identified. The experimental data shows that I_c satisfies the proceeding condition for most conditions addressed in this study.

Figure 6.1: Effect of crowding factor (N_c) on gas holdup: (a) U_l = 10 cm/s and (b) U_l = 2 cm/s.

(a)

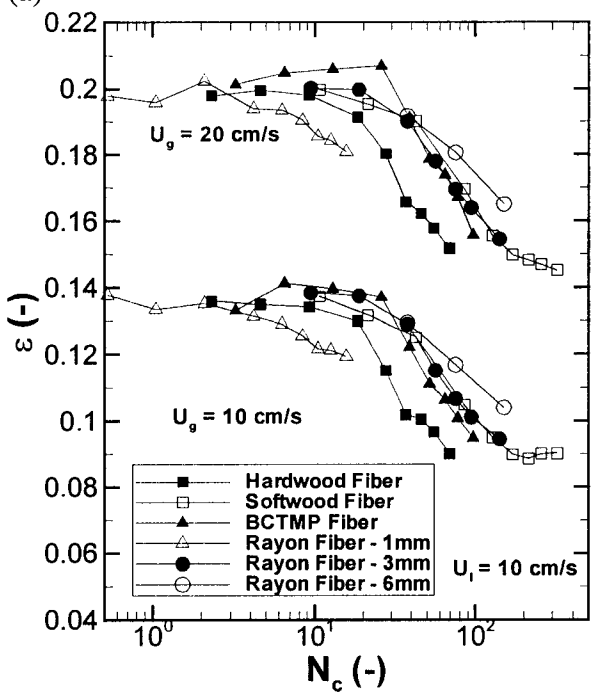

(b)

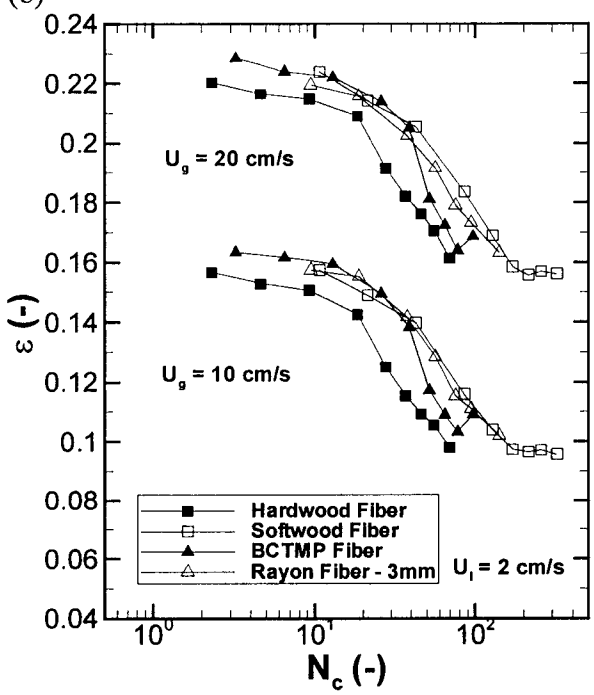

Figure 6.2: Effect of crowding factor ($N_{c,LA}$) on gas holdup: (a) U_l = 10 cm/s and (b) U_l = 2 cm/s.

(a)

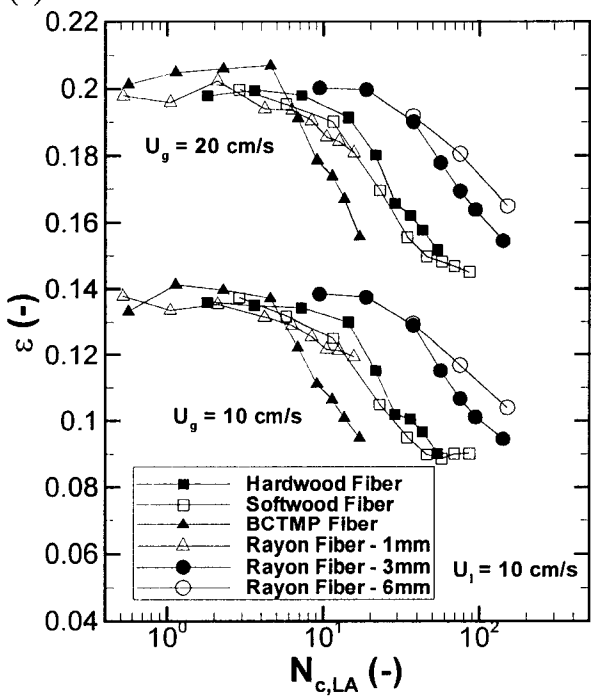

(b)

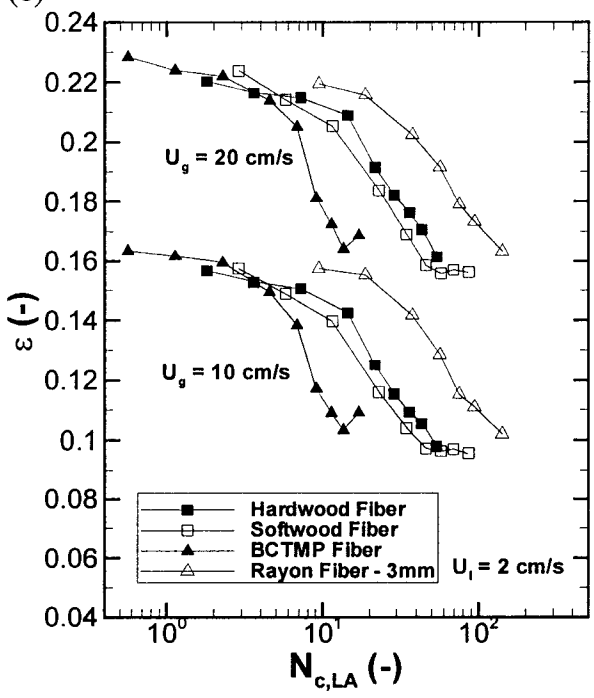

Figure 6.3: Effect of fiber number density on gas holdup: (a) U_l = 10 cm/s and (b) U_l = 2 cm/s.

(a)

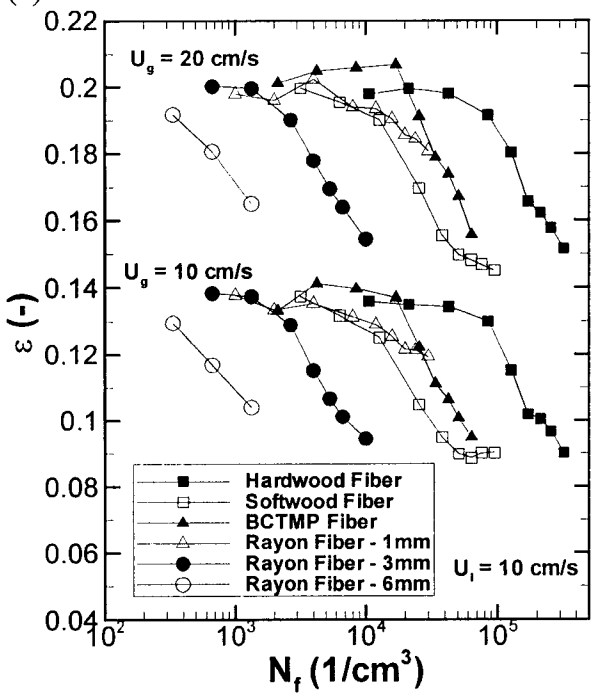

(b)

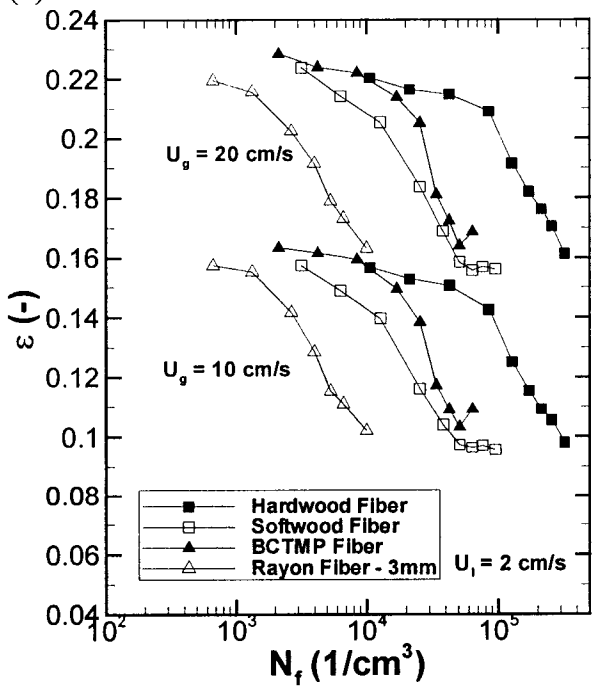

Figure 6.4: Variation of gas holdup with N_{c1}: (a) U_l = 10 cm/s and (b) U_l = 2 cm/s.

(a)

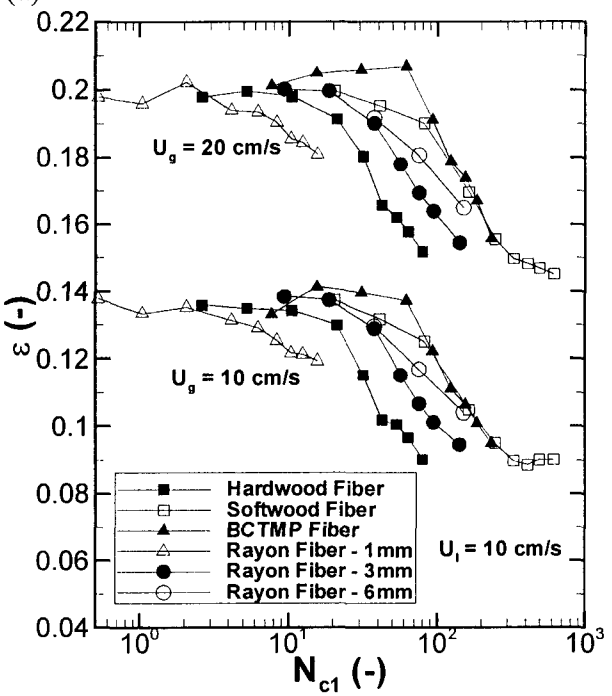

(b)

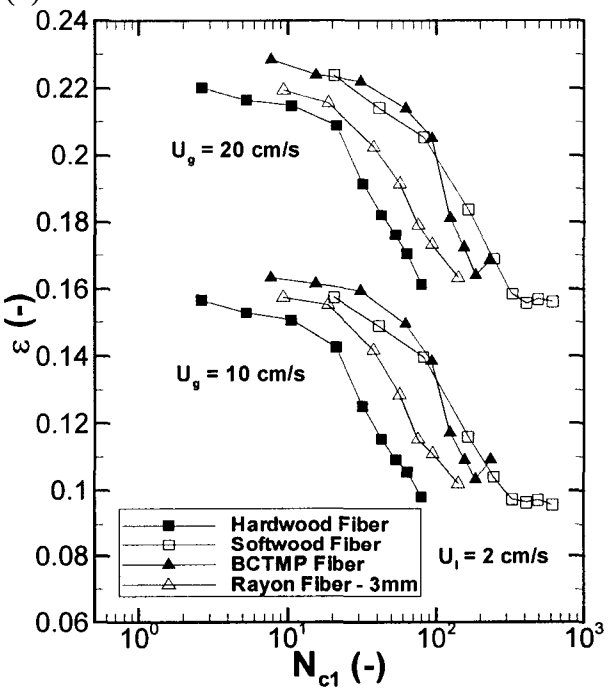

Figure 6.5: Variation of gas holdup with N_{c2}: (a) U_l = 10 cm/s and (b) U_l = 2 cm/s.

(a)

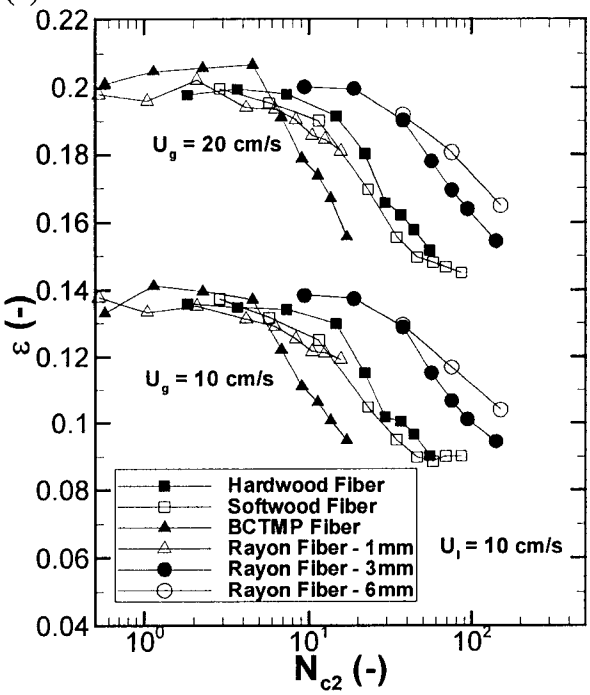

(b)

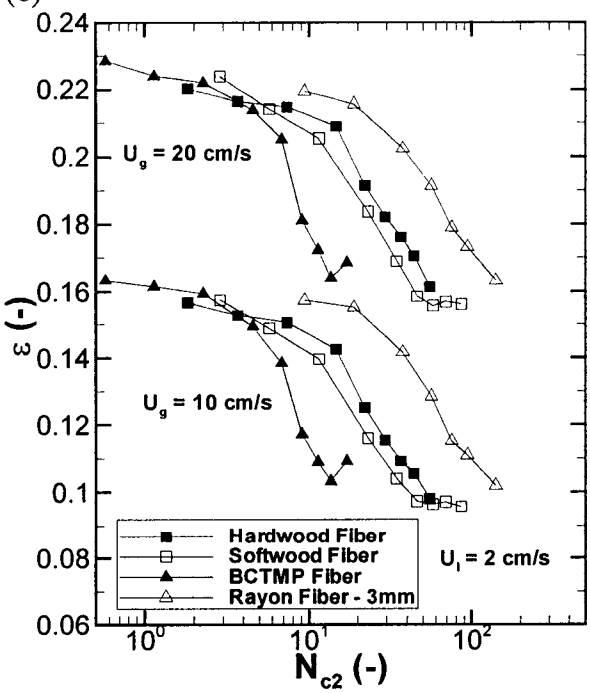

Figure 6.6: Variation of gas holdup with I_c in different fiber suspensions: (a) U_l = 2 cm/s; (b) U_l = 4 cm/s; (c) U_l = 8 cm/s; and (d) U_l = 10 cm/s.

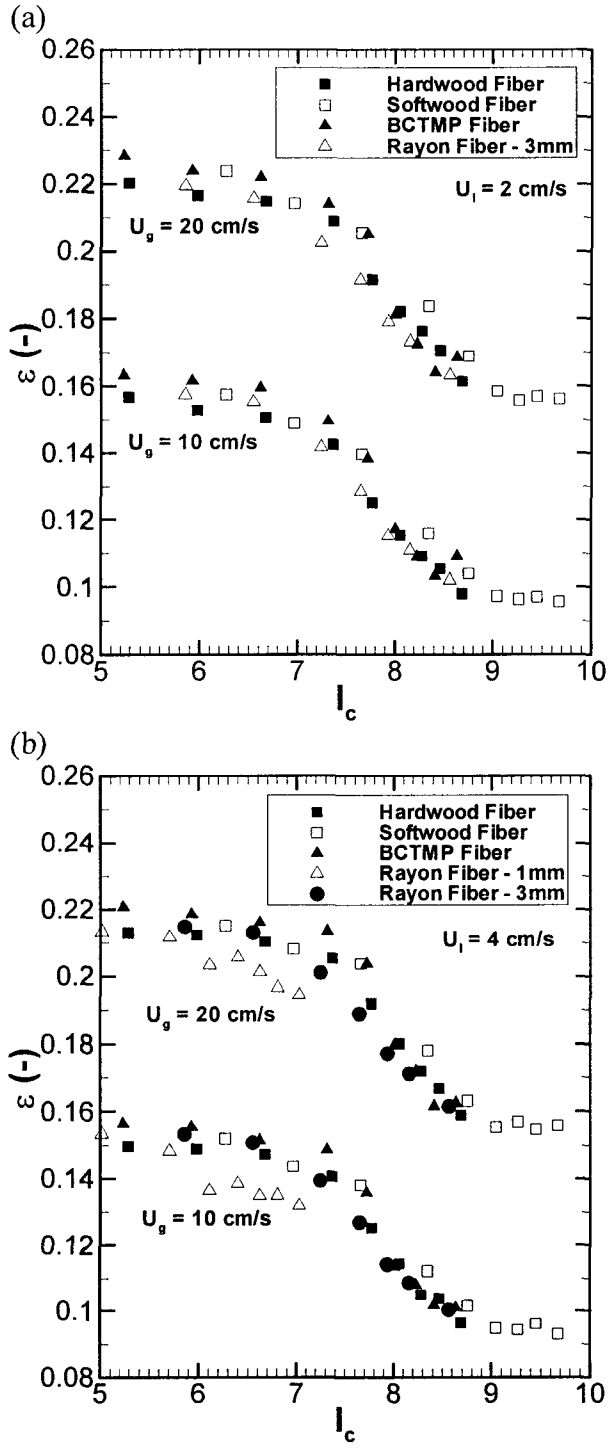

Figure 6.6: Continued.

(c)

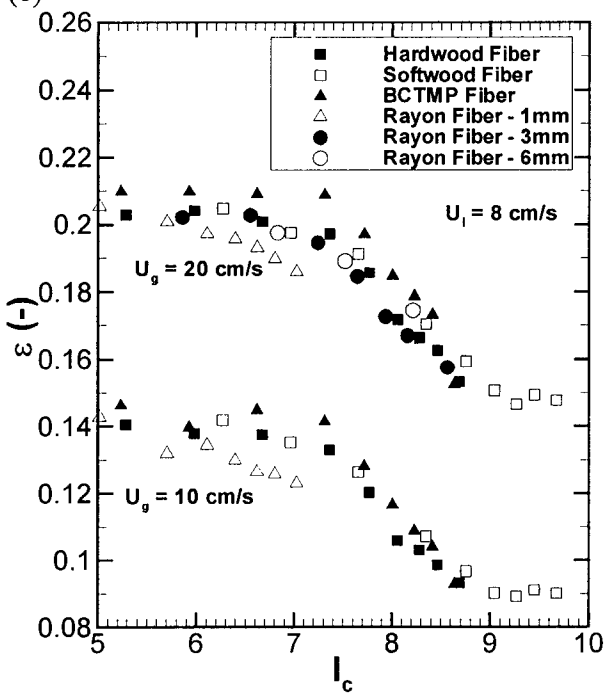

(d)

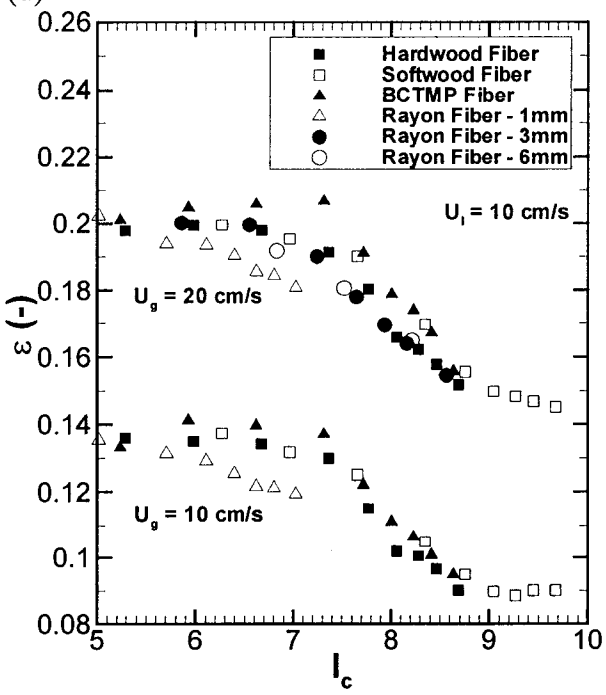

Figure 6.7: Variation of I_c with fiber mass fraction for different fibers.

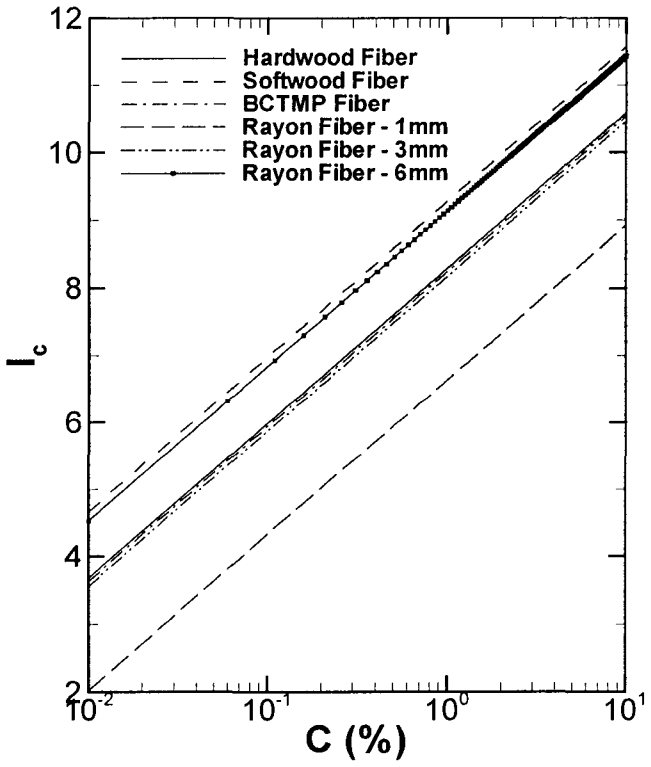

Chapter 7: GAS HOLDUP MODEL DEVELOPMENT

In this chapter, a gas holdup model is developed for cocurrent air-water-fiber bubble column flows, and correlates gas holdup (ε) with superficial gas (U_g) and liquid (U_l) velocities and I_c, the parameter identified in Chapter 6, which characterizes the influence of fiber type and mass fraction. The model can be used by various industries to predict system performance when fibers are added to a desired process. The model is also useful to control air-water-fiber systems by adjusting superficial gas velocity, superficial liquid velocity, and/or amount of fibers in the system, so that optimal or required performance can be reached.

The gas holdup in the present cocurrent air-water-fiber bubble column can be modeled based on the modified drift-flux model using a curve fitting method. The modified drift-flux model includes two radial distribution parameters and is formulated as (Clark and Flemmer, 1986; Miller and Cain, 1986)

$$\frac{\langle U_g \rangle}{\langle \varepsilon \rangle} = C_l \langle U_l \rangle + C_g \langle U_g \rangle + \frac{\langle j_{gm} \rangle}{\langle \varepsilon \rangle} \tag{7.1}$$

It can be used to correlate gas holdup data and identify gas flow regimes in gas-liquid and gas-liquid-solid bubble columns (Clark and Flemmer, 1986; Miller and Cain, 1986). Equation (7.1) can be rewritten as

$$\frac{\langle U_g \rangle}{\langle \varepsilon \rangle} = C_g \langle U_g \rangle + B_0 \tag{7.2}$$

where $B_0 = C_l \langle U_l \rangle + \frac{\langle j_{gm} \rangle}{\langle \varepsilon \rangle}$ is a constant for a given flow regime and U_l. The <> nomenclature is omitted when U_g, U_l, and ε refer to the data acquired in the present study. According to Eq. (7.2), the U_g/ε versus U_g plot can be used to identify the superficial gas velocity at which flow regime transition occurs for a given U_l. In Sec. 5.3, based on Eq. (7.2), three or two gas flow regimes are identified in air-water-fiber cocurrent bubble column flows,

depending on fiber mass fraction and type. For a given U_l , C, and fiber type, each U_g/ε versus U_g curve comprises three or two straight-line segments, as shown in Figs. 5.18-5.20.

In this Chapter, the gas holdup model will only be developed for $U_g > 4$ cm/s, where the two heterogeneous gas flow regimes, i.e., vortical-spiral and turbulent flow, are found. This is because the gas holdup error due to small bubble entrainment, which typically occurs when $C > 0.4\%$, constitutes a significant fraction of the total gas holdup at $U_g < 4$ cm/s and consequently, the U_g/ε versus U_g curves at $U_g < 4$ cm/s do not follow a consistent trend (Figs. 5.18-5.20).

7.1 Gas Holdup Model Development

The gas holdup model is developed in three steps. The first step is to find a correlation for gas holdup at a given superficial liquid velocity, fiber mass fraction, and fiber type based on Eq. (7.2). The next step is to correlate the gas holdup data at a given fiber mass fraction and type with a single model. And the final step is to identify a suitable model that can correlate the gas holdup data acquired at all conditions with all 6 fibers and estimate the model coefficients using curve-fitting techniques.

7.1.1 Gas holdup correlation at a given U_l, C, and fiber type

As shown in Sec. 5.3 (Figs. 5.18-5.20), when *$U_g > 4.0$ cm/s*, there are only two gas flow regimes for all conditions of this study. The data for a given U_l and C can be fitted by a curve comprising two straight-line segments connected at U_{gt}, i.e., the superficial gas velocity corresponding to the gas flow regime transition from vortical-spiral to turbulent flow, as shown in Fig. 7.1. U_{gt} can be directly estimated from the U_g/ε versus U_g plot. Because at each gas flow regime, the gas holdup data can be correlated with Eq. (7.1), hence, data points are correlated as

$$\frac{U_g}{\varepsilon} = \begin{cases} C_{g,1}U_g + B_{0,1}, & U_g \le U_{gt} \\ C_{g,2}U_g + B_{0,2}, & U_g > U_{gt} \end{cases} \tag{7.3}$$

where the parameters $C_{g,1}$, $C_{g,2}$, $B_{0,1}$, and $B_{0,2}$ are evaluated by fitting data in each gas flow regime using least square estimation (LSE) (Neter *et al.*, 1990). The data used for each segment is determined by U_{gt}.

This method, however, requires improvement due to the following two reasons: (i) the coefficients from Eq. (7.3) do not guarantee the adjacent two segments are connected at U_{gt}, because this is not considered as a condition when evaluating the coefficients using the LSE method; and (ii) this method requires data plotting before model fitting to estimate the superficial gas velocity at which gas flow regime transitions, i.e., U_{gt}, which is extremely time intensive because the work must be repeated for each superficial liquid velocity, fiber mass fraction, and fiber type.

Recognizing these two shortcommings, a constraint is added to Eq. (7.3) to force the two straight lines meet at U_{gt}:

$$C_{g,1}U_{gt} + B_{0,1} = C_{g,2}U_{gt} + B_{0,2} \tag{7.4}$$

Combining Eqs. (7.2) and (7.3) yields

$$\frac{U_g}{\varepsilon} = B_{0,1} + C_{g,1}U_g + (C_{g,2} - C_{g,1})(U_g - U_{gt})^+ \tag{7.5}$$

where the operator "$()^+$" is defined as

$$(x)^+ = \begin{cases} x, & x > 0 \\ 0, & x \le 0 \end{cases} \tag{7.6}$$

Thus, adding the constraint specified by Eq. (7.4) eliminates one model parameter, $B_{0,2}$. Equation (7.5) is equivalent to Eqs. (7.3) and (7.4), but explicitly includes U_{gt} as a model parameter. Rewrite Eq. (7.5) as

$$\frac{U_g}{\varepsilon} = B_1 + C_{g,1}U_g + C_{g,2-1}(U_g - U_{gt})^+ \tag{7.7}$$

where $B_1 = B_{0,1}$ and $C_{g,1}$ are the intercept and slope of the first segment, respectively and $C_{g,2-1} = C_{g,2} - C_{g,1}$ is the slope change when the flow regimes transition from vortical-spiral to turbulent flow. Equation (7.7) can be used to fit the data at both gas flow regimes for a given superficial liquid velocity, fiber mass fraction, and fiber type. The model parameters, including B_1, $C_{g,1}$, $C_{g,2\text{-}1}$, and U_{gt} can be determined using nonlinear least square estimation (NLSE) (Dennis, 1977). This is implemented with a program developed with the

MATLAB™ software (The MathWorks Inc., 2004, 2005). Thus, there is no need to determine the gas flow regime transition from U_g/ε versus U_g plots.

At each given superficial liquid velocity, fiber mass fraction, and fiber type, 4 fitting coefficients (i.e., B_1, $C_{g,1}$, $C_{g,2\text{-}1}$, and U_{gt}) are obtained for Eq. (7.7). Thus, each model coefficient in Eq. (7.7) is potentially a function of superficial liquid velocity, fiber mass fraction, and fiber type. These coefficients are studied in the next section to generate a gas holdup model capable of correlating all data at a given fiber mass fraction and type.

7.1.2 Gas holdup correlation at a given C and fiber type

To correlate the gas holdup data at a given fiber mass fraction and type, superficial liquid velocity (U_l) should be included in the gas holdup model as an independent variable. This is accomplished by modeling the coefficients in Eq. (7.7) as functions of U_l at the given C and fiber type.

The relationship between B_1, $C_{g,1}$, $C_{g,2\text{-}1}$, and U_{gt} and superficial liquid velocity for a given C and fiber type is studied. Figure 7.2 shows the variation of B_1, $C_{g,1}$, $C_{g,2\text{-}1}$, and U_{gt} with U_l at different C in hardwood fiber suspensions. B_1 consistently increases with increasing superficial liquid velocity at all fiber mass fractions. However, there is no consistent $C_{g,1}$, $C_{g,2\text{-}1}$, and U_{gt} trend with superficial velocity at the studied fiber mass fractions. Hence, it is assumed that

$$B_1 = A_1 + C_1 U_l \tag{7.8}$$

and $C_{g,1}$, $C_{g,2\text{-}1}$, and U_{gt} are constant with U_l. Equation (7.8) is reasonable, because substituting Eq. (7.8) for B_1 in Eq. (7.7) yields

$$\frac{U_g}{\varepsilon} = A_1 + C_1 U_l + C_{g,1} U_g + C_{g,2\text{-}1}(U_g - U_{gt})^+ \tag{7.9}$$

Equation (7.9) agrees with the modified drift-flux model (Eq. (7.1)), which includes a linear U_l term. Equation (7.8) is also seen from Fig. 5.18, where the intercept of each U_g/ε versus U_g curve (i.e., B_1) is a linear function of U_l. The assumption that $C_{g,1}$, $C_{g,2\text{-}1}$, and U_{gt} are constant with U_l also agrees with Fig. 5.18, where the slopes of the U_g/ε versus U_g curves at different superficial liquid velocities are constant.

With superficial liquid velocity included as an independent variable, Eq. (7.9) is able to fit all the data collected at a given C and fiber type. The 5 coefficients A_l, C_l, $C_{g,1}$, $C_{g,2\text{-}1}$, and U_{gt} in Eq. (7.9) are expected to be only functions of fiber mass fraction and type. Another program is written in MATLAB^{TM} to estimate the coefficients of Eq. (7.9). As an example, the data collected at C = 0.1% and 1.0% in hardwood fiber suspensions are fitted by Eq. (7.9) with the coefficients presented in Table 7.1. Figure 7.3 compares the experimental gas holdup values and their corresponding predicted values by Eq. (7.9) for 0.1% and 1.0% hardwood fiber suspensions. All the experimental data can be reproduced with Eq. (7.9) within ±5% error. Using Eq. (7.9), gas holdup data in other fiber suspensions can also be fitted within ±5% error, albeit the given coefficients differ.

Table 7.1: Coefficients of Eq. (7.9) for 0.1% and 1.0% hardwood fiber suspensions.

C (%)	A_l (cm/s)	C_l (-)	$C_{g,1}$ (-)	$C_{g,2\text{-}1}$ (-)	U_{gt} (cm/s)
0.1	23.25	1.18	3.90	-1.62	12.38
1.0	58.10	0.93	3.16	-1.13	12.52

7.1.3 Gas holdup correlation for all fiber suspensions

The goal of this chapter is to find a gas holdup model to correlate all gas holdup data from all six fiber suspensions. Thus, fiber mass fraction and fiber type must be considered in the final gas holdup model. This can be implemented by modeling Eq. (7.9) coefficients (i.e., A_l, C_l, $C_{g,1}$, $C_{g,2\text{-}1}$, and U_{gt}) as functions of fiber mass fraction and type. Hence, the relationship between A_l, C_l, $C_{g,1}$, $C_{g,2\text{-}1}$, and U_{gt} and fiber mass fraction and type should be studied.

Recall in Chapter 6, a parameter $I_c = \ln(N_c^{4/5}N_f^{1/5})$ is found capable of simultaneously accounting for the effects of both fiber mass fraction and type on gas holdup in bubble columns. An I_c value can be calculated for each C and fiber type as described in Chapter 6. Hence, to simplify the process, potential relationships between the coefficients (A_l, C_l, $C_{g,1}$, $C_{g,2\text{-}1}$, and U_{gt}) and I_c are analyzed. To reach this end, at first, Eq. (7.9) is used to fit the data at each C and fiber type. Then all the coefficients are plotted versus their corresponding I_c

values. The trends of A_1, C_l, $C_{g,1}$, $C_{g,2\text{-}1}$, and U_{gt} with I_c are analyzed and suitable models for the five coefficients are determined.

Figure 7.4 shows the variation of A_1, C_l, $C_{g,1}$, $C_{g,2\text{-}1}$, and U_{gt} with I_c for all fiber types. Notice that I_c is calculated with N_f having units of $1/cm^3$. As shown in Fig. 7.4a, A_1 is a nonlinear function of I_c. It remains approximately constant when $I_c \lesssim 6$ and then increases significantly with increasing I_c when $6 \lesssim I_c \lesssim 10$. When $I_c \gtrsim 10$, A_1 does not increase with increasing I_c, which is different from that at $6 \lesssim I_c \lesssim 10$. Although there are insufficient data points to show an obvious A_1 trend with I_c when $I_c \gtrsim 10$, it is expected that A_1 is approximately constant in this range. This is because at such a high I_c, which is only obtained in softwood fiber suspensions at $C \gtrsim 0.8\%$, gas holdup is nearly constant with increasing C (see Fig. 5.12), as further addition of fibers can not cause further increase in bubble coalescence. With this observation, A_1 can be modeled as a function of I_c with the following equation:

$$A_1 = a_1 + \frac{a_2}{1+\exp[a_3(I_c - I_0)]} \tag{7.10}$$

where the coefficients a_1, a_2, a_3, and I_0 can be determined with nonlinear least square estimation. With all A_1 and I_c values presented in Fig. 7.4a, the coefficients of Eq. (7.10) are estimated as: $a_1 = 24.20$ cm/s, $a_2 = 48.60$ cm/s, $a_3 = -2.27$, $I_0 = 7.98$. The A_1 values estimated from experimental data and calculated with Eq. (7.10) are compared in Fig. 7.5. It is shown that Eq. (7.10) can represent the relationship between A_1 and I_c with reasonable accuracy.

Figures 7.4b-e show the relationship between other coefficients (C_l, $C_{g,1}$, $C_{g,2\text{-}1}$, and U_{gt}) and I_c. The data points in these plots scatter significantly. The scattering is due to the nonlinear least square estimation procedure, which minimizes the total error between the experimental data at a given C and fiber type and their predicted values by Eq. (7.9). The trends of C_l, $C_{g,1}$, $C_{g,2\text{-}1}$, and U_{gt} with increasing I_c are not consistent for all fiber types. From Figs. 5.19 and 5.20, it is observed that the slope of the U_g/ε versus U_g curve does not significantly change with fiber mass fraction and type in both the vortical-spiral and turbulent flow regimes. Thus, it is assumed $C_{g,1}$, $C_{g,2\text{-}1}$ are constant with I_c. From these two figures, the superficial gas velocity at which gas flow regime transitions (U_{gt}) is also found

approximately constant with I_c. The relationship between C_l and I_c can be seen from Figs. 5.2 and 5.14, which compare the variation of gas holdup with U_l at constant U_g for different fiber mass fractions (Fig. 5.2) and different fiber types (Fig. 5.14), respectively. Although the slope of ε with U_l decreases with increasing C when U_g is low (e.g., U_g = 4 cm/s, Fig. 5.2a). This trend is insignificant when U_g is high (e.g., U_g = 13 or 20 cm/s, Fig. 5.2a and b). From Fig. 5.14, the slope of ε with U_l does not change significantly with fiber type. Therefore, the coefficient C_l is also assumed to be constant with I_c.

Thus, it is expected that the addition of fiber only changes the constant term (A_l) in Eq. (7.9). Substituting Eq. (7.10) for A_l in Eq. (7.9) results in a gas holdup model able to correlate the data acquired in all fiber suspensions investigated in the present study:

$$\frac{U_g}{\varepsilon} = a_1 + \frac{a_2}{1+\exp[a_3(I_c - I_0)]} + C_l U_l + C_{g,l} U_g + C_{g,2-l}(U_g - U_{gt})^+ \qquad (7.11)$$

where $I_c = \ln(N_c^{4/5} N_f^{1/5})$; N_c is the crowding factor; N_f is the fiber number density. To obtain an optimal model, the coefficients in Eq. (7.11) are estimated using all fiber suspension data with a nonlinear least square estimation method (NLSE) (Dennis, 1977) implemented in MATLAB™. The estimated values of the 8 coefficients are listed in Table 7.2. Their 95% confidence intervals are also estimated and given in Table 7.2. Note that "to say a numerical interval is a 95% confidence interval for a parameter is to say that in obtaining it, one has applied methods of data collection and calculation that would produce intervals bracketing the parameter in about 95% of repeated applications" (Vardeman and Jobe, 2001). The higher the confidence level (e.g., 95%), the more likely that the estimation numerical interval contains the parameter. Also, at the same confidence level, the narrower the interval, the more accurate the estimation is.

Table 7.2: Estimated values and confidence intervals of the overall gas holdup model (Eq. (7.11)) coefficients.

Coefficients	Estimated values	95% Confidence intervals	
		Lower bound	Upper bound
a_1 (cm/s)	28.08	27.63	28.54
a_2 (cm/s)	41.61	41.01	42.22
a_3 (-)	-2.38	-2.46	-2.31
I_0	8.12	8.10	8.14
C_l (-)	1.14	1.11	1.17
$C_{g,1}$ (-)	3.41	3.36	3.45
$C_{g,2-1}$ (-)	-1.25	-1.34	-1.15
U_{gt} (cm/s)	13.23	12.88	13.57

7.2 Model Evaluation

The gas holdup model represented by Eq. (7.11) and the coefficients listed in Table 7.2 are evaluated with experimental data (including data used or not used in estimating coefficients).

Figure 7.6 compares all the data acquired with the six fibers at $U_g > 4$ cm/s (3839 data points in total) and their corresponding reproduced values by Eq. (7.11). It shows that Eq. (7.11) can reproduce most experimental data points within ±10% error. Only a few data points are reproduced out of the ±10% error bound. All but 3 of the 3839 experimental data points are reproduced within the ±15% error bound.

Figure 7.7 compares the experimental data and their reproduced values for each individual fiber type. The hardwood (Fig. 7.7a), softwood (Fig. 7.7b), 3 mm Rayon (Fig. 7.7e), and 6 Rayon (Fig. 7.7f) fiber data are reproduced with Eq. (7.11) with a larger accuracy than the BCTMP (Fig. 7.7c) and 1 mm Rayon (Fig. 7.7d) fiber data. The BCTMP fiber data is reproduced with a smaller accuracy because the effect of the foam promoting lignosulfonates is not accounted for in Eq. (7.11). The smaller reproduction accuracy for the 1 mm Rayon fiber data is attributed to the much shorter fiber length, which caused negligible fiber deformation (i.e., bending). Nevertheless, all but one of the 1507 BCTMP and 1 mm Rayon fiber data points are still reproduced within ±15% error.

Figures 7.8-7.10 compares selected experimental data and their reproduced values at specific superficial liquid velocities and fiber mass fractions for hardwood, softwood, and 3 mm Rayon fiber suspensions. The model (Eq. (7.11)) accurately reflects the gas holdup trends with superficial liquid and gas velocity at both C = 0.1% and 1.0% for all the three fibers. This is also seen at other conditions and for other fiber types.

Figure 7.11 shows how Eq. (7.11) can be used to predict gas holdup in air-water bubble column flows. The proposed model (Eq. (7.11)) predicts the experimental data with high accuracy. Most gas holdup values are predicted with an error much less than ±5% and most data points on the parity plot are located tightly around the y = x line. There are several data points at U_l = 0 cm/s which deviate from the y = x line. But the predictions for these data points are still within ±5%. *Notice that the air-water bubble column data have not been used in estimating the model coefficients (Table 7.2) and I_c for air-water bubble column flows is -∞, which is out of the I_c range covered by the fiber suspensions used in the present study. Hence, Eq. (7.11) can be extrapolated toward the lower limit I_c = -∞.*

7.3 Discussion of Model Coefficients

Expanding Eq. (7.11), the modified drift-flux models for the spiral-vortical ($U_g \le U_{gt}$) and turbulent ($U_g > U_{gt}$) flow regimes are obtained separately:

$$\frac{U_g}{\varepsilon} = \begin{cases} \left[a_1 + \dfrac{a_2}{1+\exp[a_3(I_c - I_0)]} \right] + C_l U_l + C_{g,1} U_g, & U_g \le U_{gt} \\ \left[a_1 + \dfrac{a_2}{1+\exp[a_3(I_c - I_0)]} - C_{g,2\text{-}1} U_{gt} \right] + C_l U_l + (C_{g,1} + C_{g,2\text{-}1}) U_g, & U_g > U_{gt} \end{cases} \tag{7.12}$$

Thus, the drift-flux model coefficients can be obtained for each gas flow regime.

7.3.1 Radial distribution parameters C_l and C_g

Comparing Eq. (7.12) with Eq. (7.1), the radial distribution parameters for the vortical-spiral flow regime are C_l, and $C_{g,1}$; they are C_l and ($C_{g,1}$ + $C_{g,2\text{-}1}$) for turbulent flow

regime. The slope with superficial liquid velocity does not change when the flow regime changes. The slope with superficial gas velocity, however, decreased by $|C_{g,2\text{-}l}|$ (notice that $C_{g,2\text{-}l}$ is negative, Table 7.2). Both radial distribution parameters are not affected by superficial liquid velocity (U_l) and fiber (I_c).

The radial distribution parameters in the modified drift-flux model (Eq. (7.1)), C_l and C_g, are related with the radial distribution parameter of the Zuber-Findlay drift-flux model (Zuber and Findlay, 1965)

$$\frac{U_g}{\varepsilon} = C_0(U_l + U_g) + \frac{\langle j_{gm} \rangle}{\langle \varepsilon \rangle} \tag{7.13}$$

by Clark and Flemmer (1986):

$$C_0 = \frac{C_l U_l + C_g U_g}{U_l + U_g} \tag{7.14}$$

With the C_l and C_g values obtained in the present study, C_0 at different superficial gas and liquid velocity is calculated with Eq. (7.14) and presented in Fig. 7.12. It is obvious that C_0 is not constant with superficial gas and liquid velocity when $U_l > 0$ cm/s, even in the same gas flow regime. Also C_0 assumes very large values, which are larger than the usually recommended values, which are typically ~1.2 for fast upward bubble flows in small diameter (e.g., 50 mm) columns (Zuber and Findlay, 1965; Wallis, 1969; Hewitt, 1977; Ishii, 1977). The C_0 values in the present study are also higher than those recently obtained by Xie *et al.* (2003a), who identified that $C_0 \approx 1.1$ in a 5.08 cm diameter cocurrent air-water-fiber bubble column with $0 \leq U_g \leq 26$ cm/s and $21 \leq U_l \leq 51$ cm/s.

However, high C_0 values have been found in many studies with low superficial liquid velocities and large column diameters. Kara *et al.* (1982) found that $3.61 \leq C_0 \leq 5.13$ and increased with particle size in a 15.2 cm diameter cocurrent upflow air-water-coal and dried mineral ash bubble column with $3.0 \leq U_g \leq 30$ cm/s and $0 \leq U_l \leq 10$ cm/s. In a similar cocurrent bubble column experimental system under similar operating conditions, Kelkar *et al.* (1983) found that when alcohols were added in the liquid phase, C_0 increased with decreasing alcohol chain length and had a value of 2.41 in methanol solutions but was insensitive to the alcohol concentrations; Kelkar *et al.* (1984) obtained C_0 values as high as 3.02 in various gas-liquid-solid systems with slurries having different liquid (surface tension

and viscosity) and particle (size and density, and concentration) properties. In a 5 cm diameter cocurrent air-water-glass beads (40-80 μm) bubble column with $0.15 \leq U_l \leq 1.646$ m/s and $0.009 \leq U_g \leq 1.328$ m/s with solid concentration up to 40%, Miller and Cain (1986) found C_g increased with solid concentration and was ~2.6 when the solid concentration was 40% and C_l was less sensitive to solid concentration and had a value of ~0.5, which implies that C_0 (calculated with Eq. (7.14)) can have a value much larger than 1.2 at some conditions.

Clark *et al.* (1990) showed that C_0 was determined by two competing effects present in bubble columns, i.e., buoyancy and wall effects. It increases with the dominance of buoyancy effects. In large diameter columns, C_0 is always larger than unity and assumes very high values at low superficial liquid velocity (it can be larger than 10 under some extreme conditions) because the velocity profile is dictated by buoyancy effects rather than by a net flow up the column (i.e., wall effects). In small diameter pipes, C_0 can still have high values at low superficial liquid velocities if buoyancy effects are still significant. At higher superficial liquid velocities where buoyancy effects are negligible, C_0 tends to assume values between 1 and 1.5.

Equation (7.14) can be written as

$$C_0 = \frac{R_U \cdot C_l + C_g}{R_U + 1} \tag{7.15}$$

where

$$R_U = \frac{U_l}{U_g} \tag{7.16}$$

is the superficial velocity ratio. In Fig. 7.13, C_0 is plotted as a function of R_U for the two gas flow regimes in the present study. It can be seen that C_0 decreases with R_U and the decrease is more significant at lower R_U. This agrees with Clark *et al.* (1990) since at higher R_U the buoyancy effects have less dominance over the velocity profile. Rewriting Eq. (7.15) yields

$$C_0 = C_l \frac{1 + \left(\frac{C_g}{C_l} \Big/ R_U \right)}{1 + (1/R_U)} \tag{7.17}$$

Because C_g/C_l is finite (e.g., in the present study, $C_g/C_l = 2.75$ and 1.89 for vortical-spiral and turbulent flows, respectively), when superficial velocity ratio (R_U) is large, C_0 will be very

close to C_1, which is 1.14 in the present study and similar to the C_0 values widely reported and recommended for fast bubble flows (Zuber and Findlay, 1965; Wallis, 1969; Hewitt, 1977; Ishii, 1977).

In the present study, the bubble column diameter is large and the superficial liquid velocity is only up to 10 cm/s, buoyancy effects are significant at all investigated operating conditions. Hence, it is reasonable that C_0 assumes higher values.

7.3.2 Weighted average drift velocity $\langle j_{gm}\rangle/\langle\varepsilon\rangle$

The weighted average drift velocity can be obtained for both gas flow regimes by comparing Eq. (7.12) with Eq. (7.1). Because the difference between the weighted average drift velocities for the two gas flow regimes is a constant ($C_{g,2\text{-}1}U_{gt}$), the discussions on $\langle j_{gm}\rangle/\langle\varepsilon\rangle$ will be focused on that for vortical-spiral flow.

For vortical-spiral flows ($U_g < U_{gt}$), the weighted average drift-velocity is

$$\frac{\langle j_{gm}\rangle}{\langle\varepsilon\rangle} = a_1 + \frac{a_2}{1+\exp[a_3(I_c - I_0)]} \tag{7.18}$$

It is significantly affected by fiber (I_c).

The weighted average drift velocity may be approximated by the terminal bubble rise velocity ($U_{b\infty}$) in an infinite medium (Miller and Cain, 1986; Clark *et al.*, 1990) because the local slip velocity U_s ($= \frac{U_g}{\varepsilon} - \frac{U_l}{1-\varepsilon}$) changes little over the pipe diameter and $j_{gm} = U_s(1-\varepsilon)$, with $\varepsilon < 0.25$ in most situations for bubble flows. Thus, for vortical-spiral flow,

$$U_{b\infty} \approx a_1 + \frac{a_2}{1+\exp[a_3(I_c - I_0)]} \tag{7.19}$$

Because $a_3 < 0$, when $I_c >> I_0$,

$$U_{b\infty} \rightarrow a_1 + a_2 \tag{7.20}$$

When $I_c << I_0$,

$$U_{b\infty} \rightarrow a_1 \tag{7.21}$$

The variation of the terminal bubble rise velocity ($U_{b\infty}$) with I_c is plotted in Fig. 7.14. $U_{b\infty}$ is constant when $I_c \lesssim 6$ and $I_c \gtrsim 10$; its values are equal to a_1 and $a_1 + a_2$, respectively. The lower limit a_1 is the average terminal bubble rise velocity when there is negligible fiber present in the bubble column, and it equals $U_{b\infty}$ in an air-water bubble column. The parameter a_2 represents the ultimate increase in average terminal bubble rise velocity when sufficient fibers are added in bubble columns.

The average bubble diameter (d_b) can be derived from the average terminal rise velocity ($U_{b\infty}$) using a general bubble terminal velocity correlation proposed by Jamialahmadi *et al.* (1994):

$$U_{b\infty} = \frac{U_{b\infty}^{sp} U_{b\infty}^{w}}{\sqrt{\left(U_{b\infty}^{sp}\right)^2 + \left(U_{b\infty}^{w}\right)^2}} \tag{7.21}$$

where

$$U_{b\infty}^{w} = \sqrt{\frac{2\sigma}{d_b\left(\rho_l + \rho_g\right)} + \frac{g d_b}{2}} \tag{7.22}$$

$$U_{b\infty}^{sp} = \frac{1}{18}\frac{\rho_l - \rho_g}{\mu_l} g d_b^2 \tag{7.23}$$

and σ, μ_l, and ρ_l are the liquid surface tension, viscosity, and density, respectively, and ρ_g is the gas density. In the present study, it is estimated that in air-water vortical-spiral flow, $U_{b\infty}$ = 28.08 cm/s. Using the air and water properties recommended by Munson *et al.* (2002): σ = 73.4 mN, $\mu_l = 1.12\times10^{-3}$ Pa·s, ρ_l = 999 kg/m^3, and ρ_g = 1.23 kg/m^3, the average bubble diameter d_b is estimated as 13.9 mm. This is close to visual observations on the air-water bubble column flows. For air-water-fiber flows, the fiber suspension rheological properties are non-Newtonian when fiber flocculation occurs and bubble behavior may be different, hence, the Jamialahmadi *et al.* (1994) correlation (Eqs. (7.21)-(7.23)) may not apply. Thus, no attempt has been made to estimate the bubble size in air-water-fiber flows using $U_{b\infty}$. However, it is expected that bubble size will be larger because of enhanced bubble coalescence due to fiber flocculation.

In Fig. 7.14, there is a transitional region when $6 \lesssim I_c \lesssim 10$, where $U_{b\infty}$ varies significantly with I_c. The width of the transitional region ($\Delta I_{c,t}$) is a function of $|a_3|$. If $\Delta I_{c,t}$ is defined as the I_c range where

$$a_1 + a_2 \cdot 0.01 \le U_{b\infty} \le a_1 + a_2 \cdot 0.99 \tag{7.24}$$

then from Eq. (7.14) the transitional region is estimated as

$$0.01 \le \frac{1}{1+\exp[a_3(I_c - I_0)]} \le 0.99 \tag{7.25}$$

or

$$I_0 - \frac{\ln 99}{|a_3|} \le I_c \le I_0 + \frac{\ln 99}{|a_3|} \tag{7.26}$$

Thus, the transitional region width

$$\Delta I_{c,t} = \frac{2 \ln 99}{|a_3|} \tag{7.27}$$

Substituting the fitted values $I_0 = 8.12$ and $a_3 = -2.38$, the I_c range for the transitional region is $6.19 \le I_c \le 10.05$ and the transitional region width is $\Delta I_{c,t} = 3.86$.

Within the transitional region, there is an I_c range where $U_{b\infty}$ increases linearly with increasing I_c (Fig. 7.14). This is called a linear region. This region is located near $I_c = I_0$. For I_c values in the neighborhood of $I_c = I_0$, i.e., if $I_c = I_0 + \delta$,

$$\begin{aligned} U_{b\infty} &= a_1 + \frac{a_2}{1+\exp(a_3\delta)} \\ &= a_1 + \frac{a_2}{1+(1+a_3\delta+O(\delta^2))} \\ &= (a_1 + \frac{a_2}{2}) - a_2 a_3 \delta + O(\delta^2) \end{aligned} \tag{7.28}$$

where δ is a small number ($\delta < 1$) representing a deviation from I_0 and $O(\delta^2)$ means a small change in $U_{b\infty}$ on the order of δ^2. Hence,

$$U_{b\infty} \approx (a_1 + \frac{a_2}{2}) - a_2 a_3 \delta = (a_1 + \frac{a_2}{2}) + |a_2 a_3| \delta \tag{7.29}$$

in the linear region. Recall in Chapter 6 it is found that I_c is related to fiber mass fraction (C):

$$I_c = \ln(N_c^{4/5} N_f^{1/5}) \approx \ln(C) + \frac{1}{5}\ln\left[\left(\frac{\rho_l n_f}{100}\right)\left(\frac{\pi L_L^{\,2}\rho_l}{600\omega}\right)^4\right] \tag{7.30}$$

Assume the fiber mass fraction corresponding to $I_0 = 8.12$ is C_{l0} (which is estimated from Fig. 5.7 as ~0.35% for softwood fiber and ~0.9% for hardwood, BCTMP, and 3 mm Rayon fibers), then from Eq. (7.30) it is obtained

$$\delta = \ln(C) - \ln(C_{l0}) \tag{7.31}$$

for a given fiber type and hence,

$$U_{b\infty} \approx (a_1 + \frac{a_2}{2} - |a_2 a_3| \ln(C_{l0})) + |a_2 a_3| \ln(C) \tag{7.32}$$

Therefore, in the linear region, $U_{b\infty}$ is approximately a linear function of ln(C) when the fiber type is given and the slope has a value of $|a_2 a_3|$.

7.4 Gas Holdup Model Development Summary

In this chapter, a gas holdup model was developed for cocurrent air-water-fiber bubble flows based on the modified drift-flux model. The gas holdup model correlates gas holdup with superficial gas and liquid velocity and fiber type and mass fraction. The model can reproduce most experimental data within ±10% error and all experimental data within ±15% error. It can also predict air-water bubble column gas holdup data. The physical implications of the model coefficients were also discussed.

Figure 7.1: Segmented gas holdup model at a given superficial liquid velocity, fiber mass fraction, and fiber type.

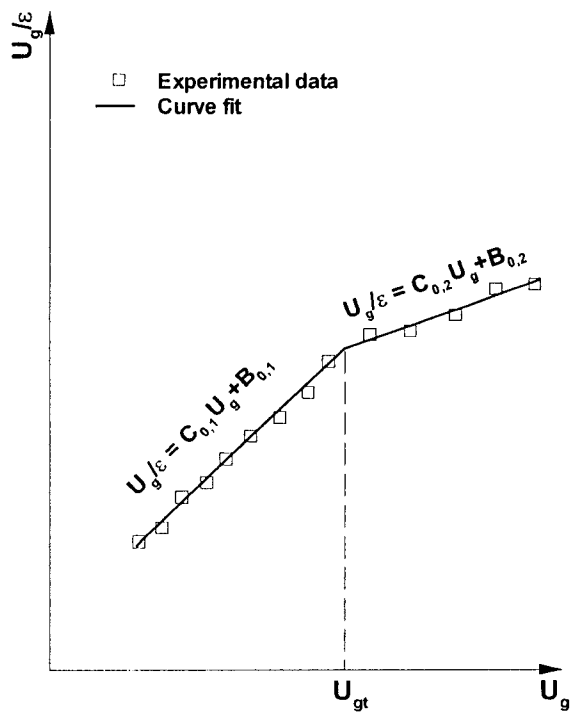

Figure 7.2: Variation of Eq. (7.7) coefficients with U_l at different fiber mass fractions in hardwood fiber suspensions: (a) B_1; (b) $C_{g,1}$; (c) $C_{g,2\text{-}1}$; and (d) U_{gt}.

(a)

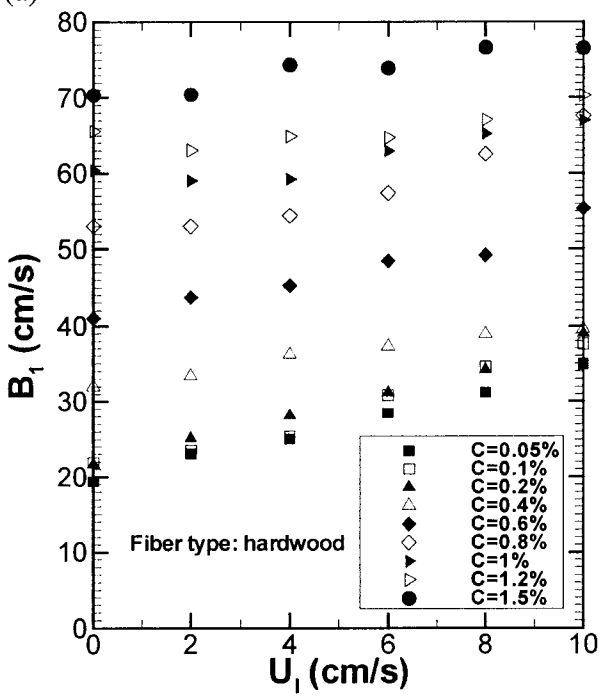

(b)

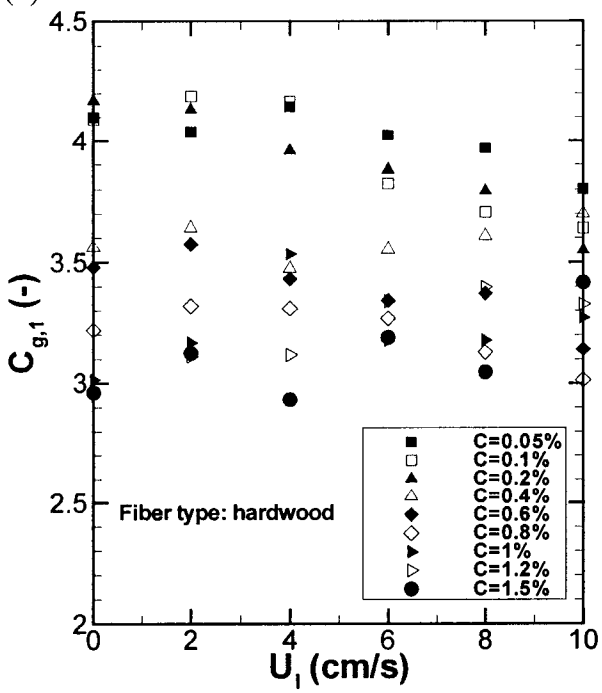

Figure 7.2: Continued.

(c)

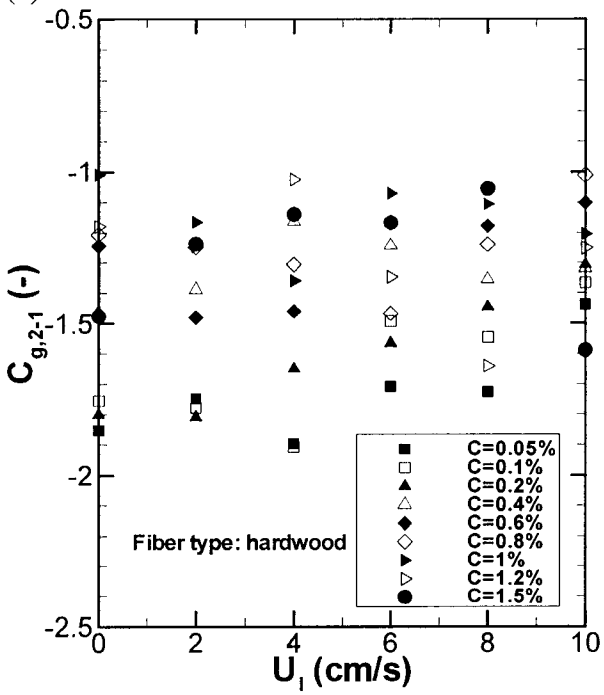

(d)

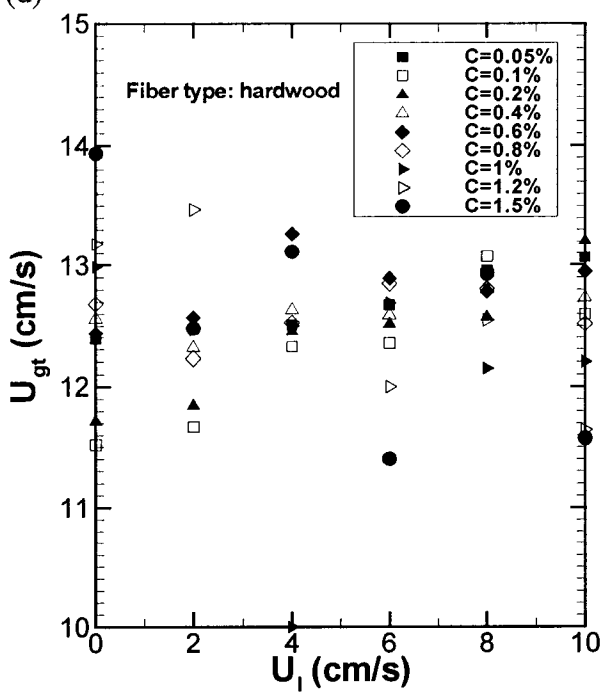

Figure 7.3: Parity plot for all data points acquired at C = 0.1% and 1.0% in hardwood fiber suspensions: (a) C = 0.1% and (b) C = 1.0%.

(a)

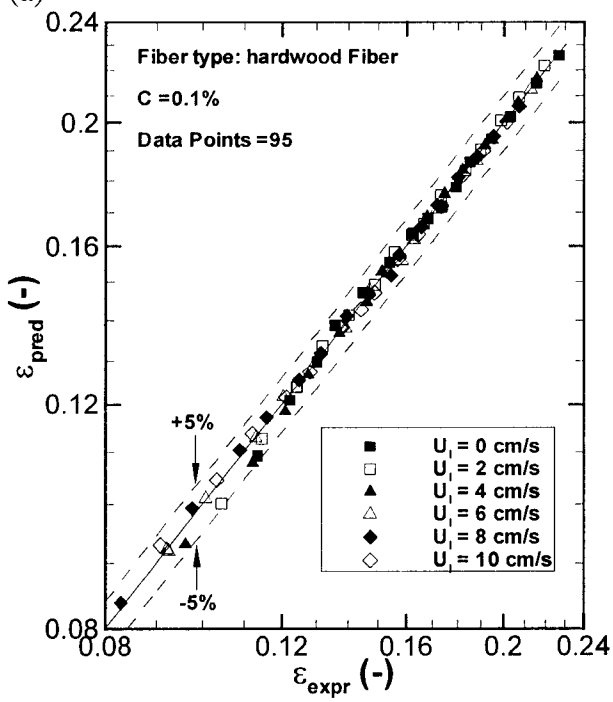

(b)

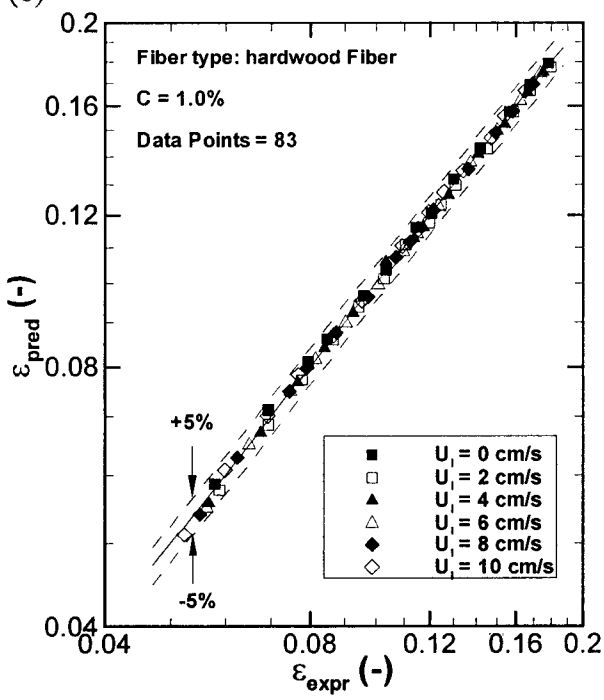

Figure 7.4: Variation of Eq. (7.9) coefficients with U_l at different fiber mass fractions in hardwood fiber suspensions: (a) A_1; (b) C_1; (c) $C_{g,1}$; (d) $C_{g,2\text{-}1}$; and (e) U_{gt}.

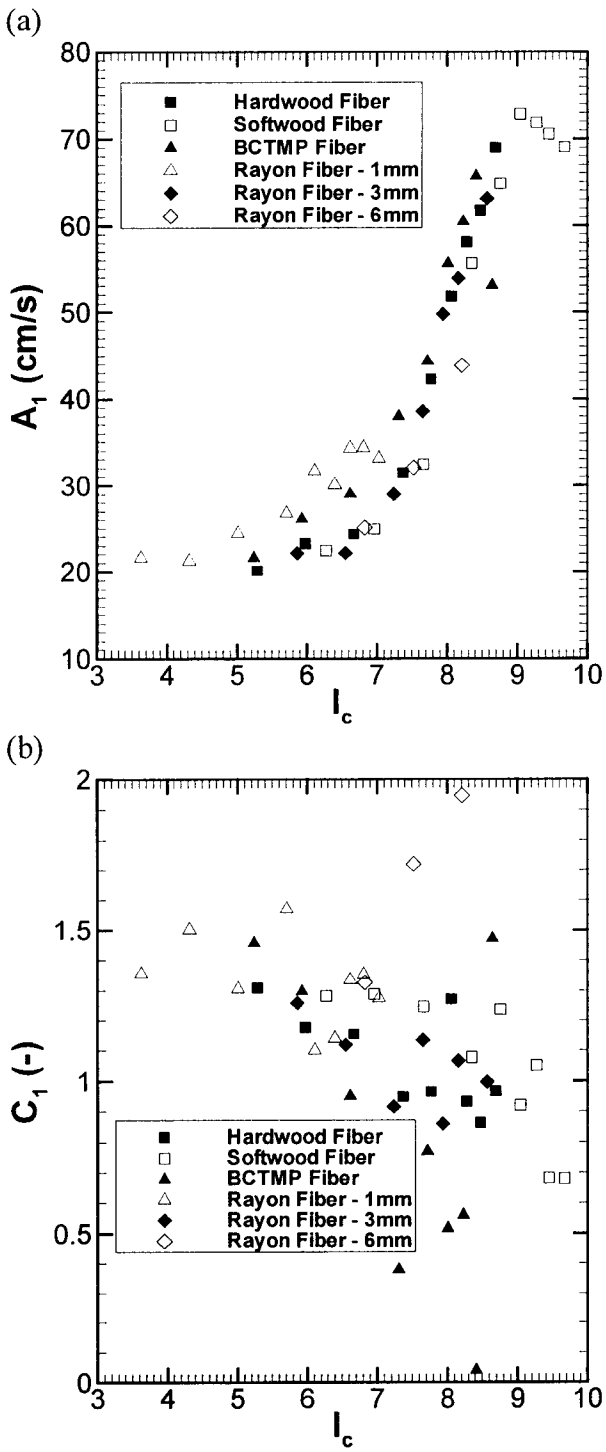

Figure 7.4: Continued.

(c)

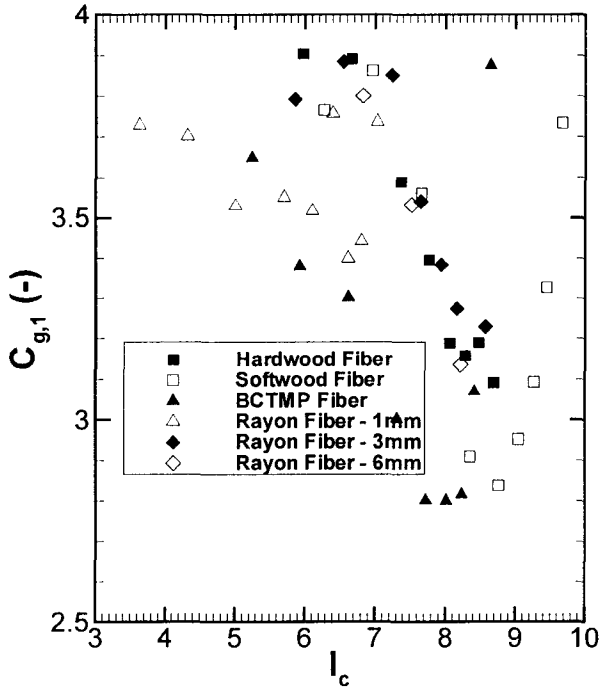

(d)

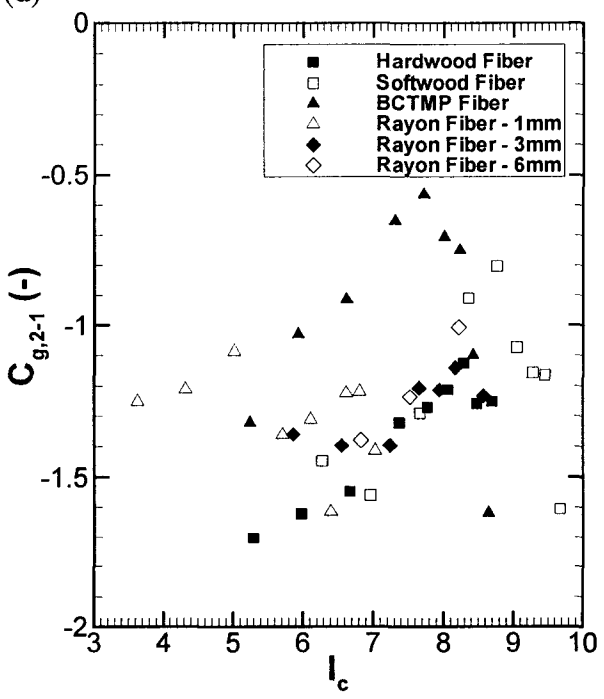

Figure 7.4: Continued.

(e)

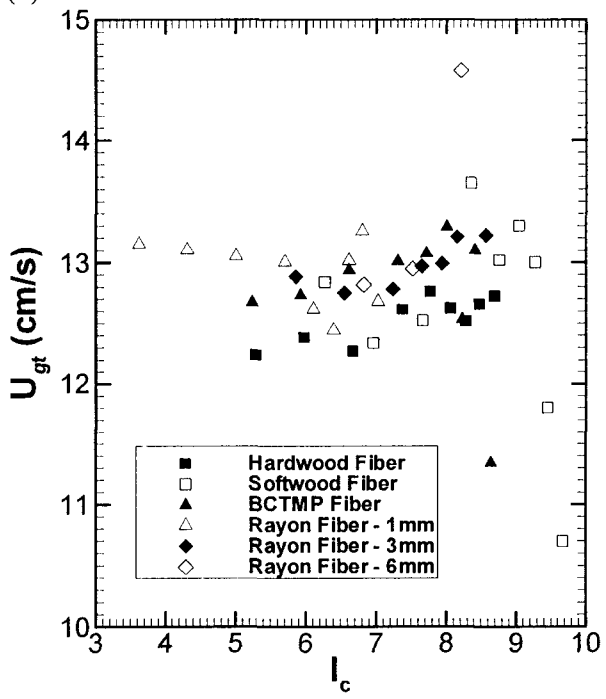

Figure 7.5: Comparison between A_1 estimated from experimental data and calculated with Eq. (7.10).

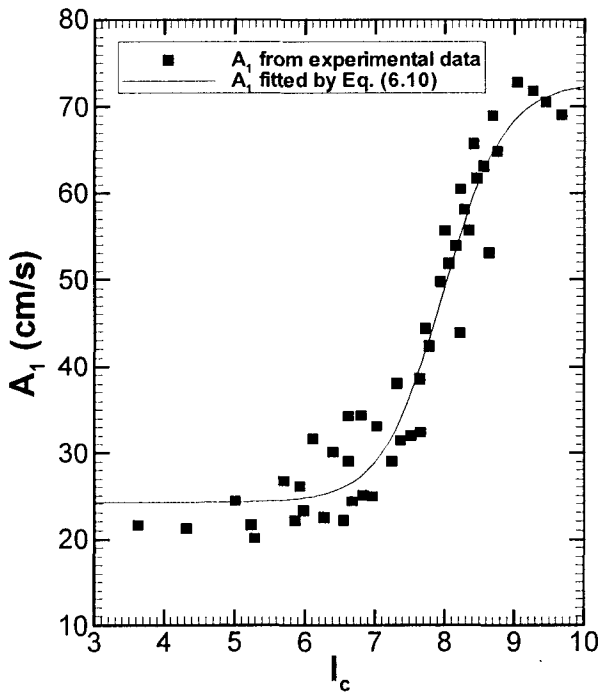

Figure 7.6: Parity plot for all data points acquired at $U_g > 4$ cm/s.

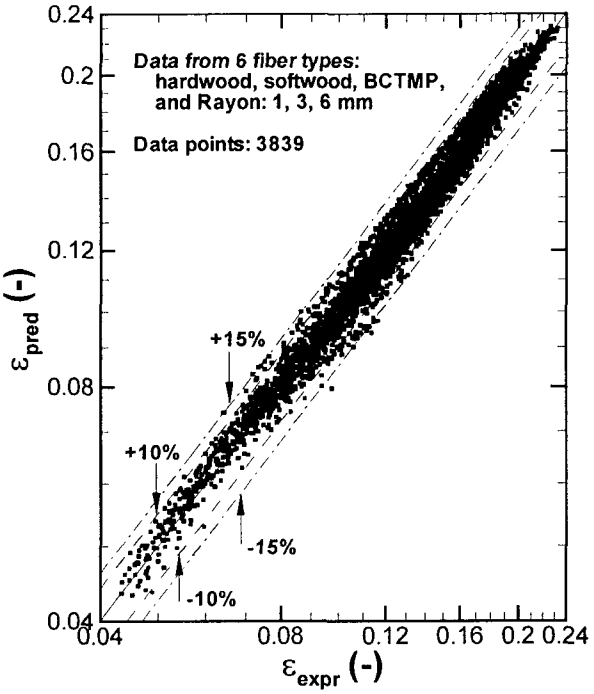

Figure 7.7: Parity plot for data points acquired with each fiber type at $U_g > 4$ cm/s: (a) hardwood; (b) softwood; (c) BCTMP; (d) 1 mm Rayon; (e) 3 mm Rayon; and (f) 6 mm Rayon.

(a)

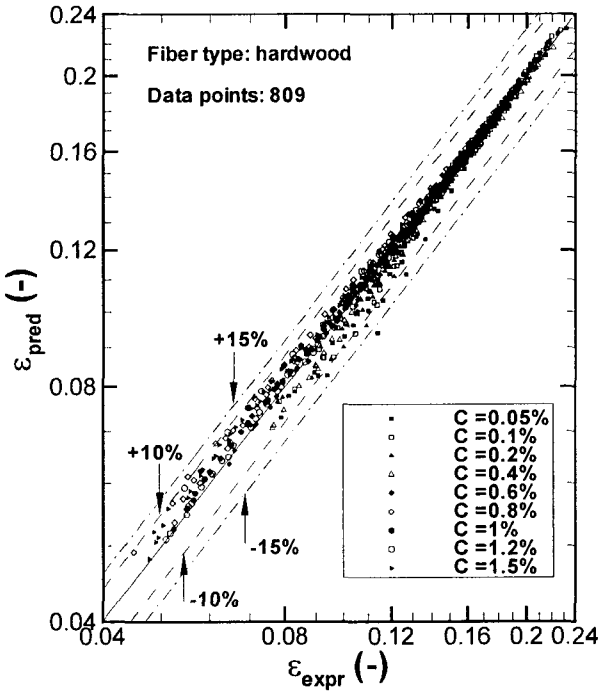

(b)

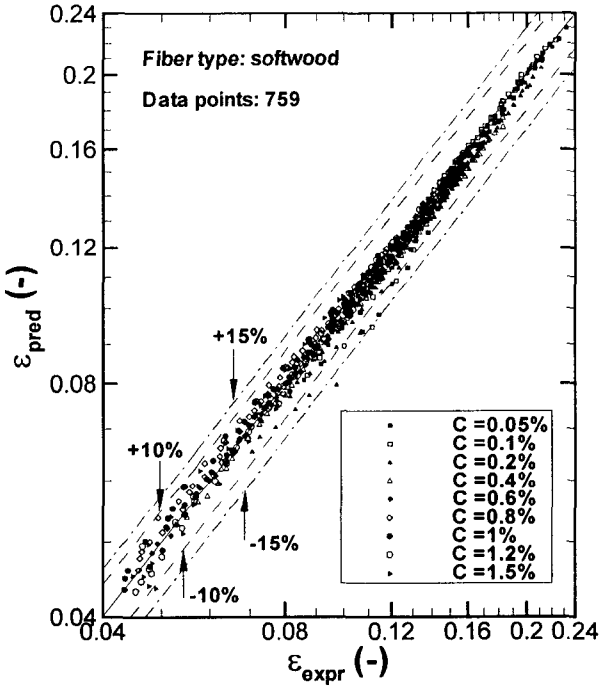

Figure 7.7: Continued.

(c)

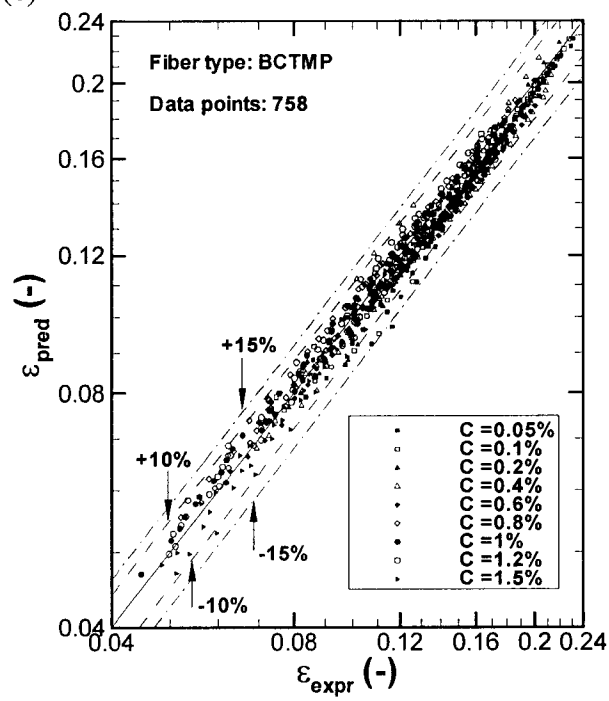

(d)

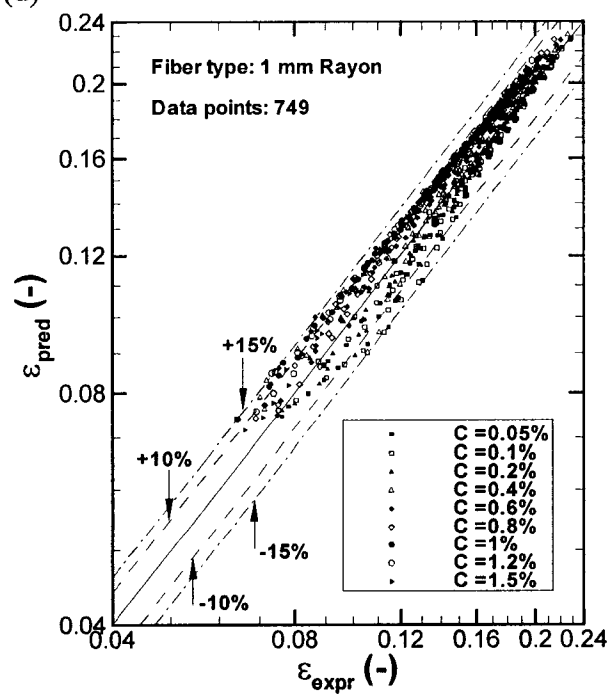

Figure 7.7: Continued.

(e)

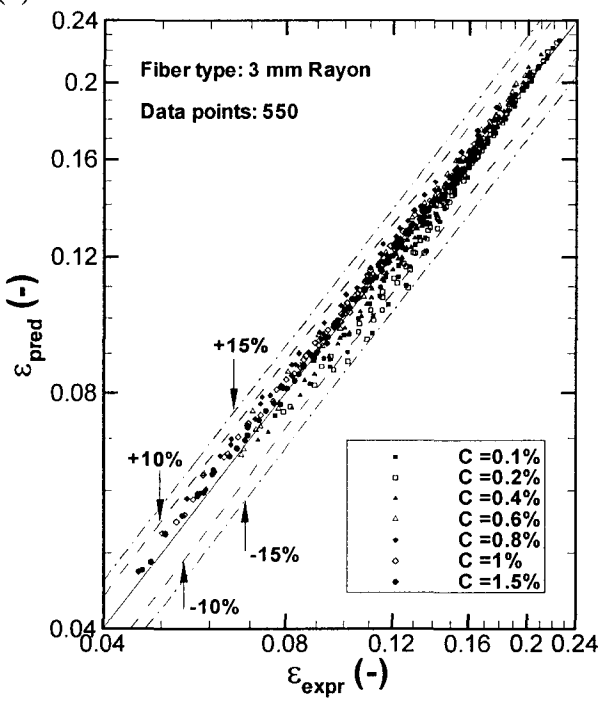

(f)

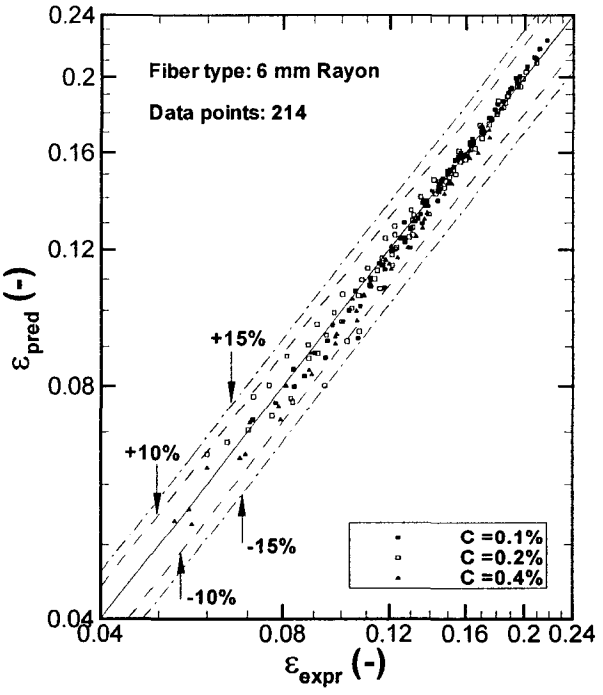

Figure 7.8: Comparison between experimental data and their reproduced values at specific fiber mass fractions in hardwood fiber suspensions: (a) C = 0.1% and (b) C = 1.0%.

(a)

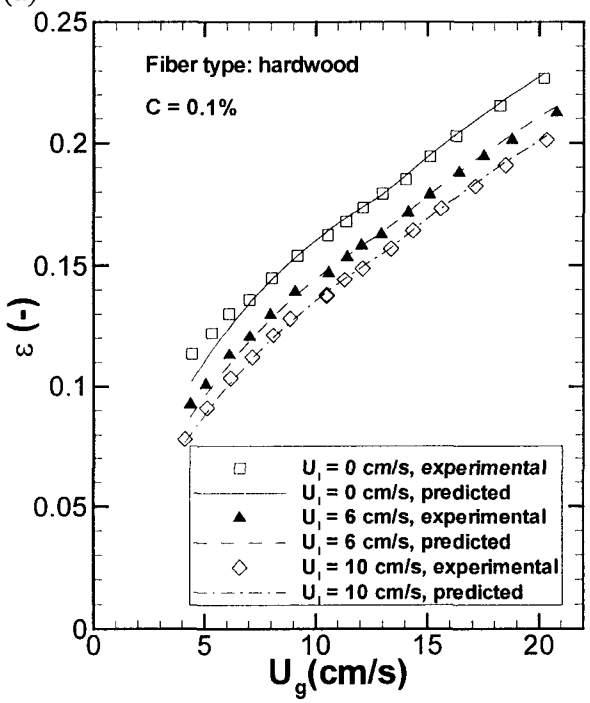

(b)

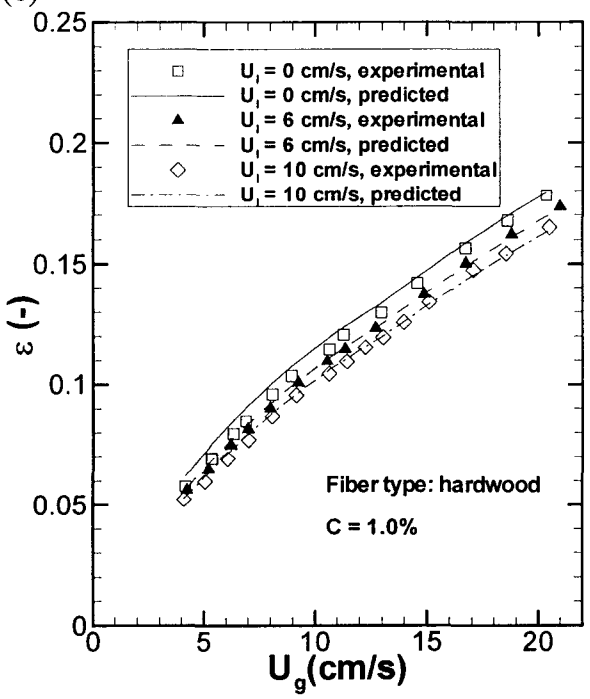

Figure 7.9: Comparison between experimental data and their reproduced values at specific fiber mass fractions in softwood fiber suspensions: (a) C = 0.1% and (b) C = 1.0%.

(a)

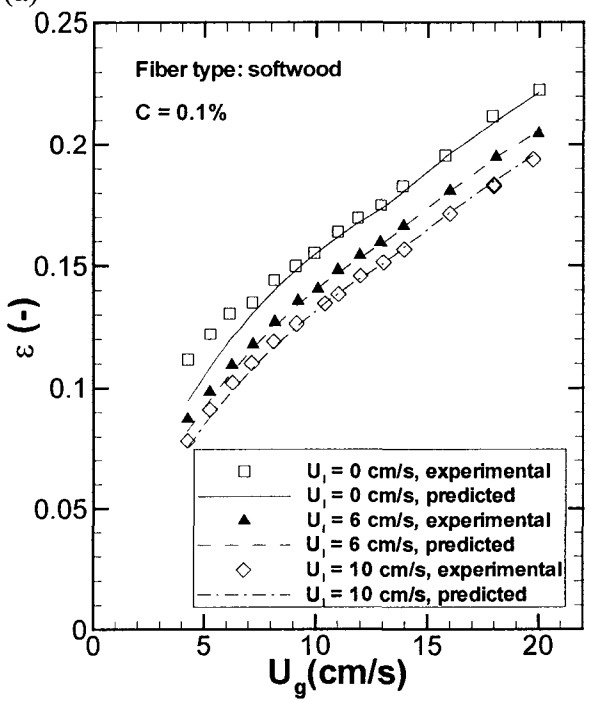

(b)

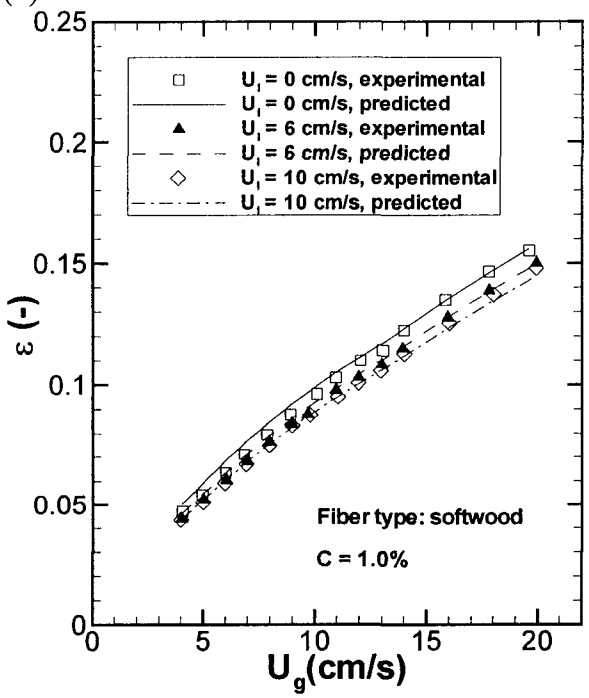

Figure 7.10: Comparison between experimental data and their reproduced values at specific fiber mass fractions in 3 mm Rayon fiber suspensions: (a) C = 0.1% and (b) C = 1.0%.

(a)

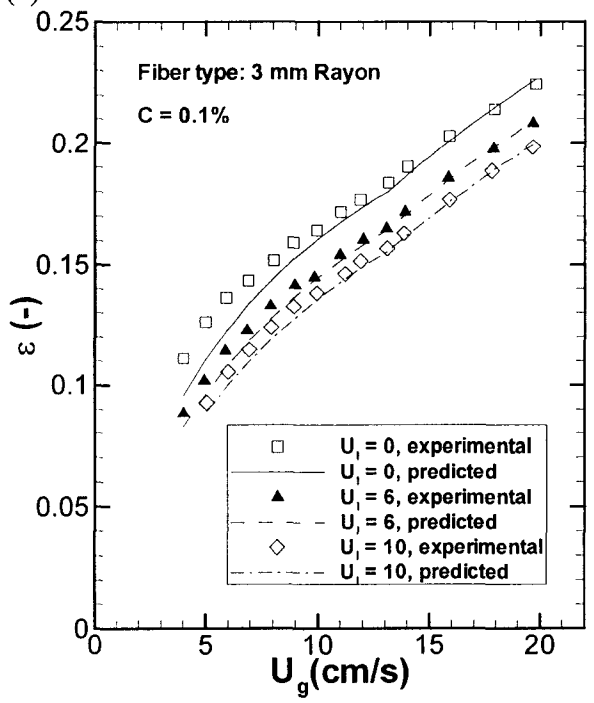

(b)

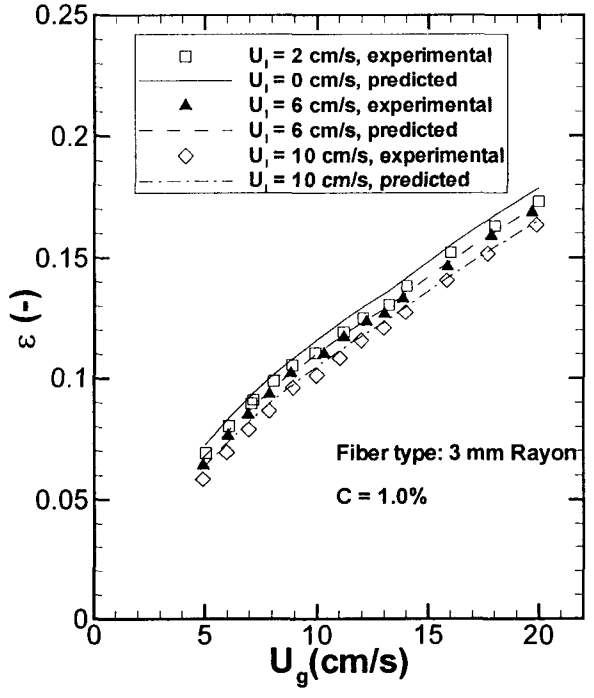

Figure 7.11: Parity plot for data points acquired in air-water bubble column at $U_g > 4$ cm/s.

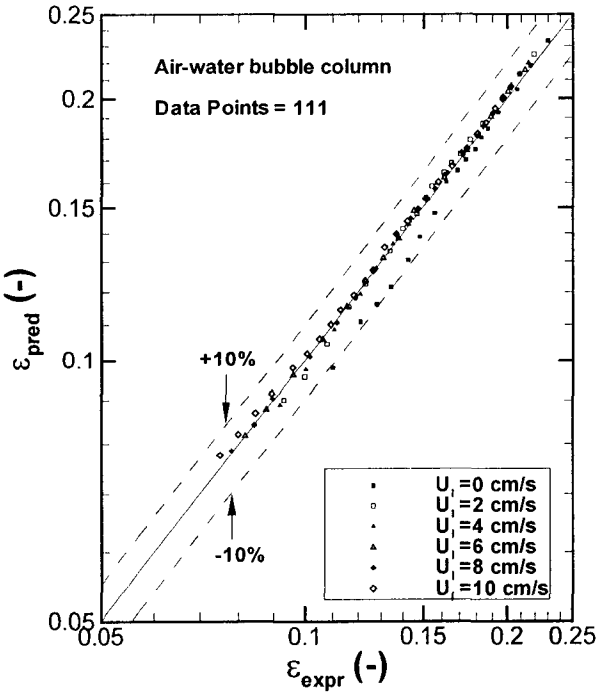

Figure 7.12: Estimated Zuber-Findlay drift-flux model distribution parameter as a function of U_g and U_l.

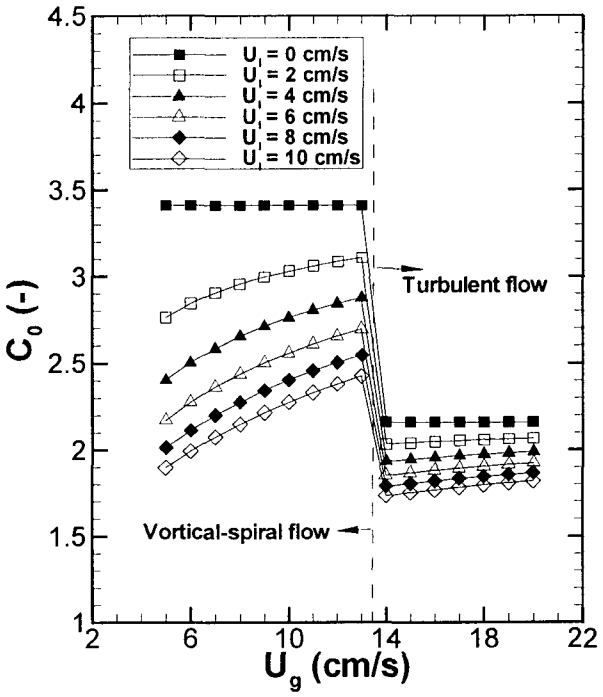

Figure 7.13: Variation of C_0 with R_U for different gas flow regimes.

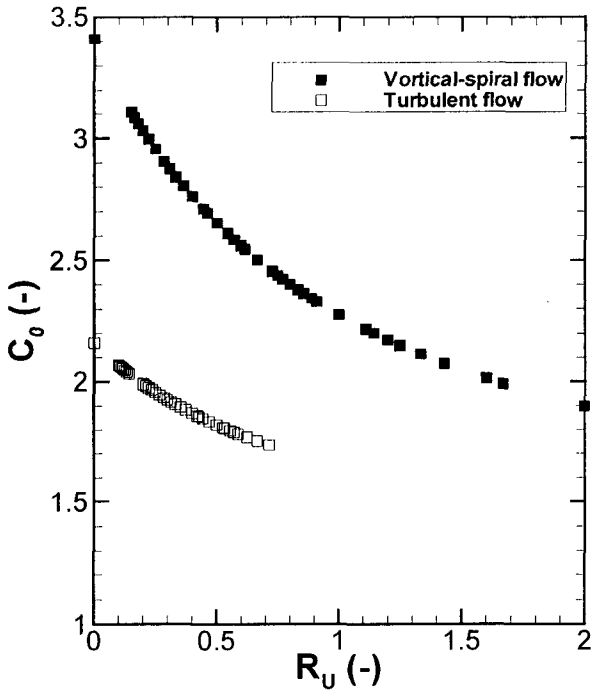

Figure 7.14: Variation of terminal bubble rise velocity with I_c for vortical-spiral flows ($U_g < U_{gt}$).

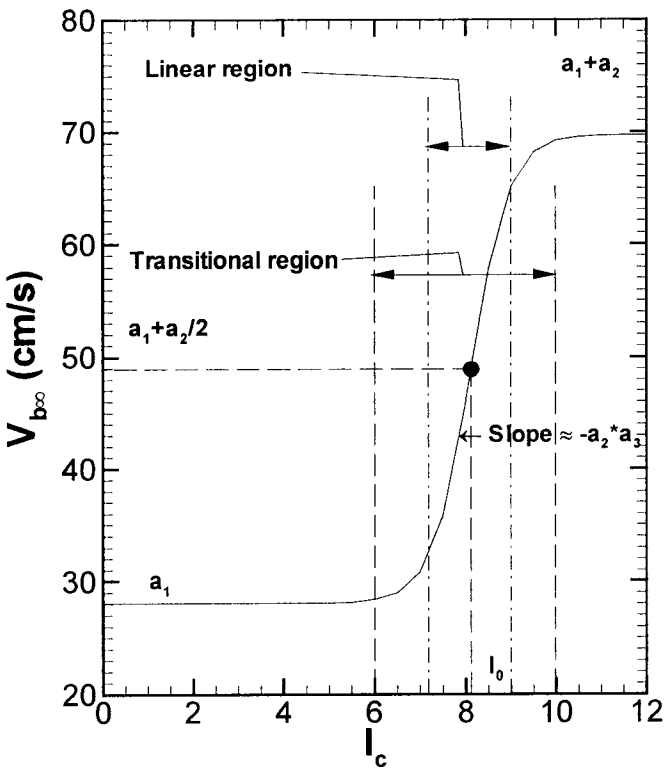

Chapter 8: CONCLUSIONS AND RECOMMENDATIONS FOR FUTURE WORK

In the present study, the hydrodynamics and gas holdup in a cocurrent air-liquid-fiber bubble column were systematically examined with an emphasis on the role of fibers. The fundamental mechanisms behind the fiber influences were connected to the unique behavior of fibers in fiber suspensions, i.e., flocculation, and its influence on bubble behavior. Effects of operating conditions, including superficial gas and liquid velocity, fiber mass fraction, and fiber type on gas holdup in the cocurrent air-water-fiber bubble column were investigated experimentally. Based on extensive data acquisition, a parameter was identified to quantify the fiber effect on gas holdup in the air-water-fiber bubble column for various cellulose and Rayon fibers. Utilizing this new parameter, a gas holdup was developed based on the drift-flux model, which is able to accurately predict the gas holdup in a cocurrent air-water-fiber bubble column.

In the first part of this chapter, the conclusions obtained in this study are summarized. In the second part, recommendations are provided on further work.

8.1 Conclusions

8.1.1 Influences of fiber suspensions on bubble motion and gas holdup

- Flocculated fiber suspensions were considered as a mixture of fiber and suspending liquid comprising flocs and inter-floc regions. Fiber suspension properties are affected by the formation and disruption of fiber flocs as well as their size and strength.

- Bubble entrainment and movement in fiber suspensions were explained by considering the bubble buoyancy and confinement forces the flocs and inter-floc structures exert on the bubble.

- When a swarm of bubbles is in a fiber suspension, inter-bubble interactions significantly affect their behavior. Seven inter-bubble interaction modes were summarized,

with three of them considered specifically for bubbles in flocculated fiber suspensions. Fiber flocculation has significant effects on the seven inter-bubble interactions.

- Single bubbles or bubble swarms behave differently in a flowing fiber suspension because fiber suspension rheological properties and bubble contact probability change due to the flowing conditions.

- Six mechanisms were identified for fiber influences on gas holdup in gas-liquid-bubble columns. One or more of these mechanisms are usually significant in a system and determine the overall gas holdup trends in fiber suspensions.

8.1.2 Experimental results on gas holdup in the cocurrent air-water-fiber bubble column

- The influence of superficial gas and liquid velocity and fiber mass fraction on gas holdup in the cocurrent air-water-fiber bubble column were analyzed, mainly based on the data acquired in hardwood fiber suspensions. Generally, gas holdup increased with increasing superficial gas velocity without a local maximum, decreased with increasing superficial liquid velocity, and changed nonlinearly with increasing fiber mass fraction. When flocculation was significant in the fiber suspension, gas holdup decreased with increasing fiber mass fraction. Similar trends were also found in 5 other fiber suspensions (softwood, BCTMP, and Rayon (1, 3, and 6 mm) fibers).

- By comparing with available literature results, the gas distribution method was found to significantly affect the gas holdup trend with increasing superficial liquid velocity or fiber mass fraction.

- Fiber type had a significant effect on gas holdup in the cocurrent air-water-fiber bubble column because fiber physical properties significantly affected flocculation in fiber suspensions, and consequently influenced bubble column hydrodynamics.

- The air-water-fiber to air-water gas holdup ratio ($\varepsilon/\varepsilon_{A-W}$) represented the effect of fiber addition on gas holdup and the degree to which an air-water-fiber bubble column flow deviates from an air-water flow. The gas holdup ratio was a nonlinear function of superficial gas velocity. It reached a local minimum at $U_g \approx 4\sim5$ cm/s when the fiber mass fraction was sufficiently high to form fiber flocs.

- Gas flow regimes were identified using the modified drift-flux model (Eq. (5.8)). Three gas flow regimes (i.e., dispersed bubble, vortical-spiral, and turbulent flow) were identified. When fiber mass fraction was higher than a certain value (which was a function of fiber type), the dispersed bubble flow regime disappeared because bubble coalescence was enhanced at low U_g by flocculating fibers. Superficial liquid velocity did not affect gas flow regime transition.

8.1.3 Quantifying fiber effects on gas holdup

- A parameter was identified that characterizes the fiber effect on gas holdup in gas-liquid-fiber bubble columns and satisfies the following condition: when this parameter is constant, the gas holdup in different fiber suspensions is generally similar at most operating conditions.

- The crowding factor estimated with various methods and fiber number density did not satisfy this criterion.

- A method was outlined to identify a characterization parameter by combining the crowding factor and fiber number density. With this method, a parameter $I_c = \ln(N_c^{4/5} N_f^{1/5})$ was identified. The experimental data showed that I_c satisfies the preceeding condition for most conditions addressed in this study.

8.1.4 Gas holdup model development

- A gas holdup model (Eq. (7.11)) was developed for cocurrent air-water-fiber bubble flows based on the modified drift-flux model. The model coefficients were estimated using a nonlinear least square error curve fitting method. The gas holdup model correlates gas holdup with superficial gas and liquid velocity and fiber type and mass fraction. It reproduced most experimental data within ±10% error and all but 3 of the 3839 experimental data points within ±15% error. It also predicted the air-water bubble column (where $I_c = -\infty$) gas holdup data within ±5% error; these data were not used in estimating the model coefficients. Hence, the gas holdup model can be extrapolated toward the lower limit $I_c = -\infty$.

- The physical implications of the model coefficients, including the radial distribution parameters and weighted average drift velocity, were discussed. Two different radial distribution parameters (C_l and C_g) were used in the modified drift-flux gas holdup model (Eq. (7.11)); their values were larger than the values recommended for fast upward and small diameter columns. This was attributed to the large column diameter and low superficial liquid velocities used in this study, which caused the flow to be dictated by buoyancy effects rather than wall effects. The weighted average drift velocity increased nonlinearly with increasing I_c with a linear region near $I_0 = 8.12$, where the average terminal bubble rise velocity increased linear with I_c or ln(C).

8.2 Recommendations for Future Work

Gas-liquid-fiber flows are widely used in the pulp and paper industry, especially in the flotation deinking and gaseous bleaching processes. The knowledge of gas-liquid-fiber systems may also be useful to understand other processes involving flocculating filamentous substances (e.g., fungi) (see Chapter 1) and develop new cellulose fiber applications (Tang and Heindel, 2005a). To obtain a further understanding of the gas-liquid-fiber flows, more work is recommended. This includes experimental and theoretical studies.

8.2.1 Further work on factors influencing hydrodynamics in gas-liquid-fiber bubble columns

Gas-liquid-fiber bubble column flows are extremely complex and affected by as many as 23 factors at constant pressure and temperature (see, for example, Appendix B). Among these factors, important factors such as bubble column diameter and height and liquid properties have not been studied. The effects of fiber stiffness and length distribution and gas distributor have not been systematically investigated either. Thus, the following experimental work is recommended:

- Investigate the effect of liquid phase surface tension on hydrodynamics in gas-liquid-fiber bubble column flows. Surface tension directly affects bubble stability in the liquid. In practical applications such as flotation deinking, surface active-agents are intentionally added to control bubble size and behavior and enhance the hydrophobicity of the ink particles. Under this condition, the effect of fiber addition on gas holdup and bubble size may be different from what was observed in this study.

- Investigate the effect of liquid viscosity on the hydrodynamics in gas-liquid-fiber bubble column flows. This is recommended because liquid viscosity affects fiber flocculation (Zhao and Kerekes, 1993), which is the most important reason that a gas-liquid-fiber flow is different from other gas-liquid-solid ones.

- In industrial applications like flotation deinking, there are usually other particles (e.g., stickies and ink particles) present in the fiber suspensions. Such particles may also influence the hydrodynamics in a gas-liquid-fiber bubble column. An investigation from this aspect will further the understanding of real industrial processes.

- Investigate the effect of bubble column geometry parameters (including diameter and height) on the hydrodynamics in gas-liquid-fiber bubble column flows. In industrial applications, bubble columns are usually much larger than that used in laboratory studies. To apply the knowledge of gas-liquid-fiber flows obtained with laboratory bubble columns to design industry processes and bubble columns, the difference in size must be considered.

- The effect of gas distribution method on the gas holdup trend with superficial liquid velocity and fiber mass fraction was revealed to be significant. It is useful for industrial applications to explore in more detail (qualitatively or quantitatively) the effects of gas distributor type and design and its position and orientation on the hydrodynamics in gas-liquid-fiber bubble column flows.

- Fiber elastic modulus and surface friction coefficient also affect fiber flocculation and hence, the hydrodynamics and gas holdup in gas-liquid-fiber suspensions. These effects should be studied using a fiber with an elastic modulus and/or surface friction coefficient significantly different from those of cellulose fibers.

- Usually cellulose fibers are not uniform in length. Fiber length distribution was found to affect fiber flocculation (Huber *et al.*, 2003). Therefore, it is believed that gas holdup in fiber suspensions is related to the fiber length distribution. Although it was concluded that the fiber effect characterization parameter, I_c, which was identified in Chapter 6, includes the effect of the standard deviation of a fiber length distribution, this parameter does not consider the entire information of a fiber length distribution (i.e., its probability density function). The modified definition of the crowding factor proposed by Huber *et al.* (2003) may serve as an important clue to qualitatively account for the fiber length distribution effect on gas holdup in fiber suspensions and should be investigated.

8.2.2 Further work on modeling gas-liquid-fiber flows in bubble columns

The modified drift-flux gas holdup model developed in this study is simple and convenient for application and provides accurate predictions of gas holdup in air-water-fiber bubble columns. However, a lot of information is omitted from this model. It only provides volume and time averaged gas holdup. It does not provide information about phase velocities in a bubble column. Gas holdup alone is insufficient for estimating gas-liquid momentum, heat, and mass transfer rates. Information on bubble size distribution is also very important. Hence, a more complex model considering more details is needed. To achieve this,

investigations on local dynamics in gas-liquid-fiber bubble columns are necessary. Thus, the following further work is recommended:

- Measure the local gas holdup and bubble size and velocity at different operating conditions. With such measurements, radial and axial profiles of local gas holdup and bubble size and velocity can be revealed.

- Model the rheological properties of flocculating fiber suspensions. Fiber suspensions have been considered as pseudofluid in many studies. However, due to their unique structures (as described in Chapter 4), flocculating fiber suspensions are inherently heterogeneous. In discussing the importance of mechanistic-based models in fiber suspension flow, Duffy (2000) concluded that: "Just as rheologists have separated homogeneous, non-settling suspension flow characteristics from inhomogeneous solid-liquid systems, the pulp and paper industry must strive to show that there is a third class of structured solid-liquid systems which have their own flow models and shear mechanisms." The understanding of fiber suspension rheological properties is critical to model gas-liquid-fiber bubble column flows.

- Qualitatively investigate floc formation and dispersion, floc size distribution evolution, fiber network formation and breakup, and bubble-fiber network interactions for various conditions, especially under turbulent mixing similar to that in a bubble column. Such investigations will provide insight for modeling the complex transport processes involved in gas-liquid-fiber flows.

- The bubble formation process in floccultated fiber suspensions may be different from that observed in pure liquids because of the inherent heterogenerous fiber suspension structure, as described in Chapter 4. Observations of the bubble formation process in fiber suspensions using flow visualization techniques will further our understanding of the bubble formation process and bubble-fiber network interactions. Numerical modeling of the bubble formation process, while considering the unique fiber suspension structure, is highly recommended.

- The parameter I_c was identified to characterize the fiber suspension effect on gas holdup in gas-liquid-fiber bubble columns based on experimental data acquired over a wide range of conditions. It is simple to use. However, the fundamental physical mechanism behind the parameter is not quite clear. Theoretical study is needed to further the understanding and provide confidence in applying such a parameter in a wide range of practical applications.

REFERENCES

Ajersch, M., and Pelton, R., 1993. The growth of bubble on pulp fibers and on carbon black dispersed in supersaturated carbon dioxide solutions. *Proceedings of the 2nd Research Forum on Recycling*, Ste-Adele, Que, Canada, October 5-7, pp. 129-134.

Ajersch, M., and Pelton, R., 1999a. The behavior of air bubbles in aqueous wood pulp suspensions. *Proceedings of the 5th Research Forum on Recylcing*, Ottawa, Ont, Canada, September 28-30, pp. 97-112.

Ajersch, M., and Pelton, R., 1999b. Modelling fibre loss by entrainment during flotation of flocculated pulps. *Journal of Pulp and Paper Science*, 25: 30-36.

Akosman, C., Orhan, R., and Dursun, G., 2004. Effects of liquid property on gas holdup and mass transfer in co-current downflow contacting column. *Chemical Engineering and Processing*, 43: 503-509.

Al-Masry, W.A., 2001. Gas holdup in circulating bubble columns with pseudoplastic liquids. *Chemical Engineering & Technology*, 24: 71-76.

Andersson, S.R., and Rasmuson, A., 2000. Flow measurements on a turbulent fiber suspension by laser Doppler anemometry. *AIChE Journal*, 46: 1106-1119.

Barnea, D., Shoham, O., and Taitel, Y., 1980. Flow pattern characterization in 2-phase flow by electrical conductance probe. *International Journal of Multiphase Flow*, 6: 387-397.

Beghello, L., 1998. Some factors that influence fiber flocculation. *Nordic Pulp and Paper Research Journal*, 13: 274-279.

Behkish, A., 2004. *Hydrodynamic and Mass Transfer Parameters in Large-Scale Slurry Bubble Column Reactors*. Ph.D. Thesis, Univesity of Pittsburgh, Pittsburgh, PA, 316 pp.

Bejar, P., Casas, C., Godia, F., and Sola, C., 1992. The influence of physical properties on the operation of a 3-phase fluidized-bed fermenter with yeast-cells immobilized in Ca-alginate. *Applied Biochemistry and Biotechnology*, 34-5: 467-475.

Bennington, C.P.J., Azevedo, G., John, D.A., Birt, S.M., and Wolgast, B.H., 1995. The yield stress of medium- and high- consistency mechanical pulp fiber suspensions at high gas contents. *Journal of Pulp and Paper Science*, 21: J111-J118.

Bennington, C.P.J., and Kerekes, R.J., 1996. Power requirements for pulp suspension fluidization. *TAPPI Journal*, 79 (2): 253-258.

Bennington, C.P.J., Kerekes, R.J., and Grace, J.R., 1990. The yield stress of fiber suspensions. *Canadian Journal of Chemical Engineering*, 68: 748-757.

Bessler, W.F., and Littman, H., 1987. Experimental studies of wakes behind circularly capped bubbles. *Journal of Fluid Mechanics*, 185: 137-151.

Beyerlein, S.W., Cossmann, R.K., and Richter, H.J., 1985. Prediction of bubble concentration profiles in vertical turbulent 2-phase flow. *International Journal of Multiphase Flow*, 11: 629-641.

Bhaga, D., Pruden, B.B., and Weber, M.E., 1971. Gas holdup in a bubble column containing organic liquid mixtures. *Canadian Journal of Chemical Engineering*, 49: 417-420.

Bjorkman, U., 2002. Floc behaviour in flowing fiber suspension. PMT-2002-1, Paper Technology, Royal Institute of Technology, Stockholm, Sweden.

Bjorkman, U., 2003a. Break-up of suspended fiber networks. *Nordic Pulp and Paper Research Journal*, 18: 32-37.

Bjorkman, U., 2003b. Stress generation and transmission in suspended fiber networks. *Nordic Pulp and Paper Research Journal*, 18: 38-43.

Bly, M.J., and Worden, R.M., 1992. The effects of solids density and void fraction on the bubble rise velocity in a liquid-solid fluidized bed. *Chemical Engineering Science*, 47: 3281-3288.

Boultonstone, J.M., and Blake, J.R., 1993. Gas bubbles bursting at a free surface. *Journal of Fluid Mechanics*, 254: 437-466.

Buckingham, E., 1914. On physically similar systems; Illustrations of the use of dimensional equations. *Physcial Review*, 4: 345-376.

Camarasa, E., Vial, C., Poncin, S., Wild, G., Midoux, N., and Bouillard, J., 1999. Influence of coalescence behaviour of the liquid and of gas sparging on hydrodynamics and bubble characteristics in a bubble column. *Chemical Engineering and Processing*, 38: 329-344.

Casey, J.P. (Editor), 1960. *Pulp and Paper: Chemistry and Chemical Technology*, 2nd ed., Vol: 1. Interscience Publishers, Inc., New York, NY, 580 pp.

Catchpole, J.P., and Fulford, G., 1966. Dimensionless Groups. *Industrial and Engineering Chemistry*, 58: 46-60.

Chaiarrekij, S., Dhingra, H., and Ramarao, B.V., 2000. Deinking of recycled pulps using column flotation: energy and environmental benefits. *Resources, Conservation and Recycling*, 28: 219-226.

Chase, W.C., Donatelli, A.A., and Walkinshaw, J.W., 1989. Effects of freeness and consistency on the viscosity of hardwood and softwood pulp suspensions. *TAPPI Journal*, 72 (5): 199-204.

Chen, F., Chen, H., and Gong, X.D., 1997. Mixotrophic and heterotrophic growth of *Haematococcus lacustris* and rheological behaviour of the cell suspensions. *Bioresource Technology*, 62: 19-24.

Chen, R.C., Reese, J., and Fan, L.-S., 1994. Flow structure in a three-dimensional bubble column and three-phase fluidized bed. *AIChE Journal*, 40: 1093-1104.

Chen, W.B., and Tan, R.B.H., 2002. Theoretical analysis of bubble formation in a co-flowing liquid. *Journal of Chemical Engineering of Japan*, 35: 952-962.

Chhabra, R.P., Farooqi, S.I., and Richardson, J.F., 1984. Isothermal 2-phase flow of air and aqueous polymer-solutions in a smooth horizontal pipe. *Chemical Engineering Research & Design*, 62: 22-32.

Chisti, Y., 1998. Pneumatically agitated bioreactors in industrial and environmental bioprocessing: hydrodynamics, hydraulics, and transport phenomena. *Applied Mechanics Review*, 51: 33-112.

Clark, N., and Flemmer, R., 1986. The effect of varying gas voidage distributions on average holdup in vertical bubble flow. *International Journal of Multiphase Flow*, 12: 299-302.

Clark, N.N., van Egmond, J.W., and Nebiolo, E.P., 1990. The drift-flux model applied to bubble columns and low velocity flows. *International Journal of Multiphase Flow*, 16: 261-279.

Clift, R., Grace, J.R., and Weber, M.E., 1978. *Bubbles, Drops, and Particles*. Academic Press, New York, NY, 380 pp.

Crabtree, J.R., and Bridgwater, J., 1967. Wakes behind 2-dimensional air bubbles. *Chemical Engineering Science*, 22: 1517-1518.

Deckwer, W.D., 1992. *Bubble Column Reactors*. Wiley, New York, 533 pp.

Deindoerfer, F.H., and West, J.M., 1960. Rheological examination of some fermentation broths. *Journal of Biochemical and Microbiological Technology and Engineering*, 2: 165-175.

Delnoij, E., Kuipers, J.A.M., and vanSwaaij, W.P.M., 1997. Dynamic simulation of gas-liquid two-phase flow: effect of column aspect ratio on the flow structure. *Chemical Engineering Science*, 52: 3759-3772.

Dennis, J.E., Jr., 1977. Nonlinear least squares. In: D. Jacobs (Editor), *State of the Art in Numerical Analysis: Proceedings of the Conference on the State of the Art in Numerical Analysis Held at the University of York, April 12th-15th, 1976.* Academic Press, London, pp. 269-312.

Dessureault, S., Barbe, M.C., and Levesque, M., 1995. Column flotation: a new technology for deinking recycled pulp. *TAPPI Proceedings of 1995 Recycling Symposium*, New Orleans, LA, February 20-23, pp. 251-255.

Dessureault, S., Carabin, P., Thom, A., Kleuser, J., and Gitzen, P., 1998. Column flotation: a significant simplification of the flotation deinking process. *Progress in Paper Recycling*, 8(1): 23-33.

DeSwart, J.W.A., vanVliet, R.E., and Krishna, R., 1996. Size, structure and dynamics of "large" bubbles in a two-dimensional slurry bubble column. *Chemical Engineering Science*, 51: 4619-4629.

Dodson, C.T.J., 1996. Fiber crowding, fiber contacts, and fiber flocculation. *TAPPI Journal*, 79 (9): 211-216.

Dodson, C.T.J., and Sampson, W.W., 1999. Spatial statistics of stochastic fiber networks. *Journal of Statistical Physics*, 96: 447-458.

Doi, M., and Edwards, S.F., 1978a. Dynamics of Rod-Like Macromolecules in Concentrated-Solution .1. *Journal of the Chemical Society-Faraday Transactions II*, 74: 560-570.

Doi, M., and Edwards, S.F., 1978b. Dynamics of Rod-Like Macromolecules in Concentrated-Solution .2. *Journal of the Chemical Society-Faraday Transactions II*, 74: 918-932.

Doi, M., and Edwards, S.F., 1987. *The Theory of Polymer Dynamics*. Clarendon Press, Oxford, 391 pp.

Drahos, J., Zahradnik, J., Puncochar, M., Fialova, M., and Bradka, F., 1991. Effect of operation conditions on the characteristics of pressure fluctuations in a bubble column. *Chemical Engineering and Processing*, 29: 107-115.

Duchemin, L., Popinet, S., Josserand, C., and Zaleski, S., 2002. Jet formation in bubbles bursting at a free surface. *Physics of Fluids*, 14: 3000-3008.

Dudukovic, M.P., Larachi, F., and Mills, P.L., 1999. Multiphase reactors - revisited. *Chemical Engineering Science*, 54: 1975-1995.

Duffy, G.G., 2000. The importance of mechanistic-based models in fiber suspension flow. *54th APPITA Annual General Conference*, Melbourne, Australia, April 3-6, 2000, Vol: 1, pp. 337-342.

Duffy, G.G., Titchener, A.L., Lee, P.F.W., and Moller, K., 1976. Mechanisms of flow of pulp suspensions in pipes. *APPITA*, 29: 363-370.

Fan, L.-S., 1989. *Gas-Liquid-Solid Fluidization Engineering*. Butterworths, Boston, MA, 763 pp.

Fan, L.-S., and Tsuchiya, K., 1990. *Bubble Wake Dynamics in Liquids and Liquid-Solid Suspensions*. Butterworth-Heinemann, Stoneham, MA, 363 pp.

Fan, L.-S., Yang, G.Q., Lee, D.J., Tsuchiya, K., and Luo, X., 1999. Some aspects of high-pressure phenomena of bubbles in liquids and liquid-solid suspensions. *Chemical Engineering Science*, 54: 4681-4709.

Farnood, R.R., Loewen, S.R., and Dodson, C.T.J., 1994. Estimation of intra-floc forces. *Appita Journal*, 47: 391-396.

Fawkner, R.D., Kluth, P.P., and Dennis, J.S., 1990. Bubble formation at orifices in pulsed, flowing liquids. *Chemical Engineering Research & Design*, 68: 69-73.

Figliola, R.S., and Beasley, D.E., 2000. *Theory and Design for Mechanical Measurement*, 3rd ed. John Wiley & Sons, Inc, New York, 536 pp.

Finkelstein, D.B., and Ball, C. (Editors), 1992. *Biotechnology of Filamentous Fungi: Technology and Products*. Butterworth-Heinemann, Boston, MA, 520 pp.

Forest Products Laboratory, 1999. Wood handbook - wood as an engineering material. Gen. Tech. Rep. FPL-GTR-113, USDA Forest Service, Forest Products Laboratory, Madison, WI.

Forgacs, O.L., Robertson, A.A., and Mason, S.G., 1958. The hydrodynamic behaviour of paper making fibers. In: F. Bolam (Editor), *Fundamentals of Papermaking Fibers, Transactions of The Symposium Held at Cambridge, 1957*. Technical Section of BP&BMA, Surrey, England, pp. 447-479.

Forrester, S.E., and Rielly, C.D., 1998. Bubble formation from cylindrical, flat and concave sections exposed to a strong liquid cross-flow. *Chemical Engineering Science*, 53: 1517-1527.

Garner, A.E., and Heindel, T.J., 2000. The effect of fiber type on bubble size. *Journal of Pulp and Paper Science*, 26: 266-269.

Gharat, S.D., and Joshi, J.B., 1992. Transport phenomena in bubble column reactors. II. Pressure drop. *Chemical Engineering Journal*, 48: 153-166.

Gibbs, P.A., Seviour, R.J., and Schmid, F., 2000. Growth of filamentous fungi in submerged culture: problems and possible solutions. *Critical Reviews in Biotechnology*, 20: 17-48.

Glover, S.M., Yan, Y.D., Jameson, G.J., and Biggs, S., 1999. Characterisation of the structural compactness of bridging flocculated aggregates using settling. *Proceedings of the 27th Australasian Chemical Engineering Conference (Chemeca 99)*, Newcastle, Australia, September.

Gomez, C.O., Watson, J.A., and Finch, J.A., 1995. Recycled-paper deinking using column flotation. *Proceedings of the 3rd Research Forum on Recycling*, Vancouver, BC, Canada, November 20-22, pp. 41-44.

Gorowara, R.L., and Fan, L.-S., 1990. Effect of surfactants on three-phase fluidized bed hydrodynamics. *Industrial & Engineering Chemistry Research*, 29: 882-891.

Groen, J.S., Oldeman, R.G.C., Mudde, R.F., and van den Akker, H.E.A., 1996. Coherent structures and axial dispersion in bubble column reactors. *Chemical Engineering Science*, 51: 2511-2520.

Guet, S., Ooms, G., Oliemans, R.V.A., and Mudde, R.F., 2004. Bubble size effect on low liquid input drift-flux parameters. *Chemical Engineering Science*, 59: 3315-3329.

Gullichsen, J., and Harkonen, E., 1981. Medium consistency technology - part 1: fundamental data. *TAPPI*, 64: 69-72.

Hardie, C.A., Gomez, C.O., and Finch, J.A., 1999a. A venturi aerated column cell for deinking: effect of design and operating parameters. *Progress in Paper Recycling*, 8 (4): 33-41.

Hardie, C.A., Leichtle, G.F., Watson, J.A., Finch, J.A., and Gomez, C.O., 1999b. Application of mineral processing techniques to the recycling of wastepaper. *CIM Bulletin*, 92: 131-137.

Heindel, T.J., 1997. The fundamentals of flotation deinking. *1997 TAPPI Pulping Conference*. TAPPI Press, Atlanta, GA, pp. 521-533.

Heindel, T.J., 1999. Bubble size measurements in a quiescence fiber suspension. *Journal of Pulp and Paper Science*, 25: 104-110.

Heindel, T.J., 2000. Gas flow regime changes in a bubble column filled with a fiber suspension. *Canadian Journal of Chemical Engineering*, 78: 1017-1022.

Heindel, T.J., 2002. Bubble size in a cocurrent fiber slurry. *Industrial & Engineering Chemistry Research*, 41: 632-641.

Heindel, T.J., 2003. A review of gas flows in fiber suspensions. *TAPPI Journal*, 2 (11): 22.

Heindel, T.J., and Garner, A.E., 1999. The effect of fiber consistency on bubble size. *Nordic Pulp and Paper Research Journal*, 14: 171-178.

Heindel, T.J., and Monefeldt, J.L., 1997. Flash x-ray radiography for visualizing gas flows in opaque liquid/fiber suspensions. *Proceedings of the 1997 ASME Fluids Engineering Division Summer Meeting, FEDSM'97*, Vancouver, BC, Canada, June 22-26, Vol: 16.

Heindel, T.J., and Monefeldt, J.L., 1998. Observations of the bubble dynamics in a pulp suspension using flash x-ray radiography. *TAPPI Journal*, 81 (11): 149-158.

Heindel, T.J., and Omberg, S.J., 2001. Gas bubble size in a synthetic fiber slurry. *4th International Conference on Multiphase Flow*, New Orleans, LA, May 27-June 1.

Helle, T.M., 2000. Effect of centrifugal force on flotation of air bubbles onto fibres and fillers. *Paperi Ja Puu-Paper and Timber*, 82: 251-254.

Herringe, R.A., and Davis, M.R., 1978. Flow structure and distribution effects in gas-liquid mixture flows. *International Journal of Multiphase Flow*, 4: 461-486.

Hesketh, R.P., Etchells, A.W., and Russell, T.W.F., 1991. Bubble breakage in pipeline flow. *Chemical Engineering Science*, 46: 1-9.

Hewitt, G.F., 1977. Vertical bubble and slug flow. In: D. Butterworth and G.F. Hewitt (Editors), *Two Phase Flow and Heat Transfer*. Oxford University Press, Oxford, pp. 91-106.

Hibiki, T., and Ishii, M., 2002. Distribution parameter and drift velocity of drift-flux model in bubbly flow. *International Journal of Heat and Mass Transfer*, 45: 707-721.

Hikita, H., Asai, S., Tanigawa, K., Segawa, K., and Kitao, M., 1980. Gas hold-up in bubble-columns. *Chemical Engineering Journal and the Biochemical Engineering Journal*, 20: 59-67.

Hills, J.H., 1976. The operation of a bubble column at high throughputs. *Chemical Engineering Journal*, 12: 89-99.

Hol, P.D., and Heindel, T.J., 2005. Local gas holdup variation in a fiber slurry. *Industrial & Engineering Chemistry Research*, 44: 4478-4784.

Hourani, M.J., 1988a. Fiber flocculation in pulp suspension flow - part 1: theoretical model. *TAPPI Journal*, 71 (5): 115-118.

Hourani, M.J., 1988b. Fiber flocculation in pulp suspension flow - part 2: experimental results. *TAPPI Journal*, 71 (6): 186-189.

Huber, P., and Martinez, M., 2003. An estimate of the level of fibre crowding for polydisperse suspensions. *APPITA Journal*, 56: 445-448.

Huber, P., Roux, J.C., Mauret, E., Belgacem, N., and Pierre, C., 2003. Suspension crowding for a general fibre-length distribution: Application to flocculation of mixtures of short and long papermaking fibres. *Journal of Pulp and Paper Science*, 29: 77-85.

Hudson, K., and Kazem, B., 2003. Highly efficient method of mixing dissimilar fluids using mechanically induced cavitation. Patent: 6,627,784 B2, Hydro Dynamics, Inc., Rome, GA.

Ilvessalo-Pfaffli, M.-S., 1995. *Fiber Altas: Identification of Papermaking Fibers*. Springer-Verlag, Berlin, 400 pp.

Ishii, M., 1977. One-Dimensional Drift-Flux Model and Constitutive Equations for Relative Motion Between Phases in Various Two-Phase Flow Regimes. ANL-77-47, Argonne National Laboratory, USA.

Isler, W., and Widmer, F., 1979. Formation and separation of air bubbles in technical pulp suspensions .2. separation of bubbles from pulp suspensions in closed and open flow channels. *Papier*, 33: 89-93.

Jacquelin, G., 1972. Method of Treating Suspension of Fibers to Form Fibrous Aggregates. Patent: 3,679,542, Societe d'Explotition des Brevets Granofibre (Sebreg), Paris, France.

Jagannadh, S.V.S., Jordan, H., and Brodkey, R.S., 1991. Formation and characterization of paper pulp flocs. *Chemical Engineering Science*, 46: 2997-3005.

Jamialahmadi, M., Branch, C., and Mullersteinhagen, H., 1994. Terminal bubble rise velocity in liquids. *Chemical Engineering Research & Design*, 72: 119-122.

Jamialahmadi, M., and Mullersteinhagen, H., 1991. Effect of solid particles on gas hold up in bubble columns. *Canadian Journal of Chemical Engineering*, 69: 390-393.

Janse, P., Gomez, C.O., and Finch, J.A., 1999. Effect of pulp fibers on gas holdup in a flotation column. *Canadian Journal of Chemical Engineering*, 77: 22-25.

Johnson, B.D., Gershey, R.M., Cooke, R.C., and Sutcliffe, W.H., 1982. A theoretical model for bubble formation at a frit surface in a shear field. *Separation Science and Technology*, 17: 1027-1039.

Joshi, J.B., 2001. Computational flow modelling and design of bubble column reactors. *Chemical Engineering Science*, 56: 5893-5933.

Joshi, J.B., Pandit, A.B., and Rao, K.S.M.S.R., 1986. Axial mixing in multiphase sparged contactors. In: N.P. Cheremisinoff (Editor), *Encyclopedia of Fluid Mechanics*, Vol: 3. Gulf Publ. Co., Huston, TX, pp. 1136-1179.

Joshi, J.B., Ranade, V.V., Gharat, S.D., and Lele, S.S., 1990. Sparged loop reactors. *Canadian Journal of Chemical Engineering*, 68: 705-741.

Joshi, J.B., Vitankar, V.S., Kulkarni, A.A., Dhotre, M.T., and Ekambara, K., 2002. Coherent flow structures in bubble column reactors. *Chemical Engineering Science*, 57: 3157-3183.

Kao, S.V., and Mason, S.G., 1975. Dispersion of particles by shear. *Nature*, 253: 619-621.

Kara, S., Kelkar, B.G., Shah, Y.T., and Carr, N.L., 1982. Hydrodynamics and axial mixing in a 3-phase bubble column. *Industrial & Engineering Chemistry Process Design and Development*, 21: 584-594.

Kawagoe, M., Hyakumura, K., Suye, S.-I., Miki, K., and Naoe, K., 1997. Application of bubble column fermentors to submerged culture of *Schizophyllum commune* for production of L-Malic Acid. *Journal of Fermentation and Bioengineering*, 84: 333-336.

Kawagoe, M., Kawakami, K., Nakamura, Y., Naoe, K., Miki, K., and Noda, H., 1999. Submerged culture of *Tricholoma matsutake* mycelium in bubble column fermentors. *Journal of Bioscience and Bioengineering*, 87: 116-118.

Kawasaki, H., and Tanaka, H., 1995. Effects of geometric properties for a perforated plate on gas holdup in a bubble column. *Journal of Chemical Engineering of Japan*, 28: 715-720.

Kelkar, B.G., Godbole, S.P., Honath, M.F., Shah, Y.T., Carr, N.L., and Deckwer, W.D., 1983. Effect of addition of alcohols on gas holdup and backmixing in bubble-columns. *AIChE Journal*, 29: 361-369.

Kelkar, B.G., Shah, Y.T., and Carr, N.L., 1984. Hydrodynamics and axial mixing in a three-phase bubble column: effects of slurry properties. *Industrial & Engineering Chemistry Process Design and Development*, 23: 308-313.

Kemoun, A., Ong, B.C., Gupta, P., Al-Dahhan, M.H., and Dudukovic, M.P., 2001. Gas holdup in bubble columns at elevated pressure via computed tomography. *International Journal of Multiphase Flow*, 27: 929-946.

Kerekes, R.J., 1983. Pulp flocculation in decaying turbulence: a literature review. *Journal of Pulp and Paper Science*, 9: TR86-TR91.

Kerekes, R.J., 1995. Perspectives on fibre flocculation in papermaking. *International Paper Physics Conference*, Niagara-on-the-Lake, ON, Canada, September 11-14, pp. 23-31.

Kerekes, R.J., 1996. Characterizing fiber suspensions. *Proceedings of TAPPI 1996 Engineering Conference*, Chicago, IL, September 16-19, Vol: 1, pp. 21-28.

Kerekes, R.J., and Schell, C.J., 1992. Characterization of fiber flocculation regimes by a crowding factor. *Journal of Pulp and Paper Science*, 18: J32-J38.

Kerekes, R.J., and Schell, C.J., 1995. Effects of fiber length and coarseness on pulp flocculation. *TAPPI Journal*, 78 (2): 133-139.

Kerekes, R.J., Soszynski, R.M., and Tam Doo, P.A., 1985. The flocculation of pulp fibers. In: V. Punton (Editor), *Papermaking Raw Materials, Transactions of the 8th Fundamental Research Symposium Held at Oxford: September 1985*, Vol: 1. Mechanical Engineering Publications Limited, London, England, pp. 265-310.

Kluytmans, J.H.J., van Wachem, B.G.M., Kuster, B.M., and Schouten, J.C., 2001. Gas holdup in a slurry bubble column: influence of electrolyte and carbon particles. *Industrial & Engineering Chemistry Research*, 40: 5326-5333.

Koetsier, W.T., Van Swaaij, W.P.M., and Van der Most, M., 1976. Maximum gas holdup in bubble columns. *Journal of Chemical Engineering of Japan*, 9: 332-3333.

Krishna, R., deSwart, J.W.A., Ellenberger, J., Martina, G.B., and Maretto, C., 1997. Gas holdup in slurry bubble columns: effect of column diameter and slurry concentrations. *AIChE Journal*, 43: 311-316.

Krishna, R., and Ellenberger, J., 1996. Gas holdup in bubble column reactors operating in the churn-turbulent flow regime. *AIChE Journal*, 42: 2627-2634.

Krishna, R., Ellenberger, J., and Hennephof, D.E., 1993. Analogous description of the hydrodynamics of gas-solid fluidized beds and bubble columns. *Chemical Engineering Journal*, 53: 89-101.

Krishna, R., Ellenberger, J., and Maretto, C., 1999a. Flow regime transition in bubble columns. *International Communications in Heat and Mass Transfer*, 26: 467-475.

Krishna, R., Urseanu, M.I., van Baten, J.M., and Ellenberger, J., 1999b. Influence of scale on the hydrodynamics of bubble columns operating in the churn-turbulent regime: experiments vs. Eulerian simulations. *Chemical Engineering Science*, 54: 4903-4911.

Krishna, R., Wilkinson, P.M., and Vandierendonck, L.L., 1991. A Model for gas holdup in bubble-columns incorporating the influence of gas-density on flow regime transitions. *Chemical Engineering Science*, 46: 2491-2496.

Kropholler, H.W., and Sampson, W.W., 2001. The effect of fibre length distribution on suspension crowding. *Journal of Pulp and Paper Science*, 27: 301-305.

Kumar, S.B., Dudukovic, M.P., and Toseland, B.A., 1997. Measurement techniques for local and global fluid dynamic quantities in two and three phase systems. In: J. Chaouki, F.

Larachi and M.P. Dudukovic (Editors), *Non-Invasive Monitoring of Multiphase Flows*. Elsevier, New York, pp. 1-45.

Lapidus, L., and Elgin, J.C., 1957. Mechanics of vertical-moving fluidized systems. *AIChE Journal*, 3: 63-68.

Larachi, F., Wild, G., Laurent, A., and Midoux, N., 1994. Influence of gas density on the hydrodynamics of cocurrent gas-liquid upflow fixed bed reactors. *Industrial & Engineering Chemistry Research*, 33: 519-525.

Lee, C.W., and Brodkey, R.S., 1987. A visual study of pulp floc dispersion mechanisms. *AIChE Journal*, 33: 297-302.

Lee, D., Macchi, A., Grace, J.R., and Epstein, N., 2001. Fluid maldistribution effects on phase holdups in three-phase fluidized beds. *Chemical Engineering Science*, 56: 6031-6038.

Lee, D.J., Luo, X., and Fan, L.-S., 1999. Gas disengagement technique in a slurry bubble column operated in the coalesced bubble regime. *Chemical Engineering Science*, 54: 2227-2236.

Letzel, H.M., Schouten, J.C., Krishna, R., and van den Bleek, C.M., 1997. Characterization of regimes and regime transitions in bubble columns by chaos analysis of pressure signals. *Chemical Engineering Science*, 52: 4447-4459.

Letzel, H.M., Schouten, J.C., Krishna, R., and van den Bleek, C.M., 1999. Gas holdup and mass transfer in bubble column reactors operated at elevated pressure. *Chemical Engineering Science*, 54: 2237-2246.

Lin, T.-J., Juang, R.-C., Chen, Y.-C., and Chen, C.-C., 2001. Predictions of flow transitions in a bubble column by chaotic time series analysis of pressure fluctuation signals. *Chemical Engineering Science*, 56: 1057-1065.

Lin, T.J., Tsuchiya, K., and Fan, L.-S., 1998. Bubble flow characteristics in bubble columns at elevated pressure and temperature. *AIChE Journal*, 44: 545-560.

Lin, T.J., Tsuchiya, K., and Fan, L.-S., 1999. On the measurements of regime transition in high-pressure bubble columns. *Canadian Journal of Chemical Engineering*, 77: 370-374.

Lindsay, J.D., Ghiaasiaan, S.M., and Abdel-Khalik, S.I., 1995. Macroscopic flow structures in a bubbling paper pulp-water slurry. *Industrial & Engineering Chemistry Research*, 34: 3342-3354.

Liu, T.J., 1997. Investigation of the wall shear stress in vertical bubbly flow under different bubble size conditions. *International Journal of Multiphase Flow*, 23: 1085-1109.

Luo, X.K., Jiang, P.J., and Fan, L.S., 1997. High-pressure three-phase fluidization: Hydrodynamics and heat transfer. *AIChE Journal*, 43: 2432-2445.

Luo, X.K., Lee, D.J., Lau, R., Yang, G.Q., and Fan, L.S., 1999. Maximum stable bubble size and gas holdup in high-pressure slurry bubble columns. *AIChE Journal*, 45: 665-680.

Magaud, F., Souhar, M., Wild, G., and Boisson, N., 2001. Experimental study of bubble column hydrodynamics. *Chemical Engineering Science*, 56: 4597-4607.

Maier, C.G., 1927. Producing small bubbles of gas in liquids by submerged orifices. Bulletin No. 260, US Bureau of Mines, Washington, DC.

Malfait, J.L., Wilcox, D.L., Mercer, D.G., and Barker, L.D., 1981. Cultivation of a filamentous mould in a glass pilot-scale airlift fermenter. *Biotechnology and Bioengineering*, XXIII: 863-867.

Marie, J.L., 1987. Modeling of the skin friction and heat-transfer in turbulent 2-component bubbly flows in pipes. *International Journal of Multiphase Flow*, 13: 309-325.

Mason, S.G., 1948. The flocculation of cellulose fiber suspension: general considerations. *Pulp and Paper Magazine of Canada*: 99-104.

Mason, S.G., 1950. The flocculation of pulp suspensions and the formation of paper. *Pulp and Paper Magazine of Canada*, 51 (10): 94-98.

Mason, S.G., 1954. Fiber motions and flocculation. *TAPPI*, 37: 494-501.

McCool, M.A., 1993. Flotation deinking. In: R.J. Spangenberg (Editor), *Secondary Fiber Recycling*. TAPPI Press, Atlanta, GA, pp. 141-162.

McIntosh, D.C., 1970. Fiber structure and properties. In: K.W. Britt (Editor), *Handbook of Pulp and Paper Technology*, 2nd ed. van Nostrand Reinhold, New York, NY, pp. 37-46.

Merchuk, J.C., and Stein, Y., 1981. Local hold-up and liquid velocity in air-lift reactors. *AIChE Journal*, 27: 377-388.

Metkin, V.P., and Sokolov, V.N., 1982. Hydraulic resistance to flow of gas-liquid mixtures having non-Newtonian properties. *Journal of Applied Chemistry of the USSR*, 55: 558-563.

Meyer, R., and Wahren, D., 1964. On the elastic properties of three-dimensional fibre networks. *Svensk Papperstidning*, 67: 432-436.

Miller, R.L., and Cain, M.B., 1986. Prediction of flow regime transitions in vertical upward 3 phase gas-liquid solid flow. *Chemical Engineering Communications*, 43: 147-163.

Mitra-Majumdar, D., Farouk, B., Shah, Y.T., Macken, N., and Oh., Y.K., 1998. Two- and three-phase flows in bubble columns: numerical predictions and measurements. *Industrial & Engineering Chemistry Research*, 37: 2284-2292.

Miyahara, T., Matsuba, Y., and Takahashi, T., 1983. The size of bubble generated from perforated plates. *International Chemical Engineering*, 23: 517-523.

Munson, B.R., Young, D.F., and Okiishi, T.H., 2002. *Fundamentals of Fluid Mechanics*, 4th ed. John Wiley & Sons, Inc., New York, 840 pp.

Myreen, B., 1989. Modeling the flow of pulp suspensions in pipes - part 1. *Paperi Ja Puu-Paper and Timber*, 71: 497-504.

Neter, J., Wasserman, W., and Kutner, M.H., 1990. *Applied Linear Statistical Models: Regression, Analysis of Variance, and Experimental Designs*, 3rd ed. Irwin, INC., Boston, MA.

Nicklin, D.J., 1962. Two phase bubble flow. *Chemical Engineering Science*, 17: 693-702.

Norman, B.G., Moller, K., and Duffy, G.G., 1978. Hydrodynamics of papermaking fibers in water suspension. *Fiber-Water Interaction in Papermaking, Transactions of the Symposium Held at Oxford.* British Paper and Board Industry Federation, London, England, pp. 195-249.

O'Donnell, K., and Peterson, S.W., 1992. Isolation, preservation, and taxonomy. In: D.B. Finkelstein and C. Ball (Editors), *Biotechnology of Filamentous Fungi: Technology and Products*. Butterworth-Heinemann, Boston, MA, pp. 7-39.

Olsvik, E., and Kristiansen, B., 1994. Rheology of filamentous fermentations. *Biotechnology Advances*, 12: 1-39.

Oolman, T., and Blanch, H.W., 1986. Non-Newtonian fermentation systems. *CRC Critical Reviews in Biotechnology*, 4: 133-184.

Otake, T., Tone, S., Nakao, K., and Mitsuhashi, Y., 1977. Coalescence and breakup of bubbles in liquids. *Chemical Engineering Science*, 32: 377-383.

Pan, N., 1993. A modified analysis of the microstructural characteristics of general fiber assemblies. *Textile Research Journal*, 63: 336-345.

Park, Y., Tyler, A.L., and de Nevers, N., 1977. The chamber orifice interaction in the formation of bubbles. *Chemical Engineering Science*, 32: 907-916.

Pelton, R., and Piette, R., 1992. Air bubble holdup in quiescent wood pulp suspensions. *Canadian Journal of Chemical Engineering*, 70: 660-663.

Petrie, C.J.S., 1999. The rheology of fibre suspensions. *Journal of Non-Newtonian Fluid Mechanics*, 87: 369-402.

Powell, R.L., Morrison, T.G., and Milliken, W.J., 2001. Apparent viscosity of suspensions of rods using falling ball rheometry. *Physics of Fluids*, 13: 588-593.

Ranade, V.V., and Tayalia, Y., 2001. Modelling of fluid dynamics and mixing in shallow bubble column reactors: influence of sparger design. *Chemical Engineering Science*, 56: 1667-1675.

Reese, J., and Fan, L.-S., 1994. Transient flow structure in the entrance region of a bubble column using particle image velocimetry. *Chemical Engineering Science*, 49: 5623-5636.

Reese, J., and Fan, L.-S., 1997. Hydrodynamics of a bubble column with a conical-shaped entrance region. *Chemical Engineering Science*, 52: 1553-1559.

Reese, J., Jiang, P., and Fan, L.-S., 1996. Bubble characteristics in three-phase systems used for pulp and paper processing. *Chemical Engineering Science*, 51: 2501-2510.

Reilly, I.G., Scott, D.S., Debruijn, T.J.W., and Macintyre, D., 1994. The role of gas-phase momentum in determining gas holdup and hydrodynamic flow regimes in bubble column operations. *Canadian Journal of Chemical Engineering*, 72: 3-12.

Ringner, J., and Rasmuson, A., 2000. Characterisation of fibre suspensions using X-ray computed tomography and image analysis. *Nordic Pulp & Paper Research Journal*, 15: 319-325.

Risso, F., 2000. The mechanisms of deformation and breakup of drops and bubbles. *Multiphase Science and Technology*, 12: 1-50.

Robertson, A.A., and Mason, S.G., 1954. Flocculation in flowing pulp suspensions. *Pulp and Paper Magazine of Canada*, 55: 263-269.

Ruzicka, M., Drahos, J., Zahradnik, J., and Thomas, N.H., 1999. Natural modes of multi-orifice bubbling from a common plenum. *Chemical Engineering Science*, 54: 5223-5229.

Ruzicka, M.C., Drahos, J., Fialova, M., and Thomas, N.H., 2001a. Effect of bubble column dimensions on flow regime transition. *Chemical Engineering Science*, 56: 6117-6124.

Ruzicka, M.C., Zahradnik, J., Drahos, J., and Thomas, N.H., 2001b. Homogeneous-heterogeneous regime transition in bubble columns. *Chemical Engineering Science*, 56: 4609-4626.

Sada, E., Yasunishi, A., Katoh, S., and Nishioka, M., 1978. Bubble formation in flowing liquid. *Canadian Journal of Chemical Engineering*, 56: 669-672.

Sarrafi, A., Jamialahmadi, M., Muller-Steinhagen, H., and Smith, J.M., 1999. Gas holdup in homogeneous and heterogeneous gas-liquid bubble column reactors. *Canadian Journal of Chemical Engineering*, 77: 11-21.

Schmid, C.F., Switzer, L.H., and Klingenberg, D.J., 2000. Simulations of fiber flocculation: effects of fiber properties and interfiber friction. *Journal of Rheology*, 44: 781-809.

Schulz, E.R., and Scott, W.E., 1993a. Analysis of air entrainment by secondary fibers .1. entrained air in a coated recycled boxboard mill. *Tappi Journal*, 76: 147-155.

Schulz, E.R., and Scott, W.E., 1993b. Analysis of air entrainment by secondary fibers .2. laboratory investigation of air release from individual fiber stocks. *Tappi Journal*, 76: 87-91.

Schulz, T.H., and Heindel, T.J., 2000. A study of gas holdup in a cocurrent air/water/fiber system. *TAPPI Journal*, 83 (6): 58-59.

Seely, T., 1968. *Turbulent Pipe Flow of Dilute Fiber Suspensions*. Ph.D. Thesis, Institute of Paper Chemistry, Appleton, Wisconsin.

Seth, R.S., Francis, W.D., and Bennington, C.P.J., 1993. The effect of mechanical treatment during medium stock concentration fluidization on pulp properties. *APPITA Journal*, 46: 54-60.

Shah, Y.T., Kelkar, B.G., Godbole, S.P., and Deckwer, W.D., 1982. Design parameters estimations for bubble column reactors. *AIChE Journal*, 28: 353-379.

Smook, G.A., 1992. *Handbook for Pulp & Paper Technologist*, 2nd ed. Angus Wilde Publications Inc., Vancouver, BC, Canada, 419 pp.

Soszynski, R.M., and Kerekes, R.J., 1988a. Elastic interlocking of nylon fibers suspended in liquid - 1. Nature of cohesion among fibers. *Nordic Pulp & Paper Research Journal*, 3: 172-179.

Soszynski, R.M., and Kerekes, R.J., 1988b. Elastic interlocking of nylon fibers suspended in liquid - 2. Process of interlocking. *Nordic Pulp & Paper Research Journal*, 3: 180-184.

Steen, M., 1989a. A concept for fibre flocculation in turbulent flow. In: C.F. Baker and V.W. Punton (Editors), *Fundamentals of Papermaking, Transactions of the Ninth Fundamental Research Symposium Held at Cambridge, September 1989*, Vol: 1. Mechanical Engineering Publications Limited, London, pp. 251-274.

Steen, M., 1989b. On turbulent structure in vertical pipe flow of fiber suspensions. *Nordic Pulp and Paper Research Journal*, 4: 244-252.

Steen, M., 1991. Modeling fiber flocculation in turbulent-flow - a numerical study. *Tappi Journal*, 74: 175-182.

Stenuf, T.J., and Unbehend, J.E., 1986. Hydrodynamics of fiber suspensions. In: N.P. Cheremisinoff (Editor), *Encyclopedia of Fluid Mechanics*, Vol: 5. Gulf Publ. Co., Huston, TX, pp. 291-308.

Stewart, C.W., 1995. Bubble interaction in low-viscosity liquids. *International Journal of Multiphase Flow*, 21: 1037-1046.

Streeter, V.L., and Wylie, E.B., 1985. *Fluid Mechanics*, 8th ed. McGraw-Hill Book Company, New York, 586 pp.

Su, X., and Heindel, T.J., 2003. Gas holdup in a fiber suspension. *Canadian Journal of Chemical Engineering*, 81: 412-418.

Su, X., and Heindel, T.J., 2005. Effect of perforated plate open area on gas holdup in rayon fiber suspensions. *Journal of Fluids Engineering*,127, 816-823.

Su, X., and Heindel, T.J., 2004b. Gas holdup behavior in Nylon fiber suspensions. *Industrial & Engineering Chemistry Research*, 43: 2256-2263.

Sundararajakumar, R.R., and Koch, D.L., 1997. Structure and properties of sheared fiber suspensions with mechanical contacts. *Journal of Non-newtonian Fluid Mechanics*, 73: 205-239.

Syrjala, M., Knuutinen, J., and Pakarinen, P., 2003. Floc size distribution measurements in stagnant fibre suspension. *Paperi Ja Puu-Paper and Timber*, 85: 150-153.

Tang, C., and Heindel, T.J., 2004a. Gas holdup in a cocurrent air-water-fiber bubble column. *Proceedings of 2004 ASME Heat Transfer/Fluids Engineering Summer Conference*, Charlotte, NC, July 11-15.

Tang, C., and Heindel, T.J., 2004b. Time-dependent gas holdup variation in an air-water bubble column. *Chemical Engineering Science*, 59: 623-632.

Tang, C., and Heindel, T.J., 2005a. Effect of fiber type on gas holdup in a cocurrent air-water-fiber bubble column. *Chemical Engineering Journal*, 111: 21-30.

Tang, C., and Heindel, T.J., 2005b. Estimation of gas holdup via pressure difference measurements in a cocurrent bubble column. *International Journal of Multiphase Flow*, In Review.

Tang, C., and Heindel, T.J., 2005c. Gas-liquid-fiber flow in a cocurrent bubble column. *AIChE Journal*, 51: 2665-2674.

Tang, W.T., and Fan, L.-S., 1989. Hydrodynamics of a 3-phase fluidized-bed containing low-density particles. *AIChE Journal*, 35: 355-364.

TAPPI, 1985. Pressure friction pressure loss of pulp suspensions: literature review and evalualtion of data and design methods. *TAPPI Technical Information Sheets*: TIS 0410-12.

TAPPI, 2002a. Coarseness of pulp fibers. *2002-2003 TAPPI Test Methods*. TAPPI Press, Atlanta, GA, pp. T234 cm-02.

TAPPI, 2002b. Fiber length of pulp and paper by automated optical analyzer using polarized light. *2002-2003 TAPPI Test Methods*. TAPPI Press, Atlanta, GA, pp. T271 om-98.

TAPPI, 2002c. Fiber length of pulp by classification. *2002-2003 TAPPI Test Methods*. TAPPI Press, Atlanta, GA, pp. T233 cm-95.

TAPPI, 2002d. Fiber length of pulp by projection. *2002-2003 TAPPI Test Methods*. TAPPI Press, Atlanta, GA, pp. T232 cm-01.

Terasaka, K., Tsuge, H., and Matsue, H., 1999. Bubble formation in cocurrently upward flowing liquid. *Canadian Journal of Chemical Engineering*, 77: 458-464.

The MathWorks Inc., 2004. *Optimization Toolbox User's Guide, Version 3*.

The MathWorks Inc., 2005. *MATLAB Programming, Version 7*.

Thorat, B.N., Shevade, A.V., Bhilegaonkar, K.N., Aglawe, R.H., Veera, U.P., Thakre, S.S., Pandit, A.B., Sawant, S.B., and Joshi, J.B., 1998. Effect of sparger design and height to diameter ratio on fractional gas hold-up in bubble columns. *Chemical Engineering Research & Design*, 76: 823-834.

Tse, K.L., Martin, T., McFarlane, C.M., and Nienow, A.W., 2003. Small bubble formation via a coalescence dependent break-up mechanism. *Chemical Engineering Science*, 58: 275-286.

Tsuchiya, K., and Nakanishi, O., 1992. Gas holdup behavior in a tall bubble column with perforated plate distributors. *Chemical Engineering Science*, 47: 3347-3354.

Tsuchiya, K., Song, G.H., Tang, W.T., and Fan, L.S., 1992. Particle drift induced by a bubble in a liquid-solid fluidized-bed with low-density particles. *AIChE Journal*, 38: 1847-1851.

Tsuge, H., Tanaka, Y., Terasaka, K., and Matsue, H., 1997. Bubble formation in flowing liquid under reduced gravity. *Chemical Engineering Science*, 52: 3671-3676.

Tzeng, J.-W., Chen, R.C., and Fan, L.-S., 1993. Visualization of flow characteristics in a 2-D bubble column and three-phase fluidized bed. *AIChE Journal*, 39: 733-744.

Ueyama, K., and Miyauchi, T., 1979. Properties of recirculating turbulent two phase flow in gas bubble columns. *AIChE Journal*, 25: 258-266.

Ueyama, K., Tsuru, T., and Furusaki, S., 1989. Flow transition in a bubble column. *International Chemical Engineering*, 29: 523-529.

van den Akker, H.E.A., 1998. Coherent structures in multiphase flows. *Powder Technology*, 100: 123-136.

Vardeman, S.B., and Jobe, J.M., 2001. *Basic Engineering Data Collection and Analysis*. Duxbury, Pacific Grove, CA, 832 pp.

Wahren, D., 1967. Proposed definitions of some basic papermaking terms. *Svensk Papperstidning-Nordisk Cellulosa*, 70: 725-729.

Wahren, D., 1979. Fiber networks structures in papermaking operations. *Proceedings of the Conference on Paper Science and Technology - the Cutting Edge*, Institute of Paper Chemistry, Appleton, WI, May 8-10, pp. 112-129.

Waldie, B., Johnston, T., Harris, W.K., and Bell, C., 1999. Bubble characteristics in a high-intensity gas/liquid contactor. *Chemical Engineering Science*, 54: 5319-5327.

Wallis, G.B., 1969. *One-Dimensional Two-Phase Flow*. McGraw-Hill, New York, 408 pp.

Walmsley, M.R.W., 1992. Air bubble motion in wood pulp fiber suspension. *APPITA 46th Annual General Conference Proceedings*, Launceston, Australia, April, pp. 509-515.

Walter, J.F., and Blanch, H.W., 1986. Bubble break-up in gas-liquid bioreactors: break-up in turbulent flows. *Chemical Engineering Journal*, 32: B7-B17.

Went, J., Jamialahmadi, M., and Muller-Steinhagen, H., 1993. Effect of wood pulp fibre concentration on gas hold-up in bubble columns. *Chemie-Ingenieur-Technik*, 65: 306-308.

Wikstrom, T., and Rasmuson, A., 1998. Yield stress of pulp suspensions: the influence of fibre properties and processing conditions. *Nordic Pulp and Paper Research Journal*, 13: 243-250.

Wikstrom, T., Ronnmark, Y., and Rasmuson, A., 2002. A new correlation for the onset of fluidisation in pulp suspensions. *Nordic Pulp and Paper Research Journal*, 17: 374-381.

Xie, T., Ghiaasiaan, S.M., and Karrila, S., 2003a. Flow regime identification in gas/liquid/pulp fiber slurry flows based on pressure fluctuations using artificial neural networks. *Industrial & Engineering Chemistry Research*, 42: 7017-7024.

Xie, T., Ghiaasiaan, S.M., Karrila, S., and McDonough, T., 2003b. Flow regimes and gas holdup in paper pulp-water-gas three-phase slurry flow. *Chemical Engineering Science*, 58: 1417-1430.

Xu, H., and Aidun, C.K., 2005. Characteristics of fiber suspension flow in a rectangular channel. *International Journal of Multiphase Flow*, 31: 318-336.

Yamagiwa, K., Kusabiraki, D., and Ohkawa, A., 1990. Gas holdup and gas entrainment rate in downflow bubble column with gas entrainment by a liquid jet operating at high liquid throughput. *Journal of Chemical Engineering of Japan*, 23: 343-348.

Yang, G.Q., Luo, X., Lau, R., and Fan, L.S., 2000. Heat-transfer characteristics in slurry bubble columns at elevated pressures and temperatures. *Industrial & Engineering Chemistry Research*, 39: 2568-2577.

Yokogawa, A., Suzuki, M., and Shimizu, T., 1985. A study on flow characteristics of pulp suspension flow - measurement of turbulence intensity and fiber concentration unevenness. *Bulletin of JSME*, 28: 846-853.

Youn, H.J., and Lee, H.L., 2002. An experimental investigation of the effect of pulp types, mechanical treatments and crill contents on fiber network strength. *Nordic Pulp and Paper Research Journal*, 17: 187-192.

Zahradnik, J., Fialova, M., Ruzicka, M., Drahos, J., Kastanek, F., and Thomas, N.H., 1997. Duality of the gas-liquid flow regimes in bubble column reactors. *Chemical Engineering Science*, 52: 3811-3826.

Zhang, J.-P., Grace, J.R., Epstein, N., and Lim, K.S., 1997. Flow regime identification in gas-liquid flow and three-phase fluidized beds. *Chemical Engineering Science*, 52: 3979-3992.

Zhao, R.H., and Kerekes, R.J., 1993. The effect of suspending liquid viscosity on fiber flocculation. *Tappi Journal*, 76: 183-188.

Zhi, C., and Rorrer, G.L., 1996. Photolithotrophic cultivation of *Laminaria saccharina gametophyte* cells in a bubble-column bioreactor. *Enzyme and Microbial Technology*, 18: 291-299.

Zhong, J.J., Seki, T., Kinoshita, S.I., and Yoshida, T., 1992. Rheological characteristics of cell-suspension and cell-culture of *Perilla-frutescens*. *Biotechnology and Bioengineering*, 40: 1256-1262.

Zlokarnik, M., 1991. *Dimensional Analysis and Scale-up in Chemical Engineering*. Spinger-Verlag, New York, 176 pp.

Zlokarnik, M., 1998. Problems in the application of dimensional analysis and scale-up of mixing operations. *Chemical Engineering Science*, 53: 3023-3030.

Zuber, N., and Findlay, J.A., 1965. Average volumetric concentration in two-phase flow systems. *Journal of Heat Transfer*, 87: 453-468.

Appendix A: ESTIMATING GAS HOLDUP VIA PRESSURE DIFFERENCE MEASUREMENTS IN A COCURRENT BUBBLE COLUMN

Estimating gas holdup via pressure difference measurements is a simple and low-cost noninvasive technique to study gas holdup in bubble columns. It is usually used in a way that the wall shear stress effect is neglected, termed Method II in this appendix. In cocurrent bubble columns, when the liquid velocity is high or the fluid is highly viscous, wall shear friction may be significant, and Method II may result in substantial error. Directly including the wall shear stress term in the determination of gas holdup (Method I) requires knowledge of the two-phase wall shear stress models and usually requires the solution of nonlinear equations.

A new gas holdup estimation method (Method III) via differential pressure measurements for cocurrent bubble columns is outlined in this appendix. This method considers the wall shear stress influences on gas holdup values without calculation of the wall shear stress. A detailed analysis shows that Method III always results in a smaller gas holdup error than Method II, and in many cases, the error is over an order of magnitude smaller. The applicability of Method III in the present study of gas holdup in a cocurrent air-water-fiber bubble column is examined. Analysis based on experimental data shows that with Method III, accurate gas holdup measurements can be obtained, while measurement error is significant when Method II is used for some operating conditions.

More details related to this appendix can be found in Tang and Heindel (2005b).

A.1 Introduction

The method to estimate gas holdup via pressure difference measurements is widely used to study the hydrodynamics in gas-liquid or gas-liquid-solid bubble columns and airlift reactors (Hills, 1976; Merchuk and Stein, 1981; Ueyama *et al.*, 1989; Luo *et al.*, 1997; Zahradnik *et al.*, 1997; Lin *et al.*, 1998; Letzel *et al.*, 1999; Al-Masry, 2001; Su and Heindel, 2003; Su and Heindel, 2004b; Tang and Heindel, 2004b, 2005c). With this method, gas holdup is measured using the time-averaged static pressure drop along the column. The

obtained gas holdup is an average value (both temporal and spatial) over the volume of the dispersion between the corresponding pressure taps.

Manometers were initially installed along multiphase flow columns to measure pressure signals (Hills, 1976; Merchuk and Stein, 1981; Zahradnik *et al.*, 1997; Al-Masry, 2001). Recently, pressure transducers have been used (Ueyama *et al.*, 1989; Luo *et al.*, 1997; Lin *et al.*, 1998; Letzel *et al.*, 1999; Su and Heindel, 2003; Su and Heindel, 2004b; Tang and Heindel, 2004b, 2005c). The pressure transducers are usually flush mounted to the column wall so that the disturbance on the flow caused by the pressure transducers is minimum.

With the price drop of piezoelectric pressure transducers and the development of computer data acquisition technology, this method becomes a simple and low-cost noninvasive gas holdup measurement technique and is applicable to systems at high temperature and pressures (Luo *et al.*, 1997; Lin *et al.*, 1998; Letzel *et al.*, 1999). This technique does not require a transparent fluid or containment vessel. It can be used to measure the overall average gas holdup in a multiphase column, as well as the average gas holdup in a column section. Thus, it can be used to probe the axial gas holdup variation in a column.

When a solid phase is present, the differential pressure gradient method can be used to measure gas holdup if the liquid-solid slurry behaves as a pseudohomogeneous mixture or if the solids concentration as a function of height is known (Kumar *et al.*, 1997).

Assuming one-dimensional isothermal flow, steady-state, constant cross-section, negligible mass transfer between the gas and liquid phases, and constant properties in a cross-section, Merchuk and Stein (1981) used a separated flow model of Wallis (1969) for vertical gas-liquid cocurrent flows to determine gas holdup in gas-liquid bubble columns and air-lift reactors:

$$\varepsilon = (1 + \frac{1}{\rho_l g}\frac{dp}{dz}) + \frac{4\tau_w}{\rho_l D_c g} + \frac{U_l^2}{g}\frac{1}{(1-\varepsilon)^2}\frac{d\varepsilon}{dz} \qquad (A.1)$$

where ε and p are the local gas holdup and pressure at position z, respectively, ρ_l is the liquid density, g is the acceleration due to gravity, D_c is the column inner diameter, U_l is the

superficial liquid velocity, and τ_w is the wall shear stress. Hills (1976) obtained a similar expression assuming a pseudohomogeneous two-phase mixture.

The first term on the right hand side of Eq. (A.1) accounts for the hydrostatic head, the second term describes wall shear effects, and the third term represents fluid acceleration due to void changes. The contribution of the acceleration term is typically ~1% of the total gas holdup (Merchuk and Stein, 1981). Hills (1976) has shown that in the worst case in a study with superficial liquid and gas velocities as high as 2.7 m/s and 3.5 m/s, respectively, the acceleration term amounted to less than 10% of the total gas holdup. As a result, the acceleration term is usually neglected in practice (Hills, 1976; Merchuk and Stein, 1981; Zahradnik *et al.*, 1997; Al-Masry, 2001; Tang and Heindel, 2004b). Without the acceleration term, Eq. (A.1) becomes

$$\varepsilon = (1 + \frac{1}{\rho_l g}\frac{dp}{dz}) + \frac{4\tau_w}{\rho_l D_c g} \tag{A.2}$$

To obtain the average gas holdup $\bar{\varepsilon}$ in a column section between two locations separated by a distance $\Delta z = z_2 - z_1$ (>0), integrate both sides of Eq. (A.2) from z_1 to z_2:

$$\frac{1}{\Delta z}\int_{z_1}^{z_2}\varepsilon dz = \frac{1}{\Delta z}\int_{z_1}^{z_2}(1 + \frac{1}{\rho_l g}\frac{dp}{dz})dz + \frac{1}{\Delta z}\int_{z_1}^{z_2}\frac{4\tau_w}{\rho_l D_c g}dz \tag{A.3}$$

Thus

$$\bar{\varepsilon} = (1 - \frac{1}{\rho_l g}\frac{\Delta p}{\Delta z}) + \frac{4\bar{\tau}_w}{\rho_l D_c g} \tag{A.4}$$

where $\Delta p = p_1 - p_2 (> 0)$ with p_1 and p_2 representing the pressures at location z_1 and z_2, respectively, and $\bar{\tau}_w$ corresponding to the average wall shear stress in the same column section. The gas holdup measurement based on Eq. (A.4) is denoted **Method I** in the following discussion. It totally accounts for the wall shear stress effect and gives accurate gas holdup values based on the assumptions above.

The wall shear term in Eq. (A.4) is usually neglected for semi-batch bubble columns (Ueyama *et al.*, 1989; Zahradnik *et al.*, 1997; Su and Heindel, 2003; Su and Heindel, 2004b). For cocurrent bubble columns and airlift reactors, this term is small at low superficial liquid velocities. When the wall shear term is negligible, Eq. (A.4) can be simplified as

$$\bar{\varepsilon}_{II} = 1 - \frac{1}{\rho_l g}\frac{\Delta p}{\Delta z} \tag{A.5}$$

The gas holdup measurement based on Eq. (A.5) is called **Method II** in the following discussion. This method totally neglects the effect of wall shear stress.

The wall shear term in Eq. (A.4) increases significantly with increasing superficial liquid (U_l) and gas (U_g) velocities and can amount to ~20% of the total gas holdup (Hills, 1976; Merchuk and Stein, 1981). This is because the wall shear stress $\bar{\tau}_w$ increases significantly with U_l and U_g (Wallis, 1969; Liu, 1997; Magaud *et al.*, 2001). When the liquid phase is highly viscous, the wall shear term can be significant even at low superficial liquid velocities (Al-Masry, 2001). Hence, it is necessary to include the wall shear effect in the total gas holdup value for most cases.

To calculate the wall shear term in Eq. (A.4) requires estimation of the two-phase wall shear stress $\bar{\tau}_w$, which is a complex function of gas holdup, superficial gas and liquid velocity, liquid phase rheological properties, and wall roughness. The models for $\bar{\tau}_w$ in gas-liquid two-phase flows are limited and most are not general and can not be extended beyond their restricted conditions (Gharat and Joshi, 1992). The two-phase wall shear stress is even more difficult to estimate when the liquid phase is non-Newtonian (Al-Masry, 2001). Even when a model for $\bar{\tau}_w$ is known, the model is usually a highly nonlinear function of gas holdup (Herringe and Davis, 1978; Merchuk and Stein, 1981; Metkin and Sokolov, 1982; Beyerlein *et al.*, 1985), and one has to solve a nonlinear version of Eq. (A.4) to obtain the gas holdup. This is challenging, especially when a large number of data points are acquired.

In this appendix, a new method (**Method III**) is outlined to estimate the gas holdup in a cocurrent bubble column. This method considers the wall shear stress effect without modeling the two-phase wall shear stress or solving a nonlinear form of Eq. (A.4). The procedure is as simple as Method II but provides more accurate gas holdup values.

A.2 Method III – A New Differential Pressure Gas Holdup Estimation Method

Consider rewriting Eq. (A.5) in the form

$$\bar{\varepsilon}_{III} = 1 - \frac{\Delta p}{\Delta p_{0,U_l}} \tag{A.6}$$

where $\Delta p_{0,U_l}$ is the pressure difference between z_1 and z_2 (the same locations corresponding to Δp) when $U_g = 0$ ($\bar{\varepsilon} = 0$) and U_l is the same superficial liquid velocity at which Δp is measured. Equation (A.6) becomes Eq. (A.5) when $U_l = 0$. The gas holdup measurement based on Eq. (A.6) is called **Method III** in the following discussion.

Substituting $\bar{\varepsilon} = 0$ into Eq. (A.4), we have

$$0 = (1 - \frac{1}{\rho_l g}\frac{\Delta p_{0,U_l}}{\Delta z}) + \frac{4\bar{\tau}_{w0}}{\rho_l D_c g} \tag{A.7}$$

So

$$\Delta p_{0,U_l} = \rho_l g \Delta z + \frac{4\bar{\tau}_{w0}}{D_c}\Delta z \tag{A.8}$$

where $\bar{\tau}_{w0}$ is the wall shear stress for single-phase liquid flow with the same superficial liquid velocity U_l corresponding to Δp.

Substituting Eq. (A.8) into (A.6)

$$\bar{\varepsilon}_{III} = 1 - \frac{1}{\rho_l g}\frac{\Delta p}{\Delta z}\left(\frac{1}{1 + \frac{4\bar{\tau}_{w0}}{\rho_l g D_c}}\right) \tag{A.9}$$

Equation (A.9) reduces to Method II (Eq. (A.5)) as $\frac{4\bar{\tau}_{w0}}{\rho_l g D_c} \to 0$.

The single-phase flow wall shear stress can be estimated by

$$\bar{\tau}_{w0} = \frac{1}{2} C_f \rho_l U_l^2 \tag{A.10}$$

where

$$C_f = \frac{1}{4} f \tag{A.11}$$

For Newtonian fluid flows, the following explicit formula can be used to estimate f (Streeter and Wylie, 1985)

$$f = \frac{1.325}{[\ln(\frac{\Delta}{3.7D_c} + \frac{5.74}{Re^{0.9}})]^2} \tag{A.12}$$

where $\frac{\Delta}{D_c}$ is relative roughness and Re is the liquid flow Reynolds number based on column diameter D_c.

According to Eqs. (A.10) – (A.12), $\frac{4\bar{\tau}_{w0}}{\rho_l g D_c} << 1$ is applicable when D_c is not too small and U_l and $\frac{\Delta}{D_c}$ are not too high. For example, in a 15.24 cm bubble column with water only flowing at U_l = 1 m/s and $\frac{\Delta}{D_c} = 0.01$, $\frac{4\bar{\tau}_{w0}}{\rho_l g D_c} = 0.013$; when D_c = 2.54 cm, for the same conditions $\frac{4\bar{\tau}_{w0}}{\rho_l g D_c} = 0.081$. With the $\bar{\tau}_{w0}$ model provided by Metkin and Sokolov (1982) for non-Newtonian power-law fluids, $\frac{4\bar{\tau}_{w0}}{\rho_l g D_c} << 1$ also holds for most conditions.

When $\frac{4\bar{\tau}_{w0}}{\rho_l g D_c} << 1$, a Taylor expansion can be used to estimate Eq. (A.9), thus

$$\bar{\varepsilon}_{III} \approx 1 - \frac{1}{\rho_l g}\frac{\Delta p}{\Delta z} + \frac{1}{\rho_l g}\frac{\Delta p}{\Delta z}\frac{4\bar{\tau}_{w0}}{\rho_l g D_c} \tag{A.13}$$

Assuming the gas holdup given by Method I is accurate, then the error of Method II is

$$\Delta\bar{\varepsilon}_{II} = \bar{\varepsilon} - \bar{\varepsilon}_{II} = \bar{\varepsilon}_{\tau} = \frac{4\bar{\tau}_w}{\rho_l D_c g} \tag{A.14}$$

where $\bar{\varepsilon}_{\tau}$ represents the contribution of wall shear stress to the total gas holdup. The error of Method III is

$$\Delta\bar{\varepsilon}_{III} = \bar{\varepsilon} - \bar{\varepsilon}_{III} = \frac{4\bar{\tau}_w}{\rho_l D_c g}\left(1 - \frac{1}{\rho_l g}\frac{\Delta p}{\Delta z}\frac{\bar{\tau}_{w0}}{\bar{\tau}_w}\right) \tag{A.15}$$

Combining Eqs. (A.4), (A.14), and (A.15) yields

$$\frac{\Delta\bar{\varepsilon}_{III}}{\Delta\bar{\varepsilon}_{II}} = 1 - \left(1 - \bar{\varepsilon} - \bar{\varepsilon}_\tau\right)\frac{\bar{\tau}_{w0}}{\bar{\tau}_w} \tag{A.16}$$

Since $\frac{\bar{\tau}_w}{\bar{\tau}_{w0}} > 1$ (Herringe and Davis, 1978; Metkin and Sokolov, 1982; Marie, 1987),

$$\frac{\Delta\bar{\varepsilon}_{III}}{\Delta\bar{\varepsilon}_{II}} < 1 \tag{A.17}$$

This shows an improvement of Method III over Method II, since the error of Method III is always smaller than that of Method II.

In air-water cocurrent upward flows, Herringe and Davis (1978) found

$$\frac{\bar{\tau}_w}{\bar{\tau}_{w0}} = 1 + 0.22\bar{\varepsilon} + 0.82\bar{\varepsilon}^2 \tag{A.18}$$

Substituting Eq. (A.18) into Eq. (A.16)

$$\frac{\Delta\bar{\varepsilon}_{III}}{\Delta\bar{\varepsilon}_{II}} \approx 1 - \left(1 - \bar{\varepsilon}\right)\frac{1}{1 + 0.22\bar{\varepsilon} + 0.82\bar{\varepsilon}^2} \tag{A.19}$$

Using a Taylor expansion on Eq. (A.19)

$$\frac{\Delta\bar{\varepsilon}_{III}}{\Delta\bar{\varepsilon}_{II}} \approx 1 - \left(1 - \bar{\varepsilon}\right)\left(1 - 0.22\bar{\varepsilon} - 0.82\bar{\varepsilon}^2\right) \tag{A.20}$$

Thus

$$\frac{\Delta\bar{\varepsilon}_{III}}{\Delta\bar{\varepsilon}_{II}} \approx 1.22\bar{\varepsilon} \tag{A.21}$$

This implies the error of Method III can be an order of magnitude lower than that of Method II.

When the liquid phase is a power-law fluid, i.e.,

$$\mu_l = K\gamma^{n-1} \tag{A.22}$$

where μ_l is the apparent viscosity, K is the fluid consistency index, γ is the shear rate, and n is the power-law index, Metkin and Sokolov (1982) recommended

$$\frac{\bar{\tau}_w}{\bar{\tau}_{w0}} = 1 + 2.4n\left(\frac{U_g}{U_l}\right)^{1/2} Re_n^{-0.0625n} \tag{A.23}$$

where

$$Re_n = \frac{8U_l^{2-n}D^n\rho_l}{K\left(\frac{6n+2}{n}\right)^n} \tag{A.24}$$

then

$$\frac{\Delta\bar{\varepsilon}_{III}}{\Delta\bar{\varepsilon}_{II}} \approx 1 - \frac{1}{1 + 2.4n\left(\frac{U_g}{U_l}\right)^{1/2} Re_n^{-0.0625n}} \tag{A.25}$$

Figure A.1 shows an example of the relationship between $\frac{\Delta\bar{\varepsilon}_{III}}{\Delta\bar{\varepsilon}_{II}}$, $\frac{U_g}{U_l}$, and Re_n. This is obtained for a 1.01% carboxymethyl cellulose solution, whose consistency index is 0.709 (Al-Masry, 2001). The value $\frac{\Delta\bar{\varepsilon}_{III}}{\Delta\bar{\varepsilon}_{II}}$ is always smaller than 1 and decreases with decreasing $\frac{U_g}{U_l}$ and increasing Re_n. When $\frac{U_g}{U_l} \approx 1$, $\Delta\bar{\varepsilon}_{III}$ is ~50-60% of $\Delta\bar{\varepsilon}_{II}$. When $\frac{U_g}{U_l} \approx 0.1$, $\Delta\bar{\varepsilon}$ is ~30% of $\Delta\bar{\varepsilon}_{II}$. The $\frac{\Delta\bar{\varepsilon}_{III}}{\Delta\bar{\varepsilon}_{II}}$ trend with $\frac{U_g}{U_l}$ and Re_n implies Method III is especially good for flows at high superficial liquid velocity and low superficial gas velocity when total gas holdup ($\bar{\varepsilon}$) is low but $\bar{\varepsilon}_\tau$ composes a significant part of $\bar{\varepsilon}$ and omitting $\bar{\varepsilon}_\tau$ results a substantial relative error. With Method III, the error can be reduced considerably.

A.3 Applying Method III to Determine Gas Holdup in a Cocurrent Air-Water-Fiber Bubble Column

In fiber suspension flows without aeration, the pressure drop per unit length ($\frac{\Delta p_\tau}{\Delta z}$) due to wall shear friction is estimated by:

$$\frac{\Delta p_\tau}{\Delta z} = \frac{\Delta p_{0,U_l} - \Delta p_0}{\Delta z} \tag{A.26}$$

where $\Delta p_0 = \rho_l g \Delta z$, i.e., the hydrostatic head of a static fluid column.

The wall shear stress for fiber suspension flows when $U_g = 0$ is calculated by

$$\bar{\tau}_{w0} = \frac{D_c \Delta p_\tau}{4\Delta z} = \frac{D_c (\Delta p_{0,U_l} - \Delta p_0)}{4\Delta z} \tag{A.27}$$

To determine the average gas holdup in an air-water-fiber suspension for fiber mass fractions $C \leq 1.5\%$, assume the Herringe and Davis (1978) model (i.e., Eq. (A.18)) for wall shear stress in two phase flow is applicable. Note that when $C \leq 1.5\%$, the fiber suspension is considered dilute and it behaves like a Newtonian fluid (Seely, 1968). Hence, the average gas holdup is

$$\bar{\varepsilon} = 1 - \frac{\Delta p}{\Delta p_0} + \frac{\Delta p_{0,U_l} - \Delta p_0}{\Delta p_0}\left(1 + 0.22\bar{\varepsilon} + 0.82\bar{\varepsilon}^2\right) \tag{A.28}$$

By measuring Δp_0, $\Delta p_{0,U_l}$, and Δp for different operation conditions, accurate gas holdup values can be obtained by solving Eq. (A.28), where,

$$\Delta\bar{\varepsilon}_{II} = \bar{\varepsilon}_\tau = \frac{\Delta p_{0,U_l} - \Delta p_0}{\Delta p_0}\left(1 + 0.22\bar{\varepsilon} + 0.82\bar{\varepsilon}^2\right) \tag{A.29}$$

The gas holdup obtained by Method II (Eq. (A.5)) can be written as

$$\bar{\varepsilon}_{II} = 1 - \frac{\Delta p}{\Delta p_0} \tag{A.30}$$

Tables A.1 and A.2 compare gas holdup values obtained using Methods I, II, and III and errors associated with Methods II and III at a fixed nominal superficial gas velocity (U_g = 20 cm/s) in air-water and air-water-fiber (C = 1.5%) systems. The pressure readings, i.e., p_l, p_{lu}, and p_{l0} (p_4, p_{4u}, and p_{40}) are measured at the bottom of section 1 (4) of the bubble column. The subscript u indicates the pressure measurement when $U_g = 0$ cm/s while U_l is the same as the superficial liquid velocity corresponding to p_l. The subscript 0 represent the pressure measured when $U_l = 0$ cm/s and $U_g = 0$ cm/s.

In air-water systems (Table A.1), both the errors resulted from Methods II and III are negligible because the superficial liquid velocity is small ($0 \leq U_l \leq 10$ cm/s). However, the error resulted from Method III is almost an order of magnitude lower than that from Method

II. In the air-water-fiber systems at C = 1.5% (Table A.2), the errors resulted from both Methods II and III increase by an order of magnitude and the relative error for Method II increases to ~5% of the total gas holdup. However, the error resulted from Method III is still lower than 1% and is only ~15% of that from Method II.

Table A.3 shows a significant advantage of Method III over Method II. In this table, the variation of gas holdup values ($\bar{\varepsilon}_{II}$ and $\bar{\varepsilon}_{III}$) and their associated errors ($\Delta\bar{\varepsilon}_{II}$ and $\Delta\bar{\varepsilon}_{III}$) from Methods II and III are compared at different superficial gas velocities when U_l = 10 cm/s and C = 1.5%. The gas holdup values obtained with the three methods and the relative errors from Methods II and III are also compared in Figs. A.2 and A.3, respectively. Although the absolute error of Method II ($\Delta\bar{\varepsilon}_{II}$) does not change significantly while that of Method III ($\Delta\bar{\varepsilon}_{III}$) increases by an order of magnitude when U_g increases from 1.96 cm/s to 20.44 cm/s, $\Delta\bar{\varepsilon}_{III}$ is always much smaller than $\Delta\bar{\varepsilon}_{II}$. Furthermore, the relative error of Method III ($\frac{\Delta\varepsilon_{III}}{\bar{\varepsilon}}$) is always lower than 1% and nearly constant in the same superficial gas velocity range, while the relative error of Method II ($\frac{\Delta\varepsilon_{II}}{\bar{\varepsilon}}$) is much higher, ranging from 5.3% at U_g = 20.4 cm/s to 30.7% at U_g = 2.0 cm/s. Hence, wall shear effects are significant at high U_l and low U_g, and if they are not properly accounted for in Method II, they can produce a significant error in gas holdup measurements.

Since results at C =1.5% (Tables A.2 and A.3) show that Method III results in a negligible error in gas holdup measurements when $0 \leq U_l \leq 10$ cm/s and $0 \leq U_g \leq 20$ cm/s, the error of Method III is also negligible at C < 1.5% since the shear friction at C < 1.5% will be lower than that at C = 1.5% in the same superficial liquid velocity range (Forgacs *et al.*, 1958).

A.4 Summary

A new gas holdup estimation method (Method III) via differential pressure measurements for cocurrent bubble columns was proposed. This method considers the wall shear stress influences on gas holdup values by modifying Eq. (A.5) into Eq. (A.6). A

detailed analysis revealed that Method III always results in a smaller gas holdup error than Method II. In many cases, the error is much smaller than that of Method II. Hence, more accurate gas holdup measurements in cocurrent bubble columns can be made with only pressure measurements, and the calculation is as simple as that required by Method II. Furthermore, no knowledge of wall shear stress is required for Method III, which is not the case for Method I. The applicability of Method III in the present study on gas holdup in a cocurrent air-water-fiber bubble column was examined. Analysis based on experimental data showed that with Method III, accurate gas holdup can be obtained, while error may be significant for selected operational conditions with Method II.

Table A.1: Comparison between Methods I, II, and III at selected operating conditions in a cocurrent air-water bubble column (C = 0%) when nominal superficial gas velocity is 20 cm/s (p_{10} = 40.42 kPa, p_{40} = 11.33 kPa).

U_g (cm/s)	U_l (cm/s)	p_1 (kPa)	p_4 (kPa)	p_{1u} (kPa)	p_{4u} (kPa)	$\bar{\varepsilon}$ (Eq. (A.4))	$\bar{\varepsilon}_{II}$ (Eq. (A.5))	$\bar{\varepsilon}_{III}$ (Eq. (A.6))	$\Delta\bar{\varepsilon}_{II}$ *	$\Delta\bar{\varepsilon}_{III}$ *	$\frac{\Delta\bar{\varepsilon}_{II}}{\bar{\varepsilon}}$ *	$\frac{\Delta\bar{\varepsilon}_{III}}{\bar{\varepsilon}}$ *	$\frac{\Delta\bar{\varepsilon}_{III}}{\Delta\bar{\varepsilon}_{II}}$ *
20.9	0.1	29.90	7.50	40.42	11.33	0.230	0.230	0.230	0	0	0	0	NA
20.5	2.1	30.83	8.10	40.49	11.40	0.219	0.219	0.219	1.72E-04	3.79E-05	0.08%	0.02%	22.03%
20.5	4.0	31.14	8.29	40.51	11.41	0.215	0.214	0.215	4.13E-04	8.93E-05	0.19%	0.04%	21.60%
20.8	6.0	31.33	8.42	40.51	11.41	0.213	0.212	0.212	4.48E-04	9.57E-05	0.21%	0.05%	21.38%
21.3	8.2	31.58	8.54	40.53	11.43	0.209	0.208	0.208	5.51E-04	1.16E-04	0.26%	0.06%	20.96%
20.8	10.0	31.91	8.69	40.48	11.38	0.203	0.202	0.202	6.20E-04	1.26E-04	0.31%	0.06%	20.36%

* Calculated using unrounded $\bar{\varepsilon}$, $\bar{\varepsilon}_{II}$, and $\bar{\varepsilon}_{III}$ values.

Table A.2: Comparison between Methods I, II, and III at selected operating conditions in an air-water-fiber bubble column when C = 1.5% and nominal superficial gas velocity is 20 cm/s (p_{10} = 40.56 kPa, p_{40} = 11.38 kPa).

U_g (cm/s)	U_l (cm/s)	p_1 (kPa)	p_4 (kPa)	p_{1u} (kPa)	p_{4u} (kPa)	$\bar{\varepsilon}$ (Eq. (A.4))	$\bar{\varepsilon}_{II}$ (Eq. (A.5))	$\bar{\varepsilon}_{III}$ (Eq. (A.6))	$\Delta\bar{\varepsilon}_{II}$ *	$\Delta\bar{\varepsilon}_{III}$ *	$\frac{\Delta\bar{\varepsilon}_{II}}{\bar{\varepsilon}}$ *	$\frac{\Delta\bar{\varepsilon}_{III}}{\bar{\varepsilon}}$ *	$\frac{\Delta\bar{\varepsilon}_{III}}{\Delta\bar{\varepsilon}_{II}}$ *
18.2	0.1	32.91	8.22	40.56	11.38	0.154	0.154	0.154	0	0	0	0	NA
20.8	2.0	32.96	8.54	40.75	11.49	0.166	0.163	0.166	2.70E-03	4.49E-04	1.63%	0.27%	16.61%
20.3	3.9	33.42	8.80	40.84	11.54	0.161	0.156	0.160	4.27E-03	6.85E-04	2.66%	0.43%	16.05%
20.5	6.0	33.65	8.93	40.95	11.58	0.160	0.153	0.159	6.63E-03	1.06E-03	4.15%	0.66%	15.91%
20.2	8.0	34.00	9.12	40.92	11.52	0.155	0.148	0.154	7.58E-03	1.17E-03	4.89%	0.75%	15.44%
20.4	10.1	34.11	9.21	40.97	11.55	0.155	0.147	0.154	8.18E-03	1.26E-03	5.28%	0.81%	15.42%

* Calculated using unrounded $\bar{\varepsilon}$, $\bar{\varepsilon}_{II}$, and $\bar{\varepsilon}_{III}$ values.

Table A.3: Comparison between Methods I, II, and III at selected operating conditions in an air-water-fiber bubble column when C = 1.5% and nominal superficial liquid velocity is 10 cm/s (p_{1u} = 40.97 kPa, p_{4u} = 11.55 kPa; p_{10} = 40.56 kPa, p_{40} = 11.38 kPa).

U_g (cm/s)	U_l (cm/s)	p_1 (kPa)	p_4 (kPa)	$\bar{\varepsilon}$ (Eq. (A.4))	$\bar{\varepsilon}_{II}$ (Eq. (A.5))	$\bar{\varepsilon}_{III}$ (Eq. (A.6))	$\Delta\bar{\varepsilon}_{II}$ *	$\Delta\bar{\varepsilon}_{III}$ *	$\frac{\Delta\bar{\varepsilon}_{II}}{\bar{\varepsilon}}$ *	$\frac{\Delta\bar{\varepsilon}_{III}}{\bar{\varepsilon}}$ *	$\frac{\Delta\bar{\varepsilon}_{III}}{\Delta\bar{\varepsilon}_{II}}$ *
2.0	10.0	39.78	11.14	0.027	0.019	0.026	8.18E-03	2.16E-04	30.68%	0.81%	2.64%
3.1	10.0	39.26	10.96	0.038	0.030	0.038	8.18E-03	3.11E-04	21.34%	0.81%	3.80%
6.1	10.0	38.19	10.57	0.062	0.053	0.061	8.18E-03	5.00E-04	13.27%	0.81%	6.11%
7.9	10.0	37.56	10.37	0.076	0.068	0.076	8.18E-03	6.20E-04	10.71%	0.81%	7.58%
10.4	10.0	36.81	10.10	0.093	0.085	0.092	8.18E-03	7.54E-04	8.81%	0.81%	9.22%
12.0	10.0	36.35	9.95	0.104	0.095	0.103	8.18E-03	8.41E-04	7.90%	0.81%	10.29%
13.8	10.0	35.85	9.79	0.115	0.107	0.114	8.15E-03	9.33E-04	7.07%	0.81%	11.45%
15.9	10.1	35.22	9.58	0.130	0.121	0.129	8.15E-03	1.05E-03	6.29%	0.81%	12.88%
18.1	10.1	34.69	9.45	0.143	0.135	0.142	8.15E-03	1.16E-03	5.69%	0.81%	14.26%
20.4	10.1	34.11	9.21	0.155	0.147	0.154	8.15E-03	1.26E-03	5.26%	0.81%	15.42%

* Calculated using unrounded $\bar{\varepsilon}$, $\bar{\varepsilon}_{II}$, and $\bar{\varepsilon}_{III}$ values.

Figure A.1: Variation of $\Delta\bar{\varepsilon}_{III}/\Delta\bar{\varepsilon}_{II}$ with Ren and U_g/U_l for power-law fluids (n = 0.709).

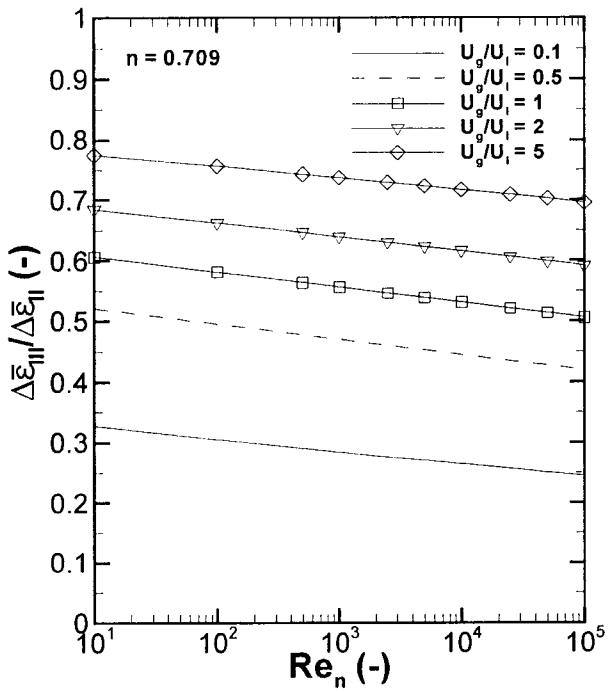

Figure A.2: Comparison between gas holdup values from Methods I, II, and III at $0 < U_g < 20$ cm/s when $U_l = 10$ cm/s and C = 1.5%.

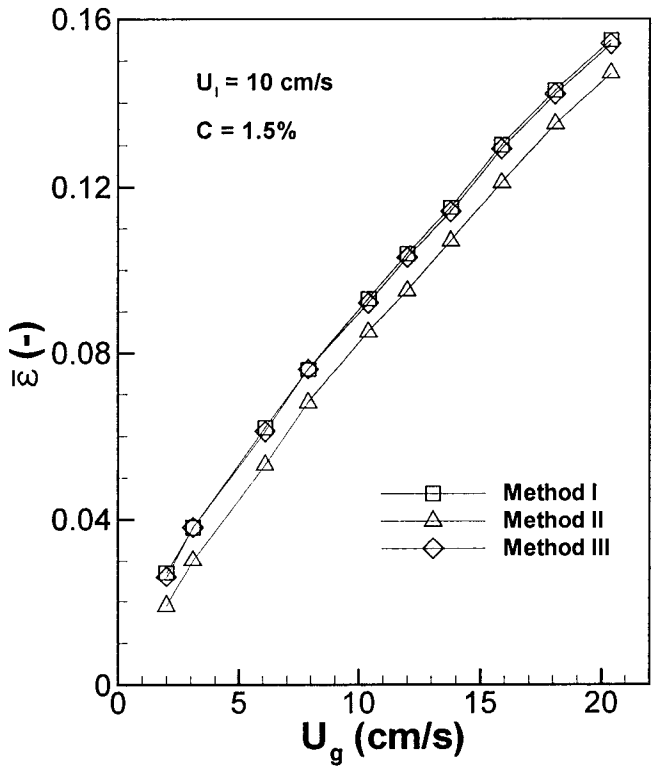

Figure A.3: Comparison between relative gas holdup error from Methods II and III at $0 < U_g < 20$ cm/s when $U_l = 10$ cm/s and $C = 1.5\%$.

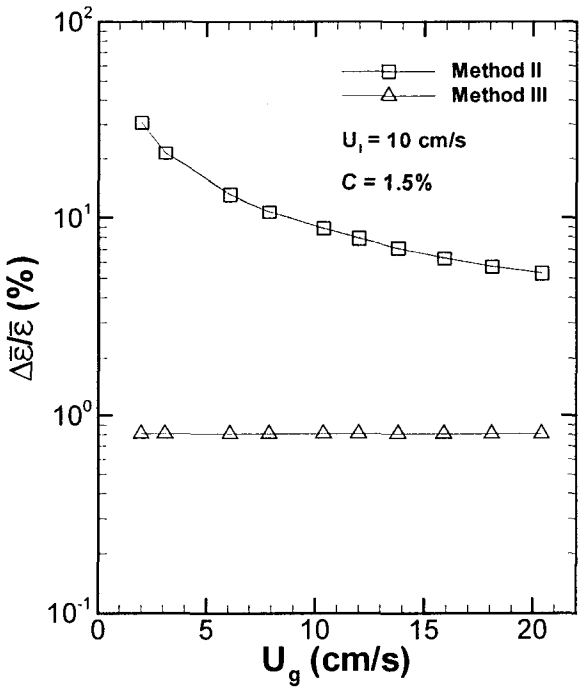

Appendix B: DIMENSIONAL ANALYSIS OF GAS HOLDUP IN COCURRENT GAS-LIQUID-FIBER BUBBLE COLUMNS

B.1 Introduction

Dimensional analysis is widely used to study the relationship between the parameters that influence a physical process. This is because it has two advantages (Zlokarnik, 1998): (1) dimensional analysis can quickly and reliably result in a group of dimensionless numbers, which usually reduce the number of parameters needed to represent the experimental results; and (2) dimensional analysis can ensure a reliable scale-up of the experimental results. A dimensional analysis usually involves two steps (Zlokarnik, 1998): (1) construct a complete list of relevant parameters which affect the process; and (2) determine the necessary dimensionless numbers to characterize the process.

Two approaches are usually used to obtain the dimensionless numbers. The first method is to non-dimensionalize the differential equations describing the process. This method may not be able to give a system of dimensionless numbers adequate to reveal the similarity laws of a complex process because: (1) differential equations may not be available that adequately describe the process; or (2) only simplified equations are available that describe special or idealized process conditions and they omit key parameters. The second method is to use the Buckingham Pi Theorem (Buckingham, 1914). This method is widely used because no models are required before the dimensional analysis.

For a complex system like the cocurrent gas-liquid-fiber bubble column studied in this investigation, there is currently no model describing the relationship between the gas holdup and all the influential factors. Thus, the Buckingham Pi Theorem (Buckingham, 1914) will be used in the current dimensional analysis.

B.2 Relevant Parameters

In this analysis, gas holdup ε is the target parameter. The gas holdup in a cocurrent gas-liquid-fiber bubble column is affected by many physical quantities, including: (1) the

geometry of the bubble column and the gas distributor, (2) the physical properties of the gas, liquid, and solid phases, and (3) the process-related parameters. In the following, the three aspects of relevant parameters we will be discussed.

B.2.1 Geometric parameters

It is extensively reported that the bubble column diameter (D) and height (H) have a significant influence on gas holdup in a bubble column (Shah *et al.*, 1982; Delnoij *et al.*, 1997; Krishna *et al.*, 1997; Thorat *et al.*, 1998; Krishna *et al.*, 1999b; Ranade and Tayalia, 2001; Ruzicka *et al.*, 2001a). There are also many investigations showing that the design of the gas distributor, through which the gas enters the bubble column, can dramatically affect the flow regime transition and gas holdup in a bubble column (Miyahara *et al.*, 1983; Tsuchiya and Nakanishi, 1992; Kawasaki and Tanaka, 1995; Zahradnik *et al.*, 1997; Thorat *et al.*, 1998; Camarasa *et al.*, 1999; Lee *et al.*, 2001; Ranade and Tayalia, 2001). A gas distributor is usually designed as a plate or sparger with many small gas-passing orifices of the same size (d_o). In this analysis, we assume that the orifices are uniformly distributed on the gas distributor. Thus, the distributor can be characterized by two parameters, i.e., the open area ratio (R_A), which is defined as the ratio of the total area of all the orifices to the cross-section of the bubble column, and the orifice diameter (d_o).

B.2.2 Physical properties

Gas holdup in a bubble column is found to be influenced by the physical properties of each phase involved in the multiphase flow. These influential physical properties can be divided into three classes according to the respective phase.

B.2.2.1 Gas phase properties

Gas density (ρ_g) and viscosity (ν_g) can significantly affect the gas holdup in a bubble column. It is reported that gas holdup increased with increasing gas density (Bhaga *et al.*, 1971; Koetsier *et al.*, 1976; Larachi *et al.*, 1994; Reilly *et al.*, 1994). It was also reported that

increasing gas density delays regime transition (Krishna *et al.*, 1991; Reilly *et al.*, 1994; Krishna *et al.*, 1999a). Hikita *et al.* (1980) showed that the effect of gas density and viscosity could be significant.

No direct conclusion has been found on the effect of gas solubility on gas holdup in bubble columns. However, Behkish (2004) studied the solubility of 5 gases (CH_4, CO, N_2, H_2, and He) in a bubble column with the liquid phase being an organic liquid (Isopar-M) and found that their solubility has the relationship: $CH_4 > CO > N_2 > H_2 >$ He. In the same study, Behkish (2004) found that the gas holdup values at the same operational conditions using different gases followed the trend: $N_2 \approx CO > CH_4 >$ He $\approx H_2$. He further pointed out that the gas holdup trend with gases is related to the gas molecular weight. Thus, according to the data reported in Behkish (2004), the influence of gas solubility on gas holdup is insignificant.

Hence, in the current dimensional analysis, two gas phase physical properties are considered: density (ρ_g) and viscosity (ν_g). The gas phase properties usually change with temperature and pressure. When applying the dimensional analysis results, the gas properties should have their values corresponding to the operating temperature and pressure.

B.2.2.2 Liquid phase properties

In a gas-liquid-solid bubble column, the solid particles and gas bubbles are suspended by a continuous liquid phase. The liquid density affects the buoyancy force acting on the particles and bubbles, and the liquid viscosity affects the drag force, both of which affect the particle and bubble motion and the resulting gas holdup. The effect of liquid viscosity on gas holdup has been extensive reported (Kelkar *et al.*, 1984; Bejar *et al.*, 1992). The liquid surface tension has significant effects on the gas holdup in a bubble column because the bubble formation, coalescence, and breakup depend on the liquid surface tension. There are extensive studies on this issue (Kelkar *et al.*, 1983; Gorowara and Fan, 1990; Zahradnik *et al.*, 1997; Janse *et al.*, 1999; Kluytmans *et al.*, 2001; Akosman *et al.*, 2004; Tang and Heindel, 2004b). All these liquid phase properties are functions of the operating temperature. Some may changes significantly with the operating pressure.

In the current analysis, we assume the liquid is a Newtonian fluid. Thus, the liquid properties included in the analysis are density (ρ_l), viscosity (ν_l), and surface tension (σ). They should be determined at the operating pressure and temperature.

B.2.2.3 Fiber physical properties

Solid phase properties can affect the hydrodynamics in a gas-liquid-solid bubble column. The axial solid concentration distribution in a 3-phase bubble column depends on the solid density and size (Tang and Fan, 1989). Bly and Worden (1992) also reported that bubble rise velocities decrease with increasing solids fraction and density. Jamialahmadi and Mullersteinhagen (1991) reported solid particle size, density, and wettability have a significantly effect on gas holdup. Wettability of carbon particles (Kluytmans *et al.*, 2001) and Nylon fibers (Su and Heindel, 2004b) on gas holdup in bubble columns were also reported.

In a gas-liquid-fiber bubble column, fibers comprise the solid phase. Fibers are different from spherical particles because they have a large length to width ratio. Fibers can move in translation and rotation. As it rotates, a fiber can sweep out a much larger volume, exceeding its own volume by a factor of r^2, where r is the fiber aspect ratio. This results in many more collisions between fibers when they are present in the same flow field. In a shear field, a fiber may have a different rotation orbit depending on its stiffness (Mason, 1954). When fibers are crowded, entanglement (or flocculation) occurs and fiber flocs (aggregation of fibers) form. Fiber flocculation is a complex function of fiber length (l_f), aspect ratio (r), stiffness (EI), surface friction coefficient (μ_f), and flow conditions (Forgacs *et al.*, 1958; Kerekes, 1983; Kerekes *et al.*, 1985; Kerekes and Schell, 1995). Wikstrom and Rasmuson (1998) also reported that the fiber length distribution had a significant effect on fiber network strength. When the fiber mass fraction of a liquid-fiber suspension is high enough, continuous fiber networks form. The presence of fiber flocs or networks can significantly modify the hydrodynamics and gas holdup in the bubble column (Pelton and Piette, 1992; Walmsley, 1992; Lindsay *et al.*, 1995; Reese and Fan, 1997; Heindel and Monefeldt, 1998; Ajersch and Pelton, 1999a; Heindel, 2000; Schulz and Heindel, 2000; Heindel, 2002; Xie *et*

al., 2003b). Furthermore, cellulose fibers have internal voids called lumens (Forest Products Laboratory, 1999), which can absorb a large amount of liquid and significantly modify the effective density of fibers in liquids. However, this is not the case for synthetic fibers, which do not have internal voids.

In the current analysis, the fiber is modeled as a hollow cylinder, with a length-weighted average length (l_f), an inner diameter (d_{fi}), and an outer diameter (d_{fo}). For a synthetic fiber, $d_{fi} = 0$. To account for the effect of fiber length distribution, a fiber length standard deviation (S_f) is also considered. Notice $S_f = 0$ if a fiber has a uniform length distribution. Thus, the fiber physical properties to be considered include length-weighted average fiber length (l_f), fiber length standard deviation (S_f), coarseness (ω), inner diameter (d_{fi}), outer diameter (d_{fo}), stiffness (EI), surface friction coefficient (μ_f), and liquid-fiber interfacial contact angle (θ_f).

Assuming a fiber lumen is filled with the liquid phase after it is suspended in a liquid and neglecting the fiber wall swell, the effective fiber density can be obtained:

$$\rho_{f,eff} = \rho_l \left(\frac{d_{fi}}{d_{fo}} \right)^2 + \frac{4\omega}{\pi d_{fo}^2} \tag{B.1}$$

Since the water held in the fiber internal voids moves with the fiber as an entity, it is better to use the effective fiber density ($\rho_{f,eff}$) as the solid phase density than the fiber wall material density (ρ_f), which is also related to fiber coarseness (ω):

$$\rho_f = \frac{4\omega}{\pi(d_{fo}^2 - d_{fi}^2)} \tag{B.2}$$

Because all the parameters in Eq. (B.1) other than ω are included in the relevant parameter list for the dimensional analysis, ω is excluded out of the relevant parameter list.

Also note that the fiber number per unit mass (n_f) can be obtained once the length-weighted average length (l_f), fiber length standard deviation (S_f), and fiber coarseness (ω) are given:

$$n_f = \frac{2}{\omega\left(l_f - \sqrt{l_f^2 - 4S_f^2}\right)} \tag{B.3}$$

Thus, the fiber number per unit mass will not be included in the dimensional analysis.

B.2.3 Process parameters

Gas and liquid throughput rates, pressure, temperature, and fiber concentration are important process conditions and affect the gas holdup significantly. In this analysis, we only consider the gas holdup in a gas-liquid-fiber bubble column under atmospheric pressure and ambient (room) temperature and neglect the effects of pressure and temperature. The superficial gas velocity (U_g), superficial liquid velocity (U_l), and fiber volumetric concentration (C_v) are chosen as process variables. Because a bubble column is a heterogeneous material system with differences in phase densities, we should also include the gravity difference between gas and liquid phases, $g(\rho_l - \rho_g)$, and the gravity difference between liquid and solid phases, $g(\rho_{f,eff} - \rho_g)$, as the process parameters (Zlokarnik, 1991).

Notice the fiber volumetric concentration (C_v) is correlated with fiber mass fraction C by Eq. (1.11). The fiber volumetric concentration is used in the present analysis because it is more frequently used in fiber suspension rheology studies (Bennington *et al.*, 1990; Bennington *et al.*, 1995; Wikstrom and Rasmuson, 1998).

B.2.4 Complete relevant parameter list

In summary, the complete list of relevant parameters for this simplified analysis includes 23 parameters, including the target parameter, ε:

$$\{\varepsilon;\ D,\ H,\ R_A,\ d_o,\ \rho_g,\ \nu_g,\ \rho_l,\ \nu_l,\ \sigma,\ \rho_{f,eff},\ l_f,\ S_f,\ d_{fi},\ d_{fo},\ EI,\ \mu_f,\ \theta_f,\ U_g,\ U_l,\ C_v,\ g(\rho_l - \rho_g),\ g(\rho_{f,eff} - \rho_g)\}. \quad \text{(B.4)}$$

B.3 Dimensional Analysis with the Buckingham Pi Theorem

There are already 5 dimensionless parameters in the list, i.e.

$$\{\varepsilon,\ R_A,\ \theta_f,\ C_v,\ \mu_f\} \quad \text{(B.5)}$$

We can exclude these dimensionless parameters from the dimensional analysis.

It is also found that the parameters in each of the following five sets have a same dimension:

(1) D, H, d_o, l_f, S_f, d_{fi}, and d_{fo};

(2) ρ_g, ρ_l, and $\rho_{f,eff}$;

(3) ν_g and ν_l;

(4) U_g and U_l; and

(5) $g(\rho_l - \rho_g)$ and $g(\rho_{f,eff} - \rho_g)$.

We can immediately obtain a list of 11 dimensionless parameters representing the ratios between the parameters having the same dimensions, i.e.,

$$\{\frac{H}{D}, \frac{d_o}{D}, \frac{l_f}{D}, \frac{l_f}{d_{fo}}, \frac{S_f}{l_f}, \frac{d_{fi}}{d_{fo}}, \frac{\rho_g}{\rho_l}, \frac{\rho_{f,eff}}{\rho_l}, \frac{\nu_g}{\nu_l}, \frac{U_g}{U_l}, \frac{\rho_{f,eff}-\rho_l}{\rho_l-\rho_g}\} \tag{B.6}$$

and leave only one parameter of each set for the dimensional analysis. As a result, we have a final relevant parameter list:

$$\{D, \rho_l, \nu_l, EI, \sigma, U_l, g(\rho_l - \rho_g)\} \tag{B.7}$$

The dimension of each relevant parameter is listed in Table B.1.

Table B.1: Dimensions of relevant parameters.

Parameter	Dimensions
D	L
ρ_l	ML^{-3}
ν_l	L^2T^{-1}
EI	ML^3T^{-2}
σ	MT^{-2}
U_l	LT^{-1}
$g(\rho_l - \rho_g)$	$ML^{-2}T^{-2}$

There are only 3 basic dimensions (L, M, and T) contained in all the 7 parameters in Table B.1. Thus, according to the Buckingham PI Theorem, the 7 parameters in Table B.1 can be reduced to 4 dimensionless parameters.

In the following, a dimensional analysis is applied to the parameters in Table 1 using the Buckingham PI Theorem.

Let

$$\Pi = D^{\alpha}\rho_l^{\beta}\nu_l^{\gamma}(EI)^{\delta}\sigma^{\tau}U_l^{\phi}[g(\rho_l - \rho_g)]^{\varphi} \tag{B.8}$$

In terms of the three basic dimensions (M, L, T), to make Π dimensionless, we have

$$\Pi = [L]^{\alpha}[ML^{-3}]^{\beta}[L^2T^{-1}]^{\gamma}[ML^3T^{-2}]^{\delta}[MT^{-2}]^{\tau}[LT^{-1}]^{\phi}[ML^{-2}T^{-2}]^{\varphi} = 1 \quad \text{(B.9)}$$

Thus, the following linear equations can be obtained:

$$\text{For M: } \beta + \delta + \tau + \varphi = 0 \quad \text{(B.10)}$$

$$\text{For L: } \alpha - 3\beta + 2\gamma + 3\delta + \phi - 2\varphi = 0 \quad \text{(B.11)}$$

$$\text{For T: } -\gamma - 2\delta - 2\tau - \phi - 2\varphi = 0 \quad \text{(B.12)}$$

Solving for α, β, and γ from Eqs. (B.10) – (B.12), assuming δ, τ, ϕ, and φ are known:

$$\alpha = -2\delta + \tau + \phi + 3\varphi \quad \text{(B.13)}$$

$$\beta = -\delta - \tau - \varphi \quad \text{(B.14)}$$

$$\gamma = -2\delta - 2\tau - \phi - 2\varphi \quad \text{(B.15)}$$

Substituting α, β, and γ into Eq. (B.8) to yield:

$$\Pi = \left(\frac{EI}{D^2\rho_l\upsilon_l^2}\right)^{\delta}\left(\frac{\sigma D}{\rho_l\upsilon_l^2}\right)^{\tau}\left(\frac{U_l D}{\upsilon_l}\right)^{\phi}\left(\frac{g(\rho_l - \rho_g)D^3}{\rho_l\upsilon_l^2}\right)^{\varphi} \quad \text{(B.16)}$$

Thus, 4 dimensionless parameters result:

$$\Pi_1 = \frac{EI}{D^2\rho_l\upsilon_l^2},\ \Pi_2 = \frac{\sigma D}{\rho_l\upsilon_l^2},\ \Pi_3 = \frac{U_l D}{\upsilon_l},\ \Pi_4 = \frac{g(\rho_l - \rho_g)D^3}{\rho_l\upsilon_l^2} \quad \text{(B.17)}$$

The dimensionless parameters in Eq. (B.17), together with those included in Eqs. (B.5) and (B.6), reveal 20 dimensionless parameters for the present dimensional analysis:

$$\{\varepsilon;\ R_A,\ \theta_f,\ C_v,\ \mu_f,\ \frac{H}{D},\ \frac{d_o}{D},\ \frac{l_f}{D},\ \frac{l_f}{d_{fo}},\ \frac{S_f}{l_f},\ \frac{d_{fi}}{d_{fo}},\ \frac{\rho_g}{\rho_l},\ \frac{\rho_{f,eff}}{\rho_l},\ \frac{\upsilon_g}{\upsilon_l},\ \frac{U_g}{U_l},\ \frac{\rho_{f,eff} - \rho_l}{\rho_l - \rho_g},$$

$$\Pi_1,\ \Pi_2, \Pi_3, \Pi_4\}. \quad \text{(B.18)}$$

The number of the resultant dimensionless parameters agrees with the Buckingham Pi Theorem, since the complete relevant list (Eq. (B.4)) consists of 23 parameters and only three basic dimensions (L, M, and T) are contained in all 23 parameters.

B.4 Resultant Dimensionless Parameters

The resulting dimensionless parameters (Eq. (B.18)) in the proceeding section are just one possible outcome of the dimensional analysis. Pi terms can be combined to form alternative dimensionless parameters which provide more specific physical implications (Zlokarnik, 1991; Munson *et al.*, 2002). Thus, in this section, some of the dimensionless parameters are combined with others to generate alternative parameters that provide physical significance for describing the hydrodynamics in the cocurrent gas-liquid-fiber bubble column. Physical explanations for important dimensionless parameters are also presented.

B.4.1 Reynolds number - Re

Among the dimensionless parameters in Eq. (B.18),

$$\Pi_3 = \frac{U_l D}{\nu_l} = Re_l \tag{B.19}$$

is the liquid flow Reynolds number, which represents the ratio of inertial and viscous forces. Note the characteristic velocity is the superficial liquid velocity and not the true liquid velocity.

B.4.2 Froude number - Fr*

The dimensionless parameter Π_4 is the Archimedes number.

$$\Pi_4 = \frac{g(\rho_l - \rho_g)D^3}{\rho_l \nu_l^2} = Ar \tag{B.20}$$

It represents the ratio of buoyant to viscous forces. Zlokarnik (1991) suggested that a dimensionless number including both U_l and $g(\rho_l - \rho_g)$ is necessary for bubble column scale-up. Thus, an alternative dimensionless parameter resulting from a combination of Π_3 and Π_4 is chosen

$$\Pi_3^2\Pi_4^{-1} = \left(\frac{U_l D}{\nu_l}\right)^2 \frac{\rho_l \nu_l^2}{g(\rho_l - \rho_g)D^3}$$
$$= \frac{\rho_l U_l^2}{g(\rho_l - \rho_g)D} \qquad (B.21)$$
$$= Fr^*$$

This is the Froude number, which is the ratio of inertial to buoyant forces.

B.4.3 Weber number - We

The dimensionless parameter Π_2 in Eq. (B.18) can be written as

$$\Pi_2 = \frac{\sigma D}{\rho_l \nu_l^2} = \frac{\rho_l \sigma D}{\mu_l^2} = \frac{1}{Oh^2} \qquad (B.22)$$

where $Oh = \mu_l / \sqrt{\rho_l \sigma D}$ is the Ohnesorge number, which represents the ratio of viscous force to the square root of the product of intertial force and surface tension force and is usually used in study of fluid atomization (Catchpole and Fulford, 1966). It is not used in characterization of bubble column hydrodynamics. Consider a combination of Π_3 and Π_2

$$\Pi_2^{-1}\Pi_3^2 = \left(\frac{\sigma D}{\rho_l \nu_l^2}\right)^{-1}\left(\frac{U_l^2 D^2}{\nu_l^2}\right) = \frac{\rho_l U_l^2 D}{\sigma} = We, \qquad (B.23)$$

to produce the Weber number. This dimension number is proportional to the ratio of inertial to surface tension forces and is widely used to characterize bubble/droplet dynamics in multiphase flows.

B.4.4 Fiber network confinement force to buoyancy force ratio - Π_1'

The physical implication of the dimensionless number Π_1 is not quite clear. It is expected that the presence of fiber has a significant effect on bubble column hydrodynamics, and this effect can be revealed with a dimensionless number. Consider combining Π_1 and Π_4

$$\Pi_1\Pi_4^{-1} = \frac{EI}{D^2\rho_l v_l^2}\frac{\rho_l v_l^2}{g(\rho_l-\rho_g)D^3} = \frac{EI}{g(\rho_l-\rho_g)D^5} \tag{B.24}$$

From Wikstrom and Rasmuson (1998), the yield stress in a fiber network is proportional to

$$\tau_y \propto E\left(\frac{l_f}{d_{fo}}\right)^2\left[1-\left(\frac{d_{fi}}{d_{fo}}\right)^4\right]C_v^3 \propto (EI)\cdot C_v^3\cdot\left(\frac{l_f}{d_{fo}}\right)^2\cdot d_{fo}^{-4} \tag{B.25}$$

where the moment of inertial of a fiber (I) is

$$I = \frac{\pi}{64}d_{fo}^4\left[1-\left(\frac{d_{fi}}{d_{fo}}\right)^4\right] \tag{B.26}$$

Combining Eq. (B.24) with other dimensionless parameters, such as C_v, $\frac{l_f}{D}$, and $\frac{l_f}{d_{fo}}$ to yield

$$\begin{aligned}\Pi_1' &= \left(\Pi_1\Pi_4^{-1}\right)\left(\frac{l_f}{d_{fo}}\right)^2 C_v^3\cdot\left(\frac{l_f}{D}\right)^{-4}\left(\frac{l_f}{d_{fo}}\right)^4 \\ &= \left[(EI)\cdot C_v^3\cdot\left(\frac{l_f}{d_{fo}}\right)^2\cdot d_{fo}^{-4}\right]\cdot\frac{1}{g(\rho_l-\rho_g)D}\end{aligned} \tag{B.27}$$

Thus, a new dimensionless parameter is obtained

$$\Pi_1' = \frac{EI}{g(\rho_l-\rho_g)D^5}C_v^3\left(\frac{l_f}{d_{fo}}\right)^2\left(\frac{d_{fo}}{D}\right)^{-4} \propto \frac{\tau_y}{g(\rho_l-\rho_g)D} \tag{B.28}$$

This dimensionless parameter is proportional to the ratio of the fiber network strength (i.e., yield stress) to the bubble buoyancy force. A critical value of Π_1', termed $\Pi_{1,cr}'$, indicates the balance between the fiber network confinement force and bubble buoyant force. A value larger than $\Pi_{1,cr}'$ means the fiber network strength is stronger than the bubble buoyancy force and the bubble will be confined under or within the fiber network. This dimensionless number must be considered when fiber flocculation is significant.

B.4.5 Crowding factor - N_c

Although the fiber volumetric concentration (C_v) is dimensionless and is related to fiber flocculation in a fiber suspension, C_v can not sufficiently characterize the flocculation trend in the fiber suspension because fiber flocculation is also significantly affected by fiber aspect ratio. Kerekes and Schell (1992; 1995) argued that a dimensionless parameter called the crowding factor (N_c) can be used to characterize the flocculation in a fiber suspension. This dimensionless parameter is obtained by combining the fiber volumetric concentration (C_v) and the fiber aspect ratio ($\frac{l_f}{d_{fo}}$):

$$N_c = \frac{2}{3} C_v \left(\frac{l_f}{d_{fo}} \right)^2 \tag{B.29}$$

The crowding factor characterizes the number of fibers in a spherical volume with a diameter equal to the fiber length.

Other dimensionless parameters in Eq. (B.18) remain the same. So the resultant dimensionless parameters are:

$$\{\varepsilon;\ R_A,\ \theta_f,\ N_c,\ \mu_f,\ \frac{H}{D},\ \frac{d_o}{D},\ \frac{l_f}{D},\ \frac{l_f}{d_{fo}},\ \frac{S_f}{l_f},\ \frac{d_{fi}}{d_{fo}},\ \frac{\rho_g}{\rho_l},\ \frac{\rho_{f,eff}}{\rho_l},\ \frac{\nu_g}{\nu_l},\ \frac{U_g}{U_l},$$

$$\frac{\rho_{f,eff} - \rho_l}{\rho_l - \rho_g},\ \mathrm{Re},\ \mathrm{We},\ \mathrm{Fr}^*,\ \Pi_1' \}. \tag{B.30}$$

All the resultant dimensionless parameters and their physical meanings are list in Table B.2.

B.5 Discussion on the Applicable Dimensionless Parameters in the Present Study

In the present study, gas holdup at different superficial gas and liquid velocities, fiber mass fractions, and fiber types are studied. The geometry parameters (D, H, R_A, and d_o), gas (air) and liquid (water) physical properties (ρ_g, ν_g, ρ_l, ν_l, and σ) are approximately constant. The effective fiber density ($\rho_{f,eff}$) is close to liquid (water) density after the fibers absorb

water and swell to a saturation point. It does not change very much with fiber type. Thus, the following dimensionless parameters are constant:

$$\{\frac{H}{D}, R_A, \frac{d_o}{D}, \frac{\rho_g}{\rho_l}, \frac{\nu_g}{\nu_l}, Fr^*, \frac{\rho_{f,eff}}{\rho_l}, \text{and } \frac{\rho_{f,eff}-\rho_l}{\rho_l-\rho_g}\} \quad \text{(B.31)}$$

Table B.2: Resultant dimensionless parameters and their physical meaning.

Dimensionless parameter	**Physical meaning**
ε	Gas holdup
R_A	Open area ratio
θ_f	Liquid-fiber contact angle
μ_f	Fiber surface friction coefficient
H/D	Column aspect ratio
d_o/D	Distributor orifice to column diameter ratio
l_f/D	Fiber length to column diameter ratio
l_f/d_{fo} (r)	Fiber aspect ratio
S_f/l_f	Coefficient of variation (COV) of fiber length
d_{fi}/d_{fo}	Fiber inner to outer diameter ratio
ρ_g/ρ_l	Gas to liquid density ratio
$\rho_{f,eff}/\rho_l$	Fiber to liquid density ratio
ν_g/ν_l	Gas to liquid viscosity ratio
U_g/U_l	Gas to liquid throughput ratio
$(\rho_{f,eff}-\rho_l)/(\rho_l-\rho_g)$	Fiber-liquid to liquid-gas density difference ratio
N_c	Crowding factor
Re	Reynolds number
We	Weber number
Fr^*	Froude number
Π_1'	Fiber network confinement force to buoyancy force ratio

In addition, in the present study, the fiber length is much less than column diameter, thus, $\frac{l_f}{D}$ is negligible. Furthermore, $\frac{l_f}{D}$ is already included in the dimension less parameter Π_1'. Thus, we can omit $\frac{l_f}{D}$ in the final dimensionless parameter list. The influence of fiber aspect ratio ($\frac{l_f}{d_{fo}}$) is mainly on fiber flocculation and network strength, and is already considered in N_c and Π_1', so $\frac{l_f}{d_{fo}}$ can also be deleted from the final parameter list. The major contribution of the fiber inner to outer diameter ratio ($\frac{d_{fi}}{d_{fo}}$) is to affect fiber stiffness. It is thus included in the fiber moment of inertial (I) and consequently considered in Π_1'. So it is not necessary to retain it in the list. The significance of the influence of the dimensionless fiber physical property, μ_f and θ_f, on gas holdup in gas-liquid-fiber bubble column has not been reported. However, in a dilute or semi-dilute fiber suspension where fiber-fiber contact is not the only dominant mechanism of fiber suspension rheological behavior, μ_f can be assumed to have limited effects on gas holdup. The fibers (cellulose and Rayon) used in the present study are all hydrophilic. Pelton and Piette (1992) reported that the main reason bubbles are held up in a fiber suspension is mechanical confinement, not bubble adhesion to fibers. Thus, the fiber contact angle can also be assumed to have a negligible effect. In summary, the following dimensionless parameters can be neglected in the present study:

$$\{\frac{l_f}{D}, \frac{l_f}{d_{fo}}, \frac{d_{fi}}{d_{fo}}, \mu_f, \theta_f\} \tag{B.32}$$

Furthermore, because surface tension σ does not change significantly in this study, the Weber number (We) only provides information of superficial liquid velocity (U_l), column diameter (D), and liquid density (ρ_l). However, in the present study, D and ρ_l are constant and U_l is also included in the Reynolds number (Re). Thus, the Weber number (We) can be neglected in the present study.

With the dimensionless parameters in Eq. (B.31) being constant and those in Eq. (B.32) and the Weber number (We) being neglected, the significant dimensionless parameters in the present study compromise:

$$\{\varepsilon;\ N_c,\ \frac{S_f}{l_f},\ \frac{U_g}{U_l},\ Re,\ \Pi_1'\}. \tag{B.33}$$

Notice that the dimensionless number $\frac{S_f}{l_f}$ (denoted as the coefficient of variation (COV) of fiber length) is kept because it represents the effects of fiber length variation, which is significant when fiber length is not uniform.

Thus the gas holdup can be written in a form:

$$\varepsilon = f(N_c,\ \frac{S_f}{l_f},\ \frac{U_g}{U_l},\ Re,\ \Pi_1') \tag{B.34}$$

for the present study.

Recall that in Chapter 7, we have obtained the following (Eq. (7.11)):

$$\frac{U_g}{\varepsilon} = a_1 + \frac{a_2}{1+\exp[a_3(I_c - I_0)]} + C_l U_l + C_{g,l} U_g + C_{g,2\text{-}l}(U_g - U_{gt})^+ \tag{B.32}$$

where a_1, a_2, a_3, I_0, C_l, $C_{g,l}$, $C_{g,2\text{-}l}$, and U_{gt} are constants estimated by a curve fitting method; $I_0 = \ln(N_f^{1/5} N_c^{4/5})$ are functions of fiber mass fraction and fiber type. Equation (B.32) can be rewritten as:

$$\varepsilon = \frac{\left(\frac{U_g}{U_l}\right)}{\frac{\left[a_1 + \frac{a_2}{1+\exp[a_3(I_c - I_0)]}\right]\left(\frac{D}{\nu_l}\right)}{Re} + \left[C_l + C_{g,l}\left(\frac{U_g}{U_l}\right)\right] + C_{g,2\text{-}l}\left[\left(\frac{U_g}{U_l}\right) - \frac{U_{gt}\left(\frac{D}{\nu_l}\right)}{Re}\right]^+} \tag{B.33}$$

From Eq. (B.33), since D and ν_l are constant in this study, it can be seen that the gas holdup (ε) can be written as a function of $\frac{U_g}{U_l}$, Re, and I_c. Notice the definition of I_c includes N_c and N_f. The fiber number density N_f is not a dimensionless number. However, it was found

related to the coefficient of variation (COV) of fiber length ($\frac{S_f}{l_f}$) in Chapter 6 (Eq. (6.19)). Recall that in Chapter 6, for a given I_c, the gas holdup values for different fiber suspensions still slightly deviated from each other and this was attributed to the fact that still a few important influential factors (e.g., fiber surface friction coefficient and elastic modulus) were not considered in I_c. These factors can be accounted for with the newly identified dimensionless number, Π_1'. In the present study, the quantitative relationship between ε and Π_1' has not been investigated, further work is recommended.

B.6 Summary

A dimensional analysis was conducted for the gas holdup in a cocurrent gas-liquid-fiber bubble column under atmospheric pressure and room temperature. A total of 23 relevant parameters were considered. A total of 20 dimensionless numbers were obtained, as listed in Eq. (B.20) and Table. B.2. With consideration of the conditions in the present study, the gas holdup can be written as a function of 6 dimensionless parameters, as shown in Eq. (B.34).